# NANOQED

## NANO Quantum ElectroDynamics

## Applied Theory in Physics and Nanotechnology

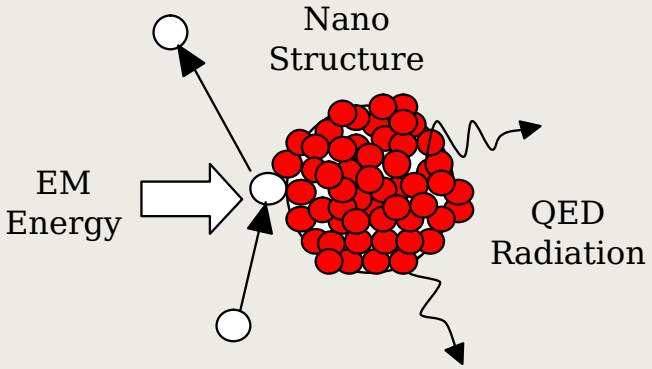


*A tribute to Thomas V Prevenslik*

Articles published posthumously

# NANOQED

A simple theory in Physics with many
applications in the world of Nanotechnology

*A tribute to Thomas V Prevenslik*

Articles published posthumously

Copyright © 2024 Nanoqed

This work by Thomas V. Prevenslik is licensed under Creative Commons Attribution 4.0 International. To view a copy of this license, visit https://creativecommons.org/licenses/by/4.0/

Use, distribution and reproduction in any medium are permitted, provided the original author, Thomas V. Prevenslik [1937-2021] and source are credited.

# Contents

**Introduction** **1**

**1 Covid-19 Treatment by Nanoparticles** **3**

1.1 The CoVid-19 in vivo Nanoparticle Vaccine . . . . . 4

1.2 Nanoparticles and efficacy of mRNA vaccines . . . . . 13

1.3 Solar UV Treatment of Covid-19 by Nanoparticles . . . . . 17

1.4 AstraZeneca Vaccination and Blood Clotting . . . . . 21

**2 Health Risks of Nanoparticles and GM Food** **27**

2.1 DNA Damage by Nanoparticles . . . . . 28

2.2 Cancer by UV radiation from nanoparticles in GM food . . . . . 33

2.3 Electronics Cigarettes and DNA Damage . . . . . 37

2.4 Protein misfolding by UV emission from nanoparticles . . . . . 41

**3 Cellular Biology** **45**

3.1 The Electrostatic Filopodia Force . . . . . 46

3.2 Endogenous UV in Warburg's Theory on the Origin of Cancer . . . . . 56

3.3 Broadband endogenous UV in Mitochondria . . . . . 68

3.4 ATP by Endogenous UV Radiation . . . . . 74

3.5 Cancer: UVC induced Nanoparticle Treatment and Metastasis . . . . . 84

**4 UV Disinfection by Heat** **85**

4.1 Disinfectant Drinking Bowl . . . . . 86

4.2 QED Disinfection of Drinking Water in the Developing World . . . . . 92

4.3 The Ebowla in the Disinfection of the Ebola virus . . . . . 95

4.4 QED Disinfection of Future Public Transport in Hong Kong . . . . . 98

**5 Simple QED** **101**

5.1 The Planck law cancelled? . . . . . 102

5.2 Simple QED induced Superconductivity . . . . . 107
5.3 QED Heat Transfer . . . . . 111
5.4 Sonoluminescence at Ambient Temperature? . . . . . 118

**6 Astronomy** **145**
6.1 Redshift in Cosmic Dust precludes Universe Expansion and Dark Matter . . . . . 146
6.2 Dark Matter only Exists because of Cosmic Dust . . . . . 149
6.3 Cosmic Dust in an Expanding Universe? . . . . . 155
6.4 CMBR as Solar illumination of the Oort Cloud modified by Cosmic Dust . . . . 160

**7 Nanoparticle Physics and Molecular Dynamics** **171**
7.1 Graphene: High Thermal Conductivity at the Nanoscale? . . . . . 172
7.2 Nanocomposites by Quantum Mechanics . . . . . 176
7.3 Molecular Dynamics by Quantum Mechanics . . . . . 181
7.4 Molecular Dynamics of Silver Nanowires Stiffened by QM . . . . . 187
7.5 Quantum Mechanics: Validity of Classical Molecular Dynamics . . . . . 192

**8 Geoengineering and Engineering** **193**
8.1 Global Cooling by Injecting Black Carbon into the Stratosphere? . . . . . 194
8.2 Heat Transfer in Nanoelectronics by Quantum Mechanics . . . . . 201
8.3 1/f Noise in Nanowires by Quantum Mechanics . . . . . 209
8.4 Cavity QED devices United States Patent . . . . . 214

**Acknowledgements** **231**

# Introduction

## Simple QED Theory

Simple QED is a nanoscale heat transfer process. As a consequence of the Planck law, atoms in nanostructures can not conserve heat by increasing temperatures – rather the atoms convert heat to electromagnetic radiation. This radiation can manifest as ultraviolet light.

QED stands for quantum electrodynamics, a complex theory based on virtual photons advanced by Richard Feynman and others. Simple QED is far simpler. This theory only requires the heat capacity of the atoms in nanostructures to vanish, allowing conservation to proceed by the creation of real photons. The photons comprise electromagnetic waves that stand across the nanostructure.

## Background of Thomas Prevenslik

Thomas Prevenslik grew up in a small town near Pittsburgh Pennsylvania. He was a serious student with a particular interest in science, wanting to know how things work and why; questioning the status quo. He attended Carnegie Mellon and the University of Pittsburgh where he obtained his Bachelor and Master Degrees in Mechanical Engineering respectively.

Moving to California in 1966, he designed the mechanical, non-vibrating structures to support and secure the telescopes and cameras aboard the Apollo 11 which landed on the moon in 1969.

Returning to Pennsylvania in 1970, he worked for major companies in the area of nuclear reactors as a source of energy for the next 20 years.

In 1990, he was invited to introduce and set up American engineering software program, ANSYS, in Japanese companies in Tokyo.

Leaving Japan in 1994, Tom began a new career in Physics and entered a doctorate program at the University of Hong Kong. He developed a theory of quantum electrodynamics (QED) based on quantum mechanics (QM) and founded his own company: QED Radiations.

In 2002, now retired, he brought QED Radiations to Berlin, Germany and continued his research in Physics – focusing on Nanotechnology. One year later, he obtained US Patent 20030178616 entitled "Cavity QED devices" and he presented his ongoing research on his newly formed website: `www.nanoqed.org`.

Tom expanded the theory of simple QED nanoscale heat transfer that began at the University of Hong Kong. Based on the Planck law that precludes atoms in NPs the heat capacity to conserve heat by an increase in temperature, conservation proceeds by creating non-thermal standing or travelling EM radiation depending on size of the nanostructure is emitted as UV radiation to the surroundings. Applications included near-field heat transfer and Covid-19 vaccinations.

In the following years, he presented his research and applications of his QED theory not only on his website but also at numerous conferences throughout Europe, Asia and the USA – that is until the Covid pandemic occurred. Nevertheless, he continued on - with Zoom and Webinar conferences - from his home in Berlin.

Even from his hospital bed in Berlin, in early November 2021, he updated his website: `nanoqed.org` - wherein he announced he had prostate cancer, which unfortunately had not been diagnosed by his urologist and the cancer had metastasized. He passed away the end of November at age 84. His legacy is this book entitled NANOQED - available in digital format and paper copy upon request.

Requests may be sent to nanoqed.book@gmail.com

# Chapter 1

# Covid-19 Treatment by Nanoparticles

The advantages and disadvantages of nanoparticles in different Covid 19 vaccines are examined. An explanation of interaction of nanoparticles with Vitamin D3 is presented.


1.1 The CoVid-19 in vivo Nanoparticle Vaccine . . . . . 4
1.2 Nanoparticles and efficacy of mRNA vaccines . . . . . 13
1.3 Solar UV Treatment of Covid-19 by Nanoparticles . . . . . 17
1.4 AstraZeneca Vaccination and Blood Clotting . . . . . 21

# The CoVid-19 *in vivo* Nanoparticle Vaccine

**Abstract**
Vaccine development in preventing CoVid-19 requires long development and testing time which is unacceptable to attendant social unrest and world economic collapse. Instead of preventative vaccines, a CoVid-19 treatment of patients already tested positive is proposed using intravenous injections of lipid nanoparticles (NPs). The NP treatment includes only biodegradable lipid NPs in saline. In contrast, preventive vaccines include the inactivated virus, aluminum adjuvants, formaldehyde, antibiotics, and stabilizers, but in the bloodstream of the CoVid-19 patient none of the preventive vaccine ingredients are likely found. Indeed, only the live virus exists. UV light can inactivate the live virus, but no UV sources are known within the human body. In this regard, simple QED theory based on the Planck law denies atoms in NPs the heat capacity to conserve heat by an increase in temperature. Instead, NPs convert heat from the blood into EM radiation at a wavelength depending on the NP size. e.g., ~ 80 nm lipid NPs emit UVC (254 nm) radiation. In the manner of an *in vivo* vaccine, the UVC kills the live virus to produce the inactivated virus that acts as the antigen in providing immunity to prevent subsequent infection. What this means is the NPs not only disinfect the patient of CoVid-19, but also provide immunity. By controlling the NP dose, the UVC is held to low levels of collateral DNA damage allowing recovery by DNA repair systems.

Keywords: CovVid-19, vaccine, antigen, UV, Nanoscale heat transfer.

## I. INTRODUCTION

Vaccines to prevent viral infection generally include the inactivated virus, aluminum adjuvants to enhance the immune system response, formaldehyde to assure inactivation is complete, antibiotics to prevent contamination during manufacturing, and stabilizers during storage. CoVid-19 vaccine [1] comprises live, inactivated, and DNA or mRNA antigens. Live vaccines are based on genetic engineering having a surface protein of CoVid-19 to trigger an immune response. Inactivated vaccines use killed CoVod-19 viruses, but are recognized by the body as foreign and produces antibodies. Gene-based vaccines are the preferred approach comprising pure genetic information in the form of DNA or mRNA of the virus processed into carrier nanoparticles (NPs) that enter cells and form harmless virus proteins to provide immunity. Compared to live and inactivated vaccines, gene-based vaccines allow quick vaccine production which is of importance in CoVid-19 because billions of doses need to be available to most of the people of the world.

However, the history of vaccinations did not originate with gene-based vaccinations. Over 150 years ago, Pasteur envisioned [2] that live or inactivated microbial pathogens could be used to protect against the pathogen itself. Today, the inactive virus is preferred [3] over live virus, but is problematic because inactivation may turn out to be incomplete leading to outbreaks after vaccination. Formaldehyde and UV radiation are generally used to completely inactivate the virus. Formaldehyde alters virus structure while UV mainly influences the virus genome and preserves structure. In CoVid-19 vaccines, the chemical inactivation of a virus is complex compared to the far simpler inactivation by UV radiation which is pursued here.

Indeed, UV inactivation in CoVid-19 vaccine development is supported by a history of UV disinfection [4] of viruses in the air or on solid surfaces, the UV supplied by external lamps. For viruses having size of about 100 mm, disinfection requires germicidal UVC (254 nm) radiation and has been used [5] to disinfect localized infections suggesting UVC is suitable in inactivated CoVid-19 vaccines as well as providing antigenicity.

The problem is the CoVid-19 is not found near or on exterior body surfaces, but rather in the lungs not accessible to external UVC lamps. Recently, UVA light was made available [6] inside the lungs by a device 'Healight' comprising a flexible catheter equipped with LEDs. But CoVid-19 is not present only in the lung, and rather spread throughout the body and even the brain, all of which cannot be accessed with UVA from the lung.

An *in vivo* UVC light source having access throughout the body is required,
but is not known to exist.

In this regard, UVC disinfection of CoVid-19 having access throughout the body comprising lipid NPs injected in the bloodstream was proposed [7] to convert heat in the blood to size dependent wavelengths of EM radiation. The conversion is a natural consequence of the Planck law that denies NPs the heat capacity to conserve heat by an increase in temperature. Instead, the NP conserves heat by emitting EM radiation at wavelengths depending on the dimensions of nanoscopic NP features. By the theory of simple QED, UVC disinfection requires solid lipid NPs having diameters ~ 80 nm. The CoVid-19 also emits EM radiation as the average diameters of the body (~ 100 nm) emit UVB with the spikes (~15 nm) emitting EUV as illustrated in Fig. 1.

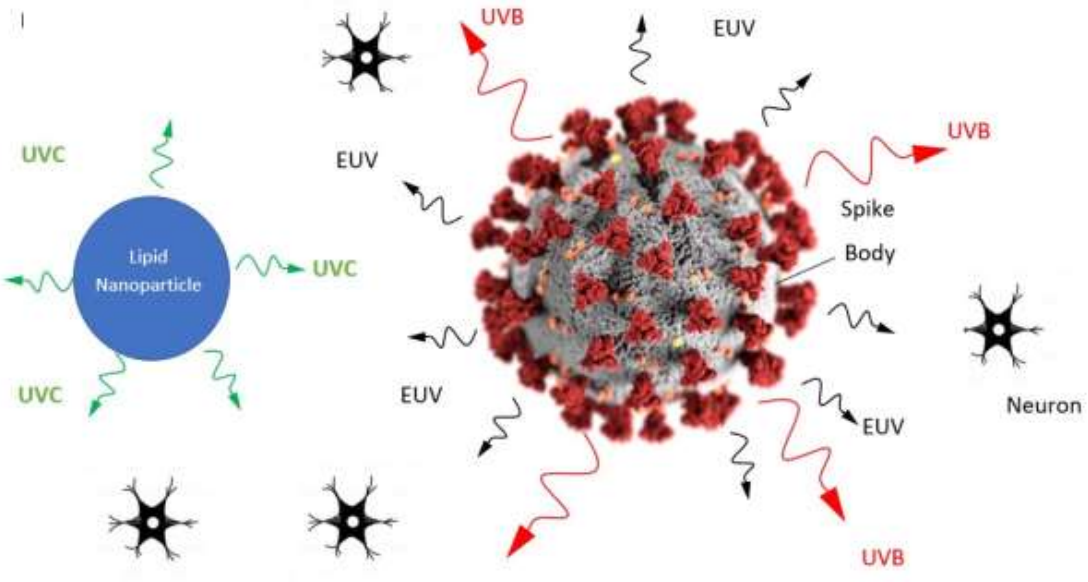


Figure 1. UVC disinfection of CoVid-19 by NPs.

In the UVC disinfection of CoVid-19 by NPs, it is of interest to consider how NPs can be used in vaccinations to protect against CoVid-19 or any other virus. For vaccines to prevent a virus infection, UV inactivated fragments of the virus from external sources would be included with the lipid carrier during NP fabrication. Even so, the vaccine would require massive amounts of UV inactivated fragments for the world population.

A more practical solution is to only treat patients already infected with the virus with UVC disinfection by NPs alone, the UVC not only inactivating the virus, but also producing *in vivo* the inactivated virus for vaccinations. Recalling Pasteur's thought that inactivated microbial pathogens could be used to protect against the pathogen itself, vaccination against the virus only requires the presence of the virus during UVC disinfection. Since UV-inactivated viruses

are able to induce an immune response, the proposed *in vivo* UVC inactivation should produce immunity. To be sure, virus vaccination by NPs is not a vaccine, but rather a treatment after the patient is infected. Nevertheless, NP treatment offers the patient a virus disinfection that may be not only life-saving, but also providing immunity against subsequent virus infections.

## II. PURPOSE

To support simple QED induced EM radiation from intravenous injections of doses of lipid NPs in saline as a rational basis for the *in vivo* CoVid-19 vaccine that also disinfects by UVC radiation from NPs. How UVC disinfection of CoVid-19 elicits immunity is discussed.

## III. BACKGROUND

Over a century ago, investigations of UV radiation discovered using avirulent antigens of a virus for vaccination, but development of the technology for complete inactivation was not available. Today, UV lamps and LEDs have improved inactivation of virus in the air or on external surfaces, but are not applicable within the human body. However, simple QED proposes NPs distributed throughout the bloodstream emit UV radiation allowing vaccine development to proceed based on *in vivo* local inactivation of viruses. Surely, if Pasteur were aware of NPs emitting UV, NP vaccines would have been developed by the UV inactivation of virus particles in an infected patient, each particle acting as an antigen in the immune response against subsequent virus infection.

Absent NPs, UV inactivated SARS-CoV virus particles [8] subcutaneously injected in mice with and without an adjuvant elicited a high level of humoral immunity, resulting in the generation of long-term antibody secreting and memory B cells. UV inactivation of the SARS virus particles was performed under 365 nm UVB lamps *ex vivo* the patient. Indeed, the vaccine containing UV inactivated SARS-CoV particles was able to induce long-term antibody production even without an adjuvant. What this means is whole killed SARS-CoV particles can serve as a candidate [9] antigen for the SARS vaccine eliciting both humoral and cellular immunity.

But can NPs inactivate virus and still elicit immunity?

Recently, the importance of NPs in adjuvants [10] of vaccines was reviewed. Since the 1920's, adjuvants of aluminum salts (alum) have been traditionally thought to stimulate immune response of vaccine antigens, although the mechanism is not known by which alum adjuvants augment immunity, particularly T-cell responses. However, since alum adjuvants are ~ 0.5 – 10 micron microparticles, each of which are aggregates of ~ 100 nm alum NPs, and since NPs alone were found [10] to significantly enhance immune response of traditional alum adjuvants, it can be concluded that over the past 100 years, NPs were present in the alum adjuvants as confirmed in Fig. 2 showing NPs everywhere in a TEM micrograph over a ~ 0.5 micron area of alum adjuvant. NPs alone are present around ~100 nm while alum adjuvant aggregation is centered at ~ 5 microns. But notice the alum adjuvant includes a NP content as otherwise alum adjuvants would not have stimulated vaccines. By simple QED, the NPs emitting UV radiation to elicit immunity by stimulating T-cells.

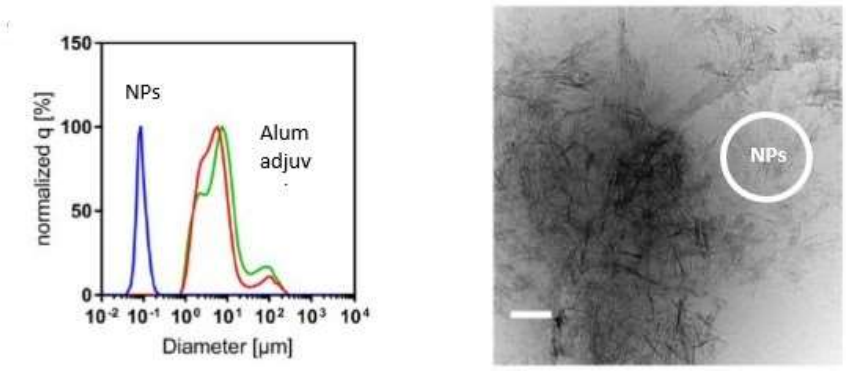


Figure 2. NPs in Alum Adjuvants

. What this means is simple QED induced UV from NPs in saline administered by intravenous injection to infected CoVid-19 patients not only disinfects the virus, but also provides immunity to prevent subsequent CoVid-19 infections. Unlike traditional vaccines, the NP vaccine does not contain any drugs - only NPs.

Other than CoVid-19, simple QED was used to support both the advantage and disadvantage of NP induced DNA damage. For CoVid-19, NPs emitting UV offer desirable disinfection and immunity, but NPs can be a disadvantage as UV induces unwanted DNA damage. Indeed, UV radiation of neurons can cause [11] DNA damage leading to neuro-degenerative diseases from aluminum adjuvants in vaccines and even genetically modified food. At the same time, nanoscale ~ 100 nm films on drinking bowls offer a means to disinfect drinking water from body heat in the hands. Simple QED induced UV explains both advantages and disadvantages of NPs.

## IV. SIMPLE QED.

Classical physics allows the atom to have heat capacity at the nanoscale, the conservation of heat proceeding by a change in temperature. However, simple QED based on the Planck law of quantum mechanics [12] denies the atom in nanostructures the heat capacity to conserve heat by a change in temperature, the consequence of which is any heat is conserved by creating standing EM radiation that is released to the surroundings.

Unlike electronic quantum states, simple QED is based on size dependent quantum states depending on the dimensions of the nanostructure over which the EM waves stand. Simple QED is a method of nanoscale heat transfer analysis that conserves heat with EM radiation instead of temperature. QED stands for quantum electrodynamics, a complex theory based on virtual photons advanced by Feynman [13] and others. In contrast, simple QED is a far simpler theory based on the Planck law of quantum mechanics (QM) that requires the heat capacity of the atoms in nanostructures to vanish allowing conservation to proceed by the creation of real photons comprising EM waves that stand within and across the nanostructure. The standing waves of interest are in the UVC that by classical physics require extreme temperatures of ~37,000 K for creation.

By classical physics, the kT heat capacity of the atom is independent of the EM confinement wavelength λ, where k is the Boltzmann constant and T absolute temperature. QM differs as the heat capacity of the atom decreases under EM confinement λ < 200 microns. At the nanoscale λ < 100 nm, the heat capacity vanishes. The Planck law at 300 K is shown in Fig. 3.

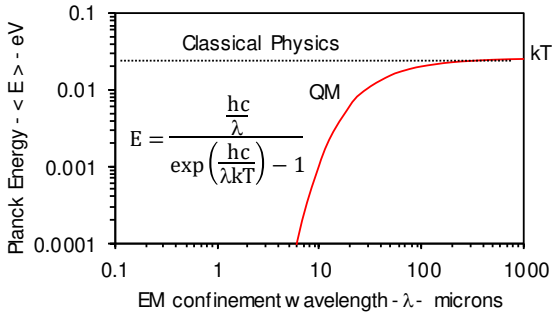


Figure. 3. Planck law of the Atom at 300 °K
In the inset, E is Planck energy, h Planck's constant, c light speed, k Boltzmann's constant, T temperature, and λ the EM confinement wavelength

Classically, the UVC photon can only be created at very high temperatures T, i.e., T = E/1.5k ~ 37,000 K. But high temperatures are not necessary under high EM confinement provided by the absorbed heat Q from the surroundings. EM confinement requires the heat Q to almost totally be confined to the nanostructure surface. For the NP, the surface heat itself absorbed in the penetration depth δ provides the brief EM confinement necessary to create EM waves standing across the diameter d as shown in Fig. 4. Heat (or light) having wavelength λ >> d, the light (yellow) immerses the NP and is absorbed over the full NP surface.

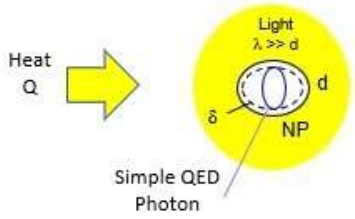


Figure 4. Heat Q (or light) absorbed in NP surface

Confinement of the light Q while creating the standing wave requires EM confinement at least equal to the Planck energy E of the absorbed light. The pressure P acting on the surface is given for bulk modulus B and volume strain ΔV/V by, $P = B \cdot \Delta V/V = 6 \cdot \delta \cdot B/d$. But $P = E / V = 6E/\pi d^3$ giving $\delta = Q/\pi B d^2$. Consider human meibomian lipids [14] at 250 nm having refractive index n ~ 1.55 (extrapolated). For 80 nm lipid NPs, the simple QED wavelength λ ~ 248 nm and E ~ 4.88 eV. Taking a lipid bulk modulus $B \sim 2 \times 10^9$ N/m$^2$, the absorption depth δ of a single UVC photon is δ ~ 20 fm - a small but necessary depth to confine the absorbed heat Q = E to the geometry of the standing wave.

Once the heat Q is absorbed in the penetration depth δ = 20 fm of the NP, the time τ to create the UVC photon as the EM heat Q travels to the NP center is, τ = 2d/(c/n) ~ 0.83 fs and prompt. What this means is the 80 nm NPs under EM confinement are continually producing UVC photons in human tissue at body temperature.

Classically, the number N of atoms created in the NP at equilibrium have temperature T equal to body temperature. The total NP thermal energy is, U = 1.5 N kT. However, by the Planck law the N atoms do not have E = kT energy. Instead, simple QED conserves the energy U that otherwise would occupy the 80 nm NP by creating standing EM radiation across the NP diameter d as shown in Fig. 4. The molecular weight of the meibomian C44H56O2 is 565 and the number N of atoms is, $N = (\rho V/565)\cdot Av$, where volume $V = \pi d^3/6 = 2.68 \times 10^{-22}$ m$^3$, density $\rho = 1000$ kg/m$^3$ and Avagadro number $Av = 6.023 \times 10^{26}$ mols/kg-mol. Hence, $N = 2.85 \times 10^5$ and U ~ 10.8 keV. For $E = hc/\lambda$ at $\lambda = 248$ nm, E ~ 5 eV and the NP creates about 2200 UVC photons upon equilibrating with the 300 °K surroundings.

Simple QED absorbs heat Q in the NP surface given by the penetration δ depth. Unable to conserve the surface heat by a change in temperature, conservation requires the creation of standing EM radiation, with a creation time $\tau = 2d/(c/n)$. The Planck energy $E \sim h/\tau = hc/2nd$ depends on the refractive index n of the NP to correct for the velocity c of light within the NP. The simple QED Planck energy E is quantized by the dimension d of the NP that defines the half-wavelength λ/2 of the nanostructure. Fig. 5 illustrates the standing EM radiation in a spherical NP of diameter d, but NP atoms still follow their quantized electron energy levels.

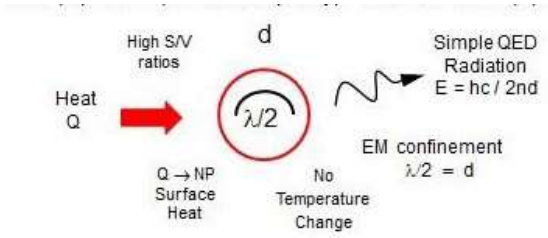


Figure. 5. Planck Energy of EM Radiation

In a rectangular NP with dimensions of width, thickness, and length there are 3 simple QED quantum states corresponding to the 3 dimensions of the NP. However, only the minimum dimension is important as by Fermat's principle, as the absorbed heat is dissipated in minimum time. Continuous variation in internal nanostructure dimensions produces a broadband spectrum of simple QED dissipated in continuous QED quantum states.

## V. APPLICATION

The simple QED radiations associated with the proposed CoVid-19 treatment include the CoVid-19 body and spikes and the 80 nm lipid NPs. For the CoVid-19, the simple QED Planck energy E and wavelength λ are based on the NP diameter d and refractive index n. The CoVid-19 body diameter d varies from 80 - 120 nm [15] with 100 nm being the average diameter for the coronaviridae family. Similar to SARS, the Covid-19 spikes are globular proteins d ~ 15 nm in diameter [16] attached to the virus body by a narrow stalk. With regard to the index n of the virus, available data is not clear. Even so, the index in the UV or EUV is required, but only data is available in VIS, e.g., n = 1.42 at λ = 830 nm [14]. Optical fringe measurements [17] show a maximum index n ~ 1.8 with the average of variations across the virus body taken as n ~ 1.6. The index n of the spikes could not be resolved [18] and is also taken at n ~ 1.6. The index n ~ 1.55 of the lipid NP is required at 248 nm corresponding to the Planck energy E of the 80 nm NP was extrapolated from data [14] at 400 nm. The simple QED summary of the CoVid-19 body and spike including the lipid NP is summarized in Table 1.

Table 1
Simple QED Energy and Wavelengths

| | Body | Spike | Nanoparticle |
|---|---|---|---|
| Material | CoVid-19 | CoVid-19 | Lipid |
| Diameter d (nm) | 100 | 15 | 80 |
| Refractive Index n | 1.6 | 1.6 | 1.55 |
| Wavelength λ (nm) | 320 | 48 | 248 |
| Planck energy E (eV) | 3.88 | 26 | 5 |

Recall EUV (< 200 nm), UVC (200 to 280 nm), UVB (280 to 320 nm), and UVA (320 to 400 nm). The CoVid-19 body emission (320 nm at long wavelength UVB) and spikes (48 nm in the EUV) while the NP emits (~248 nm near the 254 nm UVC peak). It is noted the CoVid-19 body emission increases toward the UVC peak for NP diameters < 80 nm.

## VI. TREATMENT

The history of vaccines against infectious viruses suggests a CoVid-19 vaccine developed by traditional searches for antigens will be difficult, if not impossible in the near term. In contrast, CoVid-19 treatments avoiding the serendipity search for antigens are more likely to be developed than vaccines. Indeed, blood plasma is already available, but not actively pursued because the CDC and FDA are subservient to the paradigm of vaccines to disinfect viruses. But vaccines take time for development and testing which is not an option in the current CoVid-19 pandemic. Moreover, a CoVid-19 vaccine even if found will not likely survive mutations and future viruses that will require development of yet another vaccine.

What this means is a paradigm shift from vaccines to treatment of viral infection is unavoidable. Vaccination even if successful would not be practical for the entire world population. Accordingly, CoVid-19 treatment of only the population tested to have the virus emerges as the realistic solution. Indeed, treatment instead of vaccines should be adopted by the CDC and FDA as the new paradigm.

Simple QED proposes UVC disinfection of the CoVid-19 using doses of biodegradable lipid NPs in saline delivered intravenously by injections. The interaction between the NPs and the CoVid-19 is illustrated in Fig. 1 and summarized in Table 1. Of importance is the DNA absorption spectrum [19] shown in Fig. 5.

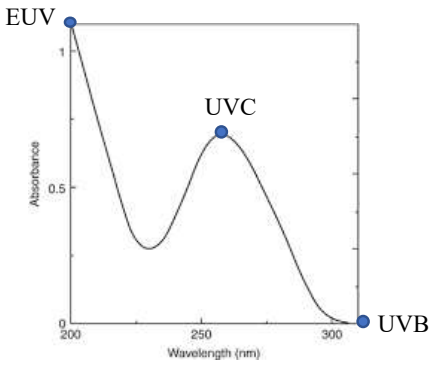


Figure 5. DNA absorption spectrum

The DNA has peaks at 260 nm in the UVC and in the EUV beyond 200 nm. The 100 nm CoVid-19 body emission in the UVB at 320 nm is not absorbed by the DNA and does not cause DNA damage to brain neurons. But DNA damage of neurons may be expected for virus diameters < 80 nm. The UVB at 320 nm finds importance [20] only in initiating the 'cytokine storm' and 'blood clot storm'.

UVC disinfection of the CoVid-19 from the 80 nm NP emission occurring at 248 nm inactivates the virus DNA. The UVC also damages brain neurons, but at low levels the DNA damage is corrected by DNA repair systems. EUV at 48 nm from the spikes does not damage brain neurons and appears to only assist burrowing through cell walls. However, these predictions depend strongly on the refractive indices of the CoVid-19.

## VII. CONCLUSIONS

In simple QED, the Planck law allows the lipid NPs to produce EM radiation to disinfect the CoVid-19 virus from heat at body temperature, a significant difference with classical physics that predicts the NPs only acquire body temperature. UVC photon are created in NPs under EM confinement at body temperature and do require ~37,000 K temperatures.

With regard to providing CoVid-19 disinfection treatments, simple QED induced UV radiation from NPs offers an easily implemented solution. Considerable theory exists to support the argument that NPs kill viruses, but a physical mechanism does not exist. However, only simple QED argues the NPs depending on size create UV radiation in equilibrating the thermal energy of the surrounding blood and tissue.

NPs convert heat from the blood into EM radiation at a wavelength depending on the NP size. For ~80 nm lipid NPs, UVC (254 nm) radiation kills the live CoVid-19 virus to create an *in vivo* vaccine comprising the inactivated virus that acts as an antigen in providing immunity to subsequent CoVid-19 infection.

The dose of NPs in saline solution can only be determined by CDC and FDA controlled testing with emphasis placed on neuron and DNA damage. The lowest NP concentration that disinfects the CoVid-19 is the goal as collateral DNA damage to adjacent tissue from low intensity UV can be corrected by DNA repair systems. For CoVid-19 patients in a life-threatening condition, DNA damage appears justified.

Over the past century, the mechanism by which adjuvants of aluminum salts are thought to stimulate immune response of vaccine antigens is nothing more than simple QED induced UV radiation from ~100 nm cylindrical particles that aggregate to form the micron size > 500 nm particles actually observed.

The vaccine paradigm as the norm in controlling infectious disease appears to no longer applicable as the CoVid-19 virus will simply mutate or other viruses may appear. Genetic basis to the CoVid-19 excludes the effect of simple QED induced EM radiation. Only a UVC treatment of patients diagnosed as having the CoVid-19 by intravenous injections of 80 nm NPs, or the equal appears relevant as vaccinations for all people in the in the world is unrealistic, if not impossible.

The CoVid-19 *in vivo* vaccine based on intravenous injection of lipid NPs is extended to the preferred oral delivery of NPs in a forthcoming paper.

## References

1. DW-News (2020) The race towards a CoVid-19 vaccine: What's the latest? https://www.dw.com/en/the-race-towards-a-CoVid-19-vaccine-whats-the-latest/a-53330975
2. Plotkin SA. (2005) Vaccines: past, present and future. Nature Medicine Supplement 11: S5-S11.
3. Delrue I, et al. (2014) Inactivated virus vaccines from chemistry to prophylaxis: merits, risks and challenges. Expert Review of Vaccines. https://doi.org/10.1586/erv.12.38
4. Downes A, Blunt TP. (1877). Researches on the effect of light upon bacteria and other organisms. Proc R Soc Lond. 26:488-500.
5. Vantasever F, et al. (2013) Can biowarfare agents be defeated with light? Virulence 4:796–825.
6. Hiltzik M. - Los Angeles Times (2020) Column: How Cedars-Sinai got sucked into the battle over Trump's claim of a COVID-19 treatment. May 1. https://www.latimes.com/business/story/2020-05-01/cedars-sinai-trump-covid-cure
7. Prevenslik T. (2020) Coronavirus by UV from Lipid Nanoparticles. https://www.nanoqed.org , 2020.
8. Takusaku N, et al. (2004) A subcutaneously injected UV-inactivated SARS Coronavirus vaccine elicits systemic humoral immunity in mice. International Immunology. 16: 1423–143.
9. Tsunetsugu-Yokota Y et al. (2008) Large-scale preparation of UV-inactivated SARS Coronavirus virions for vaccine antigen. Methods Mol Biol. 454:119-26.
10. Orr MT, et al. (2020) Reprogramming the adjuvant properties of aluminum oxyhydroxide with nanoparticle technology npj Vaccines. https://doi.org/10.1038/s41541-018-0094-0
11. Prevenslik T. Nanoparticles and DNA damage. GM Food: A Crime against Humanity; UVC disinfection of drinking water. https://www.nanoqed.org , 2017 - 2019.
12. Planck M. (1900) On the Theory of the Energy Distribution Law of the Normal Spectrum. Verhandl. Dtsch. 2: 2-37.
13. Feynman R. (1976) QED The Strange Theory of Light and Matter. Princeton University Press
14. Tiffany JM. (1986) Refractive index of meibomian and other lipids. Current Eye Research - Short Communication. 5:887-889
15. Guy JS, et al. (2006) Characterization of a Coronavirus Isolated from a Diarrheic Foal. J. Clinical Microbiology. 38:4523–4526.
16. Beniac ER, et al. (2006) Architecture of the SARS Coronavirus prefusion spike. Nature Structural Molecular Biology 13:571-572.
17. Pang Y, et al. (2016) Using optical trap to measure the refractive index of a single animal virus in culture fluid with Optics and Photonics Journal, 2016, 6, 75-86 high precision. Biomedical Optics Express. 7: 1 672-1689.
18. Hamed AM. (2016) Image Processing of Corona Virus Using Interferometry. Optics and Photonics Journal. 6:75-86.
19. Rodger A. (2013) UV Absorbance Spectroscopy of Biological Macromolecules. In: Roberts G.C.K. (eds) Encyclopedia of Biophysics. Springer, Berlin, Heidelberg.
20. Prevenslik T. (2020) Mystery pulmonary and neurological symptoms by EM radiation from the CoVid-19 https://www.nanoqed.org , 2020.

# Nanoparticles and efficacy of mRNA vaccines

**Abstract:** The CDC approach to the Covid-19 virus was traditional: quickly develop a vaccine that usually takes years, but even if successful in the near term is impossible to implement for the entire World population, let alone unacceptable because of attendant social unrest and economic collapse. On this basis alone, the traditional approach for Covid-19 is not likely to be successful. Moreover, vaccines typically contain fragments of inactivated viruses. In this regard, the current Pfizer/Biotech and Modern vaccines differ in that the inactivated virus is not used, but rather the patient receives an injection of genetic material –mRNA– that encodes the spike protein of Covid-19 virus as the antigen to elicit Covid-19 immunity, the process taking place inside the patient's body. Since the mRNA molecule is fragile and disintegrates upon entering the cell, the mRNA is dispersed inside ~ 80 nm fatty lipid nanoparticles (NPs). Unfortunately, the ~80 nm NPs emit UVC radiation that inactivates the mRNA carried making the promise of mRNA vaccines in the therapy of disease unworkable. But the mRNA vaccines by Pfizer/Biotech and Modern are reported to have a 94.5% efficacy clearly suggesting a mechanism other than mRNA is inactivating the Covid-19. In this regard, the Covid-19 NP Treatment based on NPs inducing UVC was proposed in mid-2020 as the mechanism to avoid obvious logistical problems in the World-wide delivery of cold storage requirements of Covid-19 vaccines. In the Covid-19 NP Treatment, the UVC need only inactivate a few of the live Covid-19 virus in the patient that then act as the antigen to elicit Covid-19 immunity. But UVC also damages DNA of neurons in the brain. Low NP doses reduce UVC levels to allow correction of DNA damage by repair systems. Currently, NP doses are too high as Bell's palsy and allergic reactions are reported. The concept of mRNA vaccination can be made workable if NPs > 100 nm producing IR radiation carry the mRNA as IR would not inactivate mRNA, but then efficacy is reduced to ~50% compared to the NP Treatment offering > 90% efficacy at low cost without need of mRNA and attendant cold storage.

***Keywords:*** Covid-19, Planck law, simple QED, nanoparticles, treatment, vaccine efficacy

## I. INTRODUCTION

.

In 2020, the Coronavirus known as Covid-19 became a pandemic that changed [1] the economic future of the world, although in severity only comparable to influenza. Since there was no vaccine or specific treatment known for Covid-19, the CDC approach was traditional: quickly develop a vaccine that usually takes years, but even if successful in the near term is impossible to implement for the entire World population, let alone unacceptable because of attendant social unrest and economic collapse. On this basis alone, the traditional CDC approach for Covid-19 is not likely to ever be successful.

Moreover, vaccines typically contain fragments of inactivated viruses. The current Pfizer/Biotech and Modern vaccines differ in that the inactivated virus is not used, but rather the patient receives an injection [2] of genetic material –mRNA– that encodes the virus protein *thought* to be the antigen necessary to elicit Covid-19 immunity, the process taking place inside the patient's body. For Covid-19, the spike protein was selected as encoding all proteins in the virus is difficult, if not impossible.

Making matters worse, the mRNA molecule is fragile and disintegrates upon entering the cell, the difficulty *thought* resolved by dispersing [3] the mRNA inside fatty lipid nanoparticles (NPs). Unfortunately, simple QED theory [4] claims the NPs emit UVC radiation that inactivates the carried mRNA, thereby negating [5] the concept of mRNA vaccines in NP carriers.

Nevertheless, the Pfizer/Biotech and Modern vaccines are reported [6] to have a remarkable 94.5% efficacy in protecting against Covid-19. UVC inactivation of mRNA aside, influenza vaccines based on inactivated virus have only 50% efficacy. Since Moderna's Covid-19 mRNA vaccine is the genetic equivalent of an inactivated Covid-19 spike, the efficacy of the Covid-19 mRNA vaccine should be near 50% - not over 90%.

In this regard, the Covid-19 UVC Treatment proposed [7] as an alternative to the logistical problems in the World-wide delivery of cold storage mRNA vaccines also explains the 90% efficacy without mRNA.

Based on the long history of UV inactivating viruses, simple QED theory applied to ~80 nm lipid NPs injected in the patient showed low levels of UVC radiation could be produced, the UVC only needing to

inactivate a few of the virus in the patient that then act as the antigen to elicit Covid-19 immunity, i.e., the UVC from NPs carrying the mRNA is the mechanism for the 90% efficacy.

However, the UVC from NPs has a dark-side. The NPs in injections rapidly enter the brain, the UVC causing collateral DNA damage to neurons. Low NP doses allow correction of DNA damage by repair systems. But if NP doses are too high, DNA repair systems are overwhelmed and neurological symptoms appear. Since Bell's palsy [8] and neuronal allergic modulations [9] have already been reported, DNA damage from mRNA vaccines should be included with vaccine efficacy as NP doses are likely too high.

Nevertheless, the Pfizer/BioNTech and Moderna vaccines have received CDC/FDA approval [10] and are now are in the process of being distributed around the World even though the vaccines may be ineffective [11] against Covid-19 variants.

Since there are 8 billion people in the World and cold storage temperatures for the Pfizer/ BioNTech and Moderna mRNA vaccines aside, it is still unlikely to be given to everyone. As in mid-2020, the Covid-19 UVC Treatment is once again proposed as an alternative to mRNA vaccines.

## II. PURPOSE

The purpose of this paper is to reiterate the mid-2020 proposal [6] of the NP Treatment for the Covid-19 and future pandemics. Only ~80 nm lipid NPs are used - no mRNA. The NPs injected in Covid-19 patients provide UVC within the human body to disinfect the virus as shown in Fig. 1.

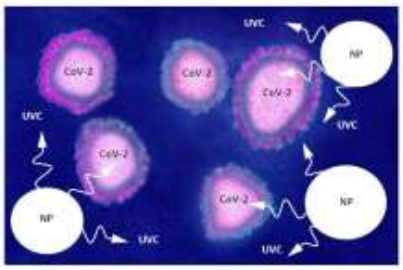


Figure 1. UVC Treatment by nanoparticles

## III. BACKGROUND AND THEORY

Simple QED is a nanoscale heat transfer process based on the Planck law [12] of quantum mechanics (QM) differing significantly from that of classical physics. Research in nanoscale heat transfer [13-15] has been reported. But despite advances, there are still challenges in understanding the mechanism of nanoscale thermal transport. Perhaps, researchers have not appreciated the significant difference between classical physics and the Planck law with regard to the heat capacity of the atom illustrated in Fig. 2.

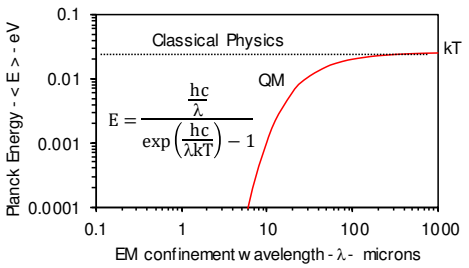


Figure. 2: Planck law of the Atom at 300 °K
In the inset, E is Planck energy, h Planck's constant, c light speed, k Boltzmann's constant, T temperature, and λ the EM wavelength.

The Planck law at 300 K shows classical physics allows the atom constant kT heat capacity over all EM confinement wavelengths λ. QM differs as the heat capacity of the atom decreases for λ < 200 microns, and vanishes at the nanoscale for λ < 100 nm.

Indeed, the Planck law denies atoms in nanostructures the heat capacity to change temperature upon the absorption of heat - a difficult notion to accept because of our training in classical physics. QM requires heat transfer to occur without changes in temperature.

Nevertheless, nanotechnology has continued [13-15] to use classical physics at the nanoscale. In effect, the Fourier law of heat conduction commonly used in nanoscale heat transfer is no longer valid. The Stefan-Boltzmann law for radiative heat transfer depending on temperature is not valid at the nanoscale. Classical Molecular Dynamics (MD) simulations [16] under periodic boundary conditions (PBC) provide the atomic response to the thermal disturbances in macrostructures are clearly valid where atoms do indeed have temperature. However, classical MD extensions to discrete nanostructures is not valid. Researchers need both new theory and computational procedures to be developed to understand nanoscale heat transfer.

Simple QED is a method [4] of nanoscale heat transfer analysis based on QM by the Planck law that conserves heat with EM radiation instead of temperature. Here, QED stands for quantum electrodynamics, a complex theory based on *virtual* photons advanced by Feynman [17] and others. In contrast, simple QED is a far simpler theory based on the Planck law that only requires the heat capacity of the atoms in nanostructures to vanish allowing conservation to proceed by the creation of *real* photons comprising EM waves that stand within and across the nanostructure.

Similar to electron level quantum states, simple QED quantum states are size dependent based on the dimension of the nanostructure over which the EM waves stand. But brief EM confinement of absorbed heat Q at the surface is necessary to form EM waves standing across and within the nanostructure. Earlier EM confinement [4] assumed the inwardly disposed heat Q over the surface was absorbed in a penetration depth δ before forming the standing wave. In this paper, the momentum of the inward heat Q flux as a Poynting vector is proposed to provide a simpler, yet brief EM confinement that forms the standing wave across the diameter d of a NP as shown in Fig. 3.

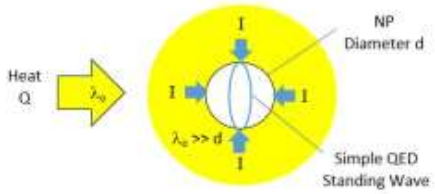


Figure 3. Brief momentum EM confinement

Importantly, the inward disposed Poynting vector is a consequence of the NP be immersed in the EM radiation of heat Q usually in as FIR radiation having wavelength $\lambda_o$, where $\lambda_o >> d$ as illustrated with heat Q (yellow) immersing the NP shown in Fig. 3. Since heat Q cannot be conserved by a change in temperature, conservation proceeds by the creation of simple QED radiation in the form of non-thermal standing waves within the geometry of the NP.

The spherically symmetric inward momentum flux I of the incident heat Q acts as the Poynting vector $S = Q/c$ giving $I = \pi d^2 S\Delta t = \pi d^2 Q\Delta t/c$, where $\Delta t$ is the duration of Q. But the momentum flux p of $N_p$ photons standing in the NP is, $p = N_p \cdot h/\lambda$, where $\lambda$ is the wavelength of simple QED radiation. For $Np \cdot E = \pi d^2 Q\Delta t$, $I = N_p \cdot E/c = N_p \cdot h/\lambda$. Hence, brief EM confinement requires $I > p$, but thereafter Q vanishes and $p > I$ allowing the standing EM radiation to be emitted to the surrounding. Earlier EM confinement [7] depending on the penetration depth δ produced by pressure of the inward momentum is avoided by using the Poynting vector.

The Planck energy E of a photon in the NP is given by the time τ required for light to travel across and back the NP diameter, $\tau = 2d/(c/n)$, where n is the index of refraction of the NP. Hence, the Planck energy E of the simple QED photons is, $E \sim h/\tau = hc/2nd$ giving the wavelength $\lambda = 2nd$. The simple QED Planck energy E is quantized by the dimension d of the NP that defines the half-wavelength $d = \lambda/2$.

In a rectangular NP with different dimensions of width, thickness, and length there are 3 simple QED quantum states corresponding to the different dimensions of the NP. However, only the minimum dimension is important as by Fermat's principle, the absorbed heat is dissipated in minimum time.

## IV. APPLICATION

The application is a NP in a thermal bath. Classically, all atoms in the NP at equilibrium have temperature T equal to the bath temperature. In terms of the Boltzmann constant k and the number N of atoms, the total NP thermal energy U is,

$$U=3/2\ NkT$$

However, by the Planck law the N atoms do not have kT energy. Instead, simple QED conserves the energy U that otherwise would occupy the ~80 nm NP by creating standing EM radiation across the NP diameter d as shown in Fig. 4. t is the duration

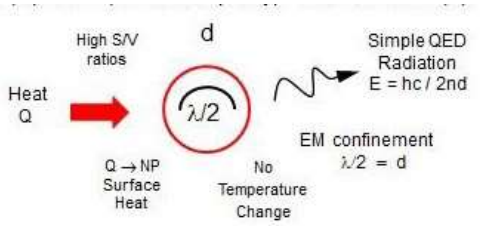


Figure. 4: Planck Energy of EM Radiation

The molecular weight of the lipid meibomian C44H56O2 is 616 and the number N of atoms is, $N = (\rho V/616)\cdot Av$, where volume $V = \rho d^3/6 = 2.68\text{x}10^{-22}$ $m^3$, density $\rho \sim 1000$ kg/$m^3$ and Av = Avagadro's. number. Hence, $N = 2.62\text{x}10^5$. Provided momentum flux $I > p$, U = 10.8 keV. For $E = hc/\lambda$ at $\lambda = 254$ nm, E ~ 4.88 eV, the lipid NP creates about ~ 2200 UVC photons upon equilibrating with the 300 K body temperature.

Once created, the emitted UVC photons are h/absorbed by the Covid-19 virus or water bath, the bath temperature T once again produces the number of ~ 2200 UVC photons repetitively. Of importance, the UVC photons based on the Planck of QM are created at body temperature. In contrast, UVC photons by classical physics requires temperature $T = E/1.5k \sim$ 37,000 K which is not possible. Need QM to validate the notion of creating UVC photons at ambient temperature.

## V. CONCLUSIONS

In simple QED, the Planck law allows ~80 nm lipid NPs to produce UVC radiation that disinfects the Covid-19 from heat at body temperature, a significant difference with classical physics that predicts the lipid NP only acquires the temperature of the bath.

With regard to Covid-19 disinfection treatments, simple QED produces UVC from ~ 80 nm lipid NPs using only the thermal energy of the surrounding blood and tissue.

In the manner of an *in vivo* Covid-19 vaccine, the UVC treatment need only inactivate a few live viruses that then act as the antigen to elicit immunity from the remaining and future Covod-19 virus in the patient.

The CDC is requested to conduct UVC Treatment tests on lipid NPs program to show:

- Lipid NPs > 100 nm produce IR but cannot inactivate live virus to produce antigens.

- UVC is required to produce antigens that requires 70 < NPs < 100 nm.

- EUV from NPs < 70 nm also inactivates live virus, but causes greater DNA damage than at UVC levels → UVC Treatment use 70–100 nm NPs.

In the blood stream, the UVC inactivation would be rapid with the NPs upon entering the brain damage the DNA of neurons. However, our DNA repair systems that evolved necessitated by survival during the UVC intense early Earth damage are expected to readily correct any DNA damage. Indeed, CDC testing to determine acceptable NP dose levels is mandatory to ensure the safety of the UVC treatment of Covid-19.

The mRNA molecule fragility thought resolved by dispersion in lipid NPs leads to other problems not anticipated by Pfizer/Biotech and Modern as the UVC produced by the 80 nm NPs inactivate the mRNA upon dispersion in the NPs.

Since influenza vaccines based on inactivated virus have only 50% efficacy, and since Modern's Covid-19 mRNA vaccine is the genetic equivalent [4] of an inactivated Covid-19 spike, the efficacy of the Covid-19 mRNA vaccine should be near 50% - not over 90%. What this means is the 80 nm NPs carrying the mRNA are the source of the significant increase in efficacy.

The concept of mRNA vaccines requires the mRNA molecules be carried in > 100 nm lipid NPs as the IR radiation created does not inactivate the carried mRNA, but then the Covid-19 efficacy will not be > 90%, rather near 50%.

**REFERENCES**

[1] Kluthe A. "Social Unrest Is the Inevitable Legacy of the Coved Pandemic," https://www.bloomberg.com/opinion/articles/2020-11-14/2020-s-covid-protests-are-a-sign-of-the-social-unrest-to-come Bloomberg Opinion, November 13, 2020.
[2] Pardo N., et al., "mRNA vaccines — a new era in vaccinology," Nature Reviews | drug discovery vol.17, pp. 264-279, 2018.
[3] Kwon D. "The Promise of mRNA Vaccines," https://www.the-scientist.com/news-opinion/the-promise-of-mrna-vaccines-68202 The Scientist, November 25,2020.
[4] Prevenslik, T. "Simple QED Theory and Applications," nanoqed.org, 2015-2020.
[5] Ponta A., et al. "Radiation Sensitivity of Messenger RNA." Molec. gen. Genet. vol. 175, pp. 13-17, 1979.
[6] Park, A. " Modern's COVID-19 Vaccine Is 94.5% Effective. Here's What That Really Means," https://time.com/5912491/moderna-covid-19-vaccine-effectiveness/ November 17, 2020.
[7] Prevenslik, T. "The Nanoparticle Treatment" See https://nanoqed.org/resources/2020/London.mp4
[8] Lima N. A., et al., "Peripheral facial nerve palsy associated with COVID-19", J. NeuroVirology . vol. 26 pp. 941–944, 2020.
[9] Undem B. J., et al. "Mechanisms underlying the neuronal-based symptoms of allergy," J Allergy Clin Immunol., vol. 133, pp. 1521–1534, 2014.
[10] CDC Approval of Pfizer/Biotech vaccine. https://www.businesswire.com/news/home/20201212005026/en/U.S.-CDC-Committee-of-Independent-Health-Experts-Recommends-Vaccination-with-Pfizer-and-BioNTech-COVID-19-Vaccine-for-Persons-Ages-16-Years-and-Older. December 12, 2020.
[11] Stankiwiecz K. "Dr. Scott Gottlieb says new UK Covid strain 'will not slip past our vaccines very easily'," CNBC, https://www.cnbc.com/2020/12/21/covid-vaccines-likely-to-protect-against-new-uk-virus-strain-dr-scott-gottlieb.html December 21, 2020.
[12] Planck M., "On the Theory of the Energy Distribution Law of the Normal Spectrum," Verhandl. Dtsch. Phys. Ges., vol. 2, pp. 2-37, 1900.
[13] Cahill D. G., et al. "Nanoscale thermal transport," Appl. Phys. vol. 93, pp. 93–818, 2003.
[14] Chen G., Nanoscale energy transport and conversion: parallel treatment of electrons, molecules, phonons, and photons, Oxford University Press, 2005.
[15] Cahill D. G, et al. "Nanoscale thermal transport. II. 2003–2012," Appl. Phys. Rev. vol. 1, pp. 011305, 2014.
[16] Poulikakos D., et al. " Molecular Dynamics simulation in nanoscale Heat Transfer: a review,". Microscale Thermophysical Eng., vol. 7, pp.181–206. 2003.
[17] Feynman R., QED: The Strange Theory of Light and Matter, Princeton University Press, 1976.

★★★

# Solar UV Treatment of Covid-19 by Nanoparticles

## I. Introduction

Covid-19 vaccines differ from the traditional. In Moderna, the patient receives an injection of mRNA that encodes the virus spike protein and once inside the patient's body produces the antigen to elicit immunity.

However, mRNA molecules are fragile and disintegrate upon entering the cell making mRNA unsuitable as a therapeutic. Research showed mRNA is a workable therapeutic by delivery to the cell inside lipid nanoparticles (NPs). Moderna uses ~ 80 nm NPs. Pfizer/BioNTech uses larger lipid NPs, but actual NPs data are proprietary and not known to the public.

## II. Problem and Purpose

The problem is simple QED theory predicts NPs emit EM radiation depending on NP size. For Moderna's ~80 nm NPs, the UVC is produced that at body temperature inactivates or at least degrades the mRNA before ever reaching the cell. Therefore, the mRNA has nothing to do with the success of the Moderna vaccine

Early-on, Moderna reported a remarkable 94.5% efficacy compared to 50% efficacy of traditional vaccines. Since UV inactivated the mRNA, what produced Moderna's high efficacy?

In late 2020, Covid-19 side effects (muscle pain, etc) in animals were shown caused [1] by NPs without mRNA. But the cause of NP induced side effects was not known. Simple QED explains side effects by the NPs emitting UV radiation that excites muscle and brain neurons which may also explain high vaccine efficacy.

Since the mRNA is inactivated, the success of Moderna and others have inadvertently proven that the UV radiation from NPs is somehow providing > 90% efficacy against Covid-19. The purpose of this short paper is to answer the question,

How does the UV do this?

## III. Solutions

Mid-2020 Version

Treat only Covid-19 patients tested positive having the live virus in their bodies. The UV only needs to inactivate a few virions in the patient that then act as the antigen to elicit Covid-19 immunity for inactivating the remaining virus in their body, but the high efficacy of Moderna for patients tested both positive and negative suggests NP induced UV efficacy has nothing to do with the patient having Covid-19 virions in his body.

Mid-2021 Version

The NP treatment was revised based on solar UV converting 7-DHC in the skin to Vitamin D3 consistent with [2,3] showing > 90% of Covid-19 deaths correlated by Vitamin D deficiency. Unlike Covid-19 virions which are in ultra-low concentration in the bloodstream even in patients tested positive, the UV from NPs over the very large area of skin of all patients is far more likely to explain Moderna's > 90% efficacy. Solar UV passes through the epidermis to reach 7-DHC. NPs reach the 7-dehydrocholesterol (7-DHC) in the sub -dermal skin by arterial and venal blood capillaries as illustrated in Fig. 1.

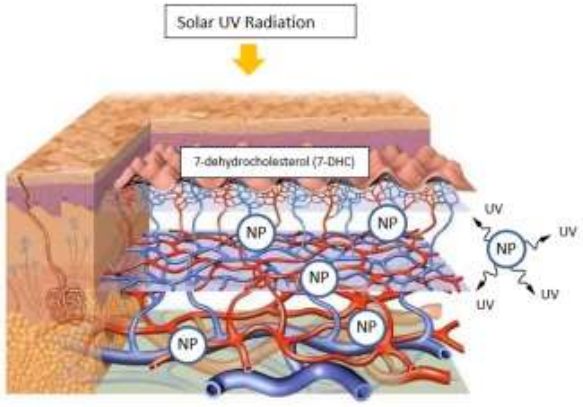


Figure 1. NPs in Capillaries at 7-DHC

For illustration, Fig. 1 depicts the NPs larger than the capillaries, but the NPs << capillary diameters allowing the NPs to reach the sub-dermal 7-DHC. The NPs emit UV that reacts with 7-DHC in basal epidermis [2] to produce Vitamin D3 which is converted in the liver into 25(OH)D the circulating metabolite. The kidneys convert 25(OH)D into bioavailable 1,25(OH)2D promoting immune regulatory T cells. Vitamin D protects against infectivity [3] from COVID-19 and deficiency in 25(OH)D is correlates with positive Covid-19.

**IV. Simple QED**

Simple QED is a method of nanoscale heat transfer that conserves heat with EM radiation instead of temperature. Based on the Planck law of quantum mechanics, simple QED allows UV to be produced at body temperature to synthesize Vitamin D3 from 7-DHC

Classical physics allows atoms in NPs to have heat capacity to conserve heat by a change in temperature. Creating a UV photon requires high temperatures, T = E/ (3/2 k). In the UVC at 254 nm, T ~ 37,000 K which is not possible in the human body.

However, heat transfer in NPs is controlled by the Planck law of quantum mechanics differing significantly from classical physics by denying atoms the heat capacity to conserve heat by a change in temperature. The Planck law precludes NP temperatures required for Fourier heat conduction, i.e., heat flux Q cannot penetrate the NP surface by conduction. Conservation of Q may only proceed by creating non-thermal EM waves carrying the heat Q across and back the NP diameter d in time $\tau = 2nd/c$. At this instant, a photon is created having Planck energy E,

$$E = h/\tau = hc/2nd$$

$\lambda = 2nd$, where n = refractive index

**V. EM Confinement**

Brief EM confinement of absorbed heat Q at the NP surface is necessary to form standing EM waves. Inward disposed Poynting vector S = heat Q flux ~ W/m$^2$ provides momentum I as EM confinement. For Q ~ W/m$^2$ , the NP absorbs U = $\pi d^2 Q$ ~ J/s. Since momentum I ~ U/c ~ Nt-s, I/s gives the EM confinement force F ~ Nt.

**VI. UV Intensity**

The UV intensity is the number N of UV photons/s, N = Q/E. For body temperature T = 37 C = 310 K, the Stefan-Boltzmann equation gives the heat Q transferred from the surroundings at 310 K to the NP that by the Planck law approaches absolute zero, Q ~ $\pi\sigma d^2 T^4$. For Moderna vaccine having d ~ 80 nm, the heat Q = 1.05x10$^{-11}$ W = 10.5 pW. Lipid NPs having n = 1.6 give $\lambda$ = 2nd ~ 254 nm which is in the UVC with E = 7.80x10$^{-19}$ J or 4.88 eV. Hence, the NPs emit N ~ 1.35x10$^7$ UVC photons/s.

Moderna and other Pharma's do not give the number $N_{NP}$ of NPs/dose. Assuming 1 mg of lipids in a Moderna 0.5 ml dose having the density of water, the total lipid volume $V_L$ = 1000x10$^{-12}$ m$^3$. The volume V = $\pi d^3/6$ of a single 80 nm NPs is 2.68x10$^{-22}$ m$^3$. Hence, the number $N_{NP}$ of NPs/dose is, $N_{NP} = V_L/V$ ~ 3.73x10$^{12}$ giving the total number $N_P$ of UVC photons/dose, $N_P = N \cdot N_{NP}$ = 5x10$^{19}$ UVC photons/s having a total UVC power of about ~ 40 W. The surface area of human skin is 1.7 m2 giving a NP induced UVC flux 23.5 W/m$^2$.

Solar radiation on the Earth's surface on a cloudless sky is about 1050 W/m$^2$. Solar UVC radiation is not present on the Earth's surface while UVB radiation (280-350 nm) is 5% of the total or 50 W/m$^2$ as shown in Fig. 2.

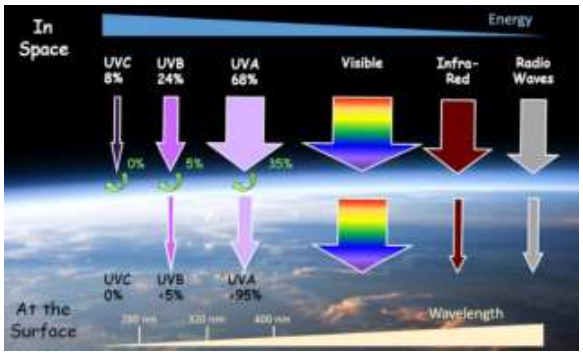


Figure 2. Solar Radiation on Earth's surface

UVC aside, the NP induced UV flux a single injection of Moderna is comparable to the solar UVB on the Earth's surface. What this means is NP induced UV is a reasonable Covid-19 therapeutic. DNA damage does occur, but based on the success of Moderna is not important. However, the FDA is required to control NP size with a tight tolerance to 80 nm.

**VII. Conclusions**

In Covid-19, the promise of mRNA vaccines in decoding the spike protein at > 90% efficacy cannot be fulfilled as the ~80 nm NPs that carry the mRNA emit UVC radiation that inactivate the mRNA before reaching the cell.

NPs alone provide the > 90% efficacy in Covid-19 immunity

To explain the success of Moderna w/o mRNA, the NP treatment was proposed in mid-2020 for patients tested positive, the NPs emitting UV to create antigens from Covid-19 virions in the patient's body. But the success of Moderna for patients tested negative suggests another mechanism is producing high efficacy.

In mid-2021, data correlating Vitamin D3 deficiency with Covid-19 suggested exposure to solar UV is preventive therapy for all Covid-19 patients. Therefore, the 2021 NP treatment using the UV from NPs is proposed to synthesize Vitamin D3 from 7-DHC in the skin, and if so,

Moderna's claim of protection for the Delta variant is likely correct.

Early estimates of heat absorbed by the NPs are grossly incorrect giving 7 UVC photons/NP/s. The Stefan-Boltzmann equation on transferring heat from the surroundings at 310 K to the NP at absolute zero is significantly higher than the Planck radiation law giving $1.35 \times 10^7$ UVC photons/NP/s.

Comments are requested.

**References**

[1] Wadman M. [2020] "Public needs to prep for vaccine side effects", Science 370 (6520), 1022.

[2] Brenner H. and Schottker B. [2020] Vitamin D Insufficiency May Account for Almost Nine of Ten COVID-19 Deaths: Time to Act. Nutrients 2020, 12(12), 3643.

[3] Charoenngam N., et al. [2021] Vitamin D and Its Potential Benefit for the COVID-19 Pandemic Endocrine Practice https://doi.org/10.1016/j.eprac.2021.03.006

## AstraZeneca Vaccination and Blood Clotting

**ABSTRACT**

Covid-19 vaccinations include AstraZeneca, Pfizer/BioNtech, and Moderna among others. Recently, blood clots have been reported after AstraZeneca vaccinations, and although a small fraction of those vaccinated, the question remains as to the cause of blood clotting. In this regard, cytokines are known to induce blood clots and EM radiation is a potent cytokine activator, but a source of EM radiation at the cellular level is required. In simple QED, EM radiation depending on nanostructure dimensions is proposed to conserve heat at the nanoscale because the Planck law precludes the atom the necessary heat capacity to conserve heat by a change in temperature. Simple QED applied to the AstraZeneca vaccine shows UVB radiation is emitted from ~ 100 nm Ads vectors that suggests the Ad vector is the source of cytokine activation and blood clots. However, the quality control of Ads sizes is difficult because AstraZeneca uses different manufacturers. Since only specific countries like Norway have reported serious blood clotting, perhaps the Ad size in the batch delivered to Norway is the problem. Regardless, the FDA should impose tight controls on Ad size in AstraZeneca vaccines. Further, the CDC is requested to perform UV-VIS spectrometry tests on Ads vectors suspended in water contained in UV transparent cuvettes to experimentally confirm the theoretical UVB emission predicted

**INTRODUCTION**

In March 2021, the AstraZeneca Covid-19 vaccine has been linked to blood clotting and brain hemorrhaging and death. Countries [1-3] that have paused AstraZeneca inoculation campaigns include Austria, Denmark, Estonia, Lithuania Norway, Iceland and Thailand. Later, the use of AstraZeneca was approved safe, but Norway has yet to resume use.

Although, the fraction of vaccinations leading to death are very small, the question remains as to the cause of blood clotting. The WHO has stated [4] that “A causal relationship … has not been shown.” Consistent with the WHO, Pharmacovigilance - the European Union medical agency risk assessment committee - concluded the vaccine’s benefits outweigh the risks. Similar arguments [5,6] in support of the AstraZeneca vaccine have been reported.

But blood clots have been a frequent complication of COVID-19. Since mid-2020, researchers have tried [7] to untangle the blood clotting mechanism with emphasis on pulmonary mechanisms in the lung. However, brain hemorrhaging suggests the Covid-19 is neurological entering the brain through the nasal path and not through the lungs. Indeed, mouse models [8] with genetically engineered human ACE2 receptors in the nose exposed to SARS-CoV virus were found in the brain and not in the lung, suggesting ACE2 receptors are not necessary for the virus to reach the brain. Absent ACE2 receptors, the nasal path to the brain requires the Covid-19 express a mechanism to burrow through the cell wall and subsequent blood-brain barrier.

In this regard, point sources of EM radiation are known to burrow through cell walls by ionization, but cannot be translated to burrowing through nose cells unless the virus itself is the source of EM radiation. Indeed, a source of EM radiation is available because the Covid-19 virus is nanoscale having a diameter d < 100 nm. Unlike the conservation of heat in classical physics by a change in temperature, the Planck law of quantum mechanics denies atoms the heat capacity to conserve heat by temperature. Instead, the theory of simple QED based [9] on the Planck law conserves heat by emitting EM radiation, the wavelength $\lambda$ of which depend on the diameter d and refractive index n of the Covid-19 virus, $\lambda = 2nd$. For Covid-19 having body diameter d ~ 100 nm, UVB radiation is emitted as illustrated in Fig. 1.

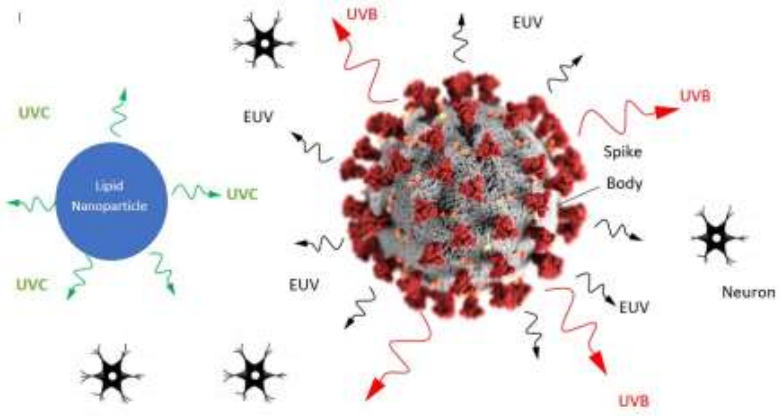


Figure 1. Coronavirus emitting simple QED induced EM radiation

In Fig. 1, nanoparticles (NPs) and Covid-19 spikes are shown emitting UVC and EUV radiation, but only UVB from the Covid-19 is of interest in blood clotting from UVB immunosuppression and inflammation leading to sepsis and coagulation similar to disseminated intravascular coagulation (DIC).

Of note, the Covid-19 virus itself is emitting UVB radiation.

UVB immunosuppression [10] is both local and systemic. Local UVB radiation inhibits the immunologic rejection of transplanted tumors. In mice, rejection was prevented when exposed to local UVB radiation. In contrast, systemic immunosuppression is the immune response at a distant location caused by UVB radiation exciting interleukin IL-10 which enters the blood circulation to suppress the immune system in a systemic manner. UVB radiation suppresses protective immune responses against viral infections and can compromise an immune response both in a local and a systemic fashion. Indeed, UVB radiation at rather low doses suppresses an immune response.

In COVID-19 infections, the thrombosis [11] is a coagulopathy similar, but not identical to DIC. Instead, there is strong local thrombotic or microvascular disease of blood vessels. Some features mimic cytokine release syndromes suggesting UVB activation. The dramatic increase in vascular complications and specific coagulation changes [12] suggest specific endothelial cell involvement in direct viral infection of endothelial cells. Indeed, the presence of ~ 150 nm viral elements within endothelial cells and an accumulation of inflammatory cells, with evidence of induced endothelial and inflammatory cell death. Fig, 2 shows the 100 nm Covid-19 body inside the spiked periphery emitting UVB.

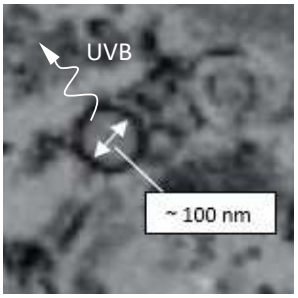


Figure 2. Covid-19 in Endothelial Cell

In sepsis characterized by the presence of infection and host inflammation, the coagulation system becomes diffusely activated as in DIC. Endothelial cellular apoptosis exacerbates inflammation and induces thrombosis leading [12] to microvascular thrombosis. COVID-19 coagulopathy differs from sepsis as hemorrhagic complications [11] are not common.

**PURPOSE**

Given UVB radiation from the Covid-19 virus itself is consistent with direct contact with endothelial cells in small vessels and activating cytokines.

But can the AstraZeneca vaccination cause blood clotting?

The purpose here is to show how the AstraZeneca vaccination could cause blood clotting by emitting UVB radiation from the adenovirus Ad vectors used to carry the DNA into the cell.

**ANALYSIS**

The AstraZeneca Covid-19 vaccine supplies DNA to the cell in nanoscale adeno vector carriers, herein designated as Ads having an approximate spherical diameter d ~ 100 nm as shown in Fig. 3.

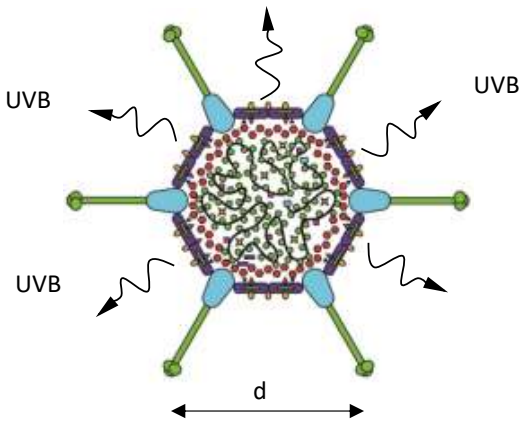


Figure 3. Adenovirus Vector- Ad

By simple QED, the Ad conserves heat from the ambient surroundings by emitting EM radiation at wavelength $\lambda$ = 2nd. For adenovirus, the refractive index n = 1.4 reported [13] as n ~ 1.4 giving a simple QED wavelength $\lambda$ - 280 nm which is in the UVB (280 to 320 nm). In comparison, the Moderna vaccine uses lipid NP to carry mRNA having average spherical diameter d ~ 80 nm. Lipids having n = 1.55 emit EM radiation [9] at $\lambda$ = 248 nm in the UVC (200 to 280 nm). In effect, both AstraZeneca and Moderna emit in the UVC at 248 nm, but it should be noted that actual average diameters are proprietary and not published. Pfizer/BioNtech vaccine data is not available, but is expected to be similar to Moderna.

Setting aside the uncertainty of NP size, the AstraZeneca vaccine having the larger size is expected to emit more UVB than Pfizer/BioNtech and Moderna. In DNA damage, the UVC is far more damaging than UVB, but in COVID-19 the systemic levels of pro-inflammatory cytokines [11,14] interleukins IL-1 and IL-6 are markedly increased by UVB.

Cytokines are glyco-proteins transiently produced that initiate biologic activities though specific cell-surface receptors. What this means is UVB light is a very potent [15] inducer of epidermal cytokine release initiating local and systemic inflammatory reactions and altering immune response.

Importantly, UVB does not directly cause blood clotting. The UVB releases cytokines from epidermal tissue, the cytokines activating the immune system to cause clotting. In this way, cytokines act as necessary intermediaries between UVB and blood clotting. However, UVB radiation is also used to remove and not induce blood clots. Indeed, UVB activation of plasminogen to form plasmin is used [16] to dissolve blood clots at 280 nm. Absent cytokines, blood clots might not be a problem in Covid-19.

In Covid-19, the cytokines activated by UVB emission can initiate systemic blood clotting. In Fig. 2, the local UVB emission from a Covid-19 virion can activate cytokines including interleukin IL-10 which enter blood circulation [10] and initiate blood clotting at distant locations.

**CONCLUSIONS**

The nanoscale Covid-19 virus emits EM radiation at a wavelength depending on its diameter and refractive index. Similarly, Covid-19 vaccines deliver mRNA and DNA to the cell in nanoscale carriers of NPs and Ads that also emit EM radiation.

The AstraZeneca Ad vector that delivers DNA to the cell is predicted by simple QED to emit UVB radiation which is well known to activate cytokines to induce blood clots. But the UVB emission depends on the size distribution of Ads which is not available in the public domain. Moreover, the quality control of Ads sizes is required as AstraZeneca uses different manufacturers. Since only specific countries like Norway and Finland have reported serious blood clotting, perhaps the Ad size distribution in the batch delivered is the problem with reported clotting. The FDA should impose tight controls on both Ad and NP size in vaccines.

The CDC is requested to confirm the simple QED prediction of UVB emission from Covid-19 virions, lipid NPs, and adenovirus Ad virions. Spectroscopy is suggested for each entity in water. The samples are placed in UV transparent cuvettes and EM radiation measured with a UV-VIS spectrometer. The only heat required is that of the water at ambient temperature.

**References**

[1] BusinessToday.In Denmark, Norway, Iceland suspend AstraZeneca vaccine supply. March 12, 2021 | Updated 12:55 IST. https://www.businesstoday.in/coronavirus/blood-clotting-incidents-raise-alarm-denmark-norway-iceland-suspend-astrazeneca-vaccine-supply/story/433650.html

[2] The Guardian, Sarah Boseley. Suspension follows similar move in Ireland due to reports in Norway of blood clots despite no proof of a link. Sun 14 Mar 2021 23.38 GMT. https://www.theguardian.com/world/2021/mar/14/ireland-suspends-oxford-astrazeneca-covid-vaccine-over-blood-clot-concerns

[3] Bensadoun E. and D'Amore R. Global News. AstraZeneca COVID-19 vaccines under investigation 'not shipped to Canada', officials say. March 14, 2021 5:12 p. https://globalnews.ca/news/7695938/astrazeneca-blood-clots-vaccine/

[4] UN News. WHO backs AstraZeneca COVID vaccine amid clotting concerns; green lights Johnson & Johnson shots. 12 March 2021. https://news.un.org/en/story/2021/03/1087222

[5] Sky News. COVID-19: AstraZeneca defends its vaccine after more countries suspend its use over clotting concerns. Monday 15 March 2021 06:33, UK. https://news.sky.com/story/ireland-should-suspend-astrazeneca-vaccine-over-clotting-concerns-health-authority-says-12245626

[6] Liotta M. 'No biological reason' to link blood clots to COVID vaccine. 12 March 2021 https://www1.racgp.org.au/newsgp/clinical/no-biological-reason-to-link-blood-clots-to-covid

[7] Willyard C. Coronavirus blood-clot mystery intensifies. Nature 581:250, 21 May 2020.

[8] Moltemi M. What Does Covid-19 Do to Your Brain? WIRED. April 15 2020
https://www.wired.com/story/what-does-covid-19-do-to-your-brain/
[9] Prevenslik T. Mystery pulmonary and neurological symptoms by EM radiation from the Coronavirus. 2020. https://nanoqed.org/resources/2020/PaperVIRAL.pdf
[10] Schwarz T. Mechanisms of UV-induced immunosuppression. Keio J Med 54: 165–171, 2005.
[11] Levi M. and Iba T. COVID-19 coagulopathy: is it disseminated intravascular coagulation? Internal and Emergency Medicine 16:309–312, 2021.
[12] Varga S., et al. Endothelial cell infection and endotheliitis in COVID-19. The Lancet. 395: 1417-1418, May 02 2020.
[13] Kowalski W. J., et al. A Genomic Model for Predicting the Ultraviolet Susceptibility of Viruses. IUVA News 11:15-28, 2009.
[14] Schwarz T. and Lugar T. A. Effect of UV irradiation on epidermal cell cytokine production. J Photochemistry and Photobiology, B: Biology, 4:1-13, 1989.
[15] Schwarz T. (1997) UV Radiation and Cytokines. In: Altmeyer P., Hoffmann K., Stücker M. (eds) Skin Cancer and UV Radiation. Springer, Berlin, Heidelberg. https://doi.org/10.1007/978-3-642-60771-4_26
[16] Correla M., et al. Photonic Activation of Plasminogen Induced by Low Dose UVB. PLOS ONE, DOI: 10.1371/journal.pone.0116737, January 30, 2015.

# Chapter 2

# Health Risks of Nanoparticles and Genetically Modified Food

It is well known that nanoparticles have had positive effects in nanomedicine, food processing, development of cosmetics, insecticides to name but a few areas. However there are disadvantages in that nanoparticles can damage DNA and that damage may lead to cancer and other illnesses.


2.1 DNA Damage by Nanoparticles . . . . . 28
2.2 Cancer by UV radiation from nanoparticles in GM food . . . . . 33
2.3 Electronics Cigarettes and DNA Damage . . . . . 37
2.4 Protein misfolding by UV emission from nanoparticles . . . . . 41

**Proceedings of ASME2010 First Global Conference on NanoEngineering for Medicine and Biology NEMB2010**
**February 7-10, 2010, Houston, TX, USA**

**NEMB2010-13198**

# DNA DAMAGE BY NANOPARTICLES

## BACKGROUND

Nanoparticles (NPs) have provided very significant technological advancements in nanomedicine in the areas of bactericidal agents in food processing, protective skin sunscreens, and the treatment of cancer tumors. However, there is a darkside. Over the past decade, experiments [1-7] have suggested NPs are a health risk by inducing DNA damage that is known to possibly lead to cancer

But what is the mechanism of DNA damage by NPs?

The oxidative stress paradigm correlates DNA damage by the number of reactive oxidative species (ROS), e.g., peroxides and hydroxyl radicals produced with the surface area of < 100 nm NPs. But particulate matter (PM) comes in all sizes that hold the oxidative stress paradigm in question. Electron spin resonance (ESR) comparisons of coarse PM 2.3-10 microns from air pollutions samples have been shown [8] to produce greater numbers of hydroxyl radicals than the fine PM <2.5 microns, but the mechanism was not defined.

Electromagnetic (EM) mechanisms based on the observation [9] that DNA damage by <100 nm NPs mimics [9] the very same pathways of conventional sources of EM radiation. On this basis, the hypothesis was formed [10] that NPs somehow produce their own EM radiation at least at ultraviolet (UV) levels, albeit at low intensity. In fact, low intensity EM radiation from NPs at UV levels is consistent with the theory [11] of QED induced EM radiation. QED stands for quantum electrodynamics. By this theory, fine < 100 nm NPs absorb low frequency thermal kT energy in the far infrared (FIR) upon collisions with solution water molecules. Here, k is Boltzmann's constant and T is absolute temperature. Since quantum mechanics precludes specific heat in NPs, absorbed kT energy cannot be conserved by an increase in temperature, and therefore is induced by QED to be frequency up-converted from the FIR to the EM frequency of the NP, usually beyond the UV. But the quasi-bound EM confinement of the NPs allows the UV to leak and thereby damages nearby DNA.

By QED induced radiation, coarse PM does not produce UV, but rather EM radiation in the near infrared (NIR) or an even lower frequency. By itself, NIR and lower radiation does not damage DNA, but compared to the FIR available from the collisions of water molecules enhances the UV from the < 100 nm NPs. What this means is the oxidative stress paradigm based on < 100 nm NPs is still a valid DNA damage mechanism, but requires qualification for enhancement of DNA damage by coarse PM.

In summary, QED induced EM radiation provides NPs with a remarkable natural source of low level continuous EM radiation that produces ROS and thereby enables the NPs to function as an antibacterial agent while at the same time may damage the DNA. Details are provided [10] elsewhere, a brief summary of which is given here in the Appendix.

## INTRODUCTION

The UV from NPs damages DNA by ionizing radiation or produces ROS that damage the DNA by chemical reaction. In contrast, traditional biology focuses on how the DNA damage by ROS is transferred by chemical reaction across cellular tissue, body fluids, and membrane walls. The source of ROS is not defined in traditional biology.

## PURPOSE

The purpose of this paper is to propose QED induced EM radiation in NPs as the mechanism which creates low-level UV radiation that:

- forms ROS and by chemical reaction damages the DNA,
- penetrates cellular membranes to damage the DNA by ionization,
- provides ROS that upon oxidative corrosion of CoCr NPs produces the Co ions that damage the DNA by entering the nucleus, and
- forms an EM potential for neurons to signal the central nervous system (CNS) that DNA has occurred.

**DISCUSSION**

Recently, QED induced radiation and the oxidative stress paradigm have been questioned [12] by DNA damage thought caused by signaling damaged DNA across multi-layers of BeWo cells. The NPs of CoCr were 30 nm in diameter while the barrier cells were grown on a 0.4 micron pore polyester filter supported on a Transwell insert, the insert positioned about 1 mm above the human fibroblast cells. Test conditions were (1) direct, (2) indirect, and (3) insert. DNA damage in direct tests occurs with the NPs in contact with the fibroblast; indirect DNA damage occurs with the NPs placed on top of the BeWo cells with the Transwell insert positioned above the fibroblast cells; and the insert test where the NPs are placed on the filter without the BeWo cells. Fibroblast DNA damage for the indirect test is claimed [12] greater than that for the insert test without BeWo cells, thereby suggesting the BeWo cells contributed to the DNA damage.

But the difference in DNA damage between indirect and insert tests is not significant, and in fact is about the same as that for the direct test. See (Fig. 1c of [12]). What this means is the 30 nm NPs or corrosion products of Co and Cr ions are passing through the BeWo cells and the 0.4 micron filter pores to enter the nucleus of the fibroblast cells. Perhaps, a thin nanoscale film instead of a porous filter would block the ions from the fibroblasts, thereby allowing the indirect effect of NP exposure to be tested with confidence.

In this regard, larger 2.9 micron sized CoCr particles that cannot pass through the 0.4 micron pores were also tested and shown [12] to produce comparable DNA damage to that found for the 30 nm NPs. Similarity is found with the greater DNA damage [8] by PM 2.3-10 than for PM < 2.5 particulate in air pollution studies. In the latter, the likelihood of < 100 nm carbon and silicate NPs in the sample allowed the argument that the coarse PM enhanced the DNA damage from the NPs. But this is unlikely for the CoCr NPs because the 2.9 micron CoCr particles were selectively processed to avoid NPs < 100 nm in the sample.

It is more likely the CoCr particles in fibroblast cells have a different DNA damage mechanism from the carbon and silica NPs embodied [1-7] in the production of ROS in the oxidative stress paradigm. Unlike NPs found in the air, CoCr particles in solution corrode into Co and Cr ions evidenced by the fact the Co ions are found in the nuclei of the fibroblast cells and not the CoCr particles themselves. Similar findings were reported in the companion study [13] of CoCr joint implants.

In contrast, carbon and silica NPs do not dissolve and are found in the cell nuclei as NP entities. Moreover, the DNA damage from Co and Cr ions for insert and indirect tests (Fig. 1c of [12]) is comparable to that for CoCr NPs and 2.9 micron particles. Cobalt has been long recognized [14] as genotoxic and carcinogenic. DNA damage by CoCr NPs is therefore more likely caused by the the toxicity of the Co ions and not the NPs and micron particles themselves.

However, the DNA damage mechanism given by the corrosion of CoCr NPs into ions cannot be construed as a signaling mechanism through the BeWo barrier cells, but simply the diffusion of Co and Cr ions through the barrier cells and the filter pores to the fibroblast cells.

The reduction in indirect DNA damage by the CoCr NPs found upon adding drugs to the BeWo cells is claimed [12] caused by the suppression of cell-to-cell communication in the junctions between cells. However, this is unlikely. The drugs included: apyrase an enzyme hydrolyzing ATP; allopurinol that inhibits xanthine oxidase; and connexin and pannexin channel blockers, all of which are UV absorptive evidenced by the fact they are detected in liquid chromatography [15] by UV spectroscopy. What this means is the drugs are absorbing the QED induced radiation from the NPs, thereby reducing the corrosion of the CoCr NPs into Co and Cr ions and subsequent DNA damage from Co ions.

Moreover, the fact the corrosion of CoCr NPs explains the DNA damage without invoking cell-to-cell communication means the NPs are indeed producing EM radiation at UV levels and beyond. Perhaps, the choice of non-corrosive NPs would resolve whether the drugs are actually blocking the transfer of Co ions between cells or absorbing QED induced radiation.

**EXTENSIONS**

DNA damage by CoCr NPs across the BeWo barrier cells is related to both bystander effects and light activated neurons.

**Bystander Effect**

Radiation biology has traditionally considered damaged DNA as a source of EM radiation. Indeed, DNA damage to neonatal mouse cerebellum has been reported [16] *in vivo* in unexposed bystander cells, the mechanism of which is thought to be cell-to-cell communication of a signal from DNA damaged cells. DNA double-strand breaks and apoptotic cell death were thought induced in signals along bystander cerebellum cells by gap-junction intercellular communication in the CNS.

The DNA damage across the multi-layered barrier cells [12] differs from the bystander effect where neurons are activated throughout the CNS of the mouse. QED induced radiation may penetrate short distances across cellular barriers, but not the distance corresponding to the body of the mouse. Traditional biology lacks EM radiation from NPs to propagate beyond local DNA damage. In contrast, QED radiations are EM and produce an EM potential signal that can propagate throughout the CNS.

**Light Activated Neurons**

The electrical conduction of stimuli in nerve cells is an active area in brain research. Usually, a sharp metal electrode is inserted into the brain to introduce a current. But the attendant damage to tissue causes electrochemical side reactions. An alternative approach [17] uses micropipette coated with lead-selenide NPs. In rat brain slices, IR light is

used to create an electrical field from the NPs on the pipette surface. The pipette can then be moved around to stimulate neurons allowing the activation of regions of the brain having damaged or cut nerves to be restored without the need for disturbing wires.

Light activated neurons by NPs is consistent with QED induced EM radiation. However, the NP coated pipette is not needed. Instead, NPs attached directly to the neuron produce an EM potential allowing electrons to propagate through the CNS. Even light is not necessary. Indeed, water molecule collisions with NPs in the interstitial water between cells should produce a steady EM potential without the need for wires.

**CONCLUSIONS**

- QED induced radiation in CoCr NPs emits a low-level source of continuous EM radiation in the UV and beyond to produce ROS of peroxides and hydroxyl radicals from water that provides the source of damage to the DNA.

- By oxidation, the ROS corrode the CoCr NPs to form Co and Cr ions that damage the DNA by entering the nucleus.

- Drugs thought to reduce NP damage of DNA by blocking cell-to-cell communication are in fact reducing DNA damage by absorbing the UV from QED induced radiation.

- The EM potential that accompanies the QED induced radiation from NPs activates signaling, thereby informing the CNS that DNA damage has occurred.

- Traditional biology that assumes the NPs damage DNA by chemical reaction with ROS needs to be revised to include QED induced EM radiation as the source of the ROS..

**REFERENCES**

[1] B.L. Razzaboni and P. Bolsaitis, "Evidence of an Oxidative Mechanism for the Hemolytic Activity of Silica Particles," Environ. Health Persp. vol. 87, pp.337-341, 1990.

[2] X. Shi, N.S. Dalal, and V. Vallyathan, "ESR evidence for the hydroxyl radical formation in aqueous suspension for quartz particle and its possible significance to lipid peroxidation in silicosis." J. Toxicol. Environ. Health, vol. 25, pp. 237-245, 1988.

[3] K. Donaldson, "The biological effect of coarse and fine particulate matter," Occup. Environ. Med., vol. 60, pp. 313-314, 2003.

[4] T. Xia, et al., "Comparison of the Abilities of Ambient and Manufactured Nanoparticles to Induce Cellular Toxicity According to the Oxidative Stress Paradigm," Nano Lett., vol. 6, pp. 1794-1807, 2008.

[5] D.B. Warheit, et al., "Pulmonary Bioassay Studies with Nanoscale and Fine-Quartz Particle in Rats: Toxicity is not Dependent upon Particle Size but on Surface Characteristics," Toxicological Sciences, vol. 95, pp. 270-280, 2007.

[6] M. Ahmed, et al., "DNA damage .response to different surface chemistry of silver nanoparticles in mammalian cells," Toxico. Appl. Pharmacol, vol. 233, pp. 404-410, 2008.

[7] L. Zastrow, et al., "The Missing Link – Light-induced (280-1600nm) Free Radical Formation in Human Skin," Skin Pharmacology and Physiology," vol. 22, pp. 31-44, 2008.

[8] D.B. Warheit, et al., "Toxicity is not Dependent upon Particle Size but on Surface Characteristics," Toxico. Sciences, vol. 95, pp. 270-280, 2007.

[9] R.M. Mroz, et al., "Nanoparticle-driven DNA damage mimics irradiation-related carcinogenesis pathways," Euro. Respir. J, vol. 31, pp. 241–251, 2008.

[10] T.V. Prevenslik, "Nanoparticle induced DNA Damage, IEEE Nanomed 2009, Tainan, 18-21 October, 2009.

[11] T.V. Prevenslik, See www.nanoqed.org

[12] G. Bhabra, et al., "Nanoparticles can cause DNA damage across a cellular barrier," Nature Nanotechnology, 5 November, 2009.

[13] I. Papageorgiou, et al., "The effect of nano- and micron-sized particles of colbalt-chromium on human fribroblasts in vitro," Vol 28, pp. 2946-2958, 2007

[14] D. Lison, et al., "Update on the geotoxicity and carcinogenicity of cobalt compounds," Occ. Env. Med., vol. 58, pp. 619-25, 2001.

[15] M.K. Reinders, et al., "A simple method for quantification of allopurinol and oxipurinol in human serum by high performance liquid chromatography with UV detection," J. Pharmaceutical and Biomedical Anal., vol. 45, pp.312-7, 2007.

[16] M. Mancusso, et al., "Oncogenic bystander radiation effects in heterozygous mouse cerebellum," Proc Natl Acad Sci U S A, vol. 105, pp, 12445-50, 2008.

[17] Y. Zhao, et al., "Wireless Activation of Neurons in Brain Slices Using Nanostructured Semiconductor Photoelectrodes," Ange. Chem. Int. Ed., vol. 48, pp. 2407-10, 2009.

**APPENDIX**

The NP conserving collision energy of water molecules by the QED induced emission of UV radiation is shown in Fig. 1. In Fig. 2, NPs that that enter the biological cell are depicted to produce hydroxyl radicals that by ionization damage the DNA. But NPs external to the cell produce UV radiation that readily penetrates the membrane wall to damages the DNA.

Quantum mechanics precludes any temperature increase in the NPs upon molecular collisions. Fig. 3 giving the Einstein-Hopf relation for the harmonic oscillator at 300 K shows the heat capacity of NP atoms vanishes at EM confinement wavelengths $\lambda < 5$ micron. For spherical solid NPs of diameter D and refractive index $n_r$, the wavelength is, $\lambda = 2Dn_r$. Fig. 4 gives the dimensionless Einstein specific heat, $C^* = c_p/3Nk$, where $c_p$ is the specific heat, N is the number of atoms, and k is Boltzmann's constant. Consistent with the heat capacity, $C^*$ at $\lambda < 5$ micron also vanishes. For NPs < 100 nm, the wavelength < 1 micron and the specific heat is far less than that at 5 microns. Power $Q_c$ absorbed from collisions of water molecules is shown in Fig. 5. For silver NPs, Fig. 6 shows the power $Q_C$ is conserved by QED induced Planck energy $E_P$ and photon rates $dN_P/dt$ depending on the NP diameter D. The power $Q_C$ for NPs < 100 nm is < 0.2 μW is upper bound by about $4x10^{11}$ photons having Planck energy $E_P$ of 4.6 eV.

QED induced EM radiation requires fine D < 100 nm NPs to damage the DNA consistent with the oxidative stress paradigm. Coarse NPs emit QED induced NIR and lower radiation that does not damage the DNA, but enhances the UV from nearby fine NPs, thereby explaining experiments showing coarse NPs produce more DNA damage than fine NPs. Fig. 7 shows coarse NP emitting QED induced NIR which enhances that from the FIR by the ratio R > 1 as shown in Fig. 8.

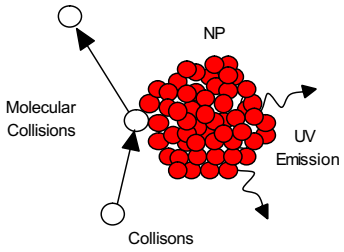


Fig. 1 NP conserving collision energy by emission of EM radiation

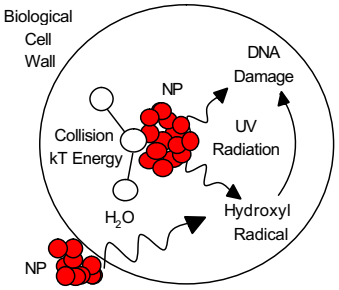


Fig. 2 DNA damage in Biological cell

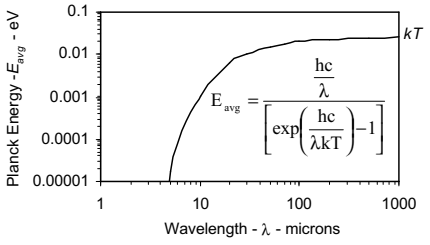


Fig. 3 Harmonic Oscillator at 300 K

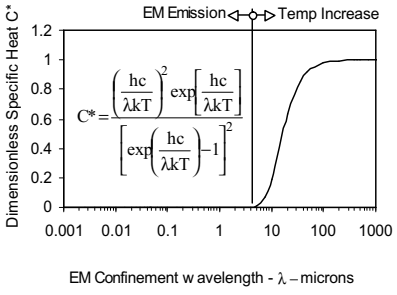


Fig. 4 Vanishing NP Specific Heat

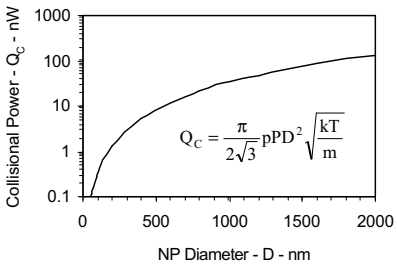


Fig. 5 Collision power in NPs

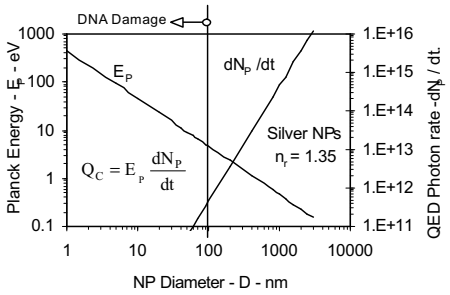


Fig. 6 QED radiation in silver NPs

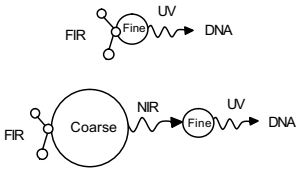


Fig. 7 Interaction of Coarse and Fine NPs

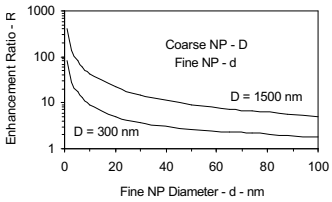


Fig 8 .Coarse NP Enhancement of Fine NPs

**Integrative Cancer Science and Therapeutics**

oat open access text

**Research Article** ISSN: 2056-4546

# Cancer by UV radiation from nanoparticles in GM food

**Thomas Prevenslik***

## Abstract

The causal link between GM food and human health is proposed to be the scrambling of genes in DNA by low-level UV radiation. GM stands for genetically modified. Modern agriculture controls weeds by spraying Roundup containing water and Glyphosate onto crop fields. To enhance Glyphosate penetration through weed leaves, the adjuvant POEA is added to Roundup. POEA stands for polyoxyethyleneamine. But weeds alone cannot be sprayed and POEA also enters the leaves of corn and soybean crops as an emulsion of NP globules that ultimately reside in the plant crop. NP stands for nanoparticle. Upon ingestion of GM food, body heat is thought to increase the NP temperature. But this is a consequence of classical physics when in fact QM governs the nanoscale. QM stands for quantum mechanics that requires the heat capacity of NPs to vanish. Conservation of body heat in NPs therefore cannot occur by the usual increase in temperature and instead proceeds by the emission of UV radiation. Nearby DNA are damaged and if the scrambled genes are not repaired by the immune system may lead to cancer. The UV radiation from NPs supports experiments over the past decade that show NPs damage the DNA. But GM food is planned for future world-wide consumption raising the question of whether cancer as a crime against humanity is being committed on the people of the world by altering their DNA.

## Introduction

Herbicide-resistant weeds now plague more than 60 million acres of US farmland. To control weeds, the non-selective herbicide Glyphosate including an adjuvant to enhance the penetration through weed leaves is widely sprayed on crop fields. But it is not possible to spray weeds alone, and therefore Glyphosate enters crop plants and ultimately resides in soy and corn crops.

Herbicide adjuvants [1] include the surfactant POEA including a declared AP which is often proprietary and kept confidential by manufacturers. POEA stands for polyoxyethyleneamine and AP for application principle, e.g., in Monsanto's Roundup, the declared AP is Glyphosate while POEA is considered an adjuvant. However, the FDA only regulates the toxicity of APs. Adjuvants like POEA are classified as chemically inert and not regulated. Moreover, if the POEA in the bulk is shown to not be toxic, NPs of POEA are not considered toxic. But studies [2] based on various Roundup formulations strongly suggest that toxicity was due to adjuvants present in the formulations and not the direct result of Glyphosate. In fact, POEA alone was found more toxic.

Upon human ingestion of GM foods, most Glyphosate and POEA are rapidly excreted, but residues remain in the gut. Of great controversy today is whether the residues are harmful to human health. Donald Huber, the prominent critic of GM foods claims [3] a pathogen is produced from Glyphosate that harms human health, e.g., residents living close to sprayed GM soybean fields in Argentina developed cancers and birth defects. However, GM food proponents argue science is still looking for, but not found Huber's pathogen to establish the causal link between Glyphosate and human health. Regardless, a single pathogen linking GM food to human health is unlikely because the diversity of problems, e.g., birth defects, autism, and so forth can only be caused by different pathogens.

One such source of different pathogens is the DNA damage from NPs. NPs stand for nanoparticles having dimensions < 100 nm. Consistent with adjuvants enhancing the penetration of Glyphosate through weed and crop plant leaves, experiments [4] show POEA upon mixing in water form a emulsion of globular NPs that adhere to and forms films on surfaces. Hence, the toxicity of POEA is proposed to be the globular NPs that attach to and disrupt cell walls allowing Glyphosate to enter and damage the DNA. If so, the scrambling of genes would lead to a variety of observed health problems. However, it is not clear how inert POEA globules disrupt cell walls or otherwise damage the DNA.

But DNA damage by NPs is not new. Over the past decade, lung cancer based on *in vivo* and *in vitro* models [5,6] show NPs induce oxidative stress and pro-inflammatory effects. At that time, the mechanisms of the generation of the oxidative stress by NPs was not understood, but thought in some way related to the large S/V ratios. S/V stands for surface-to-volume. In 2008, the DNA damage was thought [7] linked to cancer by ROS from respiration and metabolism. ROS stands for reactive oxygen species. ROS include the highly reactive hydroxyl radicals linking the activation of p53 and proteins related to DNA repair thereby mimicking irradiation-related carcinogenesis pathways. But the literature has never identified how NPs produce EM energy of at least 5 eV to create the hydroxyl radicals.

It was not until 2010 that NPs were proposed [8,9] to provide the EM energy necessary to create the ROS. Indeed, NPs were shown to create the ROS by providing a natural low-level source of continuous EM radiation beyond the UV. Here, UV stands for ultraviolet. At that time, the source of EM radiation transferred to the NPs was by molecular collisions, but since then has been superseded by any form of NP heating from the surrounding tissue. At UV levels, the NPs have sufficient EM energy at 5 eV levels to create the ROS that damage

***Key words:*** *GM food, DNA damage, UV radiation, nanoparticles, classical physics, quantum mechanics*

**Received:** December 19, 2016; **Accepted:** January 10, 2017; **Published:** January 14, 2017

nearby DNA. However, the ROS are no longer necessary as DNA damage in the irradiation-related carcinogenesis pathways are in fact activated by UV radiation.

Today, the cancer pathways linked to NPs continues to be based on ROS and not UV radiation. Recently, silver NPs linked to ROS were studied [10] in the protein interaction of the human LoVo cell line and found to depend on NP size. The 100 nm NPs indirectly effected serine/threonine protein kinase (PAK) and mitogen-activated protein kinase (MAPK), and phosphatase 2A pathways; whereas, the 20 nm NPs directly affect cellular stress and generation of ROS and protein carbonylation. But the presence of Ag+ ions suggest the NPs are producing UV radiation > 5 eV necessary to ionize silver. Indeed, the bactericidal action of silver NPs suggests UV radiation is being produced that causes [11] chromosomal damage in human hepatocarcinoma cells (HepG2) rather than by the ROS from the release of Ag and subsequent oxidation to Ag+.

The UV in the UVC at 254 nm is a lethal level for DNA damage in all living systems as the pyrimidine dimers are formed [12] that block DNA replication. If the scrambled genes are not repaired, human diseases of cancer and birth defects may occur. After all, the collateral damage of silver NPs as a bactericidal agent should not be expected to not damage DNA.

In this paper, the causal link between GM foods and varied human health problems is proposed to be the scrambling of genes in DNA by UV radiation from NPs of POEA globules that diffuse through the cell wall. Upon attaching to cell walls, the UV radiation may also disrupt cell walls by ionizing wall molecules allowing Glyphosate to enter and damage the DNA. But the DNA damage need not be limited to GM food that upon ingestion produce NP globules of POEA. Indeed, the effects of NPs in nano-medicine, e.g.,

Drug delivery vehicles, Antimicrobial agents, Treating cancer in photodynamic therapy are placed in question unless the attendant DNA damage leading to human health problems is justified alongside the celebrated beneficial effects of NPs .

## Materials and methods

### Planck law

The UV radiation from globular POEA NPs may be readily understood. Classically, NP atoms have heat capacity and conserve body heat by increasing in temperature. But QM governs the nanoscale. QM stands for quantum mechanics. The Planck law of QM [13] for the atom at 300 K is shown in figure 1.

Figure 1 shows QM allows the atom in macroscopic matter to have $kT$ energy and behave classically by increasing in temperature upon absorbing heat under EM confinement at $\lambda > 100$ microns. NPs of nanoscopic matter differ as the $kT$ energy decreases for atoms having EM confinement $\lambda < 100$ microns, and for NPs having $\lambda < 100$ nm the atoms have virtually no heat capacity to conserve absorbed heat by an increase in temperature.

Despite the fact the Planck law is known for over a century, nanotechnology today continues to assign finite heat capacity to NPs. In nanoparticle mass spectrometry, 20-50 nm carbon NPs are trapped in a quadrupole ion trap [14] and heated with lasers. Based on classical physics, NP temperatures increase to 3000 K. High temperatures were thought verified by comparing the measured NP mass loss rate with the

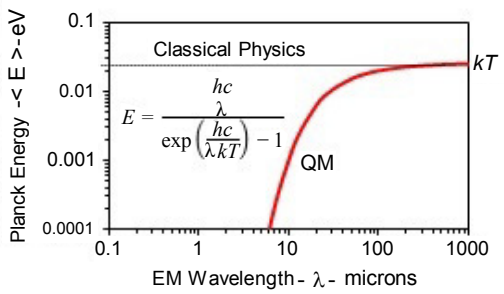


**Figure 1.** Planck law of the Atom at 300 K. In the inset, $E$ is Planck energy, $h$ Planck's constant, $c$ light speed, $k$ Boltzmann's constant, $T$ temperature, and $\lambda$ the EM confinement wavelength

temperature estimated from known sublimation rates vs temperature for bulk polycrystalline graphite. But figure 1 shows the heat capacity for carbon NPs vanishes while that for bulk graphite at $\lambda > 100$ microns is finite. Hence, high temperatures do occur in the bulk, but NPs cannot change in temperature. Lack of temperature change suggests mass loss in NPs is caused by fragmentation under charge induced Coulomb repulsion.

### EM Confinement

QM by the Planck law requires the NP atoms have vanishing heat capacity thereby precluding conservation by temperature changes. For heat capacity to vanish, the NP atoms must somehow be placed under nanoscale EM confinement. NP surfaces lack any texture that could be construed as EM confinement. But NPs have high S/V ratios that confine body heat almost entirely to their surfaces, the surface heat thereby providing the necessary EM confinement of NP atoms over nanoscale wavelengths. S/V stands for surface-to-volume. QED then conserves the surface heat by creating EM radiation standing between diametrically opposite NP surfaces.

### Simple QED

Simple QED differs from the complex relativistic QED [15] by Feynman and others. Briefly stated: QED conserves heat supplied to a NP absent heat capacity by creating EM radiation having half-wavelength $\lambda/2 = d$, where $d$ is the diameter of the NP. The Planck energy $E$ of the standing EM radiation is:

$$E = h\left(\frac{c}{n}\right)/\lambda = \frac{hc}{2nd} \quad (1)$$

where, the velocity of light $c$ is corrected for the slower speed in the solid state by the refractive index $n$ of the NP.

QED induced EM radiation differs from the speculative multi - IR photon [16] processes that excite dopant atoms, i.e., the QED radiation depends only on the NP size and refractive index. DNA damage from QED induced EM radiation is therefore always expected as the absorption of heat by a NP is excited from (1) in the EUV at wavelength $\lambda = 2nd$. EUV stands for extreme ultraviolet. Dopant atoms in lower quantum states are excited by EUV fluorescence [17] as the NP gives up EUV energy by radiationless processes. QED induced EM radiation thereby avoids the highly unlikely multi-photon process.

Prevenslik T (2017) Cancer by UV radiation from nanoparticles in GM food

### POEA surfactant

The FDA classifies Glyphosate as the AP in Roundup and claims [2] it is not toxic for human cells, except when mixed with inert components such as POEA surfactant. However, POEA causes AK and SD in human cells. AK stands for membrane damage and SD for mitochondrial activity leading to cell mortality. POEA globules may diffuse through cell walls, although the mechanism by which AK and SD occur is not identified in the literature.

### AK and SD mechanism

The proposed AK and SD mechanism is the EM radiation from NPs of POEA globules. Although the literature does not show NP globules in Roundup, POEA globules are known [4] to aggregate in water and adhere to glass surfaces to form nanoscale films. By analogy, POEA globules may adhere to cell surfaces and diffuse or burrow through the cell wall as shown in figure 2.

In POEA globular NPs, body heat is converted to EM radiation beyond the UV allowing burrowing to occur by ionization of the cell wall. Glyphosate then may enter the disrupted cell wall to damage the DNA. However, the DNA may also be damaged by UV radiation from POEA globules that simply passes through cell walls.

### Energy of QED induced EM radiation

The EM radiation energy depends on the POEA globule size. For a POEA of ethylene amine having refractive index $n = 1.51$, the Planck energy $E$ of QED induced radiation in terms of the diameter $d$ of the POEA globules is shown in figure 3.

### Toxicity

The toxicity of Glyphosate in human cells is enhanced by the disruption of membrane walls by ionizing QED induced EM radiation. Figure 3 shows the Planck energy $E$ varies from 20 to 4 eV for POEA globule diameters $d$ from 20 to 100 nm, respectively. Hence, the QED induced EM radiation from POEA globules is more than sufficient to ionize wall molecules thereby enhancing the toxicity [1,2] of Glyphosate by diffusing into the human cell.

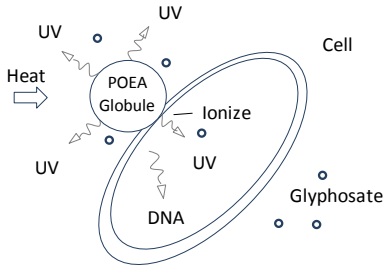


**Figure 2.** POEA Globule producing UV Radiation.

## Results

Over 100 Nobel Laureates signed a letter [18] made public urging Greenpeace to review its claims that crops and foods worldwide are not improved with biotechnology, recognize the contrary claims of scientific bodies and regulatory agencies, and abandon their campaign against GM food in general and Golden Rice in particular.

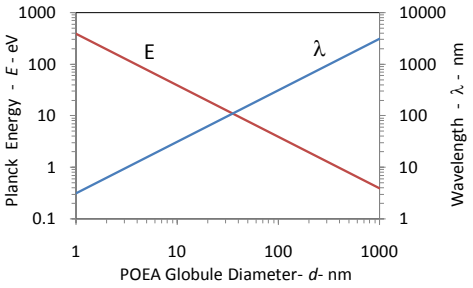


**Figure 3.** POEA globule energy and wavelength.

Greenpeace has led the opposition to Golden Rice, which has the potential to reduce or eliminate much of the death and disease caused by VAD having the greatest impact on the poorest people in the world. VAD stands for vitamin A deficiency. The WHO estimates over 250 million people suffer from VAD which compromises the immune system, putting children at great risk.

The Laureates ask the governments of the world to reject [19] Greenpeace's campaign against Golden Rice and GM foods in general and oppose Greenpeace's actions and accelerate the access of farmers to modern biology, especially GM seeds improved through biotechnology. The letter argues that Greenpeace by misrepresenting the risks of GM food based on emotion and dogma is contradicted by science, and therefore must stop.

The letter campaign was organized by Richard Roberts and Phillip Sharp, co-winners of the 1993 Nobel Prize in medicine for the discovery of DNA sequences known as introns. Roberts told *The Washington Post*:

> "We're scientists. We understand the logic of science. It's easy to see what Greenpeace is doing is damaging and is anti-science,"

The Laureates letter [18] concludes alleging Greenpeace by denying GM food has placed millions of people in the developing world at risk of VAD by asking the question:

> How many poor people in the world must die before we consider this a "crime against humanity"?

Clearly, emotion and dogma do not belong in science *even* by Nobel Laureates. The letter by the Laureates supporting the GM food industry refuting Greenpeace's actions is not based on scientific arguments, but on emotion and dogma from the GM food industry perspective.

Regardless, it is unlikely the Laureates did not know their signature to the letter would support the GM food industry argument against Greenpeace, thereby raising the question as to whether the Laureates based on their scientific expertise knew the letter was false and could only have signed the letter for personal reward, but

> Is there a scientific argument that the Laureates knew or should have known that GM food may damage human health?

If so, a jury would find the Laureates did indeed sign the letter known to be false, an unfortunate act as the Nobel Laureates hold the highest esteem in science.

## Scientific argument

Unlike Huber's pathogen, the scientific argument linking GM food

to human health requires the causal relation that the human DNA is damaged from UV radiation produced from heated NPs of POEA globules in the gut, the UV radiation being unequivocally genotoxic.

## Legal argument

Prior knowledge is the legal basis of a crime against humanity. Even if the Laureates did not know QM requires NPs conserve body heat by emitting EM radiation beyond the UV, the Laureates knew or should have known experiments over the past decade have shown NPs damage the DNA of all living cells that if not repaired may lead to cancer including a variety of health problems.

## Greenpeace *vs*. Nobel Laureates

Greenpeace is most certainly not guilty of a crime against humanity. Contrarily, the GM food industry may be alleged guilty of a crime against humanity as the DNA of the people of the world is damaged by the UV radiation from NPs that if not repaired by their immune systems may give rise to cancer including the wide range of observed health problems.

The Nobel Laureates signing the letter in support of GM foods knew or should have known the scientific basis of the letter was false and therefore are complicit in the alleged crime of the GM industry against humanity.

GM food proponents should stop their campaign against the Greenpeace claim that GM food is harmful to human health as DNA damage from NPs cannot be scientifically denied. Instead, the GM food industry should label the NPs in their products to allow the consumer to make an informed decision on its purchase.

## Conclusions

QED induced radiation from NPs is a consequence of QM that negates heat capacity of the atom under nanoscale EM confinement thereby requiring the conservation of body heat by emitting EM radiation beyond the UV that damages the DNA.

The causal link between ingested GM foods and human health is the scrambling of genes in DNA damage by UV radiation from POEA globular NPs in Glyphosate residues. Only genotoxicity can link GM food to human health because the diversity of problems, e.g., cancer, Parkinson's disease, birth defects, and autism cannot be explained by a single pathogen.

NPs provide an important link between DNA damage by UV radiation beyond the UVC within the body. Currently, UV induced DNA damage is thought to only occur in the skin exposed to solar radiation at UVB levels. The far more DNA damaging solar UVC does not reach the Earth because of ozone absorption in the upper atmosphere. But NPs as a UVC source within the body are always damaging the DNA and should be recognized as a prime cause of human health problems.

POEA globular NPs upon diffusing through cell walls emit UVC radiation that readily travels in cellular water to damage DNA at a distance. Contact is not necessary.

The beneficial effects of NPs in nano-medicine should always include companion test results of associated DNA genotoxicity.

**References**


1. Mesnage R, Defarge N, Spiroux de Vendômois J, Séralini GE (2014) Major Pesticides Are More Toxic to Human Cells Than Their Declared Active Principles. *BioMed Research International*.
2. Benachour N, Séralini GE (2009) Glyphosate formulations induce apoptosis and necrosis in human umbilical, embryonic, and placental cells. *Chem Res Toxicol* 22: 97-105. [Crossref]
3. Genetic Literacy Project: Don Huber. (October 2015) [Available: https://www.geneticliteracyproject.org/glp-facts/don-huber-science-still-looking-for-Purdue-professors-gmo-pathogen-time-bomb/]
4. Leite FL, Paterno LG, Borato CE, Herrmann PSP (2005) Study on the adsorption of poly(o-ethoxyaniline) nanostructured films using atomic force microscopy. *Polymer* 46: 12503-12510.
5. Donaldson K, Stone V (2003) Current hypotheses on the mechanisms of toxicity of ultrafine particles. *Ann Ist Super Sanita* 39: 405-410. [Crossref]
6. Donaldson K (2003) The biological effect of coarse and fine particulate matter. *Occu Environ Med* 60: 313-314. [Crossref]
7. Mroz RM, Schins RPF, Li H, Jimenez LA, Drost EM, et al. (2008) Nanoparticle-driven DNA damage mimics irradiation-related carcinogenesis pathways. *Eur Respir J*. [Crossref]
8. Prevenslik T (2010) DNA damage by Nanoparticles. Proceedings of ASME2010 First Global Conference on Nano Engineering for Medicine and Biology, NEMB2010, Houston, TX, USA, February 7-10, 2010.
9. Prevenslik T (2010) Nanoparticle toxicity and cancer. International Conference on Safe production and use of nanomaterials, NANOSAFE 2010, Minatec, Grenoble, France, November 16-18, 2010.
10. Verano-Braga T, Miethling-Graff R, Wojdyla K, Rogowska-Wrzesinska A, Brewer JR, et al. (2014) Insights into the Cellular Response Triggered by Silver Nanoparticles Using Quantitative Proteomics. *ACS Nano* 8: 2161-2175. [Crossref]
11. Zhao X, Ibuki Y (2015) Evaluating the Toxicity of Silver Nanoparticles by Detecting Phosphorylation of Histone H3 in Combination with Flow Cytometry Side-Scattered Light. *Environ Sci Technol* 49: 5003–5012.
12. Pfeifer GP, Besaratinia A (2012) UV wavelength-dependent DNA damage and human non-melanoma and melanoma skin cancer. *Photochem Photobiol Sci* 11: 90-97. [Crossref]
13. Planck M (1900) On the Theory of the Energy Distribution Law of the Normal Spectrum. *Verhandl Dtsch Phys Ges* 2: 237.
14. Howder CR, Long BA, Gerlich D, Alley RN, Anderson SL (2015) Single Nanoparticle Mass Spectrometry as a High Temperature Kinetics Tool: Sublimation, Oxidation, and Emission Spectra of Hot Carbon Nanoparticles. *J Phys Chem A* 119: 12538-12550. [Crossref]
15. Feynman R (1976) QED: The Strange Theory of Light and Matter. Princeton University Press.
16. Chen G, Qiu H, Prasad PN, Chen X (2014) Upconversion nanoparticles: design, nanochemistry, and applications in theranostics. *Chem Rev* 114: 5161-5214. [Crossref]
17. So PTC, Dong CY (2002) Fluorescence Spectrophotometry. ENCYCLOPEDIA OF LIFE SCIENCES. Macmillan Publishers Ltd, Nature Publishing Group.
18. Roberts RJ, Sharp PA. (June 29 2016) Laureates Letter Supporting Precision Agriculture (GMOs). [Available: http://supportprecisionagriculture.org/nobel-laureate-gmo-letter_rjr.html]
19. Washington Post (June 29 2016) 107 Nobel laureates sign letter blasting Greenpeace. [Available:https://www.washingtonpost.com/news/speaking-of-science/wp/2016/06/29/more-than-100-nobel-laureates-take-on-greenpeace-over-gmo-stance/?utm_term =.d768ae13ca7d]


**Copyright:** ©2017 Prevenslik T. This is an open-access article distributed under the terms of the Creative Commons Attribution License, which permits unrestricted use, distribution, and reproduction in any medium, provided the original author and source are credited.

# Electronic Cigarettes and DNA Damage

***Abstract***

*Electronic e-cigarettes are common throughout the world. E-cigarettes deliver the nicotine stimulant through aerosols to the lungs without burning tobacco. Recently, e-cigarette smokers have mysteriously expressed nicotine poisoning symptoms including nausea and vomiting, excessive salivation, headache, and dizziness followed by a period of central nervous system depression, paralysis, difficulty in breathing and even death. Unlike the immediacy of nicotine poisoning, the potential of cancer developing decades later from e-cigarette use was assessed with DNA tests that showed nicotine enhanced the UV-induced DNA mutation frequency in human lung and bladder epithelial cells by two- to fourfold. Enhanced DNA damage is consistent with simple QED that predicts nanoparticles (NPs) produced from the metal heater in the e-cigarette emit UV radiation well known to cause DNA mutations that may lead to cancer. The mystery of nicotine poisoning is solved by removing the heater producing the NPs, but then the nicotine would remain in the ground state and not enhance the stimulation of the smoker's senses*

**Keywords** — *e-cigarettes, nanoparticles, DNA damage, cancer.*

## I. INTRODUCTION

In September 2019, more than 200 people [1] across the US have come down with a mysterious illness linked to smoking e-cigarettes and a few deaths have been reported. The CDC believes their illness is associated with vaping, but cannot determine the ingredient causing the problem. Absent a known cause, doctors are treating the mystery illness as a disease of unknown origin. The patients suffered from respiratory symptoms of nicotine poisoning including: coughing, shortness of breath, chest pain, and difficulty breathing. Unlike nicotine poisoning, cancer does not appear until decades later which is of concern in that young people in their early 20s smoke e-cigarettes.

One explanation for the mystery illness is e-cigarettes produce NPs from heating metals [2,3] in the coil heater. In nanotechnology, NPs are linked to many illnesses similar to nicotine poisoning as illustrated in Fig. 1

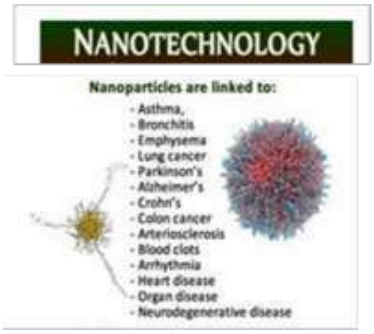


**Fig. 1. Nanoparticle linked illnesses**

In smoking e-cigarettes, puffing activates a battery that heats a liquid to produce an aerosol stimulant containing flavoring, vegetable glycerin, and nicotine. However, metal NPs are found [2,3] in the e-cigarette aerosols.

E-cigarettes produce Fe, Al, Cu, Cr, Ni, and Zn in high NP concentrations. The size of Sn, Cr, and Ni from [2] are shown in Fig. 2. Peak concentrations occur for 50 - 70 nm NPs. One puff of an e-cigarette is estimated to contain about 2 million NPs / $cm^3$. For Ni and Sn, the NPs are spherical at ~ 50 nm. The Cr NP is irregular with minimum dimension ~ 100 nm. In the simple QED of irregular NPs, the EM wave stands across the minimum dimension consistent with Fermat's principle of minimum time in conserving absorbed heat by EM emission. For spherical NPs, the minimum dimension is the diameter.

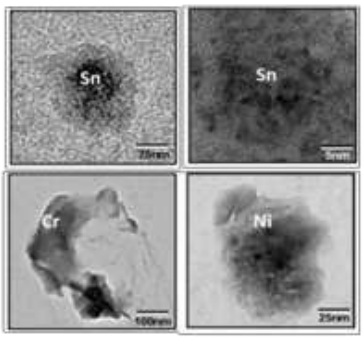


**Fig. 2. NP Size - Sn, Cr, and Ni**

An e-cigarette generation system [3] was developed for inhalation toxicology studies of size, number, and chemical compositions of metallic NPs. The Kanthal e-cigarette coil was tested without a nicotine solution to characterize the size distribution and chemical composition of the metallic NPs generated from heating of a dry e-cigarettes. Kanthal is an Fe, Cr, and Al alloy including a trace of Mn, Si, and C. Fig. 3 shows NP shapes of Fe to vary from irregular to spherical. The minimum irregular NP size is < 50 nm and spherical shapes ~ 50 nm. EDX maps show Fe and O to be dominant.

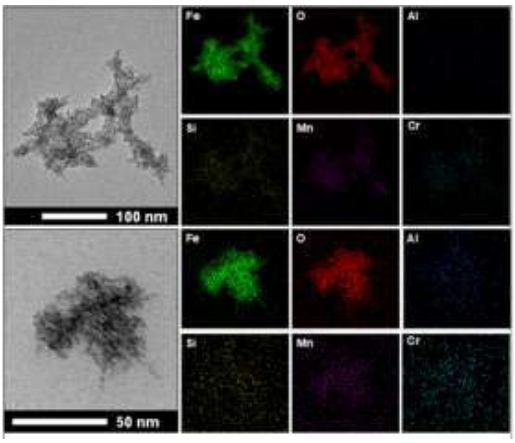


**Fig. 3. NP shapes and EDX maps from Kanthal e-cigarette coil**

Chemical carcinogenesis [4] assumes metabolism into an electrophilic metabolite that binds covalently to DNA and, if not enzymatically repaired, mutations occur, the accumulation of mutations in the genomic landscape may lead to cancer and/or damage DNA repair enzymes. Nicotine is rapidly metabolized *in vivo* to cotinine and other metabolites. In this regard, nicotine induces DNA damage and further inhibits DNA repair in human cell types.

However, chemicals are not necessary to bind DNA and induce DNA damage as UV light alone directly damages DNA to induce mutations. Of relevance to e-cigarettes is whether carcinogenesis is enhanced by nicotine irradiated with UV light in human cells. In this regard, the potential of cancer developing decades later was assessed [5] in mice showing e-cigarette aerosol enhanced UV-induced DNA mutation frequency in lung and bladder epithelial cells. Otherwise, epidemiology studies over decades would be required to assess carcinogenesis from e-cigarettes.

## II. PURPOSE

The purpose of this paper is to show the DNA mutagenesis of nicotine is enhanced by irradiated UV light produced from heated NPs. The UV light is endogenous to the e-cigarette aerosol. Exogenous UV from solar radiation is not considered.

## III. ANALYSIS

Endogenous UV light from NPs depends on simple QED - a method of analysis applicable [6,7] to nanoscale heat transfer. Simple QED is not the complex light and matter interaction advanced by Feynman and others. Instead, simple QED is readily understood by the Planck law of quantum mechanics that requires the heat capacity of constituent atoms in NPs to vanish under EM confinement. In contrast, classical physics always assumes the atom has heat capacity that produces an increase in temperature upon the absorption of heat. Simple QED differs as the NP conserves heat by the creation of standing EM radiation inside and across the diameter of the NP is illustrated in Fig. 4.

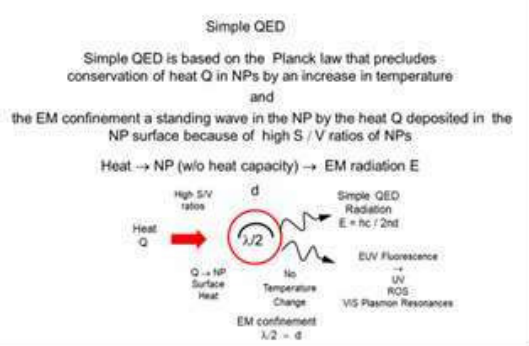
Simple QED
Simple QED is based on the Planck law that precludes conservation of heat Q in NPs by an increase in temperature
and
the EM confinement a standing wave in the NP by the heat Q deposited in the NP surface because of high S / V ratios of NPs
Heat → NP (w/o heat capacity) → EM radiation E
d
High S/V ratios
Heat Q
λ/2
Simple QED Radiation E = hc / 2nd
EUV Fluorescence
UV
ROS
VIS Plasmon Resonances
Q → NP Surface Heat
No Temperature Change
EM confinement
λ/2 = d

**Fig. 4. Simple QED - Conversion of heat to EM radiation**

The temperature of the e-cigarette aerosol is increased by the heat Q of the coil, the aerosol transferring the heat Q to the NP. Because NPs have high surface-to-volume (S/V) ratios, the heat Q is almost totally absorbed in the NP surface. The NP temperature cannot conserve the surface heat Q by an increase in temperature, and instead a standing wave is created inside and across the diameter d of the NP having half-wavelength $\lambda/2 = d$. Correcting the velocity of light c for the refractive index n of the NP gives the time $\tau = 2d/(c/n)$ for 1 cycle. Hence, the frequency of the standing wave $c/\lambda = 1/\tau = c/ 2nd$ gives $\lambda = 2nd$.

Simple QED creates standing EM waves from the EUV to UV to VIS and NIR. EUV is common in biological NP diameters d < 30 nm, otherwise the UV to the NIR are produced. The EM confinement necessary to create the standing EM wave is the momentary surface heat of the NP. EUV waves fluoresce down to lower quantum states: UVA to UVC, reactive oxygen species (ROS), and VIS plasmon resonances. Upon absorption in water surroundings, the EUV fluoresces down to lower states, but is inefficient. Fluorescence data is scarce, e.g., EUV at 120 nm in water is available from astronomy in Lyman-α fluorescence [8] to UVB (330

nm) and UVC (254 nm) but only about 8 and 13 percent efficient, respectively

The simple QED wavelength λ = 2nd for various NP metals is given in Fig. 5. The refractive index n is taken from the literature at wavelengths near the UVC at 254 nm. The Sn data is the exception at 730 nm, but was the lowest wavelength data available. The Ag, Cu, and Ni data give about the same response. Data for Fe is reasonably correct. The red lines give the NP diameter d range from 37 to 80 nm corresponding to the UVC. Experimentally, simple QED is consistent with the higher number of NPs and the NP range 50 - 70 nm reported in [2]. Also, Fig. 3 giving the average NP diameter of ~ 50 nm is near the ~ 60 nm average of the 37 to 80 nm range given by simple QED. Fig. 5 shows simple QED radiation wavelengths produced for NP diameters d < 100 nm.

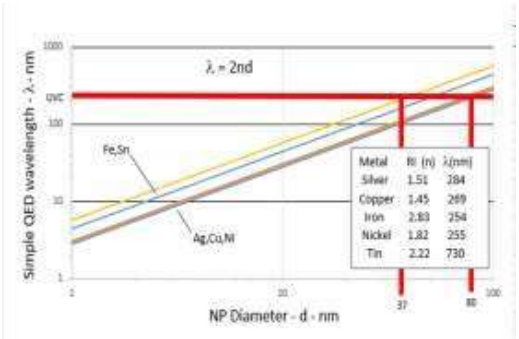


**Fig.5. Simple QED wavelength**

**IV. NP material and diameter**

Since the 1940's, UVC irradiation (225-305 nm) of nicotine is known [9] to produce oxynicotine, methylamine and nicotinic acid. Recent spectroscopy [10] shows the UVC provides a representative measure of the first excited state of nicotine in relation to water as illustrated in the absorption spectrum in Fig. 6.

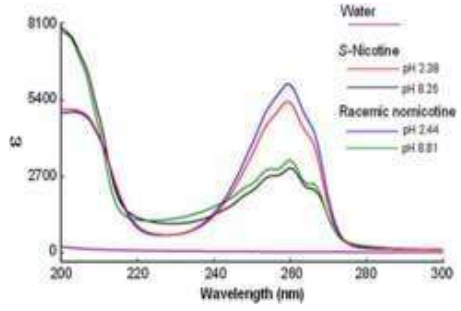


**Fig. 6. Nicotine absorption in the UV**

Similar to nicotine, the UV absorption spectrum [11] of native DNA follows the UVC peak at 254 nm depending on folded structure modified by glycation in ribose as shown in Figure 7.

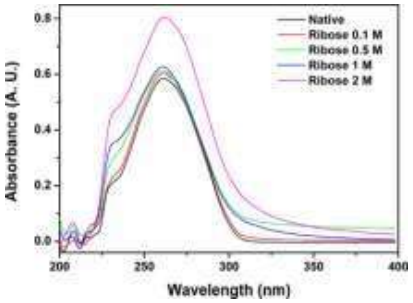


**Fig. 7. UV absorption spectra DNA (black) and glycated in D-ribose.**

The simple QED induced EM radiation analysis suggests 50-70 nm NPs of various metals produced in e-cigarettes tends to produce an average UVC radiation that excites nicotine to higher energy states coincident with absorption peak of native DNA. The UVC produced by NPs therefore enhances DNA damage above that of nicotine in the ground state. Indeed, DNA damage from NPs is not limited to e-cigarettes. Vaccinations containing NPs of aluminum adjuvants are used [12] to stimulate antigens in vaccines, the DNA damage in the vaccines more severe than e-cigarettes as the NPs reach the brain directly upon injection into the blood stream.

Unlike tobacco smoke, e-cigarette aerosols are thought to contain nicotine and relatively harmless organic solvents, and therefore e-cigarettes are considered [5] non-carcinogenic and a safer [13] substitute for tobacco. But this is questionable.

Although NPs are not the major component in e-cigarette aerosol, NPs are the most important to consumer health. NPs by emitting UV radiation excite nicotine to high electronic states to enhance mutagenic DNA and inhibit DNA repair in human lung and bladder epithelial cells, all of which are unlikely for nicotine in the ground state. NPs make e-cigarette smoking far more serious in future cancers than normal cigarettes.

**V. CONCLUSIONS**

Simple QED [6,7,12] based on the Planck law denies constituent atoms in metal NPs of e-cigarette aerosols the heat capacity to conserve absorbed heat by an increase in temperature. Because NPs have high S/V ratios, the absorbed heat is deposited in the NP surface, the surface heat itself providing the brief, but necessary EM confinement to convert the surface heat to UV radiation standing inside the NP, at which time the EM confinement

vanishes and the UV is free to excite nicotine and/or damage DNA in the surroundings.

Unlike discrete electron quantum states of the atom, the simple QED quantum state depends only on the size of the NP allowing UV photon creation by simply immersing NPs in an ambient thermal bath that otherwise is precluded unless a photon having an energy state equal or greater than the UV is absorbed.

E-cigarettes produce NPs [2,3] from the metal heating coils. Once the NPs are free in the aerosol, simple QED predicts further heating induces the NPs to emit EM radiation in the EUV-UVC-UV-VIS-NIR depending on NP size. NPs > 100 nm producing VIS and NIR are harmless. Irrespective of the NP metal, the average EM radiation of 50-70 nm NPs in the UV coincides with the UVC absorption peak of nicotine and DNA spectra. EUV produced in < 50 nm NPs produce UVC by fluorescence, but inefficiently.

Whether vaping is safer than smoking conventional cigarettes is an issue of great interest. Conventional cigarettes were found [14] to contain approximately 9000 million NPs per cigarette having diameters d from 6–50 nm. Assuming 100 puffs/day, estimates [2] suggest e-cigarettes produce about 100 million NPs which is far less than smoking one conventional cigarette per day. Based on the number of NPs alone, the e-cigarettes appear safer than conventional cigarettes as 9000 e-cigarettes puffs / day are required to inhale the same number of NPs as the one conventional cigarette.

However, the UVC from 50-70 nm NPs in e-cigarettes excites nicotine to electronic states above the ground state. Nicotine in the ground state may be considered similar to ordinary cigarettes absent NPs. On this basis, DNA damage from the higher electronic state of nicotine in e-cigarettes compared to conventional cigarettes poses a larger potential for decades later cancer.

The difficulty with the latter argument is that although the NPs in e-cigarettes include metals while conventional cigarettes do not, both emit UV radiation. Differences between metallic and non-metallic NPs are the refractive index which are not significant for the same NP diameters. What is important is the extent of DNA damage which is not assessed here or available in the literature. The FDA is recommended to conduct DNA testing of both conventional cigarette smoke and e-cigarette vapor to resolve the merits of e-cigarettes over conventional cigarettes.

## REFERENCES


[1] (2019) The VOX website. [Online] "Vaping appears to be making hundreds of people sick. No one knows exactly why." Available: https://www.vox.com/science-and-health/2019/9/3/20847219/vaping-health-risks-2019-lung-damage-death/

[2] M. Williams, A. Villarreal, K. Bozhilov, S. Lin, P. Talbot. "Metal and Silicate Particles Including Nanoparticles Are Present in Electronic Cigarette Cartomizer Fluid and Aerosol," PLOS vol. 8 pp. e57987, 2013.

[3] M. D. Wilson, K. A. Prasad, J. S. Kim, J. H. Park. "Characteristics of metallic nanoparticles emitted from heated Kanthal e-cigarette coils," Nanopart. Res: vol. 21, pp. 156, 2019.

[4] C. C. Harris. "Tobacco smoking, E-cigarettes, and nicotine harm," PNAS vol. 115, pp. 1406-1407, 2018.

[5] H. W. Lee, et al. "E-cigarette smoke damages DNA and reduces repair activity in mouse lung, heart, and bladder as well as in human lung and bladder cells," PNAS, pp. E1560–E1569, 2018.

[6] (2015-19) NanoQED website. [Online] "Simple QED Applications" Available: mamoqed.org.

[7] C. H. Rayburn, W. R. Harlan, H. R. Hanmer. "The Effect of Ultraviolet Radiation on Nicotine," J. Am. Chem. Soc. pp. 115-116. 1941.

[8] J. W. Young. et al. "Hydroxyl Radical Fluorescence and Quantum Yield Following Lyman- α Photoexcitation of Water Vapor in a Room Temperature Cell and Cooled in a Supersonic Expansion," J. Phys. Chem. A. 122:5602−5609, 2018.

[9] T. Prevenslik. "Cancer by UV radiation from nanoparticles in GM food." Integr. Cancer Sci. Therap. 4(1): 2-4, 2017.

[10] P. M. Clayton, C. A. Vas, T. Bui, A. F. Drake, K. McAdam. "Spectroscopic Studies on Nicotine and Nornicotine in the UV Region," Chirality; vol. 25, pp. 288–293, 2013.

[11] G. K. Chandra, et al. "Probing in Vitro Ribose Induced DNA-Glycation Using Raman Microspectroscopy," Anal. Chem.; vol. 87, pp. 2655−2664, 2015.

[12] T. Prevenslik. "The Causal Link Between Vaccination Adjuvants and Autism," Inter. J. Research - Granthaalayah, vol. 7, pp. 288-295, 2019.

[13] T. Cheng. "Chemical evaluation of electronic cigarettes." Tob. Control. vol. 23, pp. ii11–ii17, 2014.

[14] W. D. van Dijk, S. Gopal, P. T. Scheepers. "Nanoparticles in cigarette smoke-real-time undiluted measurements by a scanning mobility particle sizer," Anal Bioanal Chem vol. 399, pp. 3573–3578, 2011.

# Protein misfolding by UV emission from nanoparticles

Pittsburgh - Aug. 2, 2016

Amyloid diseases are proposed caused as replicating proteins are damaged by low-level UV radiation produced as heat from the surroundings is absorbed in nanoparticles By: QED Radiations

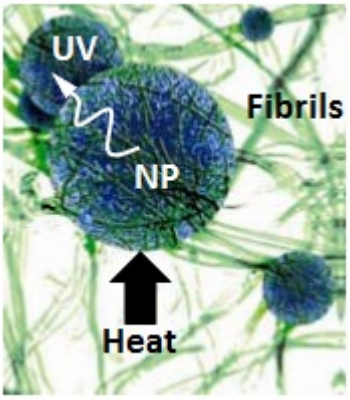


Figure 2.1: Amyloid disease: Heat induced UV from NPs causing PC and DNA damage

### Introduction

Amyloid diseases like Alzheimer's and Parkinson's are not caused by bacteria or viruses, but rather by the accumulation of fibrils from misfolded proteins. NPs having enormous S/V ratios are thought [1] to somehow enhance the rate of protein fibrils by decreasing the lag time for nucleation and growth by attaching to their surfaces. NPs stand for nanoparticles and S/V for surface-to-volume. Mature fibrils are rope-like, 5-10 nm diameter up to a few microns in length. Pre-fibrillar oligomers forming on the surface of NPs are shown in the thumbnail.

Although the DNA contains all the information for life, the replication proteins actually perform the constant repair necessary for life to be to be perpetuated. However, replication proteins themselves are subject to damage by irreversible PC modification. PC stands for protein carbonylation. Since the proteins control mutation rates in DNA replication, PC damage should determine the frequency of DNA mutations, and therefore the argument [2] was made that PC damage should cause errors in DNA replication. At various PC levels, constant levels of oxidative DNA damage from ROS were controlled with UVC light. Indeed, doubling the PC damage for Escherichia coli was found correlated with over a 100-fold increase in DNA mutation rate. ROS stands for reactive oxygen species and UVC for UV radiation at 254 nm.

### Problem

Currently, NPs are thought to induce protein misfolding by ROS induced PC. However, a NP mechanism to provide energies of at least 5 eV necessary to create the ROS is required, but not known.

### Proposal

Protein misfolding induced by NPs is proposed to be the UV radiation created as the NPs absorb heat in vivo from the surroundings. In the thumbnail, the NPs upon absorbing heat are depicted emitting low-level UV radiation that induces misfolding by photolytic fibril nucleation and growth. ROS are not required for fibrillation.

### Theory

Classical physics does not predict NPs emit UV radiation as conservation of heat proceeds by an increase in temperature. However, heat transfer in NPs is governed by the Planck law of QM that precludes conservation of heat by an increase in temperature as the heat capacity of the atoms in NPs vanishes. QM stands for quantum mechanics.

### Discussion

Unlike classical physics that allows the atom to have constant heat capacity from the macro to the nanoscale, QM by the Planck law restricts heat capacity to the macroscale. At the nanoscale, the atom heat capacity depends on the EM confinement. Since NPs have high S/V ratios, heat is momentarily confined to the NP surface, and since the NPs are nanoscale, the NP atoms are spontaneously placed under EM confinement at nanoscale wavelengths. Hence, NPs by the Planck law have vanishing heat capacity. Heat therefore cannot be conserved by an increase in temperature, and therefore QED conserves the heat by creating EM radiation standing across the NP diameter. For NP diameter $d$ and refractive index $n$, EM radiation is produced having half-wavelength $\lambda/2 = nd$. For example, silver NPs having $n = 1.32$ and $d < 95\,\text{nm}$ emit EM radiation $< 254$ nm which is beyond the UVC, a lethal level for PC and DNA damage in all living systems as the pyrimidine dimers are formed that block replication. Smaller NPs emit even higher frequency EM radiation. QED stands for quantum electrodynamics, but is a far simpler theory than the QED advanced by Feynman and others. In general, see diverse QED applications at `http://www.nanoqed.org/`, 2010 – 2016.

### Conclusions

Protein misfolding is enhanced by the UV radiation emitted from NPs upon absorbing heat from the surroundings. The UV is most intense at the NP surface thereby explaining why fibril nucleation and growth are observed at the NP surface. Amyloid diseases should therefore not be treated with NPs.

UV radiation has the Planck energy to create ROS, but ROS are not necessary for protein misfolding as fibrils nucleate and grow from the UV radiation from NPs.

High S/V ratios of NPs are important as absorbed heat is almost totally absorbed in the NP surface, thereby providing the momentary EM confinement necessary to preclude the NP atoms from having the heat capacity to increase in temperature. Therefore, conservation of heat in NPs proceeds by the creation of UV radiation standing across the NP diameter. Once the NP surface heat is expended in forming the standing EM radiation, there is no longer any EM confinement and the EM radiation escapes to the surroundings.

**References**

[1] S. Linse, et al., "Nucleation of protein fibrillation by nanoparticles", Proc. Nat. Acad. Scie. USA, 104, 8691-8696, 2007.

[2] A. Krisko and M. Radman, "Phenotypic and Genetic Consequences of Protein Damage", PLoS Genetics, 9, 1003810, 2013.

# Chapter 3

# Cellular Biology

This chapter examines in detail the development of cancers, their metastasis and proposed possible treatments using UV radiation from nanoparticles. Herein it is proposed that cancer treatment by low level nanoparticles induced UVC should not present a problem.


3.1 The Electrostatic Filopodia Force . . . . . 46
3.2 Endogenous UV in Warburg's Theory on the Origin of Cancer . . . . . 56
3.3 Broadband endogenous UV in Mitochondria . . . . . 68
3.4 ATP by Endogenous UV Radiation . . . . . 74
3.5 Cancer: UVC induced Nanoparticle Treatment and Metastasis . . . . . 84

# The Electrostatic Filopodia Force

**Abstract**

Classical physics allows the atom to have heat capacity at the nanoscale, the conservation of heat proceeding by an increase in temperature. However, simple QED based on the Planck law of quantum mechanics (QM) denies the atoms in bundles of filament the heat capacity to conserve heat by a change in temperature, the consequence of which is 60-100 nm bundles of 8 nm F-actin filaments protruding from the leading edge of cancer cells conserve thermal heat from the surroundings by producing endogenous simple QED induced EM radiation that at UVC levels charges the filopodia positive by the photoelectric effect. Cancer mitosis occurs as the endogenous UVC continuously charges the filopodia filaments positive thereby providing the electrostatic force that pulls the cancer cell to the negatively charged normal cells, but may stall if the charged filopodia is trapped in the extra cellular matrix. In muscle contraction, simple QED similarly charges the myosin heads, but differs in that the CNS produces action potentials to control charging. Herein, the latest simple QED requirement of a penetration depth in the bundle surface upon absorbing thermal heat is revised to the spontaneous conversion of thermal heat at the bundle surface to standing EM radiation inside the bundle.

Keywords: Cancer, Metastasis, Planck law, Filopodia, Neutrophils, Angiotropism.

## 1. Introduction

The Cancer Nanoparticle (NP) treatment [1] based on the simple QED induced UVC radiation from ~80 nm lipid NPs induced cancer cell apoptosis while collateral DNA damage to normal cells is corrected by DNA repair systems. Further and independent of NP induced apoptosis of cancer cells, simple QED was shown to emit UV radiation in the filopodia at the leading edge of the cancer cell to cause DNA damage and induce metastasis in nearby normal cells. However, the mechanism by which the UV radiation from filopodia spreads the cancer cell to normal cells was not described.

Cancer is generally thought [2] to spread by the process of intravasation through blood vessel walls allowing the cancer cell to enter the bloodstream and metastasize to distant sites. To penetrate the vessel wall, the cancer cell secretes substances to degrade the basement membrane and extracellular matrix. Once the cancer cell arrives at a distal point in the bloodstream, the cancer cell once again interacts with the endothelial cells by secreting substances to penetrate the vessel wall by the process of extravasation proliferates at new tissue to produce the secondary tumour.

However, the intra and extravasation of cancer cells in penetrating blood vessel walls is difficult and not efficient. In this regard, angiotropism was proposed [3] as an alternative metastasis of cancer cells and extended [4] to Extravascular Migratory Metastasis (EVMM) where cancer cells move along the outside surface of blood vessels by an interaction between the cancer cells and the vessel surface thereby avoiding the difficulty of intra and extravasation through vessel walls.

With EVMM, the cancer cells mimic pericytes on the outside of blood vessels by creeping along the blood vessel until they reach a point to form new tumors. Although not internal cancer, a mouse skin model of melanoma exposed to surface UV radiation was found [5] to accelerate the angiotropic effect leading a dramatic increase in lung metastases. The angiotrophic effect was thought to depend on the activation of neutrophils from UV damaged surface keratinocytes that promote inflammation for melanoma cells to migrate towards normal cells. However, the angiotropic effect for internal blood vessels is extremely unlikely to depend on UV damaged at distal keratinocytes in skin.

Neutrophils are cells of the immune system [6] in the extracellular medium that upon activation generate Neutrophil Extracellular Traps (NETs) of fibres that kill bacteria before entering the cell. NETs comprise globular domains of around 25 nm that aggregated into larger fibres with diameters of up to 50 nm. Like filopodia filaments, the neutrophil fibres emit simple QED induced EM radiation that inactivates bacteria before reaching normal cells, but as a bactericide causes inflammation.

In neutrophils, the activation of NET fibres by UVA and UVB radiation was shown [7] much faster than activation by chemical or biological factors. Although UV activation is prompt, the migration of neutrophils decreased within minutes most likely because the NET fibres [6] are no longer bound to the neutrophil body. After 30 minutes, UV irradiated neutrophils [7] lost all ability to migrate. What this means is simple QED induced EM radiation is charging the NET fibres positive, and therefore neutrophils still having attached fibres are attracted to the naturally negative normal cells, and if not attached, only the free NET fibres migrate - not the neutrophils. Contrary to [5], the

UV activated neutrophils do not enhance angiotropism, but the freely suspended NET fibres do provide extracellular antibiotic protection of the cell against pathogens.

With regard to forces driving angiotropism, the force exerted on the filopodia filaments attached to cancer cells measured with optical tweezers was found [8] showed no force is produced in the absence of actin polymerization, the latter defined as the assembly or disassembly of actin filaments by the addition or removal of actin monomers of actin monomers in the filopodia filament. In support of actin polymerization, a polymer bead attached to the tip of a single filament is optically trapped [9] to measure forces, the other end of the filament displaced to produce a pushing force. However, the measured force of a single filament was found to buckle and not be representative of the bundle of filaments in filopodia, perhaps explaining why F-actin filaments rarely exist [10] as isolated single filaments and instead associate into bundles.

In cancer, an overabundance of HER2 molecules in filopodia and lamellipodia was found [11] to activate protrusion growth of filaments that require no active energy sources and diffuse freely within filopodia at the leading edge of migrating tumours. HER2 activation, propagation, and functional protrusion growth is a local process in which filopodia have evolved to exploit Brownian thermal fluctuations within a barrier-free nanostructure to transduce rapid signalling. Filopodia a few microns long with a diameter of about 100 nm are illustrated in Fig. 1.

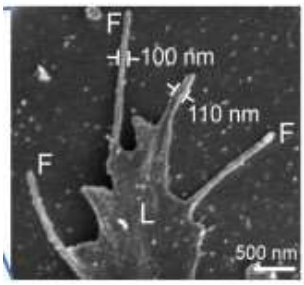


Figure 1. Filopodia (F) at leading edge of Cancer cells
(L) lamellipodium

Unlike cancer metastasis by HER2 without an energy source, simple QED requires thermal energy in the surroundings as the source to produce UV radiation within the bundle of filaments in filopodia. The UV can not only activate HER2 to produce the protrusion force of filopodia, but also the energy for UV enhanced ATP dehydration synthesis to grow the filopodia length. With regard to anti-HER2 cancer treatments, psoralen [12] in the inactivation of HER2 by UVA radiation may be extended to the Nanoparticle Treatment [11] at UVC levels.

In simple QED induced UV, the bundle of filaments in filopodia is important - the single filament inconsequential. The typical 60-100 nm bundle [13] having diameter $D_b$ comprises 25-30 filaments (yellow) of 8 nm diameter $D_{f\ separated}$ by fascin cross-linker spacers (blue) shown in Fig. 2.

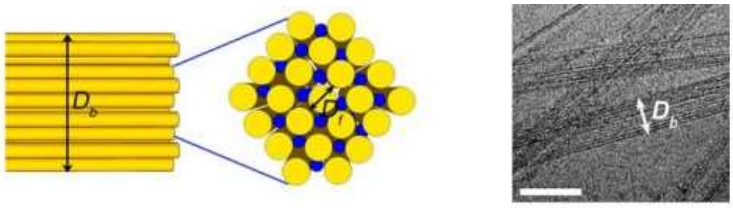


Figure 2. Actin Bundles and Filaments

The micrograph in Fig. 2 shows the side view of the bundle. Scale bar = 200 nm. Although extensively studied in the literature, the filament diameter $D_f$ is observed only as a long molecule inside the bundle. Single filaments are not found *in vivo* as separately distinct, but rather bundled. Nevertheless,

the single F-actin filament *in vitro* is found [14] to have a negative charge density of $q_n = 4$ e/nm. In the bundle, simple QED charging produces positive charge density $q_p$ depending on the bundle diameter $D_b$ from which the average net charge $q_{net}$ on the filament is, $q_{net} = q_p - q_n$ , the difference between positive and negative charge.

In contrast, the filopodia literature is not focussed on bundles of filaments, but rather on single filament mechanical and chemical models. Beyond mechanical models of buckling, chemical models of the single filament in MD simulations [15] are proposed to explain polymerization and depolymerization by ATP hydrolysis - not ATP synthesis by UV enhanced dehydration [16] in the polymerization cycle of actin as embodied in this paper.

**2.Purpose**

Cancer spreading between adjacent cells or along the exterior surfaces of blood vessels to distal organs by EVMM requires an external force to move the cancer cell. The purpose of this paper is to assess an electrostatic force based on the production of net positive charge $q_{net}$ in filopodia bundles, a net charge $q_{net} > 0$. In filopodia, at the leading edge of the cancer cell pulled to the naturally charged negative surface of adjacent cells or vessel walls in the direction of movement.

**3. Analysis**

Filopodia are protrusions of 60-100 nm bundles of actin filaments at the leading edge of cancer cells that by metastasis spread the cancer to normal cells illustrated in [17] and modified by the electrostatic filopodia parameters of simple QED induced EM radiation produced from thermal heat Q in the surroundings is shown in Fig. 3.

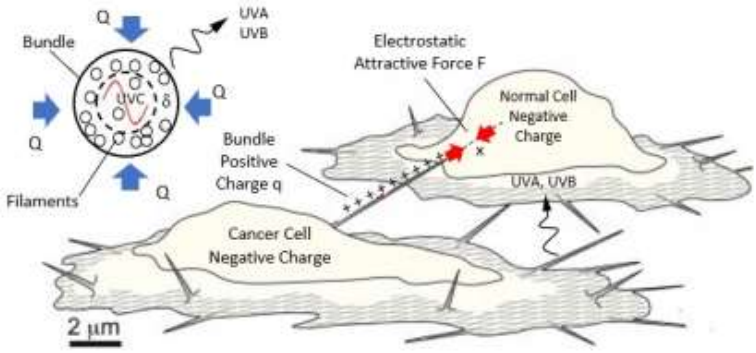


Figure 3. Electrostatic filopodia in metastasis of cancer cells to normal cells.

The simple QED analysis is based on the parameters of the electrostatic filopodia as shown in Fig. 3. A reference diameter d selected as, d = 70 mm to describe analysis parameters. Diameters d < 70 nm produce ionizing EM radiation in the UVC and beyond that upon absorption is shown to spontaneously create a net positive charge + q producing the electrostatic filopodia force F that translates the cancer cell toward the normal cells. Although less ionizing than UVC radiation, UVA and UVB are produced in bundles having d > 70 nm which do not charge the filopodia and are not involved in translational metastasis. Instead, UVA and UVB radiation emitted from the bundle initiates cancer by inducing DNA damage in adjacent normal cells, another form of metastasis.

**3.1 Simple QED**

Simple QED is a method [1] of nanoscale heat transfer that conserves heat with EM radiation instead of temperature. QED stands for quantum electrodynamics, a complex theory based on *virtual* photons advanced by Feynman and others. In contrast, simple QED is far simpler based on the Planck law that only requires the heat capacity of the atoms in nanostructures to vanish allowing conservation to proceed by the creation of *real* photons comprising EM waves standing across the nanostructure. Like electron orbitals, simple QED quantum states are size dependent based on the dimension of the nanostructure over which the EM waves stand.

By classical physics, the thermal kT heat capacity of the atom is independent of the EM confinement wavelength λ, where k is the Boltzmann constant and T absolute temperature. QM differs as the heat capacity of the atom decreases under EM confinement λ < 100 microns, and at the nanoscale for λ < 100 nm, the heat capacity may be said to vanish. The Planck law at 300 K is illustrated in Fig. 4.

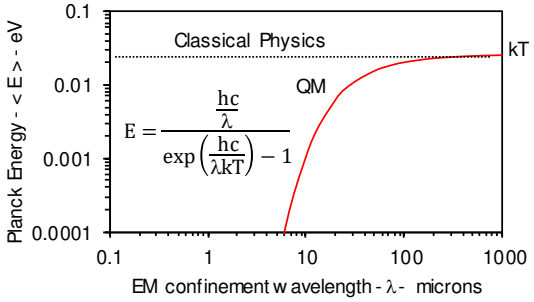


Figure 4. Planck law of the Atom at 300 °K
In the inset, E is Planck energy, h Planck's constant, c light speed, and λ EM wavelength

Unable to conserve the heat Q by a change in temperature, simple QED requires conservation of heat by the creation of EM radiation standing inside and across the bundle diameter d. The time τ to create the standing wave, τ = 2(d - 2δ)/(c/n), where the refractive index n of the actin corrects for the velocity c of light in the filament packed bundle. Since δ << d, τ ~ 2nd/c/n. Hence, the Planck energy E,

$$E = h/\tau = hc/2nd$$

having wavelength λ = 2nd as noted in Fig. 3 and illustrated in Fig. 5.

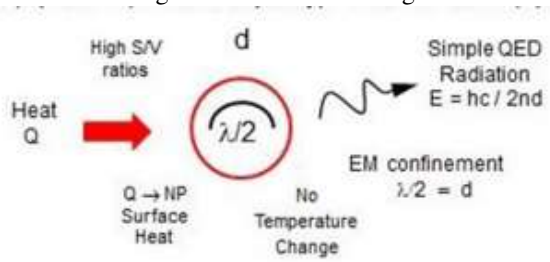


Figure 5. Planck energy of simple QED radiation in a NP

**3.2 Penetration Depth**

In the bundle, the EM confinement [1] occurred by the high surface-to-volume ratio of nanostructures that requires the thermal heat Q from the surroundings the heat itself as EM energy providing the brief EM confinement necessary to create half waves standing across the internal dimension 2(d - 2 δ) ~ 2d of the bundle, where δ is the penetration depth of the heat Q. For heat Q in the far IR having wavelength λ >> d, the absorption occurs in the penetration depth δ over the full surface noted in Fig. 3.

In this paper, simple QED is revised to not require a penetration depth δ as the Planck law precludes thermal energy Q in the nanostructure. Instead, simple QED spontaneously converts the heat Q to standing EM waves at the surface of the nanostructure. Unless the nanostructure is absorbent at wavelength λ = 2nd, the EM wave upon creation is free to be emitted to the surroundings.

**3.3 Electrostatic Charge**

The number Np of simple QED photons created in the 70 nm bundle have the same thermal energy U of all atoms in the in the bundle filaments, but not as temperature. Only non-thermal photons are allowed in the bundle as the Planck law precludes temperature at the nanoscale. The thermal energy U of the bundle is,

$$U = 3/2\ NKT$$

The volume V of a bundle is $V = \pi d^2 L/4$ and mass $W = \rho V$. Taking L = 1 nm and d = 70 nm, $V = 3.85 \times 10^{-24}$ m$^3$. For actin, $\rho = 1148$ kg/m$^3$ and $W = 4.42 \times 10^{-21}$ kg. The atomic weight of actin 536 gives the number of atoms $N = (W/536) \cdot Av \sim 5000$. For T = 300 K, the heat Q is the thermal energy $U = 3.10 \times 10^{-17}$ J ~ 200 eV/nm.

Simple QED conserves heat Q by creating standing EM radiation across the bundle diameter d having wavelength $\lambda = 2nd$, where n is the index of refraction of the filament actin. Taking DNA as representative of actin, the refractive index n = 1.5 at 400 nm [18] is *guessed* as n ~ 2 at $\lambda < 100$ nm. Hence, $\lambda \sim 280$ nm in the UVC having Planck energy E = 4.4 eV. The number Np of UV photons created is, Np = Q/E = ~ 45 UVC photons/bundle/nm.

The absorption spectrum for actin proteins (guanine, tryptophan) is taken from tubulin [19] as shown in Fig. 5.

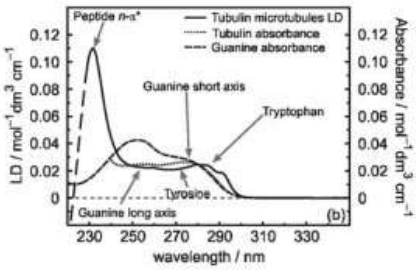


Figure 5. Near-UV absorbance tubulin spectrum

The UVC at 280 nm is absorbent and should produce q positive charge. Recall EUV (< 200 nm), UVC (200 to 280 nm), UVB (280 to 320 nm), and UVA (320 to 400 nm). Unlike UVC, the DNA absorbance vanishes for $\lambda > 300$ nm UVB and UVA radiation is not absorbed and charge q is not produced.

If the absorption of UVC is treated by Beer's law, the UVC may not be absorbed as the required absorption thickness is typically far greater than the nanoscale dimensions of the actin bundle. What this means is the heat Q on the surface of the bundle moving inward as standing EM wave is necessarily absorbed in the bundle before emission to the surroundings, i.e., Beer's law is not applicable as the UVC radiation is not passing through the bundle, but is created in the bundle.

**3.4 Electrostatic Force**

Analysis of the forces exerted by filopodia has been limited to theoretical considerations, while experimental analysis [8,9,14] has been limited to samples of isolated filaments by optical trapping a bead attached to a filament or a bundle of filaments. Measured forces range from 1 to 2 pN in isolated actin filaments and microtubules to ~ 1 nN in migrating keratocytes. The electrostatic force F between the tip of a positive charged +q filament of length L and a normal cell as a function of the separation x is illustrated in Fig. 6.

.

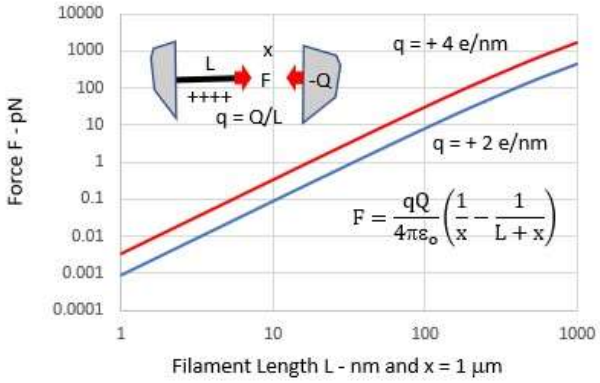


Figure 6. Cancer to normal cell attractive force at 1 □m separation

In Fig. 6, experiments in support of the electrostatic force F are not available. From Section 3.3, the positive charge density of q = + 2 e/nm for a single filament of length L interacting with a negative charged normal cell assumed to have negative charge Q = - q·L at distance x = 1 µm shows the force F of 1 - 2 pN is reached for x = 1 µm at linear charge at L ~ 60 nm. For the same x = 1 µm, the force F increases with L reaching the ~ nN level at L ~ 1.2 µm. From [14] with q = 4 e/nm, the force F is higher and similar.

## 4. Discussion

### 4.1 Charge density

In biophysics, it is well established [20] that like-charged macromolecules can aggregate under the influence of oppositely charged divalent ions, e.g., actin as an anionic rod-like polymer having a negative charge density $q_n$ = 4 e/nm. Unlike simple QED that creates positive charge, a linear distribution of positive counterions per unit length is assumed to allow like-charge attraction.

Calculated charge density [21] of $1.65 \times 10^5$ and $1.2 \times 10^5$ e/µm have been reported, although the number of filaments in an actin bundle are not clear. In this paper, the simple QED analysis of the 70 nm diameter bundle of 25 filaments absent counterions produced $0.45 \times 10^5$ UVC photons/µm or 45 UVC photons/nm.

Since each UVC photon produces 1 positive charge, and since about 25 filaments are included in typical bundle, about $q_p$ = 45 e/25 ~ 2 e /nm which is actually less than the intrinsic negative charge of $q_n$ ~ 4 e/nm predicted [14] for a single actin filament. What this means is the net $q_n$ charge, $q_{net} = q_p - q_n < 0$ and the attractive force between filaments does not occur. Instead, the filament overall is negatively charged. The $q_p$ charge is therefore localized heterogeneously at discrete atoms along the actin filament length [22] as illustrated in Fig. 7.

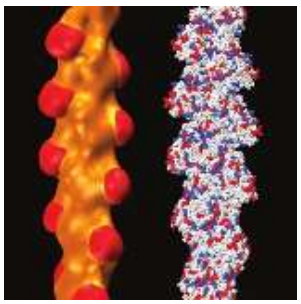

Figure 7. Heterogeneous charge distribution in actin filaments

Fig. 7 on the right is a high-resolution representation of F-actin. The interpretation [22] is negatively charged residues (red) and positive charged residues (blue) are small fractions of neutral residues (white). However, simple QED requires the dominant negative charged residue to neutralize the smaller UVC induced positive charge. Shown on the left is a low-resolution density actin map. The protrusions (red) are the highly negative charge regions thought to significantly modulate the positive counterion distribution. More study is suggested.

In contrast, the simple QED positive charges $q_p$ = 2 e/nm are insufficient to at least neutralize the filament by making the net charge $q_{net} \sim 0$. Alternatively, neutrality in the assembly of filaments to a bundle requires the net charge $q_{net}$ = 4 e/nm.

**4.2 Ambient thermal heat Q cycles**

The heat Q in creating the positive charge $q_p$ was assumed be the thermal U energy of the atoms that otherwise would have occupied the bundle at the temperature T of the surroundings. But once the heat Q is converted to 45 UVC photons/nm, the thermal energy U is regained to allow the cycle to repeat by generating an additional 45 UVC photons/nm, and so on *ad infinatum*. Hence, the net charge $q_{net}$ on the bundle continually increases until neutralized as the filopodia tip contacts the normal cell.

What this means is only 2 conversions of heat Q to 45 UVC photons/nm are necessary to neutralize the 25 filaments in the bundle, the next Q conversion producing a net charge/filament $q_{net}$ = 3x2 - 4 = 2 e /nm > 0 to provide an attractive force between the cancer and normal cells. Similarly, the assembly of filaments into a bundle only requires 2 conversions of heat Q into UVC photon achieve neutrality. Positive counter ions between adjacent filaments to offset natural acting negative charge are not necessary.

**4.3 Muscle Contraction**

Cancer mitosis by the simple QED continuous positive charging of filopodia is interrupted by neutralization upon contact with negatively charged extracellular matrix prior to eventually contacting normal cells. Similarity is found [23] in muscle contraction by the positive + charging of myosin and heads pulling the negative charged $\alpha$-actin in the Z-disks together as shown in Fig. 8.

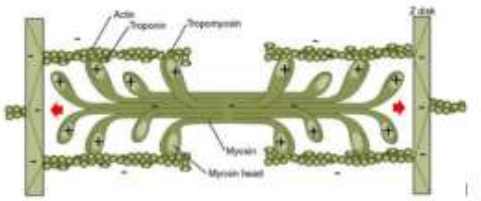


Figure 8. Electrostatic Muscle contraction

Muscle contraction is far more efficient than cancer mitosis not only because of the absence of the extracellular matrix, but more importantly as action potentials from the CNS are applied at the Z-disks that control when the muscle contraction begins. But like the filopodia filaments, simple QED is constantly charging positive the myosin and heads provided they are not in contact with the negative charged actin. The sequence in muscle contraction is shown in Fig. 9.

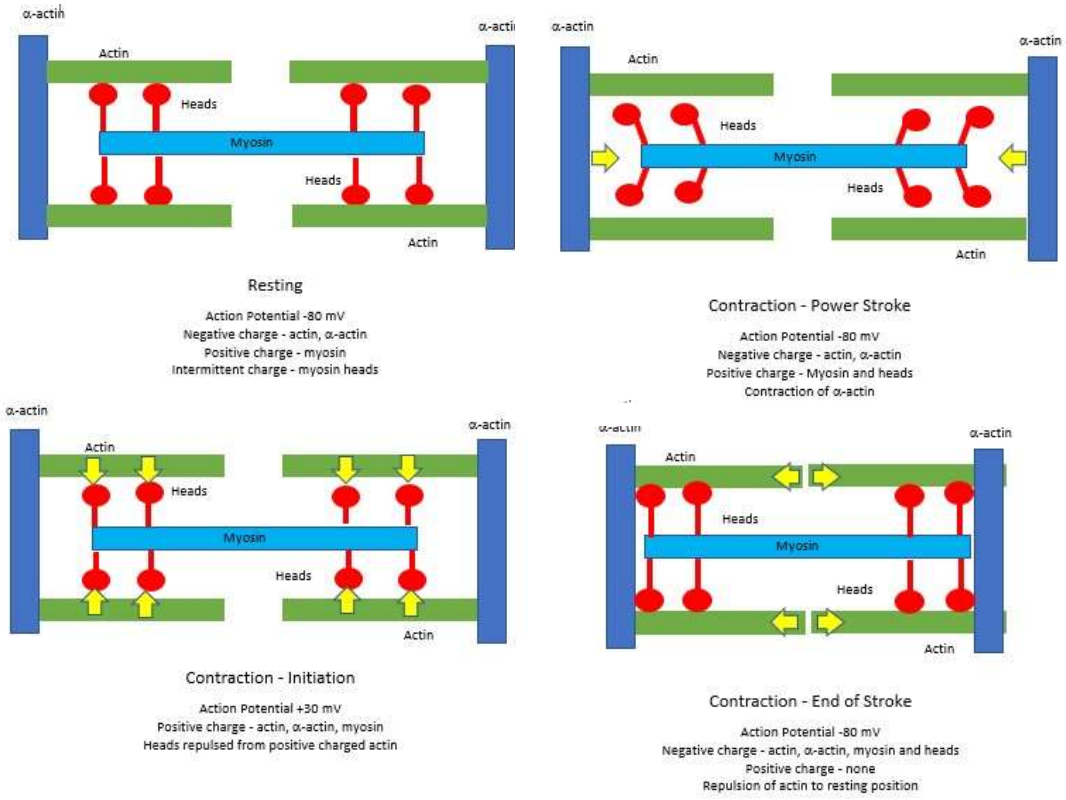


Figure 9. Muscle contraction controlled by Action Potentials

Fig. 9 shows the driving mechanism in muscle contraction is the persistent creation of simple QED radiation to charge the myosin and heads positive while the surroundings actin and α-actin remain negatively charged except during the momentary positive action potential. In muscle contraction, the myosin heads when not in contact with actin charge positive and during contact are acquire a negative charge. Only at the end of the power stroke as the myosin tip collides with the α-actin Z-disk do the myosin and heads acquire a negative charge of actin. Repulsion of the like-charged myosin and heads from the α-actin returns the muscle to the resting position

## 5. Conclusions

Metastasis of cancer by simple QED induced UVC emission produces positively charged filopodial bundles of filaments that electrostatically attract that the cancer to the negative charged normal cells including diversions to the extracellular matrix.

In bundles of 25 filaments, filopodia tips separated by 1 μm from a cancer cell in a filopodia having a net positive charge of +2 e/ nm produce electrostatic attractive force F > 2 pN for filament lengths > 100 nm.

In EVMM with cancer cells moving along the outside surface of blood vessels, the electrostatic attraction to the vessel wall is on the order of 2 pN/ μm.

Single filament filopodia not observed *in vivo* are only of academic interest. Instead, bundles of ~25 actin filaments should be the focus in cancer metastasis.

Simple QED creates UVC radiation producing positive charge in the filopodia bundles is a continuous process supplied by cycles of heating from the thermal surroundings until the tip contacts negatively charged normal cells or the extracellular matrix.

Single actin filaments are not positively charged because the number of atoms in a filament is insufficient to produce UVC radiation and is consistent with the long-standing notion of counterions to avoid like-charge repulsion and achieve neutrality in the assembly of filaments into bundles.

Unlike single filaments, assembly of 25 - 30 filaments having far more atoms produce UVC to allow assembly without the need of counterions to avoid like-charged repulsion, a notion that may be extended to actin polymerization thought to be a precursor to filopodia producing force.

The long-standing notion in biophysics that like-charged macromolecules can aggregate under the influence of oppositely charged counterions needs revision for larger numbers of macromolecules.

Single actin filaments thought to require counterions to avoid the like-like repulsion in assembly is not necessary as the number of atoms in a single filament simple QED induced positive charges cannot produce are produced bundles of 25 - 30 filaments.

Stalling of filopodia growth occurs as the bundle of filaments contact negatively charged extra cellular matrix fibers.

Neutrophil fibres having diameters ~50 nm emit simple QED induced EM radiation do indeed act as a bactericide to inactivate bacteria before reaching normal cells.

Simple QED of filopodia in cancer metastasis finds similarity with myosin bundles in muscle contraction. The basic difference is the direction of the electrostatic force from charging of myosin is well defined and controlled by action potentials from the CNS; whereas, the filopodia in cancer metastasis grow depending on the random directions of electrostatic attraction to negatively charged normal cells or the extracellular matrix.

**References**

1. Prevenslik T. (2020) Cancer: UVC in the Nanoparticle Treatment and Metastasis. See nanoqed.org, 2020.
2. Martin T. A., et al. (2013) Cancer Invasion and Metastasis: Molecular and Cellular Perspective. *Metastatic Cancer: Clinical and Biological Perspectives* edited by Rahul Jandial ©2013 Landes Bioscience.
3. Barnhill, R., Lugassy, C. (2004) Angiotropic malignant melanoma and extravascular migratory metastasis: description of 36 cases with emphasis on a new mechanism of tumour spread. Pathology 36:485–490.
4. Lugassy C., Barnhill R. (2014) Ultraviolet-radiation-induced inflammation promotes angiotropism and metastasis in melanoma. https://www.uclahealth.org/u-magazine/uv-light-aids-creeping-cancer-cells
5. Bald T., et al. (2014) Ultraviolet-radiation-induced inflammation promotes angiotropism and metastasis in melanoma. Nature 507:109–113.
6. Brinkman V., et al. (2004) Neutrophil Extracellular Traps Kill Bacteria. Science 303:1532. DOI: 10.1126/science.1092385.
7. Zawrotniak M., et al. (2019) UVA and UVB radiation induce the formation of neutrophil extracellular traps by human polymorphonuclear cells. Journal of Photochemistry & Photobiology B: Biology 196:111511
8. Cojoc D., et al. (2007) Properties of the Force Exerted by Filopodia and Lamellipodia and the Involvement of Cytoskeletal Components.
https://journals.plos.org/plosone/article?id=10.1371/journal.pone.0001072
9. Footer M.J., et al. (2007) Direct measurement of force generation by actin filament polymerization using an optical trap. PNAS: 2181–2186.

10. Haviv L., et al. (2008) Thickness distribution of actin bundles in vitro. Eur Biophys J., 37:447–454.
11. Lam W. Y., et al., (2019) HER2 Cancer Protrusion Growth Signalling Regulated by Unhindered, Localized Filopodial Dynamics. bioRxiv https://doi.org/10.1101/654988.
12. Oldham M., et al. (2016) X-Ray Psoralen Activated Cancer Therapy (X-PACT). PLoS ONE, 11: e0162078. doi:10.1371/journal.pone.0162078.
13. Haviv L., et al. (2008) Thickness distribution of actin bundles in vitro. Eur Biophys J 37:447–454.
14. Angelini T. E., et al. (2003) Like-charge attraction between polyelectrolytes induced by counterion charge density waves. PNAS 100: 8634–8637
15. Prevenslik T. (2019) ATP Synthesis by Endogenous UV Radiation. 10th Targeting Mitochondria Congress, October 27-29, 2019
16. Splettstoesser T., et al. (2011) Structural modeling and molecular dynamics simulation of the actin filament. Proteins, 79:2033–2043.
17. Bornscholgl T. (2013) How filopodia pull: What we know about the Mechanics and Dynamics of Filopodia. Cytoskeleton, 70:590-603.
18. Jung W., et al, (2017) Cationic lipid binding control in DNA based biopolymer and its impacts on optical and thermo-optic properties of thin solid films. Optical Materials Express 7: 3796.
19. Bulheller B. M., et al. (2007) Circular and linear dichroism of proteins. Phys. Chem. Chem. Phys., 7:2020–2035.
20. Sanders L. K., et al. (2007) Control of electrostatic interactions between F-actin and genetically modified lysozyme in aqueous media. Proc Natl Acad Sci USA. 104:15994–15999.
21. Cantiello H. C., et al. (1991) Osmotically induced electrical signals from actin filaments. Biophysical Journal 59:1284-1289.
22. Angelini T. E., et al. (2006) Counterions between charged polymers exhibit liquid-like organization and dynamics. PNAS 103: 7962–7967.
23. Prevenslik T. (2020) Electrostatic Muscle Contraction. See nanoqed.org, 2020.

# Endogenous UV in Warburg's Theory on the Origin of Cancer

**Abstract:** The Warburg theory on the origin of cancer proposed cancer cells undergo rapid growth by glucose fermentation upon the lack of oxygen for respiration. Once Watson and Crick discovered the DNA structure, Warburg' theory fell by the wayside to genetic explanations of cancer. But almost 70 years later, genetic theory has failed to locate the genes that explain the origin of cancer. In this paper, the Warburg theory is extended to include endogenous UV created by simple QED in peroxisomes as the cellular organelle fermenting glucose. Simple QED is a nanoscale heat transfer theory based on the Planck law that requires atoms in the nanoscale regions of the peroxisomes to conserve metabolic heat by creating endogenous UV radiation instead of increasing in temperature. Hence, high metabolic heat during rapid cancer growth produces intense endogenous UV that mutates DNA, a finding that Warburg lacking a source of UV could not explain. Geneticist argue the DNA mutations occur before rapid growth, but the mechanism is still not known. Moreover, endogenous UV in peroxisomes during fermentation allows ATP synthesis to proceed by UV enhanced dehydration instead of oxidation by chemiosmosis. Further, UV enhances glucose consumption and lactate production, but if blocked by metformin used in diabetes treatment lowers glucose consumption. Endogenous UV also activates the AKT pathway proposed for metabolic genes to control the conversion from oxidative metabolism to fermentation.

## I. Introduction

In 1956, Warburg proposed [1] cancer cells undergo glucose fermentation when oxygen is not available for respiration. Hence, cancer is caused as ATP is produced by non-oxidative breakdown of glucose by glycolysis. In contrast, healthy cells produce ATP from oxidative breakdown of pyruvate - the end-product of glycolysis. In effect, Warburg distinguished cancer cells from normal cells by the ratio of glycolysis to respiration.

Initially, Warburg's research showed sea-urchin eggs growth was fueled by oxygen consumption, but not for rat tumors that fueled their growth by consuming enormous amounts of glucose and breaking it down by fermentation. But Warburg tested human and other cancer tumors to find growth was also caused by fermentation during glucose consumption. How fermentation is initiated or how respiration is damaged leading to fermentation became the frontier of cancer research.

Given that cancer growth required energy, Warburg based subsequent research on how respiration and fermentation synthesized ATP, respiration measured by oxygen consumption and fermentation by the formation of lactic acid in the absence of oxygen. Since the respiration of all cancer cells is damaged, Warburg concluded whatever the cause it had to be gradual and irreversible as instant cell death would have stopped the cancer. Removal of oxygen causes cell damage and if then provided with oxygen, the damage is irreversible, allowing Warburg to conclude cells need respiratory energy to preserve structure, and if inhibited, both structure and respiration disappear. Even so, cancer growth not only includes irreversible damage of the respiration, but also an increase in the fermentation, the increase in fermentation compensating for the loss of respiration. But how does this increase of fermentation occur?

Warburg argued there is no physical or chemical agent with which the fermentation of cells can instantly initiate fermentation. Instead, a long time and many generations are necessary. The latency period to produce cancer is the time at which fermentation increases after a damaging of the respiration. For humans, the time is several decades. Indeed, the increase in fermentation takes a long time and only with many cell divisions. Because of this, there would be no cancers if there were no fermentation, and therefore it would be of great importance to know how fermentation occurs in the cell.

On structure and energy, Warburg thought respiration takes place in the structure of the mitochondria. Fermentation occurred in the protoplasm, but an organelle was not specified. The ATP synthesized by respiration in mitochondria involves more structure than that synthesized by fermentation. However, ATP is known synthesized in homogeneous solutions with crystallized fermentation enzymes. Like lower organisms, the structure of enzyme crystals is far less complex than mitochondria, i.e., respiration is connected to structure and fermentation with lack of structure. In this paper, fermentation takes place in peroxisomes having a far simpler structure than mitochondria.

With regard to Photodynamic Therapy (PDT), Warburg foretold the future of EM irradiation of tissue containing both normal and cancer cells. Normal cells survive PDT because of a higher residual respiration after irradiation. But descendants of the surviving normal cells may compensate the respiration decrease by fermentation increase and, thereby become cancer cells. Warburg concluded that radiation which kills cancer cells can also at the same time produce cancer - a lesson not yet learned by modern PDT research.

## II. PURPOSE

Extend Warburg's theory on the origin of cancer by proposing peroxisomes having a crystalloid core are the source of fermentation in the cell that synthesizes ATP by UV induced dehydration instead of oxidative phosphorylation by chemiosmosis. Reduced ATP production in respiration by damaged mitochondria is compensated by an increase in ATP from peroxisomes that leads to runaway cell growth. The core converts metabolic heat to UV radiation by simple QED, a nanoscale heat transfer [2] process. ATP fermentation by UV induced dehydration is similar to ATP synthesis in homogeneous solutions with crystallized fermentation enzymes.

## III. BACKGROUND

In the 1960's, the origin of life captivated biological research. Mitchell [3] proposed ATP synthesis in mitochondria followed hydrolysis given by chemiosmosis driven by the flow of H+ ions across the inner membrane. Chemiosmosis occurs by chain of complex redox reactions with electron transfer from donors to acceptors assisted by conveniently available enzymes. In contrast, Sagan et al. [4] proposed life on the early Earth began by a dehydration reaction under intense UV radiation and showed experimentally ATP was formed from ADP + Phosphate under UV. Nevertheless, ATP by hydrolysis and not UV dehydration was chosen the hallmark of modern molecular biology.

However, recent abiotic synthesis of nucleotides using UV radiation and phosphate to purify intermediates [5] supports polymerization of nucleotides into RNA, but requires high energy of which only UV radiation was indeed available on the early Earth. Nevertheless, the argument [6] is made that ionizing UV inherently destroys as much RNA as it creates and if UV was the primordial source of energy, why does no life today undergo ATP synthesis by UV radiation, thereby favoring chemiosmosis as an early bioenergetic process taking place alkaline hydrothermal vents.

Contrary to chemiosmosis, life on the early Earth recently was proposed [7] to have evolved from intense solar UV enhanced ATP synthesis by dehydration reactions as envisioned [4] by Sagan on the early Earth. UV does indeed destroy RNA, but not as much as it creates as the human species would not have populated the Earth. Indeed, survival drove mitochondria to evolve endogenous UV to replace solar UV upon ozone forming in the atmosphere. Today, the exogenous UV takes the form of EM waves standing between adjacent cristae as noted in Figure 2.

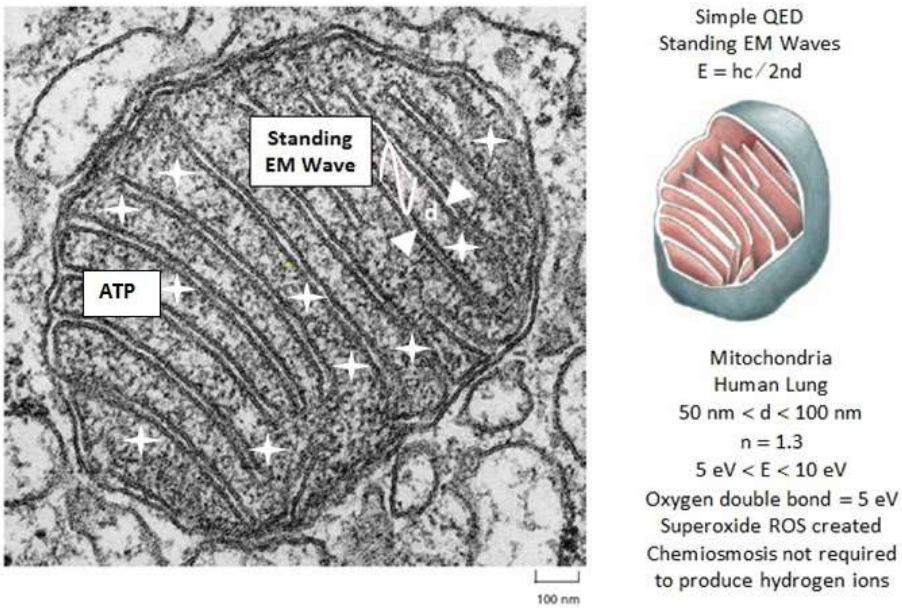


Figure 2. Human Lung Mitochondria
Showing ATP protecting DNA while providing heat source to EM standing wave

The EM wave standing in the mitochondria matrix [5] with a spacing d between adjacent cristae is defined by (50 < d < 100 nm). ATP molecules – white stars – are shown dispersed throughout the matrix. ATP binding is the likely heat source for simple QED to produce EM radiation. The Planck energy E of the standing EM waves based on a refractive index n ~ 1.4 is beyond the UV at 5 to 10 eV. The standing EM waves [3] are only shown between adjacent cristae with ATP synthase bound to lateral cristae surfaces in Figure 3.

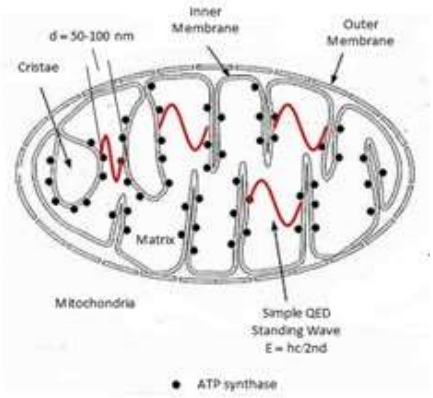


Figure 3. Standing EM waves between Cristae

Unlike exogenous UV from solar radiation, the UV radiation is endogenous to the mitochondria following the nanoscale heat transfer process of simple QED that converts [6] metabolic heat to EM radiation instead of temperature. Simple QED is based on the Planck law of quantum mechanics that denes atoms in nanostructures the heat capacity to conserve heat by a change in temperature. Hence, metabolic heat in human lung mitochondria having

nanoscopic spaces < 100 nm between adjacent cristae create EM radiation > 5 eV that produce ATP by the dehydration reaction,

$$ADP + Pi + UV \rightarrow ATP + H_2O$$

where, Pi is a phosphate group. However, Nature most likely did not choose chemiosmosis as the mechanism for ATP synthesis as a more direct path is UV enhanced dehydration, thereby avoiding complex sequential electron chain reactions that require specific enzymes to be instantly available at each step to create electrons that pass from one electron carrier to the next. Indeed, ATP synthesis is simply more direct by UV assisted dehydration reaction.

## IV. Simple QED

Simple QED is a method of nanoscale heat transfer analysis that conserves heat with EM radiation instead of temperature. QED stands for quantum electrodynamics, a complex theory based on virtual photons advanced by Feynman [8] and others. In contrast, simple QED is a far simpler theory based on the Planck law that requires the heat capacity of the atoms in nanostructures to vanish allowing conservation to proceed by the creation of real photons comprising EM waves that stand within and across the nanostructure. Unlike electron level quantum states, simple QED quantum states are size dependent based on the dimension of the nanostructure over which the EM waves stand.

The Planck law at 300 K is illustrated in Fig. 4. By classical physics, the kT heat capacity of the atom is independent of the EM confinement wavelength λ, where k is the Boltzmann constant and T absolute temperature. QM differs as the heat capacity of the atom decreases under EM confinement λ < 100 microns, and at the nanoscale for λ < 100 nm, the heat capacity may be said to vanish.

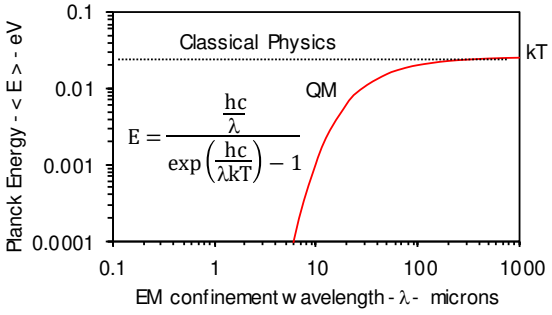


Fig. 4: Planck law of the Atom at 300 °K
In the inset, E is Planck energy, h Planck's constant, c light speed,
k Boltzmann's constant, T temperature, and λ the EM confinement wavelength

EM confinement occurs by the high surface-to-volume (S/V) ratio of nanostructures that requires the heat Q to almost totally be confined in the surface, the surface heat itself as EM energy providing the brief EM confinement necessary to create EM waves standing across the internal dimension d of the nanostructure. Specifically, heat or light having wavelength $\lambda >> d$, the light (yellow) immerses the NP and is absorbed in penetration depth $\delta$ over the full NP surface as shown in Figure 5.

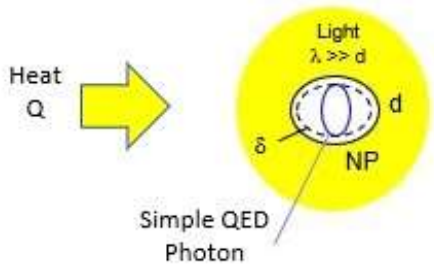


Figure 5. Heat Q absorbed in NP surface

Confinement of the light Q while creating the UVC standing wave requires EM confinement at least equal to the Planck energy E of the light. The pressure P acting on the surface is given for bulk modulus B and volume strain $\Delta V/V$ by, $P = B \cdot \Delta V/V = 6\delta B/d$. But $P = E / V = 6E/\pi d^3$ giving $\delta = Q/\pi B d^2$. For NPs, a typical absorption depth $\delta$ of a single UVC photon is $\delta \sim 0.2$ fm, a small but necessary depth necessary to confine the absorbed heat to the geometry of the standing wave.

Simple QED absorbs heat Q in the NP surface given by the penetration $\delta$ depth. Unable to conserve the surface heat by a change in temperature, conservation requires the creation of simple QED radiation, the time $\tau$ to create the standing wave, $\tau = 2d/(c/n)$. The Planck energy $E \sim h/\tau = hc/2nd$ depends on the refractive index n of the NP to correct for the velocity c of light within the NP. The simple QED Planck energy E is quantized by the dimension d of the NP that defines the half-wavelength $\lambda/2$ of the nanostructure. Fig. 6 illustrates the standing EM radiation in a spherical NP of diameter d, but NP atoms still follow their quantized electron energy levels.

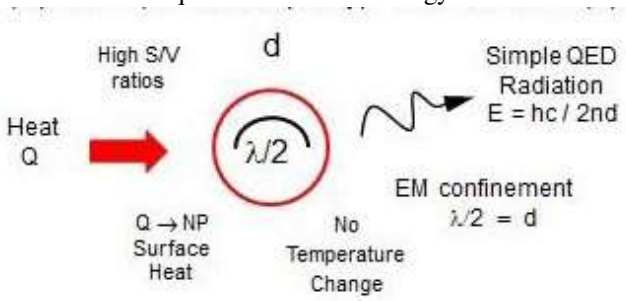


Fig. 6: Planck Energy of EM Radiation

In a rectangular NP with different dimensions of width, thickness, and length there are 3 simple QED quantum states corresponding to the different dimensions of the NP. However, only the minimum dimension is important as by Fermat's principle, the absorbed heat is dissipated in minimum time. Continuous variation in internal nanostructure dimensions produces a broadband spectrum of simple QED dissipated in continuous QED quantum states. Historically, the notion of size dependent quantum states is not found in the literature.

## V. ANALYSIS

Similar to mitochondria, peroxisomes synthesize ATP by UV enhanced dehydration. The peroxisomes [9] differ from spaced cristae in that are spherical < 1 μm membrane enclosed organelle containing catalase including a randomly disposed irregular < 100 nm crystalized electron-dense urate oxidase core as shown in Figure 7.

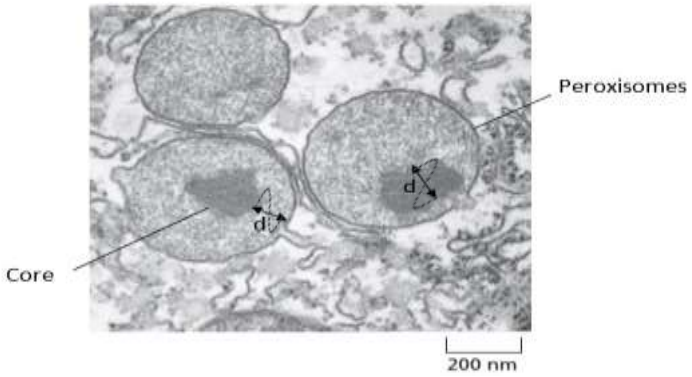


Figure 7. Peroxisomes containing crystalized cores

Not all peroxisomes contain cores. Figure 7 shows 3 peroxisomes, 2 of which contain cores and the other absent core. Unlike mitochondria with spaces between cristae, peroxisomes induce UV radiation characterized by the dimensions d representing the wavelength $\lambda = 2nd$ between irregular surfaces in the core, and between surfaces of the core and the membrane.

In applying simple QED, the peroxisome core and glucose in the space between the core and membrane have dimensions d < 100 nm. The index of refraction for the core is taken as n ~ 1.5 similar [10] to the index of the HIV-1 virus particle and for the space n = 1.333 similar to water. For UVC ($\lambda$ = 254 nm), the respective dimension d ~ 85 and 95 nm. The core UV emission is relatively constant, but the space changes with time giving broadband UV.

## IV. DISCUSSION

### Historical timeline

Warburg's theory of cancer [1] was published in 1956 before Mitchell's [2] discovery of chemiosmosis. In 1956, Warburg commented the chemical reactions where ATP is synthesized in respiration are still unknown, whereas the ATP fermentation reaction by which ADP is phosphorylated to ATP was discovered [11] in 1939. However, Warburg's ATP reaction based on an intermediate was questioned by Meyerhof' [12] who showed the intermediate was not necessary. Even so, the intermediate to ATP by fermentation could not be found, the consequence of which led to Mitchell's discovery of chemiosmosis in the 1960's.

In this historical timeline, endogenous UV activated ATP synthesis by dehydration [7] is proposed to supersede chemiosmosis in mitochondria.

### ATP synthesis

Like mitochondria, peroxisomes are major sites of oxygen utilization. It is thought [9] mitochondria made peroxisomes obsolete because oxidation carried out in peroxisomes without producing ATP was replaced in mitochondria because ATP was produced by chemiosmosis. Today, mitochondrial oxidation is thought to produce ATP, but oxidation alone in peroxisomes [13] does not synthesize ATP.

However, neither latter statements are valid as simple QED induces endogenous UV allowing ATP synthesis in mitochondria [7] to be extended to ATP synthesis in peroxisomes. In mitochondria, the UV is created in the spaces between cristae shown in Figure 2; whereas in peroxisomes, the UV is created in the core and the space between the core and membrane as shown in Figure 7. Both mitochondria and peroxisomes produce endogenous UV powered by metabolic heat.

### Glucose in ATP synthesis

Meyerhof's laboratory [1] showed glycolysis in the cytosol caused the breakdown of carbohydrates to lactic acid and provided evidence that ATP synthesis was the byproduct of glucose. Biochemists today know both respiration and fermentation produce ATP, but peroxisomes lacking an oxidative electron transfer chain (ETC) are thought [14,15] to produce small amounts of ATP by fermentation. Indeed, oxidation in peroxisomes [14] does not make ATP, and instead releases heat energy.

In contrast, metabolic heat [7] produces endogenous UV in both mitochondria and peroxisomes, but the UV level and wavelengths differ because of organelle structure. Literature supporting UV enhancement of glycolysis is limited to the skin exposed to solar radiation, but suggests dendritic cells [16] irradiated with UVB (280 to 320 nm) produced more lactate, consumed more glucose, and had greater glycolytic flux.

### Peroxisomes function

It generally thought [17] that without peroxisomes there could be no way for cells to produce peroxides necessary for metabolism, but peroxides are also toxic and there could not be any way to rid peroxides from the body. However, simple QED refutes this argument as hydrogen peroxide may be produced and detoxified by endogenous UV. Indeed, simple QED creates endogenous UV in peroxisomes and reacts with water to create hydroxyl radicals and hydrogen ions.

$$H_2O + UV \rightarrow OH^- + H^+$$

Upon UV reacting with oxygen, the superoxide anion is formed and combining with hydroxyl radicals form hydrogen peroxide.

$$O_2 + UV \rightarrow O_2^- \rightarrow \quad O_2^- + 2OH^- \rightarrow H_2O_2$$

The anti-oxidant catalase in peroxisomes is thought [15] to convert hydrogen peroxide to water. But catalase is not required as UV can directly split hydrogen peroxide into hydroxyl radicals.

$$H_2O_2 + \text{Catalase} \rightarrow H_2O \rightarrow H_2O_2 + UV \rightarrow 2OH^-$$

Endogenous UV in peroxisomes is sufficient to both produce and detoxify hydrogen peroxide without conveniently available catalase and other enzymes.

**Fatty acid β oxidation**

Mitochondria and peroxisomes both play major roles in cell metabolism, especially in fatty acid metabolism, ROS production and scavenging, and now are considered to metabolically [18] interact with each other.

Peroxisomes are involved in the β oxidation of long chain fatty acids to acetyl CoA, a process that is not possible in mitochondria. The breaking of single and double carbon bonds along the fatty acid backbone require UV energies of 3.6 and 6.3 eV, but UVC energy of 4.88 eV is not sufficient to break carbon double bonds. UV at 200 nm is required that is obtained by simple QED in peroxisome core and space at d ~ 67 and 75 nm, respectively.

Unlike mitochondrial oxidation which produces ATP, oxidation in peroxisomes is claimed [19] to not make ATP and only release heat energy. However, this claim is incorrect as simple QED induces ATP synthesis by UV enhanced dehydration in peroxisomes.

**Cancer - Genetics vs. Energy**

In the early 20th century, Sutton and Boveri [20] are credited with linking Mendel's production of gametes in peas with the behavior of chromosomes at meiosis. Boveri proposed the genetic origin of cancer based on the observation that fertilized sea-urchin eggs with two sperm instead of one having the wrong number of chromosomes later developed deformations. In the 1920's, Warburg proposed the cancer metabolism theory [1] that cells fueled by the energy of rapid growth developed deformities. Warburg's theory was independent of chromosomes describing cancer in terms of rapid metabolic growth utilizing fermentation of glucose initiate by a loss of oxygen in the cell, a theory that prevailed over genetic theory over several decades.

In 1953, Watson and Crick's structure of the DNA became the hallmark of molecular biology's gene-centered approach to cancer as a disease governed by mutated genes driving cells into a state of rapid division and proliferation. Since then, Warburg's cancer metabolism theory based on genetic mutations as the consequence of rapid cell growth was rejected with the opposite of rapid cell growth as the consequence of genetic change.

Recently, there has been a revival [21] in Warburg's theory on cancer metabolism because for over 70 years genetic research to stop cancer growth has been generally not successful. Today, the causal link between genetics as the cause of cancer metabolism appears unlikely. In 2016, an older Watson who with Crick initiated DNA structure as the control of living organisms is reportedly [21] stated that locating the genes that cause cancer is a cruel illusion. In so doing, Watson himself suggested a revival in Warburg's cancer metabolism, but still unanswered is the question of what causes the cell to activate the Warburg effect leading and cancer.

Warburg thought that rapid cancer growth was caused by defects in normal cells that reduced the available oxygen for oxidative metabolism in respiration necessary for ATP production, the lack of oxygen requiring the cell to use fermentation of glucose to maintain ATP levels, but a genetic basis was never invoked. In fact, Warburg [1] believed the origin of cancer can only be explained by physics and chemistry, and therefore mutation and carcinogenic agents are empty words, unless having a metabolic base.

Warburg's statement [1] that no physical or chemical agent can instantly initiate fermentation requires clarification. UVC and even UVB induce DNA mutations by promptly kill the cell, but lower UVA energy cannot. By simple QED, UVA energy accumulates until UVB levels in the electronic state are reached over time, a process not possible classically as UVA energy is dissipated by increasing temperature. Hence, UVA requires a delay of mutations in nanoscale regions of peroxisomes. Indeed, mutations in Chinese hamster fibroblasts [22] may be delayed many cell generations after UVA.

As though heeding Warburg, a few genetic scientists [21] have recently questioned whether cancer genes in DNA are in fact the source of rapid growth of cancer, and following Warburg's cancer metabolism suggested instead that metabolic genes in DNA were the origin of rapid consumption of nutrients and cancer growth. Without conceding to Warburg's defect of lack of oxygen initiating growth as the basis for cancer, the genetic scientists simply argued that instead of cancer genes, rapid cancer growth was caused by a DNA mutation of metabolic genes controlling consumption of nutrients.

In this controversy, DNA metabolic genes in the AKT pathway [23] need to be activated to undertake a metabolic conversion from oxidative phosphorylation to anaerobic glycolysis, initiate rapid cancer growth when mitochondria are deprived of oxygen. But the direct UV activation [24] of the AKT pathway is excluded in favor of complex chemistry. By extending Warburg to include simple QED induced UV produced in peroxisomes, the AKT pathway is activated, but may not be necessary as ATP is also produced in peroxisomes.

Metabolic genes aside, simple QED induced UV from peroxisomes enhances glucose consumption. As described above, UV irradiated mice are known [16] to produce more lactate, consume more glucose, and had greater glycolytic flux. By Warburg, cancer may be stopped by removing the glucose necessary for fermentation, and in effect, drugs blocking peroxisome UV from glucose lower fermentation. In this regard, metformin [25] used by diabetics may be used to treat cancers by absorbing peroxisome UV. The UV absorption of metformin and sitagliptin (another diabetic drug) are shown in Figure 8.

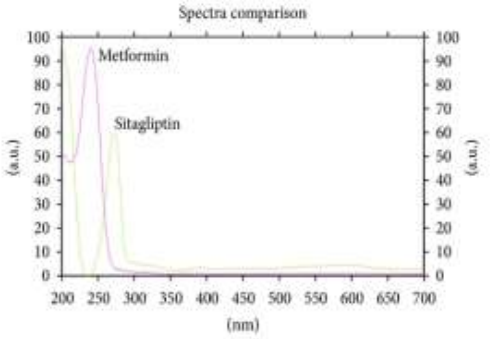


Figure 8. UV absorption of Metformin and Sitagliptin

The UV absorption peak for glucose [26] is 260-270 nm which is in the sharp decreasing region of metformin. But glucose metabolism from UV produced in peroxisomes is still blocked. Sitagliptin would appear optimum in blocking glucose metabolism. But cancer is likely to find a pathway other than glucose for peroxisomes to fuel cancer growth, e.g., glutamine and fatty acids.

## V. CONCLUSIONS

Warburg's theory that cancer develops every time cells in respiration are deprived of oxygen for a sufficient period of time followed by fermentation by anaerobic glycolysis. In this paper, the Warburg theory is paraphrased:

> In a cell, cancer develops as runaway UV enhanced fermentation in peroxisomes cannot compensate for the loss of oxygen of respiration in mitochondria.

Warburg's theory modified to include endogenous UV in peroxisomes produced by the simple QED conversion of rapid metabolic heating explains the DNA mutations observed in cancer cells after rapid growth, a claim Warburg lacking a UV source could not make.

Warburg foretold the future of EM irradiation of tissue containing both normal and cancer cells. Normal cells survive PDT because of a higher residual respiration after irradiation concluding that radiation which kills cancer cells can also at the same time produce cancer - a lesson not yet learned by modern PDT research.

On the latency period to produce cancer, Warburg argued there is no physical or chemical agent by which the fermentation of cells can occur instantly, the latency period corresponding to the time at which fermentation increases after damaging. However, DNA mutagens from endogenous UVA produced in peroxisomes do delay fermentation.

Endogenous UV enhances glycolysis by increasing glucose consumption, lactate rate, and glycolytic flux. Conversely, diabetic drugs metformin and sitagliptin that block UV from glucose decrease fermentation and by Warburg reduce cancer growth.

DNA metabolic genes in the AKT pathway are activated by endogenous UV to make the metabolic conversion from oxidative phosphorylation to anaerobic glycolysis, but may not be necessary ATP is produced from dehydration synthesis.

The argument: "Without peroxisomes there could be no way for cells to produce peroxides necessary for metabolism, but peroxides are also toxic and there could not be any way to rid peroxides from the body" is false. Endogenous UV can both produce and rid peroxides.

Peroxisomes involved in the β oxidation of long chain fatty acids to acetyl CoA, a process that is not possible in mitochondria. The breaking of single and double carbon bonds along the fatty acid backbone require UV energies of 3.6 and 6.3 eV. UVC energy of 4.88 eV is not sufficient to break carbon double bonds, but simple QED can produce UV at 200 nm in peroxisomes.

Geneticists who agree with Warburg on the mechanism of metabolism cancer argue that metabolic gene mutations still explain cancer. But explanations of detailed mutation mechanisms are complex including the availability of convenient enzymes to complete chemical equations, i.e., empty words as mutations are far too complex.

Instead, any and all mutation mechanisms to explain cancer are proposed explained by Warburg's cancer theory extended to include endogenous UV.

The controversy between Warburg and geneticists on the origin of cancer is not resolved by endogenous UV. But endogenous UV raises Warburg's cancer metabolism to the level that the search for a metabolic gene initiating cancer may no longer be important.

**References**

[1] Warburg O. (1956). On the Origin of Cancer Cells. Science 123, 309-314.

[2] Prevenslik T. Applications of Simple QED. See www.nanoqed.org, 2010-2020.

[3] Mitchell P. (1961). Coupling of phosphorylation to electron and hydrogen transfer by a chemiosmotic type of mechanism. Nature, 191, 144–148.

[4] Ponnamperuma, C., et al. (1963). Synthesis of Adenosine Triphosphate under possible primitive Earth conditions. Nature 199, 222

[5] Powner MW, Gerland, B, Sutherland JD. (2009). Synthesis of activated pyrimidine ribonucleotides in prebiotically plausible conditions. Nature 459: 239–42.

[6] Lane N, Allen JF, Martin W. (2009) How did LUCA make a living? Chemiosmosis in the origin of life. BioEssays 32:271–280'

[7] Prevenslik T. ATP Synthesis by Endogenous UV Radiation. 10th Congress Targeting Mitochondria, Oct. 28-29, 2019 - Berlin, Germany.

[8] Feynman R. QED: The Strange Theory of Light and Matter. Princeton University Press, 1976.

[9] Alberts et al. Molecular Biology of the CELL, 5th Edition, Taylor Francis 2008.

[10] Pang Y, Song H, Gheng W. (2016) Using optical trap to measure the refractive index of a single animal virus in culture fluid with high precision. Biomedical Optics Express. 7:1672-1689.

[11] Warburg, O., and Christian, W. (1939) Biochem. Z. 303, 40

[12] Kresge N, Simoni RD, Hill RL. (2005) Otto Fritz Meyerhof and the Elucidation of the Glycolytic Pathway. J. Biol. Chem. 280:e3.

[13] Lodish HF, et al. (2016) Molecular Cell Biology. 8th edition New York: W.H. Freeman Macmillan Learning. 2016.

[14] Glycolysis: regulation, processes, and diseases / editor, Paul N. Lithaw. Chapter 2. Nova Science Publishers, New York 2009.

[15] Peskin, BS. The Cancer-Hypoxia/Decreased Respiration-Glycolysis Connection. In: Glycolysis: Regulation, Processes and Diseases. Editor: Paul N. Lithaw © 2009 Nova Science Publishers, Inc.

[16] McGonigle TA, et al. (2017) UV Irradiation of Skin Enhances Glycolytic Flux and Reduces Migration Capabilities in Bone Marrow Differentiated Dendritic Cells. The American Journal of Pathology, 187:2046-2059.

[17] Peroxisomes and disease. https://www.1sthealthinsurancequotes.com/peroxisomes.html

[18] Demarquoy J, Le Borgne F. (2015) Crosstalk between mitochondria and peroxisomes. World J Biol Chem. 6: 301-309.

[19] Beta Oxidation of Very Long Chain Fatty Acids https://smpdb.ca/view/SMP0000052

[20] Martins LA-CP. (1999) Did Sutton and Boveri Propose the So-Called Sutton-Boveri Chromosome Hypothesis? Genetics and Molecular Biology, 22: 261-271.

[21] Apple S. (2016) An Old Idea, Revived: Starve Cancer to Death New York Times Health Issue May 12.

[22] Dahle J, Kvam E. (2003) Induction of Delayed Mutations and Chromosomal Instability in Fibroblasts after UVA-, UVB-, and X-Radiation. Cancer Research 63: 1464–1469.

[23] Plas DR, Thompson CB. (2005) Akt-dependent transformation: there is more to growth than just surviving. Oncogene 24:435–7442.

[24] Huang C, et al. (2001) UV Induces Phosphorylation of Protein Kinase B (Akt) at Ser-473and Thr-308 in Mouse Epidermal Cl 41 Cells through Hydrogen Peroxide. J. Biological Chemistry 276: 40234–40240.

[25] Kasznicki J, Sliwinska A, Drzewoski. (2014) Metformin in cancer prevention and therapy. Ann Transl. Med. 2:57-68.

[26] Kaijanen L, et al. (2015) Ultraviolet Detection of Monosaccharides: Multiple Wavelength Strategy to Evaluate Results after Capillary Zone Electrophoretic Separation Int. J. Electrochem. Sci., 10: 2950 - 2961.

# Broadband endogenous UV in Mitochondria

**Abstract**

In the 1960's, the hallmark of molecular biology was Mitchell's discovery of ATP synthesis in mitochondria by chemiosmosis based on oxidative phosphorylation across the inner membrane through a chain of complex redox reactions with electron transfer from donors to acceptors assisted by enzymes. But consistent with Sagan's finding that mitochondria evolving on the early Earth under intense solar UV radiation, ATP synthesis more likely occurred by UV enhanced dehydration reactions of ADP and phosphate instead of redox reactions by hydrolysis. Under constant UV absorption over time, mitochondria naturally evolved nanoscale spaces between cristae tissue similar to the half-wavelengths of the absorbed solar UV radiation. Upon ozone forming in the atmosphere, solar UV was significantly reduced, and for survival mitochondria utilized the cristae spaces to produce their own endogenous UV source. But cristae spaces alone do not produce UV radiation. Recently, metabolic heat within mitochondria was proposed to produce UV standing between adjacent cristae by the process of simple QED, a nanoscale heat transfer process that conserves heat by creating EM radiation instead of increasing in temperature. To allow UV excitation of diverse molecules, the UV standing between adjacent cristae is extended to broadband UV comprising standing UV over a number of nearby cristae in *drosophila* and human lung species. However, the specific UV wavelength which optimizes UV enhanced ATP synthesis of mitochondria species must be determined by experiment.

## I. INTRODUCTION

In the 1960's, the origin of life captivated biological research. Mitchell proposed [1] ATP synthesis in mitochondria followed hydrolysis given by chemiosmosis and driven by the flow of H+ ions across the inner membrane. Chemiosmosis occurs by chain of complex redox reactions with electron transfer from donors to acceptors assisted by conveniently available enzymes. In contrast, Sagan et al. [2] proposed life on the early Earth began by a dehydration reaction under intense UV radiation and showed experimentally ATP was formed from ADP + Phosphate under UV. Nevertheless, ATP by hydrolysis and not UV dehydration was chosen the hallmark of modern molecular biology.

However, recent abiotic synthesis of nucleotides using UV radiation and phosphate to purify intermediates [3] supports polymerization of nucleotides into RNA, but requires high energy of which only UV radiation was available on the early Earth. Nevertheless, the argument [4] is made that ionizing UV inherently destroys as much RNA as it creates and if UV was the primordial source of energy, why does no life today undergo ATP synthesis by UV radiation, thereby favoring chemiosmosis as an early bioenergetic process taking place alkaline hydrothermal vents.

Contrary to chemiosmosis, life on the early Earth recently was proposed [5] to have evolved from intense solar UV enhanced ATP synthesis by dehydration reactions as envisioned [2] by Sagan on the early Earth. Mitochondria likely evolved endogenous UV to replace solar UV upon ozone forming in the atmosphere. Today, the exogenous UV takes the form of EM waves standing between adjacent cristae as noted in Figure 1.

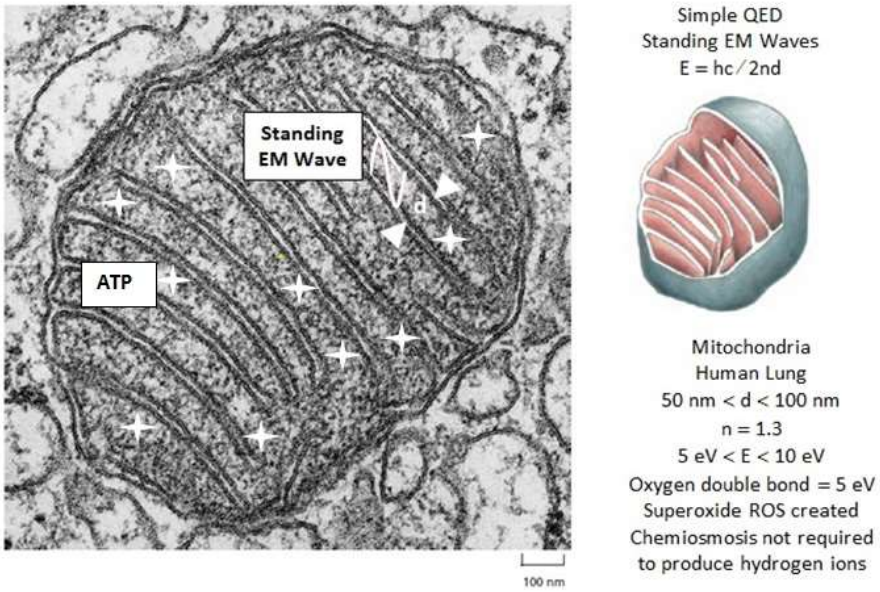


Figure 1. Human Lung Mitochondria
Showing ATP protecting DNA while providing heat source to EM standing wave

The EM wave standing in the mitochondria matrix [5] with a spacing d between adjacent cristae is defined by ($50 < d < 100$ nm). ATP molecules – white stars – are shown dispersed throughout the matrix. ATP binding is the likely heat source for simple QED to produce EM radiation. The Planck energy E of the standing EM waves based on a refractive index $n \sim 1.3$ is beyond the UV at 5 to 10 eV. The standing EM waves [3] are only shown between adjacent cristae with ATP synthase bound to lateral cristae surfaces in Figure 2.

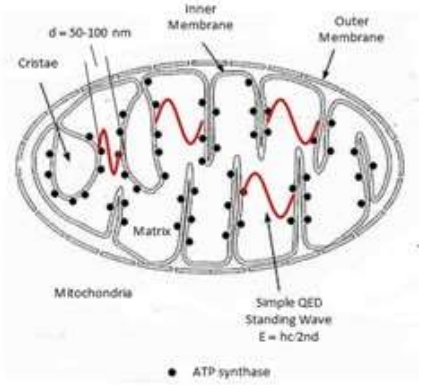


Figure 2 Standing EM waves between Cristae

Unlike exogenous UV from solar radiation, the UV radiation is endogenous to the mitochondria following the nanoscale heat transfer process of simple QED that converts [6] metabolic heat to EM radiation instead of temperature. Simple QED is based on the Planck law of quantum mechanics that denes atoms in nanostructures the heat capacity to conserve heat by a change in temperature. Hence, metabolic heat in human lung mitochondria having nanoscopic spaces < 100 nm between adjacent cristae create EM radiation > 5 eV that produce ATP by the dehydration reaction,

$$\mathrm{ADP + Pi + UV \rightarrow ATP + H_2O}$$

where, Pi is a phosphate group. However, Nature most likely did not choose chemiosmosis as the mechanism for ATP synthesis as a more direct path is UV enhanced dehydration, thereby avoiding complex sequential electron chain reactions that require specific enzymes to be instantly available at each step to create electrons that passed from one electron carrier to another. Alternatively, ATP synthesis is simply more direct by UV assisted dehydration reaction

Although dehydration reaction by UV is simpler than chemiosmosis, the difficulty is UV damages DNA directly, and indirectly by creating reactive oxygen species (ROS). In this regard, chemiosmosis also creates ROS by errant interaction with oxygen along the electron chain of reactions. But ROS is not a problem as mitochondria release ATP to protect against UV damage, i.e., the ability of ATP to protect mitochondria [7] allows both chemiosmosis and dehydration reactions to proceed during UV radiation. Regardless, Nature took advantage of the simplicity of UV induced ATP synthesis over chemiosmosis to sustain life at the expense of expending some ATP in protecting the mitochondria.

In mitochondria, ATP synthesis of human lung was based on simple QED induced [5] endogenous UVC radiation between adjacent cristae having spacings 50-100 nm as noted in Figure 1. But mitochondria of fruit fly *Drosophila* have [8] far smaller cristae spacings of the matrix at 13 nm with cristae width of 17 mn as shown in Figure 3.

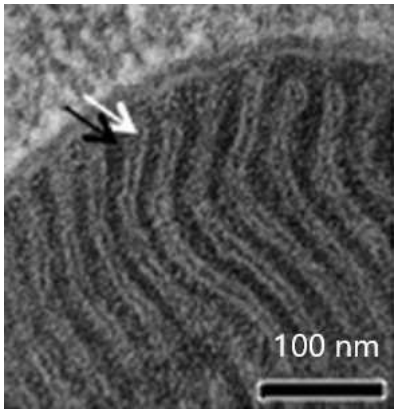


Figure 3. Mitochondria *Drosophila* Cristae
White arrow, cristae 17 nm; black arrow, matrix 13 nm

The problem is *Drosophila* having adjacent cristae spacings of 13 nm induce standing simple QED induced EM radiation in the EUV >> UVC and can only enhance ATP synthesis by fluorescing down to UVC levels. However, fluorescence is inefficient. It is therefore desirable to have the EM waves stand over longer spacings to produce broadband UV to not only enhance ATP synthesis with UVC, but also process the synthesis of ~1500 proteins necessary in maintaining diverse cell functions.

## II. PURPOSE

The purpose of this paper is to extend ATP synthesis by UVC radiation standing between adjacent cristae to multiple nearby cristae in producing broadband UV spectrum.

## III. ANALYSIS

The molecular arrangement of ATP synthase dimers on cristae from bovine heart, potato, and three types of fungi [9,10] comprising long rows of ATP synthase dimers on tightly curved cristae tips were found conserved in all species studied. Proton pumps of chemiosmosis theory [1] were arranged on flat cristae surfaces as illustrated with attendant protons in Figure 4.

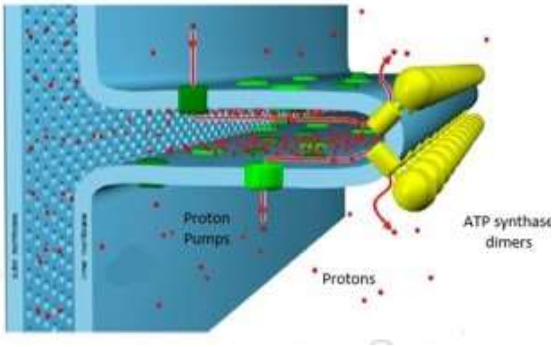


Figure 4. ATP synthase dimers on Cristae tips

By chemiosmosis, the ATP synthase forms yellow dimer rows at the cristae tips, the green proton pumps of the electron transfer chain pump red protons into the cristae space that flow back into the matrix through the ATP synthase rotor to produce ATP. But UV enhanced ATP synthesis differs as red EM radiation stands in the matrix between adjacent dimers shown in Figure 5.

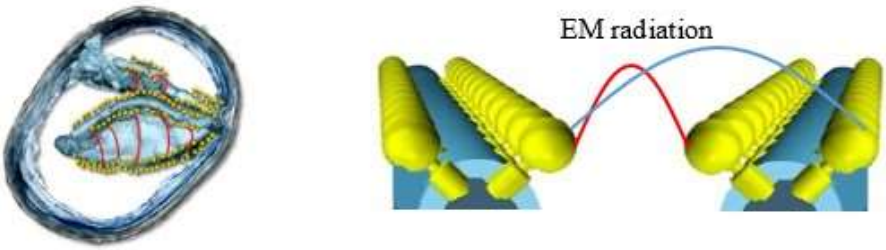


Figure 5. Standing EM radiation in Matrix between dimers of adjacent Cristae

In chemiosmosis, dimers arranged along tip of cristae serves no purpose as the dimers and proton pumps could just as well be located on the flat cristae surfaces. Figure 5 depicts the importance of the dimers in UV enhanced ATP synthesis in that the dimer heads on adjacent cristae closest each other uniquely define the nodes of red standing EM radiation across the matrix instead of the geometrically unlikely blue standing EM waves.

But in mitochondria, the broadband UV process takes advantage of EM waves standing over a number N of cristae spaces separated by a matrix of dimension Δ shown in Figure 6.

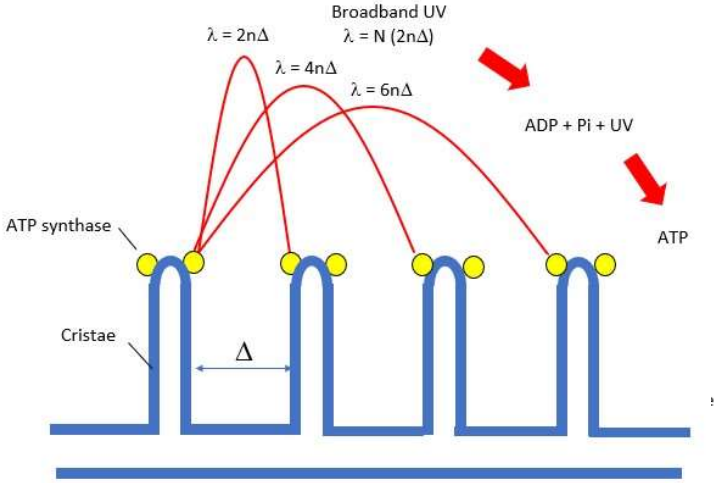


Figure 6. Broadband UV radiation in Mitochondria

The broadband UV consists of the sum of EM radiation E between dimer ATP synthase,

$$\mathrm{UV} = \mathrm{n}\Delta \sum_{1}^{\mathrm{N}} \mathrm{K} = \mathrm{n}\Delta \frac{\mathrm{N}}{2}(\mathrm{N}+1)$$

where, n is the refractive index of the matrix and N is the number of cristae in the mitochondria. Taking the refractive index n = 1.3 for water, the wavelengths λ of each standing wave is given in Table 1

Table 1. Broadband UV near UVC = 254 nm

| Mitochondria Species | λ = 2nΔ·K ~ nm K | | | | | | | | |
|---|---|---|---|---|---|---|---|---|---|
| | 1 | 2 | 3 | 4 | 5 | 6 | 7 | 8 | 9 |
| *Drosophila* Δ = 13 nm | 33.8 | 67.6 | 91.3 | 121.6 | 169.1 | 202.8 | 236.7 | 270.5 | 304.2 |
| Human Lung Δ = 50 nm | 130 | 260 | 390 | | | | | | |

Taking UVC = 254 nm, Table 1 is marked in blue arrows showing the K value at which UVC occurs for *Drosophila* and the human lung. Both mitochondria require fluorescence down to 254 nm for ATP synthesis. For *Drosophila* from K = 8 at 270.5 nm, and for human lung K = 2 at 260 nm. The advantage of broadband UV is the efficiency of fluorescence is enhanced.

## IV. CONCLUSIONS

Broadband UV enhances ATP synthesis by dehydration by increasing the efficiency of fluorescence.

The UV level for mitochondria species may not be UVC. Experiments are required to determine the optimum UV wavelength to enhance ATP synthesis by dehydration.

**References**

[1] Mitchell, P. (1961). Coupling of phosphorylation to electron and hydrogen transfer by a chemiosmotic type of mechanism. Nature, 191, 144–148.
[2] Ponnamperuma, C., et al. (1963). Synthesis of Adenosine Triphosphate under possible primitive Earth conditions. Nature 199, 222
[3] Powner MW, Gerland, B, Sutherland JD. (2009). Synthesis of activated pyrimidine ribonucleotides in prebiotically plausible conditions. Nature 459: 239–42.
[4] Lane N, Allen JF, Martin W. (2009) How did LUCA make a living? Chemiosmosis in the origin of life. BioEssays 32:271–280'
[5] Prevenslik, T. ATP Synthesis by Endogenous UV Radiation. 10th Congress Targeting Mitochondria, Oct. 28-29, 2019 - Berlin, Germany.
[6] Prevenslik T. Simple QED Applications. http//www.nanoqed.org, 2010-2020.
[7] Beyer RE. (1959). The Effect of Ultraviolet Light on Mitochondria. I. Inactivation and Protection of Oxidative Phosphorylation during Far-Ultraviolet Irradiation. Archives of Biochemistry and Biophysics. 79, 269-274.
[8] Jiang YF, et al. (2017) Electron tomographic analysis reveals ultrastructural features of mitochondrial cristae architecture which reflect energetic state and aging. Scientific Reports 7:45474.
[9] Davies K.M., et al. (2011). Macromolecular organization of ATP synthase and complex I in whole mitochondria. PNAS 108, 14121–14126.
[10] Blum TB, et al. (2019). Dimers of mitochondrial ATP synthase induce membrane curvature and self-assemble into rows. PNAS 4250–4255.

**ATP by Endogenous UV Radiation**

**Abstract**
Chemiosmosis in mitochondria is thought to synthesize ATP by oxidative phosphorylation in an inward flow of H+ protons across the inner membrane. However, ATP synthesis has a history of controversy. Although a high-energy chemical intermediate provided a more rational explanation, chemiosmosis survived as the ATP mechanism because the high-energy intermediate was never found. Chemiosmosis in chloroplasts differed as ATP was produced by photosynthesis from an outward flow of H+ protons across the thylakoid membrane. Oxidative phosphorylation in both mitochondria and chloroplasts occur by a chain of complex redox reactions with electron transfer from donors to acceptors assisted by enzymes. In this paper, chemiosmosis comprising electron chain reactions is superseded by simple QED conserving heat in nanoscopic features within the mitochondria and chloroplasts by creating endogenous UV radiation instead of increasing in temperature. ATP synthesis therefore proceeds from ADP and a phosphate group in a dehydration reaction mediated by UV instead of hydrolysis.

**Background**
Chemiosmosis (1) in mitochondria assumes a proton H+ gradient across the inner membrane to explain ATP synthesis by oxidative phosphorylation and in chloroplasts by photosynthetic phosphorylation across the thylakoid membrane. The main differences are the mitochondrion produces an inward proton flow by fuel-consuming redox reactions while the chloroplast produces an outward proton flow by photochemical charge separation. Both mitochondria and chloroplast phosphorylate ADP + Pi to ATP by a chain of complex chemistry. In chloroplasts, sunlight absorbed by chlorophyll produces heat that creates a charge separation across the thylakoid membrane, the outward H+ flow through the membrane-bound ATPase producing ATP from ADP and Pi. The mitochondrion differs as the proton flow across the inner membrane is inward, opposite to that of the chloroplast. Unlike charge separation in chloroplasts which is uniform, the inward H+ flow in mitochondria need not be uniform to pass through the ATP synthase to produce ATP. In 1961, chemiosmosis in mitochondria by a proton gradient was not accepted. A later review (2) claimed a high-energy chemical intermediate provided a more rational explanation with chemiosmosis surviving as the chosen ATP mechanism because the high-energy intermediate was never found.

Later on, chemiosmosis by oxidative phosphorylation in mitochondria using a H+ gradient was supported (3) by photosynthetic phosphorylation in chloroplasts using the reconstituted purple membrane *Bacteriorhodopsin* (bR) in a lipid membrane shown in Figure 1.

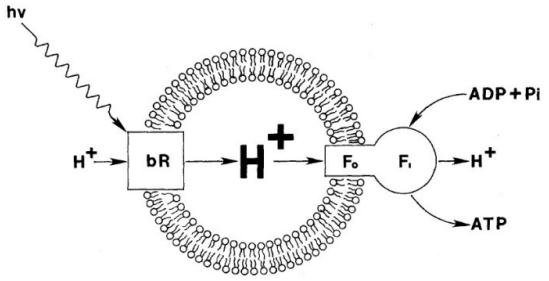


Figure 1. Chemiosmotic photophosphorylation in artificial lipid vesicles.

Figure 1 illustrates combining bR with the F0-FI ATPase from mitochondria into lipid vesicles formed an inside-out model. Upon illumination with VIS light, the protons then flow outward through the ATPase, causing it to phosphorylate ADP + Pi to ATP. In contrast, oxidative phosphorylation in mitochondria differs in that oxidation first produces H+ protons that flow outward. ATP is produced as the $H^+$ protons flow back into the cell, the subsequent inward proton flow producing ATP from ADP + Pi consistent with oxidative phosphorylation.

Similar to mitochondrial oxidative phosphorylation, chloroplasts use the photosynthetic thylakoid membranes to phosphorylate ADP + Pi to ATP. Pi stands for phosphate group. In 1967, the oxidative chemiosmosis was first supported by photosynthetic phosphorylation (4) in acidified spinach chloroplasts suddenly subjected to a basic medium. The pH gradient was created by holding the chloroplasts in a pH 4 solution for several hours and then rapidly mixed them with a neutral pH 8 buffer containing ADP and Pi. ATP synthesis was observed as the pH gradient across the membrane disappeared. The so-called acid-bath experiment was thought to unequivocally support the chemiosmosis theory that ATP synthesis is driven by pH gradients.

**Problem**

Chemiosmosis in mitochondria supported by the acid-bath chloroplast experiment showing ATP produced in a pH gradient across the thylakoid membrane is depicted in Figure 2(a).

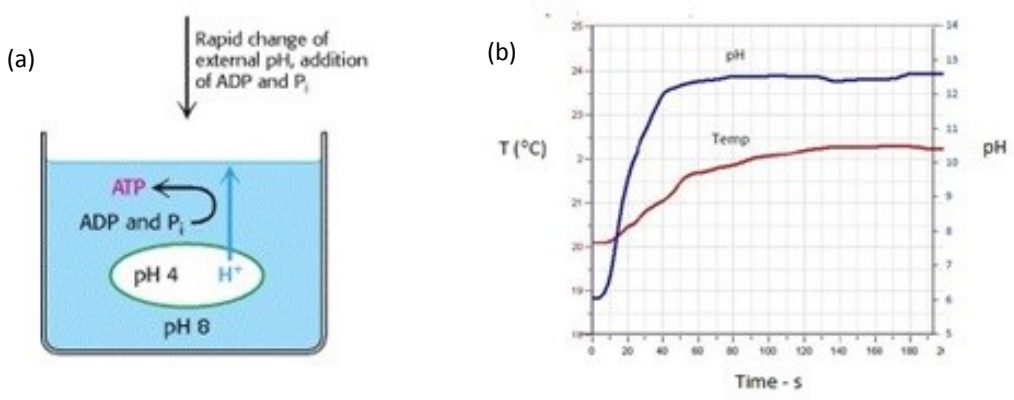


Figure 2. Chloroplast Acid-bath Experiment

However, ATP may not be produced by the pH gradient, but rather by a release (5) of anaerobic heat that increases bath temperature. In the titration of a weak acid with a base, Figure 2(b) shows rapidly changing an acidic pH 4 solution to a basic pH 8 produces a pH gradient of 4 also increases bath temperature. But the nanoscopic grana cannot increase in temperature as the heat capacity vanishes by the Planck law. Instead, thylakoid grana conserve the anaerobic heat by simple QED creating EM radiation beyond the UV that produce the ATP by the dehydration reaction,

$$ADP + Pi + UV \rightarrow ATP + H_2O$$

Simple QED was developed (6) for nanoscale heat transfer. Unlike classical physics that conserves heat by an increase in temperature, simple QED based on quantum mechanics denies atoms under the high EM confinement in nanostructures denies constituent atoms the heat capacity to conserve heat by an increase in temperature.
Instead, simple QED conserves heat by creating EM radiation at UV levels.

**Photo Oxidation**
Chemiosmosis explains ATP synthesis in mitochondria by oxidative phosphorylation through complex chemistry with enzymes in a sequential electron transport chain. The flow of electrons pumps H+ protons out of the matrix across the inner membrane into the intermembrane space, whereupon the H+ protons flow back through the F1-Fo ATPase to provide the energy for ATP synthesis.

Setting aside the difficulty in chemiosmosis of H+ protons flowing back through the F1-Fo ATPase and not elsewhere in the membrane, the electron transport chain is otherwise consistent with modern chemistry. However, Nature may not have chosen chemiosmosis as the mechanism for ATP synthesis as a more direct path is UV photo oxidation of food glucose similar to the photosynthetic phosphorylation in chloroplasts. If so, chemiosmosis with complex sequential electron chain reactions would not be required, specific enzymes in the inner membrane would not need to be instantly available, electrons from the reduced coenzymes would need not be passed from one electron carrier to another. Alternatively, the final oxidative electron transfer forming $O_2$ oxygen is more directly reached by UV assisted dehydration reactions (7) to produce ATP from ADP + Pi, where Pi is a phosphate group.

Although dehydration reaction by UV radiation is simpler than chemiosmosis, the difficulty is UV creates reactive oxygen species (ROS) that damage DNA in mitochondria and chloroplasts. But ROS is not a problem as mitochondria release ATP to protect against UV damage. The ability of ATP to protect mitochondria (8) allows the dehydration reaction to proceed during UV radiation. Perhaps, Nature took advantage of the simplicity of UV oxidation of food to glucose by allowing ATP synthesis to sustain life at the expense of expending some ATP in protecting the mitochondria.

**Purpose**
In this paper, ATP synthesis is proposed to occur by simple QED induced endogenous UV radiation assisted dehydration reactions of ADP + Pi preceded by UV conversion of glucose to ADP. The ATP expended in protecting the mitochondria against UV damage is only a fraction of the ATP produced. Moreover, the fraction of ATP protecting the mitochondria is not lost, but rather is a source of heat to produce the endogenous UV that allows ATP synthesis to proceed by dehydration.

**Analysis**
EM Radiation
Simple QED induced UV requires mitochondrial and chloroplast having nanoscopic features with at least one dimension $< 100$ nm. Otherwise, the EM confinement produces VIS and IR radiation that lacks the energy to activate ATP synthesis by UV mediated dehydration and food oxidation. The Planck energy E of the EM radiation,

$$E = \frac{hc}{2nd}$$

where, h is Planck's constant, c the speed of light, n and d are the refractive index and minimum dimension of the nanoscopic feature. For protein structures, n ~ 1.5 having d ~ 10 nm, E ~ 40 eV which is in the EUV. Although EUV fluorescence produces UV, the efficiency is reduced. With EUV fluorescence, structures having $10 < d < 80$ nm more efficiently produce UV $> 5$ eV. Regardless, simple QED requires the heat supplied to the nanostructure to produce EM radiation. The source of heat is the UV oxidation of food molecules and the binding of ALP to the nanostructure. Absent heat, simple QED does not produce EM radiation.

Experimentally, the efficiency of UV emission from EUV fluorescence data of ATP binding to nanoscopic mitochondrial and chloroplast structures is not available. But controlled oxidation of glucose to gluconic acid and other monosaccharides (9) by UVA fluorescence from d < 8 nm Ag/TiO2 nanoparticles shows < 10% efficiency.

**Applications**
In the application of simple QED induced UV activation of ATP synthesis by dehydration, the EUV produced in mitochondria and chloroplasts are presented in the following.

Mitochondria
ATP synthesis in mitochondria is proposed to occur by simple QED induced UV radiation standing between adjacent cristae surfaces. The human lung showing the mitochondria with the EM wave standing in the fold formed between adjacent cristae is noted in Figure 3.

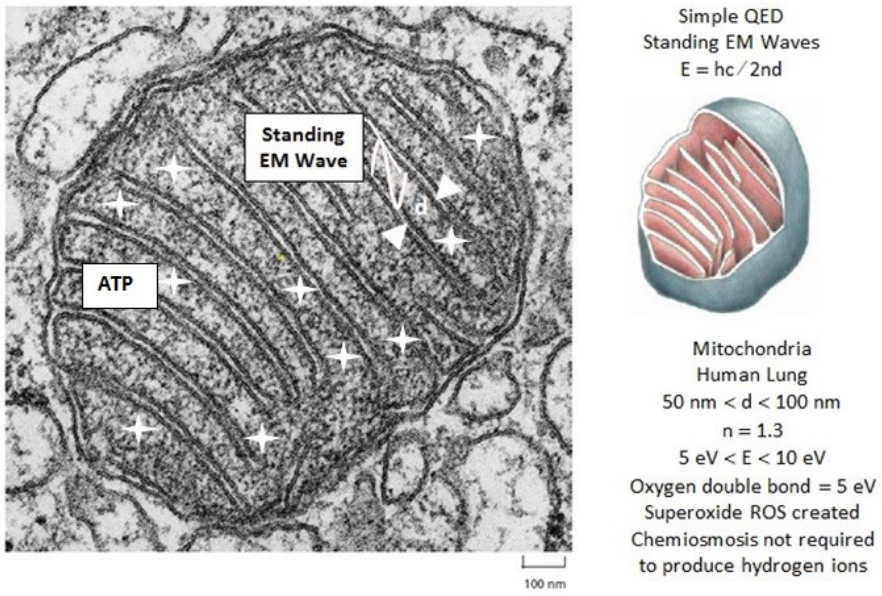


Figure 3. Human Lung Mitochondria
Showing ATP protecting DNA while providing heat source to EM standing wave

The EM wave standing in the mitochondria matrix with a spacing d between adjacent cristae is defined by ( 50 < d < 100 nm). ATP molecules – white stars – are shown dispersed throughout the matrix in Figure 3. ATP binding is the likely heat source for simple QED to produce EM radiation. For simplicity, glucose food molecules oxidized by UV radiation to produce ADP are not shown. The Planck energy E of the standing EM waves based on a refractive index n ~ 1.3 is beyond the UV at 5 to 10 eV.

In the oxidation of food molecules, the UV produces the oxygen anion superoxide by breaking the double bond of dissolved oxygen and the H+ protons from the OH radical. The UV radiation creates ADP from breaking down glucose from foods, the ATP produced from UV enhanced dehydration in the presence of ADP and Pi, but also forms ROS. In the mitochondria, simple QED is both the source of ATP synthesis and ROS.

Unlike chemiosmosis, simple QED does not depend on the H+ gradient across the inner membrane to produce ATP by hydrolysis. For over 50 years, chemiosmosis claimed the unlikely sequence of electron chain reactions powered by the H+ proton gradient across the inner membrane produced ATP by hydrolysis , when in fact simple QED in the UV and beyond actually mediated ATP synthesis by dehydrogenization of ADP + Pi.

Submicron Particles

In 1964, after chemiosmosis was proposed, mitochondria were mechanically treated with ultrasound. Electron microscopy (10) revealed numerous submicron spherical vesicles of inner mitochondrial membrane. A typical micrograph is shown in Fig. 4.

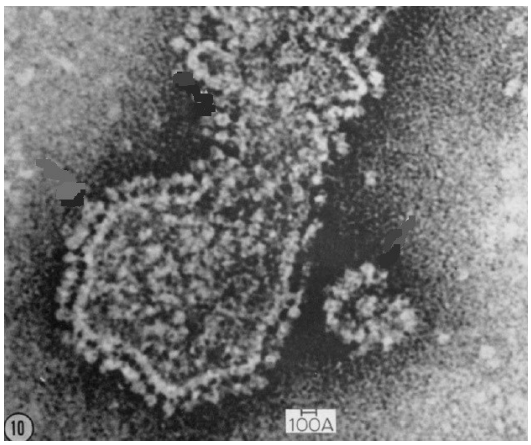


Figure 4. Submicron Spherical Vesicles from Ultrasonic treated Mitochondria

The submitochondrial particles (SMP), were spherical having diameters of 8-10 nm located on the surface of the cristae, but are also dispersed throughout the matrix. Comparison with intact mitochondria for bovine heart muscle shows the SMP display an inside-out orientation of ATPase compared with intact mitochondria, i.e., the globular SMP structures seen facing the matrix on the surface of cristae are found on the outer face of SMP outside the matrix as shown in Figure 5.

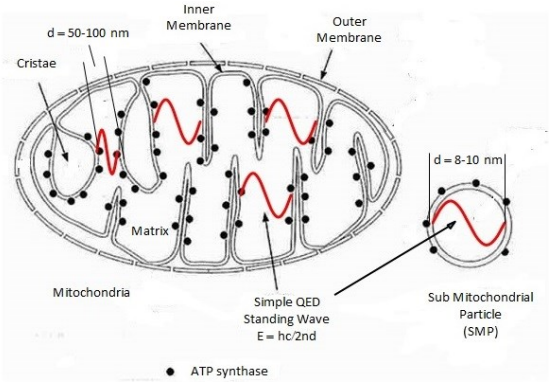


Figure 5. Simple QED standing EM waves in Mitochondria and SMP

Simple QED produces standing EM radiation in the UV and beyond as shown everywhere in the mitochondria and SMP depending on the ATP energy release regardless of which surface the ATP synthase is bound, i.e., the EM waves are conserved from ATP regardless of the binding surface. In the mitochondria, the spacing d between crista is, d = 50-100 nm producing EM radiation in the UV and beyond. However, the EM radiation in the spherical SMP having d = 8-10 nm is far higher in the EUV at about 40 eV, the lower quantum states in the UV excited by EUV fluorescence at the expense if low efficiency.

Chloroplasts

In chemiosmosis for chloroplasts, photophosphorylation of ADP to ATP occurs by light absorption in the thylakoid membrane producing H+ protons moving outward through membrane-bound ATPase to make ATP from ADP and Pi. The ATPase comprise a stalk segment (F0) embedded in the membrane with a head (F1) which extends into the aqueous stroma as shown in Fig. 4. When the intact F0--F1 ATPase is inserted into a phospholipid membrane and a pH difference is imposed across the membrane, the ATPase is thought (1) to consume protons while phosphorylating ADP with Pi to ATP. However, a pH gradient may not be necessary as cleaving the F1 head from the F0 stalk, the F1 head alone (3) in aqueous solution, produces ATP from ADP + Pi. Regardless, whether the pH difference or anaerobic heating produced the ATP in the acid-bath experiment is an open question.

Heat Q is the commonality in ATP production in chloroplasts. The outer membrane of the chloroplasts absorbs VIS radiation to provide heat Q to the lumen thylakoids. Hence, VIS cannot reach the thylakoids. Depending on dark or light adapted conditions, the lumen space (11) is about 17 nm containing water including plastocyanin (PC) and photosensitive PSII complexes. The ATP synthase located on the convoluted ends of the thylakoid membranes along the side of the stack exposed to the stroma is shown in Figure 7.

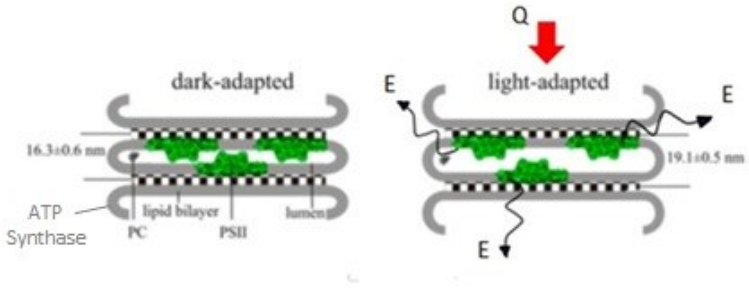


Figure 7. Lumen structure containing OEC and PC

VIS radiation wavelengths $\lambda > 400$ nm is excluded in the 17 nm EM confinement space of the lumen having EUV wavelengths $\lambda < 50$ nm. Hence, PC can only be absorbent below 300 nm. What this means is VIS photosensitivity of PC and PSII complexes has no meaning in chloroplasts. The EM absorption spectra (12) of oxidized and reduced PC peaks at UV wavelengths < 200 nm are shown in Figure 8(a). Only UV radiation is important in ATP synthesis. Similarly, the UV spectra of adenine in forming ADP shows peaks at about 205 and 265 nm is given in Figure 8(b).

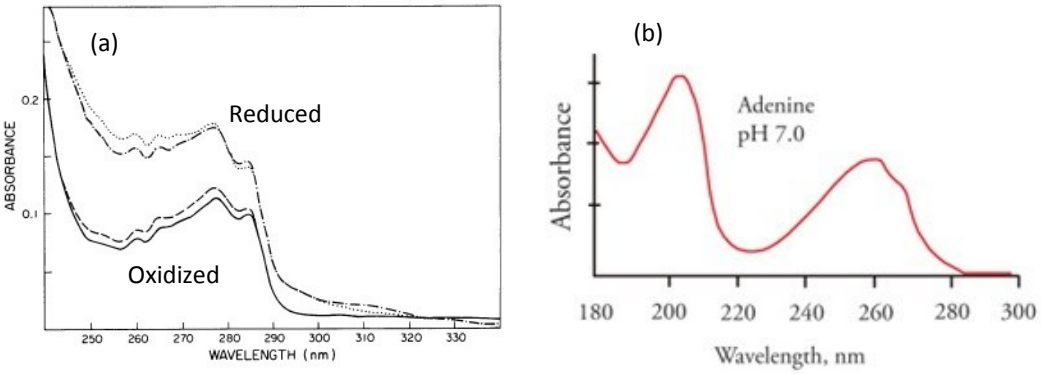


Figure 8. PC and Adenine absorption spectra

Of interest is the UV absorption spectra of glucose, ATP, and ADP spectra shown in Figure 9. Figure 9(a) shows ATP and ADP spectra (13) are almost identical at 300 nm, but differ in the VIS. The inset shows the ATP spectra below 300 nm to peak at about 260 nm. Figure 9(b) gives the UV absorption spectra (14) of glucose solution before and after irradiation for alkaline pH 11.5 and acidic pH 2 conditions. The spectral peak of the alkaline glucose solution at 267 nm is proximate the ATP peak at 260 nm consistent with the 260 nm peak of adenine shown Figure 8(b). Contrarily, chloroplast photosynthesis today is based on VIS and not UV light.

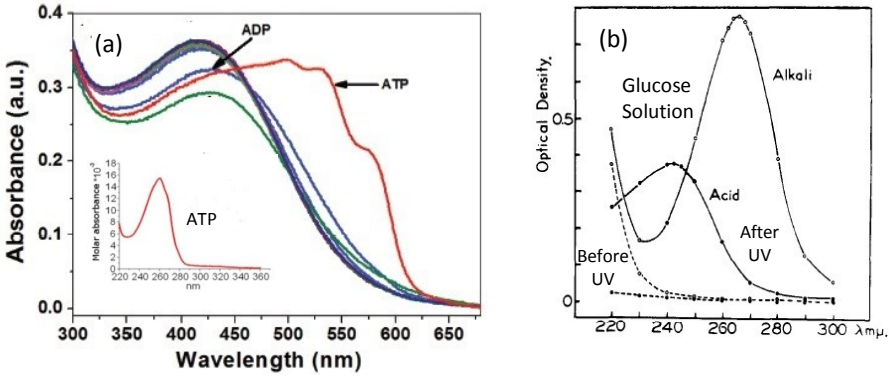


Figure 9. ATP and Glucose absorption spectra

Since ADP is converted to ATP in the stroma adjacent to the convoluted ends of thylakoid membrane in the grana stack which cannot be reached by solar light, ATP synthesis may only proceed by EUV radiation from the heat Q absorbed in the outer chloroplast membrane. Upon reaching the lumen, the heat Q is precluded by QM from increasing in temperature., and instead is conserved by simple QED creating EUV radiation within the lumen space. For water having refractive index $n = 1.33$, the Planck energy E in the EUV radiation produced in the lumen space of $d \sim 17$ nm is, $E \sim 27$ eV and $\lambda \sim 45$ nm. At the convoluted ends of the thylakoid membranes exposed to the stroma, the EUV fluorescence excites adenine, glucose and ADP near their spectral peak at 267 nm to overcome the barrier to dehydration of ADP + Pi to ATP without the complex electron chain reactions of chemiosmosis. In chloroplasts, simple QED is summarized in Figure 10.

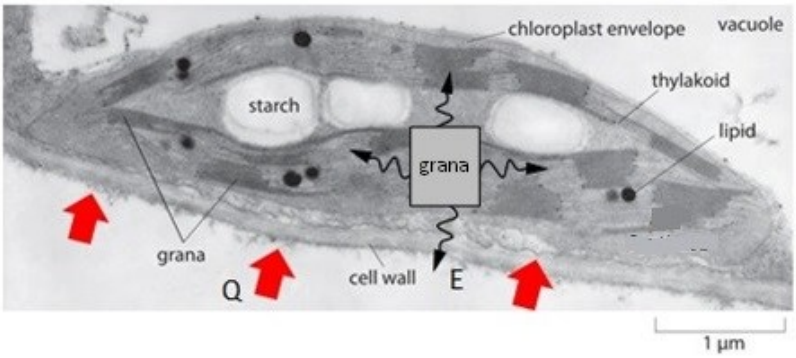


Figure 10. Simple QED in Chloroplasts

In summary, EUV is common to other sources of ATP created from EM confinement in nanoscopic structures. In 1976, ATP synthesis was reported (15) from aqueous suspensions of inorganic nanoparticles of ZnO and CdS heated by UV light, again without a pH gradient across a membrane. Indeed, the direct utilization of the hydrogen and oxygen in water for organic reactions (16) in glucose was realized by splitting water upon heating Pd/TiO2 nanoparticles with UVB irradiation at 350 nm. But for ATP synthesis and water splitting to occur, simple QED requires heating the nanoparticles and nano structural features of mitochondria and chloroplasts to produce the EUV energy to split water or assist the dehydration reaction ADP + Pi to ATP.

**Discussion**

Unlike hydrolysis in chemiosmosis, ATP synthesis by dehydration is a condensation reaction common in amino acids to proteins, sugars to carbohydrates, sugars to sugar phosphates, purines to nucleosides, and nucleosides to nucleotides. Although dehydration is direct chemistry compared to hydrolysis, an endergonic source of energy is required to activate the non-enzymatic production of ATP. On the primitive Earth, the energy source was suggested (7) to be UV radiation from outer space, i.e., pH gradients across membranes not required. UV irradiation of dilute solutions of purine or pyrimidine bases, specifically adenine, and phosphorus compound produced the nucleoside adenosine. Since adenosine has strong UV absorption peaks near 260 nm, the transparency of the early terrestrial atmosphere may have allowed ATP synthesis by dehydration reactions to proceed from dilute solutions of adenine. In ethyl metaphosphate, adenine yielded ADP and ATP.

Although exogenous UV radiation provides an understanding of the mechanism of ATP production in the evolution of life on the primitive Earth, only endogenous UV produced within the mitochondria and chloroplasts is relevant to the question of how molecular evolution proceeded. Perhaps, the lack of an endogenous UV source was implicit in the acceptance of hydrolysis in chemiosmosis theory driven by H+ proton gradients instead of dehydration reactions. The simple QED induced endogenous UV energy source proposed here to activate dehydration reactions in producing ATP from ADP + Pi groups is proposed to supersede chemiosmosis.

Endogenous UV within the mitochondria and chloroplasts not only allows ATP production, but also is the source of ROS. The literature is silent on the source of ROS, simply stating ROS are just present in biological systems. However, UV beyond UVC having energy $E > 5$ eV is required to create hydroxyl and super oxides. ROS damage to DNA is proposed (17) as the cause of neurodegenerative diseases by disrupting ATP synthase in chemiosmotic electron chain reactions, but the mechanism of ROS

production is not identified. In contrast, endogenous UV as the source of ROS may at first appear a detriment to the ATP synthase by dehydration reactions, but may not be a problem as mitochondria release ATP to protect (8) against UV damage. Perhaps, Nature took advantage of the simplicity of UV oxidation of food to glucose by allowing ATP synthesis to sustain life at the expense of some ATP in protecting the mitochondria.

In the origin of life, the concept of primordial soup remains central to mainstream thinking. But soup is homogeneous in pH and so has no capacity (18) for energy coupling by chemiosmosis. Instead, chemiosmosis is claimed central to the origin of life as proton gradients form naturally at alkaline hydrothermal vents allowing ATP synthesis powered by the ion gradient by means of vectorial electron transfer from a donor to acceptor. As described above, however, the notion of pH gradients across the thylakoid membrane of the chloroplasts as the source of ATP production in the acid-bath experiment is questionable (1,3,4) because of the anaerobic heat released in mixing acids and bases. Instead of chemiosmosis, the simple QED induced UV produced by the anaerobic heat of mixing provides the activation energy (7) for the ATP synthesis by dehydration reactions. Extended to mitochondria, the heat required to produce UV assisted ATP synthesis is the binding of a fraction of the total ATP produced to the cristae surfaces.

In support of chemiosmosis as the basis for the origin of life, heat flow across the inner membrane of mitochondria as the mechanism for sustaining pH gradients was simulated (19) by thermophoresis for specified temperature gradients across sub-millimeter sized water-filled channels. For heat flow based on a temperature difference $\Delta T = 30$ K across channel widths $> 153$ μm, pH differences of $\sim 2$ were found after 4 hours. The pH differences are caused by the heat from temperatures specified across the channel. Perhaps applicable to rock fissures, the relevance of temperature changes across $> 153$ μm wide channels in producing pH gradients is hardly support for ATP chemiosmosis across the $< 5$ nm inner membrane of mitochondria. Moreover, the simulation of pH gradient based on temperature differences is not relevant. Perhaps, simulating the heat flow in nanoscale channels based on specifying a pH gradient would be meaningful. Regardless, thermophoresis based on temperature differences across channel widths $< 100$ nm are meaningless as temperature changes are denied by QM. Consistent with QM precluding temperature changes, simple QED conserves heat from ATP binding to the membrane wall producing the UV radiation that activates ATP synthesis from ADP + Pi by dehydration.

**References**

1. Mitchell, P. (1961). Coupling of phosphorylation to electron and hydrogen transfer by a chemiosmotic type of mechanism. Nature, 191, 144–148.
2. Weber, M. (2002). Theory testing in experimental biology: the chemiosmotic mechanism of ATP synthesis. Stud. Hist. Phil. Biol. & Biomed. Sci. 33, 29–52.
3. Bahn, P. R. and Fox, S. W. (1981) Models For Protocellular Photophosphorylation. BioSystems. 14, 3–14.
4. Kaplan, A. H., et al. (1967). ATP Hydrolysis Caused by Acid-Base Transition of Spinach Chloroplasts. Archives Of Biochemistry And Biophysics. 120, 365-375.
5. Nakamura, T. and Matsuoka, I. (1978). Calorimetric Studies of Heat of Respiration of Mitochondria. J. Biochem. 84, 39-46 .
6. Prevenslik, T. Applications of Simple QED. https//www.nanoqed.org 2010–2019.
7. Ponnamperuma, C., et al. (1963). Synthesis of Adenosine Triphosphate under possible primitive Earth conditions. Nature 199, 222.
8. Beyer, R. E. (1959). The Effect of Ultraviolet Light on Mitochondria. I. Inactivation and Protection of Oxidative Phosphorylation during Far-Ultraviolet Irradiation. Archives Of Biochemistry And Biophysics. 79, 269-274.
9. Da Via, L. et al. (2016). Visible-Light-Controlled Oxidation of Glucose using Titania-Supported Silver Photocatalysts. ChemCatChem. 8, 3475 –3483.
10. Fernandes Moran, H. et al., (1964). A macromolecular repeating unit of Mitochondrial structure and function. J. Cell Biology, 22, 63.
11. Kirchoff, H., et al. (2016). Dynamic control of protein diffusion within the granal thylakoid lumen. PNAS, 108, 50, 20248–20153.
12. Draheim, J. E., et al. (1986) Plastocyanin conformations : An analysis of its near ultraviolet absorption and circular dichroic spectra, Biophys. J. 49, 891-900.
13. Ito, A. and Ito, T. (1986). Absorption spectra of deoxyribose, ribosephosphate, atp and dna by direct transmission measurements in the vacuum-uv (150—190 nm) and far-uv (190—260 nm) regions using synchrotron radiation as a light source. Photochem. and Photobiol. 44, 355-358.
14. Laurent, T. C. and Wertheim, E. M. (1952). Effect of Ultraviolet Light on Alkaline Solutions of Glucose and Certain Other Sugars. Acta Chem. Scand., 6, 678.
15. Fan, I-J., et al. (1976). Inorganic photophosphorylation of adenosine diphosphate to adenosine triphosphate. Sci. Sin. 19, 805--810.
16. Zhou, B., et al. (2016) Using the hydrogen and oxygen in water directly for hydrogenation reactions and glucose oxidation by photocatalysis. Chem. Sci. 7, 463.
17. Guo, C.. et al. (2013). Oxidative stress, mitochondrial damage and neurodegenerative diseases. Neural Regen Res. 8: 2003–2014.
18. Lane, N., et al. (2010). How did LUCA make a living? Chemiosmosis in the origin of life. BioEssays 32:271–280.
19. Keil, L. M. R., et al. (2017). Proton gradients and pH oscillations emerge from heat flow at the microscale. Nature Communications, 8: 1897

## Cancer: UVC induced Nanoparticle Treatment and Metastasis

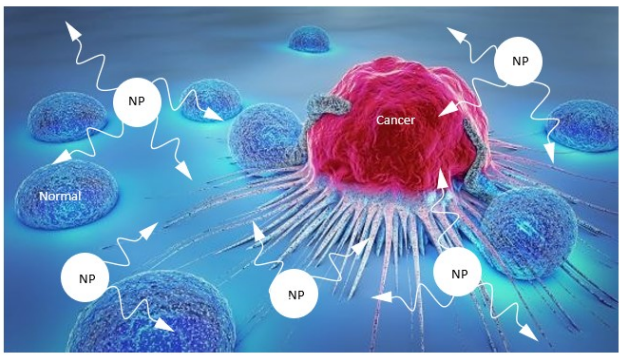


Classical physics allows the atom to have heat capacity at the nanoscale, the conservation of heat proceeding by an increase in temperature. However, simple QED based on the Planck law of quantum mechanics (QM) denies the atoms in nanoparticles (NPs) the heat capacity to conserve heat by a change in temperature, the consequence of which is embodied in the proposed Cancer NP Treatment: $\sim$ 80 nm NPs injected intravenously in cancer patients convert body heat to UVC radiation allowing DNA damage to accumulate in cancer cells to initiate apoptosis.

Collateral DNA damage to normal cells does occur, but is corrected by DNA repair systems. CDC tests to determine safe NP dosage levels in the NP treatment are required to confirm the expectation that UVC levels will not compromise normal cells based on the argument that survival of organisms on the primitive Earth required evolution of DNA repair systems to continuously correct for DNA damage from the far more intense solar UVC. If so, cancer treatment by low level NP induced UVC should not be problematic.

Simple QED not only emits UVC from NPs to treat cancer, but is the source of cancer metastasis as UVC emitted from $\sim$ 100 nm filopodial protrusions at the leading edge of cancer cells damages DNA in distal normal cells.

# Chapter 4

# UV Disinfection by Heat

There have been many inventions and methods through the years to develop ways of disinfecting water for human consumption as well as ways of disinfecting common surface areas to prevent spread of diseases. In this chapter a novel, yet simple way of disinfecting drinking water is presented. Further, a method of disinfecting public surface areas is introduced.


4.1 Disinfectant Drinking Bowl . . . . . 86
4.2 QED Disinfection of Drinking Water in the Developing World . . . . . 92
4.3 The Ebowla in the Disinfection of the Ebola virus . . . . . 95
4.4 QED Disinfection of Future Public Transport in Hong Kong . . . . . 98

DISINFECTANT DRINKING BOWL

SUMMARY OF THE INVENTION

Disclosed is a germicidal UV radiation device for disinfecting pathogens in drinking water without electricity using a hand-held bowl provided with a nanoscale silver coating that produces UV radiation powered only by body heat from the palm of the hand. The source of UV radiation embodies a bowl with a 100 nm silver coating at the water interface that converts body heat produces UVC radiation having a wavelength of about 254 nm that disinfects the water in the bowl of pathogens.

FIELD OF THE INVENTION

This invention relates to a water disinfection of water in a drinking bowl held in the palm of the hand disinfecting pathogens with UVC radiation source powered only by body heat.

BACKGROUND OF THE INVENTION

Contaminated drinking water is Universal. WHO/UNICEF estimates (WHO/UNICEF, 2012) almost 1 billion people do not have access to safe drinking water. Even if bottled water is available, the consumer never knows if it is indeed safe. The most direct water disinfection is by boiling, but except for water boiling units in restaurants is not available to the individual consumer at the point of use.

Unequivocally, water purification by filtration at the point of use is desirable. Water purifiers require pumping through ceramic or resin filters coated with silver NPs. NP stands for nanoparticle. Silver NPs are known to provide antimicrobial action by damaging the DNA of bacteria, but NPs that come off the filter and enter the body also damage human DNA that if not repaired, leads to cancer.

In contrast, UVC disinfection of drinking water outside the body avoids the danger of cancer posed by NPs in filters. Currently, LEDs in the UVC are thought (Ferrero 2014) to provide the individual with point of use disinfection of drinking water, but still require a source of electrical power. LEDs stand for light emitting diodes.

UVC radiation can deactivate pathogens such as anthrax, smallpox, viral hemorrhagic fevers, pneumonic plague, tularemia and drug resistant tuberculosis. Table I gives the dose of UVC radiation required to deactivate various pathogens (Eccleston et al., 1998). The dose is based on the average flux used in the experiment not the actual absorbed energy.

However, filters and LEDs require sources of electricity that are not always available, especially in the developing world. Therefore, it is desirable to invent a device that produces UVC radiation to disinfect drinking water without an external source of electricity. In the instant invention, a photograph of the hand-held drinking bowl is shown in Figure 1.

The theory of the drinking bowl is based on QED induced UV radiation. QED stands for quantum electrodynamics, but is a simple form of the complex relativistic light-matter interaction advanced by Feynman and others. QED disinfection is a consequence of QM that precludes the atoms in nano-coatings to have the heat capacity to conserve body heat by an increase in temperature. QM stands for quantum mechanics. Instead, the heat is induced by QED to produce UV radiation.

Classically, the atoms in coatings always have the heat capacity to increase in temperature upon the absorption of heat irrespective of their thickness. QM by the Planck law differs (Planck, 1900) in that the heat capacity of the atom vanishes in nanocoatings, and therefore heat cannot be conserved by an increase in temperature. Figure 2 shows the Planck law at 300 K. The thermal kT energy (or the heat capacity) of the atom depends on the wavelength $\lambda$ of EM confinement. For nanocoating having EM confinement wavelengths $\lambda$ < 100 nm, the heat capacity of the atom vanishes. However, for heat capacity to vanish, the nanocoating atoms must somehow be placed under nanoscale EM confinement. But nanocoatings have high S/V ratios that confine body heat almost entirely to their surfaces, the surface heat thereby providing the necessary EM confinement of nanocoating atoms over nanoscale wavelengths. S/V stands for surface-to-volume. QED then conserves the surface heat by creating EM radiation standing between nanocoating surfaces.

QED here differs from the complex relativistic QED by Feynman and others. Briefly stated: QED conserves heat supplied to a nanocoating absent heat capacity by creating EM radiation having half-wavelength $\lambda/2 = d$, where $d$ is the nanocoating thickness. The Planck energy $E$ of the standing EM radiation is:

$$E = h\left(\frac{c}{n}\right)/\lambda = \frac{hc}{2nd}$$

where, the velocity of light $c$ is corrected for the slower speed in the solid state by the refractive index $n$ of the nanocoating.

The wavelength of QED radiation emission from the conservation of heat in nanoscale coatings having refractive index $n$ = 2 and 4 is shown in Figure 3. Most indices vary from, 1.5 to 3. For a silver the nanocoating having = 1.35, the QED emission from 100 nm coating thicknesses produces EM radiation at 270 nm close to UVC to at 254 nm. The UVC may be transmitted over distances comparable to the size of the drinking bowl without any absorption.

The effectiveness of drinking bowl in disinfecting water depends on amount of body heat available in the palm of the hand. Total human body heat is about 100 W. Since the average surface area for adult men and women is about 1.75 $m^2$, the heat flow Q = 5.71 mW / $cm^2$ = 5710 $\mu$W/ $cm^2$. From Table I, the dose D to destroy most water pathogens is 16,000 to 38,000 $\mu$J / $cm^2$ may be provided by keeping the water in the drinking bowl from 3 to 6 seconds.

SUMMARY OF THE INVENTION

In accordance with the present invention, a device for disinfecting water in a hand-held drinking bowl in the palm of the hand powered by body heat is disclosed, the device including a UVC radiation source comprising a nanocoating having a thickness $d$ and refractive index $n$ to produce radiation having a wavelength $\lambda = 2nd \cong$ 254 nm. The radiation source is powered by body heat of about 5710 $\mu$W/$cm^2$ of UVC radiation capable of disinfecting water of most pathogens in 3-6 seconds.

These and other aspects, features and advantages will be apparent from the following description of certain embodiments and the accompanying drawing figures.

BRIEF DESCRIPTION OF THE DRAWINGS

The features of the present invention will be more readily apparent from the following description and drawings of the illustrative embodiments of the invention:

Drawing 1 illustrates a plan and elevation view of the drinking bowl in accordance with the present invention.

DETAILED DESCRIPTION OF CERTAIN PREFERRED EMBODIMENTS

The present invention comprises a device that can provide the rapid and effective disinfection of drinking water, in remote locations at points of use where a source of electricity is not available. The device contains a passive UVC radiation source having a wavelength of about 254 nm powered only by the body heat of the hand thereby disinfecting pathogens in the water of the drinking bowl.

With reference to Drawing 1, the drinking bowl device **100** is illustrated in accordance with one embodiment of the present invention. The UVC radiation source includes a thin-walled plastic bowl **110** held upright in the palm of the hand containing pathogens **120** in water **130** to be disinfected. The bowl **110** is provided with a 100 nm nano-coating **140** of silver and powered by body heat **150** from the palm of the hand.

While the invention is disclosed for a silver nano-coating **140**, it would be appreciated by one of skill in the art that other conductive metals such as aluminum and copper may be employed provided the thickness *d* and refractive index *n* are selected to achieve UVC radiation at 254 nm.

REFERENCES

Eccleston, B., et al., 1998. UV intensity levels affected by water quality. *Water Technology* 21:61-68

Planck, M., On the Theory of the Energy Distribution Law of the Normal Spectrum, *Verhandl. Dtsch. Phys. Ges.*, vol. 2, pp. 237, 1900.

Ferrero, G. 2014. UV disinfection in developing Countries. UNESCO IHE, Delft, The Netherlands, November 6, 2014.

Feynman R.: QED: The Strange Theory of Light and Matter, Princeton University Press, 1985.

National Academy of Sciences. 2007. Safe Drinking Water is Essential. *Global Health & Education Foundation.*

WHO/UNICEF, 2012. Progress on Drinking Water and Sanitation: 2012 Update.

FIGURES

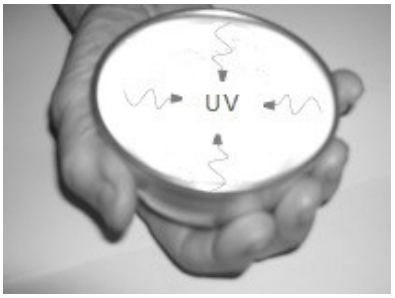


Figure 1. QED induced UV radiation from body heat disinfecting drinking water

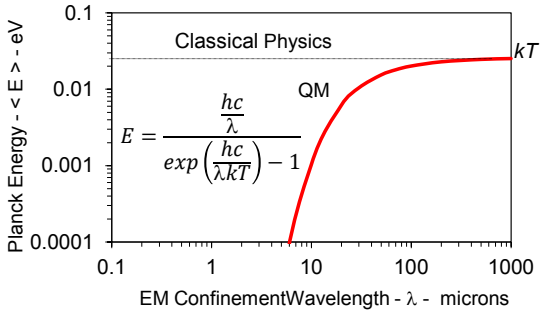


Figure 2. Heat Capacity of the Atom at 300 K

In the inset, *E* = Planck energy, *h* = Planck's constant,
*c* = speed of light, *k* = Boltzmann's constant, *T* - temperature, and λ = wavelength

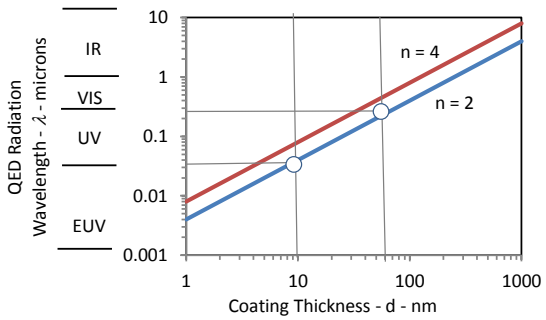


Figure 3. Wavelength of QED Emission v. Coating Thickness

DRAWINGS

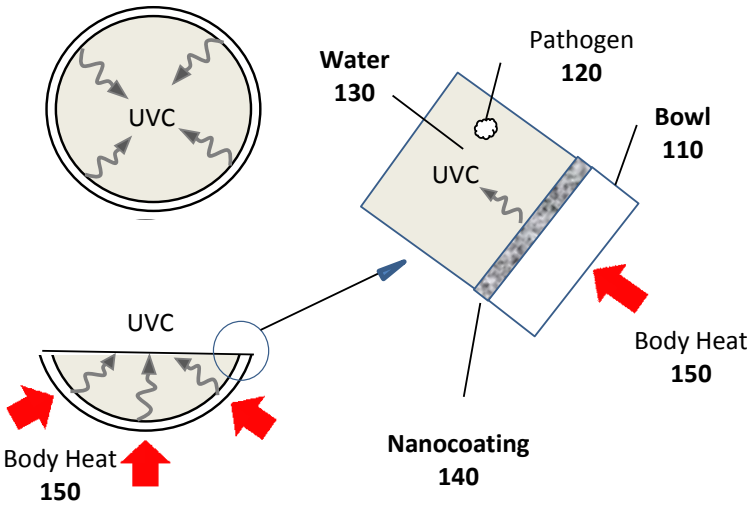


Drawing 1. Device Plan and Elevation View

TABLES

**Ultraviolet Dosage Required For 99.9% Destruction of Various Organisms**
**(μW-s/cm² at 254 nanometer)**

| Bacteria | | Mold Spores | |
|---|---|---|---|
| *Bacillus anthracis* | 8,700 | *Aspergillus flavus* | 99,000 |
| *B. enteritidis* | 7,600 | *Aspergillus glaucus* | 88,000 |
| *B. Megatherium* sp. (vegatative) | 2,500 | *Aspergillus niger* | 330,000 |
| *B. Megatherium* sp. (spores) | 52,000 | *Mucor racemosus A* | 35,200 |
| *B. paratyphosus* | 6,100 | *Mucor racemosus B* | 35,200 |
| *B. subtilis* (vegatative) | 11,000 | *Oospora lactis* | 11,000 |
| *B. subtilis* (spores) | 58,000 | *Penicillium digitatum* | 88,000 |
| *Clostridium tetani* | 22,000 | *Penicillium expansum* | 22,000 |
| *Corynebacterium diphtheria* | 6,500 | *Penicillium roqueforti* | 26,400 |
| *Eberthella typhosa* | 4,100 | *Rhizopus nigricans* | 220,000 |
| *Escherichia coli* | 7,000 | | |
| *Leptospira interrogans* | 6,000 | | |
| *Micrococcus candidus* | 12,300 | **Algae / Protozoa** | |
| *Micrococcus sphaeroides* | 15,400 | *Chlorella vulgaris* (algae) | 22,000 |
| *Mycobacterium tuberculosis* | 10,000 | Nematode eggs | 92,000 |
| *Neisseria catarrhalis* | 8,500 | Paramecium | 200,000 |
| *Phytomonas tumefaciens* | 8,500 | | |
| *Proteus vulgaris* | 6,600 | | |
| *Pseudomonas aeruginosa* | 10,500 | **Virus** | |
| *Pseudomonas fluorescens* | 6,600 | Bacteriophage (*E. coli*) | 6,600 |
| *Salmonella enteritidis* | 7,600 | Hepatitis virus | 8,000 |
| *Salmonella paratyphi* | 6,100 | Influenza virus | 6,600 |
| *Salmonella typhimurium* | 15,200 | Polio virus | 6,000 |
| *Salmonella typhosa* (Typhoid) | 6,000 | Rotavirus | 24,000 |
| *Sarcina lutea* | 26,400 | Tobacco mosaic | 440,000 |
| *Serratia marcescens* | 6,200 | | |
| *Shigella dysenteriae* (Dysentery) | 4,200 | | |
| *Shigella paradysenteriae* | 3,400 | | |
| *Spirillum rubrum* | 6,160 | **Yeast** | |
| *Staphylococcus albus* | 5,720 | Baker's yeast | 8,800 |
| *Staphylococcus aureus* | 6,600 | Brewer's yeast | 6,600 |
| *Streptococcus hemolyticus* | 5,500 | Common yeast cake | 13,200 |
| *Streptococcus lactis* | 8,800 | *Saccharomyces cerevistae* | 13,200 |
| *Streptococcus viridans* | 3,800 | *Saccharomyces ellipsoideus* | 13,200 |
| *Vibrio cholerae* | 6,500 | *Saccharomyces sp.* | 17,600 |

Table I UVC Dosage for 99.9% Destruction of Various Pathogens

8th International Conference on Thermal Engineering: Theory and Applications
May 18-21, 2015, Amman-Jordan

# QED Disinfection of Drinking Water in the Developing World

**Abstract**

WHO/UNICEF estimates almost 1 billion people in the developing world do not have access to safe drinking water. Conventional water treatment is unfeasible because of costs and lack of electricity. QED induced UV radiation using hand-held nano-coated drinking bowls is proposed to inexpensively disinfect water without electrical power. QED stands for quantum electrodynamics. QED disinfection is a consequence of QM that forbids the atoms in nano-coatings under TIR confinement to have the heat capacity to increase in temperature. QM stands for quantum mechanics and TIR for total internal reflection. Instead, conservation proceeds by QED inducing the heat to be converted to EM radiation that can be tuned to UV-C radiation to by selecting the proper coating thickness. EPA guidelines for disinfection require the minimum UV-C dose of 16 to 38 mJ / $cm^2$. With body heat of about 6 mW / $cm^2$, the drinking bowl disinfects drinking water in 3 to 6 seconds. Extensions of QED radiation in the drinking bowl are made to the disinfection of the Ebola virus.

*Keywords: nano-coated bowl, disinfection, drinking water, Ebola virus, quantum mechanics, QED*

## 1. Introduction

Currently, WHO/UNICEF estimates [1] almost 1 billion people in the developing world do not have access to safe drinking water. Moreover, about 2 million childhood deaths have been attributed to water-borne diseases. Conventional water treatment is unfeasible because of costs. Lacking municipal water supplies, the water is collected from rivers or lakes and stored in containers for later use which may also be contaminated. The most direct disinfection is by boiling small quantities of water, but this requires a source of heat which, except for fire, is usually not available. However, focusing sunlight to boil small quantities of drinking water avoids the need to build fires, but would be expensive and only be available during daylight hours. In the developing world, alternative low-cost methods are desirable.

Unfortunately, there are no known low-cost alternatives to purifying water other than by boiling. If, however, portable electrical power is available, the water could be pumped through ceramic or resin filters [2] coated with silver NPs. NP stands for nanoparticle. Silver NPs are widely known to provide antimicrobial action by damaging the DNA of bacteria, but NPs that come off the filter and enter drinking water also [3] damages human DNA that if not repaired, may lead to cancer. Regardless, NP coated filters are unfeasible because electrical pumping power is not available and costly if available.

In contrast, UV disinfection [4] of drinking water occurs outside the body and avoids the danger of cancer posed by NPs in filters. Solar-UV mediated pathogen disinfection for municipal water and wastewater treatment avoids the need for electricity, but is otherwise too costly for the developing world. Currently, LEDs in the UV-C are thought [4] to provide personal disinfection of drinking water. LEDs stand for light emitting diodes. The benefits of UV-C LEDs are mercury free and low voltage sources, but still require a source of electrical power.

## 2. Proposal

QED induced UV radiation using hand-held nano-coated drinking bowls is proposed by which drinking water is disinfected inexpensively with body heat as depicted in Fig. 1

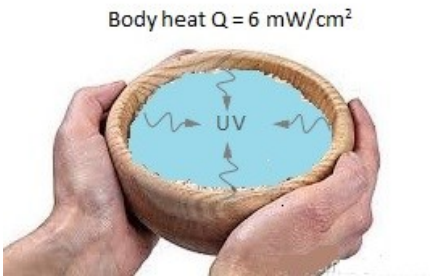


**Fig. 1 QED induced UV radiation from body heat in hands disinfecting bowl of water**

QED induced disinfection of drinking water is a consequence of QM that precludes the atoms in nano-coatings to have the heat capacity to conserve body heat by an increase in temperature. Instead, the heat is induced by QED to produce UV radiation.

## 3. Theory

### 3.1. QM Restrictions

Classically, the atoms in nano-coatings always have the heat capacity to increase in temperature upon the absorption of heat irrespective of their thickness, i.e., there is no size effect in classical physics. QM differs in that the heat capacity of the atom depends on the thickness of the coating. A comparison of the thermal kT energy (or the heat capacity) of the atom by classical physics and QM by the Einstein-Hopf relation [4] for the atom as a harmonic oscillator is shown in Fig. 2.

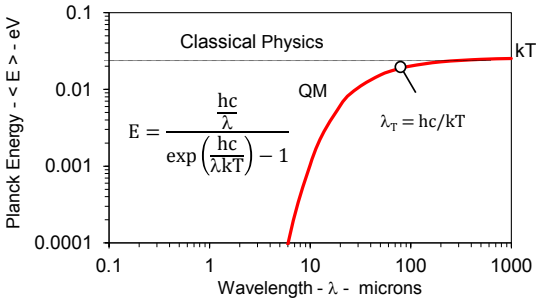


**Fig. 2 Heat Capacity of the Atom at 300 K . In the inset, E is Planck energy, h Planck's constant, c speed of light, k Boltzmann's constant, T temperature, and λ wavelength**

QM allows the atom in supramicron coatings to have kT energy and increase in temperature for $\lambda > \lambda_T$. However, atoms in micron sized coatings confined to $\lambda <$ 6 microns have kT < 0.0001 eV or little heat capacity, while at the nanoscale for $\lambda <$ 100 nm virtually no heat capacity is available to conserve absorbed heat by an increase in temperature.

### 3.2. Confinement and QED Radiation

TIR has a long history. In 1870, Tyndall showed light is trapped by TIR in the surface of a body if its RI is greater than that of the surroundings. RI stands for refractive index. Tyndall used water to show TIR confinement allowed light to be observed moving along the length of transparent curved tubes. TIR may confine any form of EM energy, although in the nano-coating of the drinking bowl the confined EM energy is the body heat from hands holding the bowl.

TIR confinement requires the deposited heat to be concentrated in the coating surface that is a natural consequence of nanoscale coatings having high S / V ratios, i.e., surface to volume ratios. Hence, QED creates standing wave photons within the TIR confinement formed between the coating surfaces, the number of photons conserving the heat absorbed. The wavelength $\lambda$ of the standing photons is, $\lambda = 2$ d, where d is the coating thickness.

However, TIR confinement by the coating surfaces is not permanent, sustaining itself only during heat absorption, i.e., absent absorption there is no TIR confinement for QED to conserve the heat by creating standing photons in the coating.

QED relies on complex mathematics as described by Feynman [5] although the underlying physics is simple to understand, i.e., EM radiation of wavelength $\lambda$ is created by supplying heat to a QM box having sides separated by $\lambda$ / 2. In this way, QED conserves absorbed EM energy by frequency up-conversion to the TIR resonance described by the thickness d of the coating. The Planck energy E of the QED radiation,

$$E = h\upsilon, \ \upsilon = \frac{c/n}{\lambda}, \ \lambda = 2d \qquad (1)$$

where, n is the RI of the coating.

### 3.3. UV Disinfection

UV light as a disinfectant penetrates an organism's cell walls and disrupts the genes to preclude reproduction. Research [6] has shown that the optimum UV wavelength range to destroy bacteria is between 250 and 270 nm. At 185 nm, UV light is powerful enough to produce ozone, hydroxyl, and other free radicals that destroy bacteria. The US HEW set guidelines for UV light disinfection require a minimum dose of 16 mJ / $cm^2$ at all points throughout the water disinfection unit, but recently the National Sanitation Foundation International set the minimum UV light requirement at 38 mJ / $cm^2$ for treat visually clear water.

## 4. Analysis

The wavelength of QED radiation emission from the conservation of heat in nanoscale coatings having n = 2 and 4 is shown in Fig. 3.

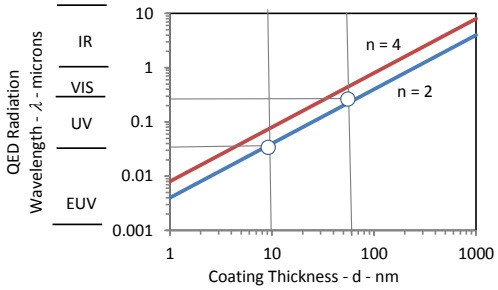


**Fig. 3 Wavelength of QED Emission v. Coating Thickness**

Insuring TIR confinement requires the RI of the coating to be greater than that of the substrate. Most RI vary from, 1.5 to 3. For the coating having = 2, the QED emission from 10 – 60 nm coating thicknesses produces EM radiation from UV-C to the near EUV. In water, the near UV-C at 254 nm may be transmitted over distances comparable to the size of the drinking bowl without any absorption. For n = 4, smaller coating thicknesses are required to produce UV-C.

Taking $\lambda$ = 260 nm UV as the optimum UV wavelength for disinfection in a coating of n = 2, the coating thickness is 65 nm and a substrate having n < 2. Materials should be selected that are resistant to corrosion and readily cleanable. Of course, the RIs of the coating and substrate depend on wavelength and require evaluation at $\lambda$ = 260 nm.

Total human body heat is about 100 W. Since the average surface area [8] for adult men and women is about 1.75 $m^2$, the heat flow Q = 5.71 mW / $cm^2$. Hence, the dose to destroy water pathogens of 16 to 38 mJ / $cm^2$ may be provided by keeping the water in the drinking bowl from 3 to 6 seconds.

### 5. Conclusions

An inexpensive drinking bowl is proposed for the third world that is simple to use and UV-C disinfects drinking water from body heat in the hands holding the bowl. Unlike other kinds of UV disinfection, no electricity is required.

### 6. Extensions

Similar to drinking water, the Ebola virus is a worldwide concern. In the U.S., Ebola disinfection includes electric powered hand-held systems that produce a blade-like light beam having an area of 50 mm x 500 mm. However, the protocol for Ebola disinfection in the U.S. is too complex and costly in the developing world requiring unavailable sources of electricity.

In this regard, QED induced EM radiation from body heat in a hand-held nano-coated bowl called an EBOWLA is proposed to provide the UV-C to inexpensively disinfect Ebola without the need for electricity. In operation, the 80 mm diameter EBOWLA provides a cylindrical beam of UV-C light from the body heat transferred to the nano-coating as shown in Fig. 4.

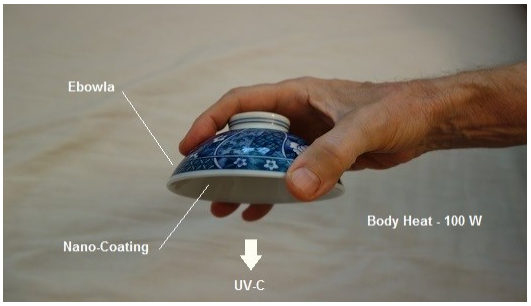


**Fig. 4 Hand-held EBOWLA disinfecting Ebola virus using body heat**

But like the drinking bowl, the temperature of the nano-coating cannot increase as its heat capacity vanishes by QM. Instead, QED induces the conversion of body heat to EM radiation having wavelength $\lambda = 2\ n\ d$, where, n and d are the RI and thickness of the coating. For example, QED induces the creation of UV-C radiation at 254 nm in a coating having n = 2 and d = 63 nm. Since the heat Q supplied by the hand is about 6 mW / $cm^2$, and since the minimum UV-C dose necessary to destroy [9] the Ebola virus is 0.4 mJ / $cm^2$, the Ebowla moved in 1 second scans is more than capable of disinfecting patients of the Ebola virus.

The QED induced UV-C radiation from the EBOWLA is especially suited for disinfecting Ebola in the developing world that lacks sources of electricity. Costs are minimal allowing free distribution by governments to individuals.

Moreover, the EBOWLA may be used to disinfect drinking water as suggested in the body of this paper. But even in the developed world, the EBOWLA would allow simple germicidal disinfection for nurses in hospitals or the public in their homes as well as assuring drinking water is free of pathogens.

Where drinking water disinfection is not so important, the EBOWLA need not be a drinking bowl and replaced with a flat nano-coated surface, say carried in the pocket of a nurse or worn as a badge.

Once exposed to the virus, Ebola workers discard protective suits– an expensive procedure in West Africa. By adding an appropriate nano-coating, the suits continually emit UV-C to remove attached Ebola viruses and allow repetitive re-use.

The applications of QED induced UV-C radiation in the disinfection of infectious diseases are numerous and diverse, the development of which is beyond the capability of the author. Collaboration with interested parties is solicited.

**References**

[1] WHO/UNICEF, Progress on Drinking Water and Sanitation: 2012 Update. 2012
[2] Mpenyana-Monyatsi L, Nomcebo H, Mthombeni NH, Onyango MS, Momba, MNB. Cost-Effective Filter Materials Coated with Silver Nanoparticles for the Removal of Pathogenic Bacteria in Groundwater. Int J Environ Res Public Health 2012; 9: 244–271.
[3] Prevenslik T. Cancer by Nanoparticles. NanoSafe 2010, November 18-20, Minatec, Grenoble
[4] Ferrero G. UV disinfection in developing Countries. UNESCO IHE, Delft, The Netherlands, November 6, 2014.
[5] Einstein A, Hopf L. Statistische Untersuchung der Bewegung eines Resonators in einem Strahlungsfeld. Ann. Physik 1910;33:1105-1120.
[6] Feynman R: QED: The Strange Theory of Light and Matter, Princeton University Press, 1985.
[7] Ultraviolet Disinfection, National drinking water clearinghouse fact sheet, Tech Brief
[8] Wikipedia, Surface Body Area. Wikipedia, the free encyclopedia
[9] Vatansever F, Ferraresi C, Pires de Sousa, MV, Yin R, Rineh A, Sharma SK, Hamblin MR. Can biowarfare agents be defeated with light? Virulence 2013;4:796–825.

# The Ebowla in the Disinfection of the Ebola virus in the developing world

Youngwood, Pa. - Dec. 1, 2014

QED induced UV-C radiation from the *Ebowla* - a hand-held nano-coated bowl - that provides inexpensive sterilization of drinking water from body heat in areas of the world lacking sources of electricity also disinfects the Ebola virus

Figure 4.1: The "Ebowla" disinfecting the Ebola virus with QED induced UV-C from body heat

### Background

The Ebola virus outbreak is a worldwide concern. Governments have instituted quarantine measures for communities and individuals that are affected by the Ebola outbreak. In the United States, the CDC has issued guidelines for how Ebola is to be disinfected in hospital and healthcare centers. CDC stands for Center for Disease Control. Currently, robotic UVGI systems are proposed to decontaminate healthcare facilities. UVGI stands for Ultraviolet Germicidal Irradiant. Hospital staff controls the robot, but vacate the room during the application of UVGI light pulses that continue for 5 minutes.

Greater flexibility than robots is provided with hand-held UVGI systems [1] that allow mobile and rapid disinfection of Ebola on surfaces and the surrounding air. Electrically powered 400 W hand-held devices producing a blade-like UV-C light beam (50 mm wide $\times$ 500 mm high) achieves 99% reduction of the Ebola virus in 5 seconds. Large areas are decontaminated using slow scanning of the UV-C light beam.

The UVGI systems disinfect Ebola including Tuberculosis and Lassa by irradiating surfaces and air using 254 nm UV-C light. But UV-C disinfection may be used for other pathogens, e.g., the CDC states that "about 1 in 20 patients [2] have an infection while receiving health care treatment in U.S. hospitals." Disinfecting health care facilities of all pathogens is challenging scientists to develop more advanced technology for better disinfection.

### Problem

The recent Ebola outbreak in West Africa highlights the inability of countries in the developing world to control the spread of the Ebola virus. Indeed, the protocol for Ebola disinfection available in the U.S. is too complex and costly. Simply put, lack of money has hampered healthcare facilities and personnel from controlling the spread of the Ebola. In the developing world, robotic and manually operated UVGI systems in the U.S. are simply too costly let alone requiring

sources of electricity which are usually not available. The developing world needs an inexpensive alternative to control Ebola that does not require electricity.

### Proposal

QED induced EM radiation from body heat in hand-held nano-coated bowls called *Ebowlas* is proposed to provide the UV-C from which Ebola on surfaces or in the air may be disinfected inexpensively without electrical power. QED stands for quantum electrodynamics and EM for electromagnetic. The 80 mm diameter *Ebowla* forms a cylindrical beam of UV-C light for disinfection. The protocol is to scan holding the *Ebowla* in one hand as illustrated in the thumbnail. In principle, the *Ebowla* is similar to the recently disclosed hand-held water bowl that uses body heat to kill water borne pathogens in drinking water, again without the need for electricity. See Press Release in *QED induced water purification* at `http://www.nanoqed.org`, 2015.

### Theory and Analysis

UV-C disinfection occurs as the body heat from the hand of the person holding the *Ebowla* is transferred to the nano-coating. Because of QM, the body heat cannot increase the temperature of the coating as its heat capacity vanishes under TIR confinement. QM stands for quantum mechanics and TIR for total internal reflection. Instead, the heat is conserved by QED inducing the heat to be converted to QED induced EM radiation at the TIR frequency of the coating. See numerous QED applications,*Ibid*, 2010-2015

The TIR confinement only occurs as body heat flows into the nano-coating, i.e., absent body heat there is no TIR confinement and UV-C radiation is not produced. The TIR wavelength $\lambda$ of the EM radiation is, $\lambda = 2nd$, where, $n$ and $d$ are the refractive index and thickness of the coating. Any suitable coating may be used. However, TIR requires the coating have a refractive index n greater than that of the *Ebowla*. For a zinc oxide coating having $n = 2$, QED induces the creation of EM radiation in the UV-C at $\lambda = 254\,\text{nm}$ for a coating having thickness $d = 63.5\,\text{nm}$.

The Planck energy $E$ of the UV-C is, $E = hc/\lambda$, where $h$ is Planck's constant and $c$ the velocity of light. For UV-C light, $E = 3.82 \times 10^{-18}\,\text{J} = 4.89\,\text{eV}$. The rate $R$ of UV-C photons created is, $R = Q/E$, where $Q$ is the body heat from the hand transferred into the nano-coating. Available body heat $Q$ may be estimated [3] from the total body heat of about 100 W distributed over the average surface area for adult men and women of $1.75\,\text{m}^2$ giving $Q = 5.71\,\text{mW/cm}^2$. Hence, the rate $R$ of QED induced UV-C created is, $R = 1.5 \times 10^{15}$ /cm$^2$s.

Guidelines [4] for the minimum UV-C intensity necessary to kill the Ebola virus suggests a dose of $0.4\,\text{mJ/cm}^2$ over a 0 to 30 s duration. For 1 s durations, the required UV-C power is $0.4\,\text{mW/cm}^2$. Since $Q = 5.71\,\text{mW/cm}^2$ is far greater than the power required for Ebola disinfection, the 80 mm diameter *Ebowla* using 1 second back and forth scanning is capable of disinfecting large areas of rooms in healthcare facilities.

### Conclusion

The QED induced UV-C radiation from the *Ebowla* is especially suited for disinfecting Ebola in the developing world that lacks sources of electricity. Costs are minimal allowing the *Ebowla* to be distributed to individuals by governments without costs. Moreover, the *Ebowla* may also be used to disinfect drinking water. But even in the developed world, the *Ebowla* would allow simple germicidal disinfection for nurses in hospitals or the public in their homes as well as assuring

drinking water is free of pathogens. Where drinking water disinfection is not so important, the *Ebowla* may be replaced with a flat nano-coated surface, say carried in the pocket of a nurse or worn as a badge.

### Extensions

Ebola disinfection by QED induced UV-C from body heat using hand-held *Ebowlas* is new, but not the use of body heat to power electronics. Recently, body heat in holding a flashlight was shown [5] to produce light. Peltier cells were built into the flashlight's casing to absorb body heat from a person's hand. Although QED induced radiation is far more efficient than the Peltier effect, only monochromatic light for a given coating thickness is produced. Therefore, using QED to make, say red or blue flashlights is possible, but not white light comprising a mix of frequencies. Whether the nano-coating thickness can be structured to produce QED induced white light remains to shown.

### References

[1] BBH, UV light technology, "UV hand-held lamp kills Ebola in seconds", Oct. 17, 2014

[2] IUVA, Ultraviolet-C Promises to be an Excellent Disinfection Technology For Use in Addressing Ebola Virus and other Hospital Acquired Infections, Oct. 17, 2014.

[3] Wikipedia, "Surface Body Area", Wikipedia, the free encyclopedia

[4] F. Vatansever, et al., "Can biowarfare agents be defeated with light?", Virulence 4, 796–825; 2013.

[5] T. Nguyen, "This Flashlight Is Powered by the Touch of Your Hand", Smithsonian.com, March 24, 2014

# QED Disinfection of Future Public Transport in Hong Kong

Pittsburgh - April 2, 2015 - PRLog

QED induced UV-C radiation produced in heated nano-coated surfaces of handrails and grab poles in future train cars and buses offers the Hong Kong Government a simple and permanent way to continuously disinfect SARS and other infectious viruses

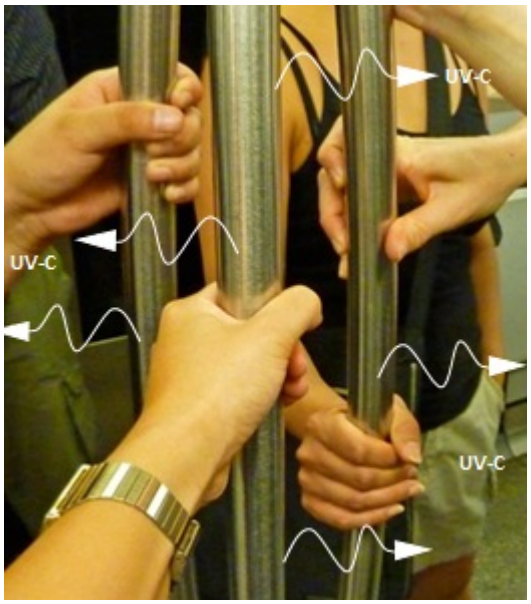


Figure 4.2: QED producing continuous UV-C radiation from grab poles in train cars and buses

### Background

Today, infectious diseases including SARS and H1N1 continue to haunt Hong Kong. SARS stands for severe acute respiratory syndrome and H1N1 for human swine flu virus. Since 2003, SARS was identified [1] by the WHO as a corona virus never before seen in humans. SARS is spread [2] by droplets from sneezing and coughing, but may be transmitted by touching contaminated objects.In fact, infectious diseases are usually transmitted through the hands by touching public surfaces. The hands then pass the virus into our bodies upon rubbing our eyes, nose or mouth before washing our hands. In Hong Kong, over 2.5 million commuters use the public transit system every day, and can easily spread infectious viruses to each other by contacting handrails and grab poles commonly used to hold and avoid falling under abrupt train car and bus motions.

In this regard, the Hong Kong authority constantly reminds commuters through automated announcements to hold handrails and grab poles for their own safety, but avoiding touching them is almost impossible making the transmission of infectious viruses by contacting public surfaces a virtual certainty.

In 2006, handrails in Hong Kong trains were disinfected by applying a spray of NSTDC to public surfaces to avoid the transmission of infectious viruses. NSTDC stands for nano silver-titanium

dioxide coating. All escalator handrails, the buttons on ticket issuing machines and all handrails and buttons in elevators including grab poles in train cars and buses were coated.

More recently in 2010, an anti-microbial coating was developed [3] that is thought to set a new standard in the disinfection of infectious viruses. Transparent, colorless and odorless, this smart coating can sustain surface disinfection by simply spraying on public surfaces. Compared with other disinfecting coatings, the smart coating is effective for at least 30 days. Test results show the smart coating can kill 99.9% of bacteria within 1 minute and 99% of the H1N1 virus within 3 minutes. The effectiveness of the smart coating lasts significantly longer than the conventional disinfectants, many of which will lose their disinfection capability as they evaporate. On the other hand, laboratory tests showed smart coatings are indeed capable of long-term disinfection with 100% effectiveness even after 30 days. The smart coating is not permanent and can be removed by washing off with detergent-in-water solution.

### Problems

Spraying NSTDC's and smart coatings on existing handrails and grab poles is a reasonable solution to disinfection of infectious viruses while allowing commuters to avoid accidental falling in train cars and buses, but spray coatings are at best a temporary solution. Future public transport need not be so restricted by including alternative designs with permanent coatings. Permanent nano-coatings capable of providng a continuos supply of UV-C are desirable in future handrail and grab pole designs. Moreover, claims that sprayed coatings containing colloidal silver are non-toxic must be questioned as nano-silver that enters the body unequivocally damages the DNA and can cause cancer. Alternative handrail and grab pole designs using permanent anti-microbial coatings emitting UV-C radiation are suggested.

### Proposal

QED induced EM radiation emitted from the surfaces of handrails and grab poles produced from internal heaters is proposed to provide the UV-C from which infectious viruses on their surfaces may be disinfected. QED stands for quantum electrodynamics, EM for electromagnetic, and UV-C for ultraviolet radiation at 254 nm. Similarly, handrails can be coated with UV-C emitting surfaces. During fabrication, the handrails and grab poles would be provided with a permanent 50-60 nm ZnO coating that can be periodically cleaned to minimize pathogen residue. The UV-C from a typical grab pole arrangement is illustrated in the thumbnail, but the electrical heaters inside the poles are not shown. The QED grab pole is similar to the recently proposed hand-held drinking bowl that uses body heat to disinfect water borne pathogens from water without electricity. See `http://www.prlog.org/12379390-nanotechnology-in-purifying-drinking-water-in-the-developing-world.html`

### Theory and Analysis

Handrails and grab poles in future public transit train cars and buses disinfect infectious viruses with UV-C radiation as the heat supplied to the inside of the handrail and poles is transferred to the surface ZnO nano-coating. Because of QM, the supplied heat cannot increase the temperature of the coating as its heat capacity vanishes under TIR confinement. QM stands for quantum mechanics and TIR for total internal reflection. Instead, the heat is conserved by QED inducing its conversion to QED induced EM radiation. See numerous QED applications at `http://www.nanoqed.org`

The TIR confinement only occurs as the heat supplied from the inside of the handrail and pole flows into the surface ZnO nano-coating. The TIR wavelength $\lambda$ of the EM radiation is, $\lambda = 2nd$, where, $n$ and $d$ are the refractive index and thickness of the coating. The ZnO coating having $n = 2.4$ only needs to have a higher refractive index than the pole material which is typically steel. Hence, QED induces the creation of EM radiation in the UV-C at $\lambda = 254\,\text{nm}$ in a coating having thickness $d = 53\,\text{nm}$.

### Conclusion

In future public transport, QED induced UV-C radiation from heated handrails and grab poles offers the Hong Kong government a direct and permanent solution for disinfecting infectious diseases in public transport train cars and buses. The nano-coatings of ZnO are permanently applied to the outside surface of the handrails and grab poles. Electrical heating must be provided inside the handrails and grab poles, but costs are minimal because of the low required power.

### References

[1] "SARS Virus", WHO, April 16, 2003.

[2] "SARS virus", WHO, Reuters, April 25, 2003.

[3] "HKUST Develops World's First Smart Anti-microbial Coating to Control Infectious Diseases" See `http://www.ust.hk/about-hkust/media-relations/press-releases/hkust-develops-worlds-first-smart-anti-microbial-coating-control-infectious-diseases/`

# Chapter 5

# Simple QED

Classical physics states heat is transferred by conduction, convection and radiation at the macroscale level. According to simple QED, the classical theory does not apply at the nanoscale level. Diverse applications of simple QED heat transfer are described in this chapter. A discussion of sonoluminescence is included with the suggestion of a possible application of simple QED, as the exact mechanism behind sonoluminescence currently remains unknown.


5.1 The Planck law cancelled? . . . . . 102
5.2 Simple QED induced Superconductivity . . . . . 107
5.3 QED Heat Transfer . . . . . 111
5.4 Sonoluminescence at Ambient Temperature? . . . . . 118

# The Planck law cancelled?

**Abstract:** Currently, the cancel culture in the USA driven by identity politics threatens not only the traditions of the USA as a country, but also the future of Science. Some scientists have placed their perception of Science above those of traditional values, the perceptions of which have consequences. Over the past decades, the consequence of US scientists cancelling the Planck law of quantum mechanics (QM) at the nanoscale in favor of classical physics has led to countless numbers of meaningless papers in the literature returning science to the dark ages at the exorbitant expense of the US taxpayer. Contrary to classical physics that allows atoms at the nanoscale to fluctuate in temperature, the Planck law denies atoms the heat capacity for temperature fluctuations. What this means is all known theories of Near-Field Radiation Heat Transfer (NFRHT) based on temperature fluctuations in nanoscale gap surfaces are invalid. In effect, the Planck law requires NFRHT theories that do not depend on temperature. One such theory is simple QED based on the Planck law that describes NFRHT by temperature independent EM travelling waves that carry heat flow, the EM waves by the photoelectric effect producing a plasma that increases heat flow. A similar photoelectric argument to replace quantum fluctuations in the attractive Casimir force by electrostatics was made over a decade ago. Recent NFRHT theory applied to single-digit nanoscale gaps is discussed.

***Keywords:*** NFRHT, Planck law, simple QED, EM waves, photoelectric effect, Casimir force

## I. INTRODUCTION

NFRHT began over a decade ago with the finding the Stefan-Boltzmann law could not explain the heat flux between hot and cold bodies separated by a nanoscale gap d as illustrated in Fig. 1.

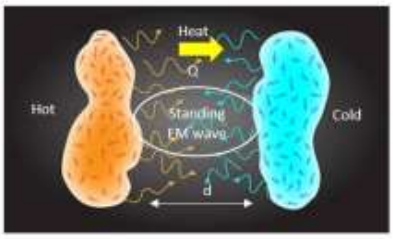


Figure 1. Near-field Heat Transfer

In NFRHT, the mechanisms by which heat Q flows from hot to cold bodies was extensively sought, all of which assumed surface temperatures of hot and cold bodies, the difficulty of measuring surface temperature in nanoscale gaps avoided by assuming bulk values. Non-thermal EM waves standing across the gap do not require surface temperatures, but presumably were excluded because since Fourier, temperature differences alone were thought necessary for heat Q flow. In Fig. 1, an EM wave is shown transferring heat Q across the gap d absent a temperature difference.

Today, all known NFRHT mechanisms transfer heat Q by gap surface temperature. What this means is temperature dependent phonons and evanescent waves known to exist in surfaces of bodies separated by large distances are assumed to exist in nanoscale gaps.

Contrarily, the Planck law [1] of QM denies atoms in the surfaces of nanoscale gaps the heat capacity to change in temperature which may be understood by considering the average Planck energy E of the atom mediated by the Bose distribution,

$$E = \frac{\frac{hc}{\lambda}}{\left[\exp\left(\frac{hc}{\lambda kT}\right) - 1\right]} \qquad (1)$$

and at 300 K is plotted in relation to classical physics in Fig. 2.

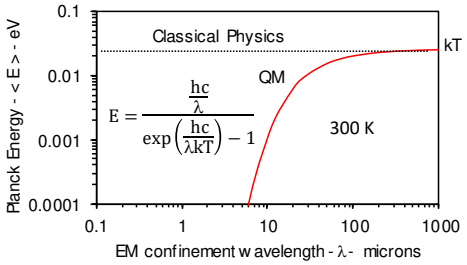


Figure. 2: Planck law of QM at 300 K
In the inset, E is Planck energy, h Planck's constant, c light speed, k Boltzmann's constant, T temperature, and λ the EM wavelength.

The Planck law at 300 K shows classical physics allows the atom to have constant thermal kT heat capacity over all EM wavelengths λ. QM differs as the kT heat capacity decreases for λ < 200 μm, and vanishes at the nanoscale for λ < 0.1 μm = 100 nm. Lacking heat capacity, atoms in nanoscale gap surfaces are absent temperature.

Today, NFRHT faces a dilemma in that all known theories based on phonons and evanescent waves, or variants thereof which require the atoms in the surface of nanoscale gaps to have temperature are invalid. In effect, the Planck law requires any NFRHT theory to be independent of temperature.

## II. PURPOSE

The purpose of this paper is to propose temperature independent simple QED heat transfer [2] as the NFRHT theory at the nanoscale. To illustrate how Science has cancelled the Planck law, the literature for NFRHT theory in single-digit nanoscale gaps is discussed and compared to simple QED.

## III. THEORY

Simple QED is the consequence of the Planck law denying atoms in nanostructures the heat capacity to increase in temperature upon the absorption of heat. QED stands for quantum electrodynamics, a complex theory based on *virtual* photons advanced by Feynman [3] and others. Simple QED is far simpler only requiring the heat capacity of the atoms in nanostructures to vanish allowing conservation to proceed by the creation of *real* photons comprising EM waves that stand across the nanostructure.

Similar to atomic quantum states described by electrons in discrete orbitals, simple QED quantum states are dependent on the dimension of the nanostructure over which the EM waves stand. The Planck energy E of a simple QED photon standing across a distance d is given by the time τ for light to travel across and back, $\tau = 2d/(c/n)$, where n is the index of refraction of the nanostructure material. Hence, the Planck energy E of the simple QED photons is, $E \sim h/\tau$ having wavelength $\lambda = 2nd$,

$$E = \frac{hc}{2nd} \qquad (2)$$

To illustrate simple QED, consider heat flux Q having wavelength $\lambda_o$ heating a nanoparticle (NP) of diameter d. For $\lambda_o >> d$, the NP is immersed in the heat flux Q as illustrated in Fig. 3.

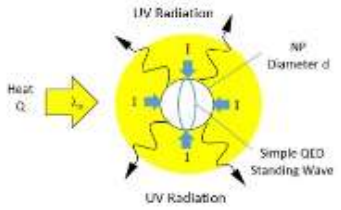


Figure 3. Heating of a NP

Importantly, heat flux Q absorbed by the NP must be placed under brief EM confinement to create the simple QED photons, the process of which depends on the Planck law denying NP atoms the heat capacity to allow the temperature changes required for Fourier heat conduction. Hence, the heat flux Q cannot penetrate the NP surface, and therefore conservation of Q at the NP surface can only proceed by creating non-thermal EM waves to carry the heat Q across and back the NP diameter d in time $\tau = 2nd/c$ that defines the energy E of the simple QED photon.

The EM confinement at the NP surface is caused by the brief inward spherical Poynting vector S = Q carrying momentum I (shown as blue arrows in Fig. 3). Here, U is the energy from the heat flux Q acting over an increment of time Δt, $U = QA \cdot \Delta t$, where A is the NP surface area, units of S and Q ~ $Wm^{-2}$ and U ~ J giving momentum I = U/c ~ Nt·s. Over time Δt, N simple QED photons having momentum $I_P = h/2nd$ are created, where $N < I/I_P$. Once $NI_P > I$, the simple QED photons are emitted to surroundings.

In the interest of whether simple QED photons absent a discrete heat Q may be created from the thermal surroundings alone, consider a NP in the ambient environment at temperature T. The Planck law gives the heat flux $Q_T$ as radiant thermal power energy density,

$$Q_T = \left(\frac{2c}{\lambda^4}\right)\frac{\frac{hc}{\lambda}}{\left[\exp\left(\frac{hc}{\lambda kT}\right) - 1\right]} \qquad (3)$$

The $Q_T$ momenta $I_T = U_T/c$ driven by the NP at absolute zero, provide the confinement of the simple QED photons, the number $N_T$ of which at temperature T is $N_T = Q_T V/E$, where V is NP volume, and $E = hc/\lambda$. At 300 K, $Q_T = 2.71 \times 10^5$ J/s·$m^3$. For Covid-19 vaccines [2] having d ~ 80 nm lipid NPs, $V = 2.68 \times 10^{-22}$ $m^3$. Taking n = 1.6, $\lambda = 2nd \sim 254$ nm or UVC with $E = 7.80 \times 10^{-19}$ J = 4.88 eV. Hence, the NPs emit $N_T \sim 100$ UVC photons/s to stimulate the immune system (Fig. 3). Depending on size, simple QED radiation from the IR to EUV may be emitted from NPs in ambient surroundings, albeit at low intensity.

The EM confinement of simple QED photons in the NP by the inward spherical momenta is not applicable to NFRHT in gaps between hot and cold bodies as illustrated in Fig. 4.

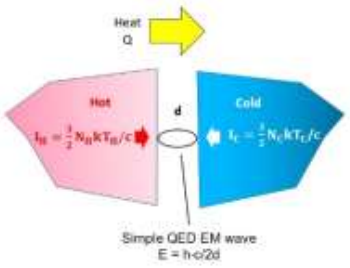


Figure 4. NFRHT.

Heat Q is transferred from hot to cold bodies across a nanoscale gap with vanishing thermal kT energy of atoms in hot and cold gap surfaces as required by the Planck law. To compensate for the surface atoms effectively at absolute zero, the number of adjacent atoms in hot $N_H$ and cold $N_C$ bodies having finite thermal kT energy $U_H = \frac{3}{2} N_H\, kT_H$ and $U_C = \frac{3}{2} N_C \cdot kT_C$ form the Poynting vectors of momentum $I_H = U_H/c$ and $I_C = U_C/c$ directed toward the respective gap surfaces, the momenta providing the EM confinement to form the simple QED photons.

Heat Q flows if the momentum $I_H > I_C$. In the gap, the Planck law precludes conservation of Q by a change in temperature, and instead proceeds by the creating a number N of EM waves, the heat Q/N ~ W/wave delivered to the gap d in time $\Delta t = 2d/c$ is,

$$\frac{Q}{N} = \frac{E}{\Delta t} = \frac{h}{4}\left(\frac{c}{d}\right)^2 \qquad (4)$$

The NFRHT time $\Delta t = d/2c$ is the same as the NP time $\tau = d/2nc$ having refractive index n = 1.

Q/N is based on evacuated gaps assumed in NFRHT theories. However, the simple QED wave energy E for small gaps at UV and EUV levels ionize the atoms in the gap surfaces to produce a plasma that upper bounds Q/N. In Casimir experiments, both plates usually gold plated were charged positive [4] by the simple QED induced photoelectric effect. But one plate was always grounded to avoid stray effects, and therefore the Casimir force is one of electrostatic attraction - not quantum fluctuations.

Similar to Casimir, NFRHT nanoscale gap surfaces of gold are charged positive but lacking a ground the electrons create a negative charged plasma with increased thermal conductivity [5] by one order of magnitude over uncharged conductivities. For gold having an ionization potential of E = 9.22 eV, the electron plasma forms in NFRHT gaps d < 70 nm.

## IV. APPLICATIONS

NFRHT between bodies separated by nanoscale vacuum gap distances d > 20 nm have been extensively studied and thought [6-8] to exceed the blackbody limit by the tunneling of evanescent waves. But for d at single-digit gaps, the heat flow Q was found [9] in disagreement with NFRHT theories as shown in Fig. 5.

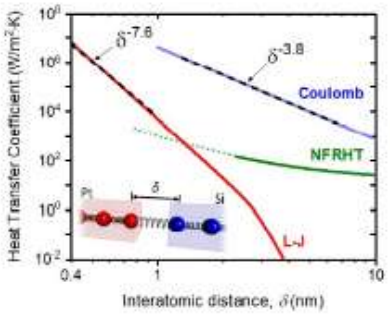


Figure 5. NFRHT and other theories.

Generally, the heat transfer coefficient H was found much higher than predicted by NFRHT theories of fluctuating temperatures. Fig. 5 shows L-J and Coulomb theories based on contact of opposing gap surfaces giving ~ 6 orders of magnitude higher H prompting [9] to suggest resolution by acoustic phonon tunneling.

Indeed, $H = 1.11 \times 10^6$ W/m$^2$K were reported [10] comparable to contact estimates shown in Fig. 5. However, the high H values were promptly rebutted in [11] on the basis of surface contamination. Today, the validity of NFRHT theories explaining single-digit nanoscale gaps remains in question.

Contrary to the suggestion [9] that acoustic phonon tunneling can account for the disparity is refuted as surface phonons only exist at ambient temperatures in the IR at 10-15 microns. Along gap surfaces, the intensity normal to the surface [7] at 100 nm is intensified, but still in the IR cannot propagate across the nanoscale gap. Surface phonon polaritons can be excited in the UV, but are more difficult to excite thermally.

Regardless, the Planck law denies gap surface atoms the heat capacity necessary for the temperature to create acoustic phonons to support NFRHT theories at single-digit nanoscale gaps. Indeed, simple QED based on the Planck law refutes Rytov's theory of temperature fluctuations at the nanoscale by requiring heat to be conserved by temperature independent EM waves, e.g., the Pt and Si atoms (Fig. 5) are at the same temperature. What this means is Rytov's theory is a classical notion not applicable to the nanoscale. By continuing this falsity, Science has in effect cancelled the Planck law.

More importantly, the focus of NFRHT over the past decades to show the heat Q transferred across in nanoscale gaps exceeds the blackbody limit was ill-conceived. Placing a nanoscale gap d in the middle a rod of length L having area A can never increase the heat flow $Q = \kappa A(T_1-T_2)/L$, where $\kappa$ is thermal conductivity and $T_1 > T_2$ are temperatures at the rod ends. Numerous NFRHT analysis showing high heat transfer H coefficients suggesting the gap increases heat flow Q are simply not correct as Q only depends on temperatures of the rod ends. Indeed, the heat transfer coefficient H = Q/A upper bounds NFRHT by the gap filled with a material having the same thermal conductivity $\kappa$ of the rod,

$$H = \frac{\kappa}{d} \sim \frac{W}{m^2K} \qquad (5)$$

which always exceeds the Planck blackbody limit. Therefore, NFRHT analyses over decades to support the argument that H exceeds the blackbody limit were never necessary.

In [9] Fig 2(e) gives the NFRHT theory computed Q ~ 35 nW/K at d = 1 nm. For tip area $A = 2.88x10^{-14}$ $m^2$, $H = Q/A = 1.2x10^6$ $W/m^2K$. But Eqn. 5 for gold having $\kappa$ = 320 W/mK increased to 3200 W/mK for ionization [5] gives $Q/A = 3200x10^9$ $W/m^2K >> 1.2x10^6$ $W/m^2K$ measured. Therefore, the heat flow $Q/A = 1.2x10^6$ $W/m^2K$ in [9] is not ionized.

The Planck blackbody radiation [10] is estimated as H = 2.1 $W/m^2K$. Since the measured $H = 1.11x10^6$ $W/m^2K$, the measured H is $5x10^5$ X greater than blackbody radiation. However, for gaps from a few Å to 5 nm [11] suggests the large deviations from NFRHT theory in [10] are caused by surface contamination effects. Further, [11] states H as large as 3 nW/K are reported in the literature which is overstated and instead should be H = 0.5 nW/K, but this is incorrect. Paper [9] gives 35 nW/K and [11] Fig. 3 (b-e) shows cleaning reduces H, but the mean minimum is closer to 2 nW/K not 0.5 nW/K.

In contrast to NFRHT theory, simple QED conserves power across the gap by creating EM waves at zero temperature difference consistent with the Planck law. For d = 1 nm, Eqn. 4 gives Q/N = 14.9 W/wave. But simple QED based on EM waves requires heat flow Q > 14.9 W, as otherwise heat does not flow across the gap. From [9] giving Q = 35 nW/K evaluated for $\Delta T$ = ~ 170 K gives $Q \sim 6x10^{-6}$ W < 14.9 W, and therefore simple QED requires heat flow Q = 0 across the 1 nm gap, as well as other single-digit nanoscale gaps.

Unlike simple QED, NFRHT theory based on fluctuating temperatures lacks a criterion for heat flow Q = 0 suggested from experiments on single-digit nanoscale gaps.

## V. CONCLUSIONS

NFRHT theory is based on the falsity that temperatures fluctuate in evacuated nanoscale gaps contrary to the Planck law that denies gap surface atoms the heat capacity necessary for temperature fluctuations.

All known NFRHT theories assume temperature fluctuations in gaps and implicitly require temperature differences between gap surfaces are therefore invalid by the Planck law.

Only temperature independent NFRHT theories are valid at the nanoscale, one of which is simple QED based on the Planck law itself.

Evanescent waves and phonons on the surface of macroscopic bodies do not exist in the surfaces of nanoscale gaps.

The Planck law aside, NFRHT touted as the method to show the Planck blackbody heat transfer is an unnecessary effort as simple thought experiments on rods shows a nanoscale gap does not increase the heat flow along its length.

Experiments to verify NFRHT based on temperature fluctuations are perhaps near impossible as the Planck law denies temperatures in nanoscale gaps. Measurements reported in the literature of temperature differences across nanoscale gaps which do not exist are shown to be fraught with error.

The Casimir effect by charging of plates by the simple QED induced photoelectric effect and not by quantum fluctuations is related to NFRHT by ionizing the gap surfaces, but is not significant for NFRHT in 1 nm gaps.

The Science acceptance of NFRHT theory based on Rytov fluctuational electrodynamics from classical physics does not bode well for the future of nanotechnology as cancelling the Planck law is a step back into the dark ages.

## REFERENCES

[1] Planck M. [1900] On the Theory of the Energy Distribution Law of the Normal Spectrum. Verhandl. Dtsch. Phys. Ges., 2:2-37.
[2] Prevenslik T. Simple QED Theory and Applications. nanoqed.org, 2015-2021.
[3] Feynman R., QED: The Strange Theory of Light and Matter. Princeton University Press, 1976.
[4] Prevenslik T. [2009] The Casimir Effect https://www.nanoqed.org/2009.php
[5] Petrro Y. V., et al. [2015] Thermal conductivity of condensed gold in states with the strongly excited electron subsystem. Journal of Physics: Conference Series 653 012087.
[6] Mulet, J. P., et al., [2002] Enhanced radiative heat transfer at nanometric distances. Microscale Thermophysical Engineering 6:209-222.

[7] Joulain, K., et al. [2005] Surface electromagnetic waves thermally excited: Radiative heat transfer, coherence properties and Casimir forces revisited in the near field. Surface Science Reports, 57: 59-112.
[8] Shen, S., et al. [2009] Surface phonon polaritons mediated energy transfer between nanoscale gaps. Nano Letters. 9:2909-2913.
[9] Jarzembski A. et al. [2018] Force-Induced Acoustic Phonon Transport Across Single-Digit Nanometre Vacuum Gaps. arXiv:1904.09383v2 [cond-mat.mes-hall].
[10] Kloppstech K., et al. [2017] Giant heat transfer in the crossover regime between conduction and radiation. Nature Communications 8:14475.
[11] Cui L., et al. [2017] Study of radiative heat transfer in Ångstrom- and nanometre-sized gaps. Nature Communications, 8:14479.

# Simple QED induced Superconductivity

**Abstract:** Almost a century ago, Cooper theorized a pair of electrons in a positive-charged metal lattice containing free electrons could attract each other by electron–phonon interaction, the phonon being the collective motion of the positively-charged lattice. The attraction only required a small binding energy of $10^{-3}$ eV, but thermal energy would rapidly break the pair which required lattice temperatures approaching absolute zero in order to allow a significant number of Cooper pairs to exist to explain superconductivity. But this is questionable as a crystal lattice near the ground state at absolute zero lacks the temperature necessary to even create phonons. Later, Bardeen suggested the exciton (electron-hole pairs) mechanism of electron attraction instead of phonons. In a sandwich structure consisting of alternate thin layers of metal and semiconductors, the metal electrons would tunnel into the semiconductor to form excitons that provide electron attraction. To this day, electron attraction by exciton mechanisms remains complex. In contrast, simple QED induced zero resistance instead of superconductivity is self-evident from first principles. Simple QED is a nanoscale heat transfer theory based on the Planck law of quantum mechanics (QM) that conserves heat with EM radiation instead of temperature. Hence, simple QED avoids the Cooper pair requirement of lattice temperatures approaching absolute zero by conserving attendant Joule heating by EM radiation which at EUV levels ionizes the silver lattice atoms and increases the free electrons to approach zero resistance in compensating for Joule heat. In effect, simple QED replaces superconductivity at absolute zero by zero resistance at ambient temperature. Only valid at the nanoscale, simple QED is applied to a nanowire comprising a stack of 200 nm diameter silver disks along the wire length, the disk thickness corresponding to the 82 nm half-wavelength of the 7.57 eV ionization potential of silver, the stack housed in an insulative evacuated tube. Separate circuits are provided for wire ionization and use of the wire in the nano-electronic application. An alternative nanowire design is presented comprising a stack of 100 nm spherical silver nanoparticles (NPs).

***Keywords:*** superconductivity, simple QED nanoscale heat transfer, Planck law

## I. INTRODUCTION

In 1956, Cooper proposed [1] a pair of electrons in a positive-charged metal lattice containing free electrons may attract each other by electron–phonon interaction, the phonon being the collective motion of the positively-charged lattice. But since the attraction only required binding energy of $10^{-3}$ eV, thermal energy in resistance heating would rapidly break the pair that in turn required absolute zero lattice temperatures. On this basis, Cooper concluded temperatures at absolute zero were necessary to offset resistance heating in superconductivity. But this is questionable as a crystal lattice near the ground state at absolute zero lacks the temperature necessary to even create phonons making the notion Cooper pairs unlikely in superconductivity.

Later in 1973, Bardeen [2] suggested the exciton (electron-hole pairs) mechanism of electron attraction instead of phonons, the exciton allowing the possibility of superconductivity at ambient temperature. In a sandwich structure consisting of alternate thin layers of metal and semiconductors, the metal electrons were thought to tunnel into the semiconductor to form excitons that provide electron attraction in Cooper pairs. Very thin metal layers are required and the formation of excitons by electron tunneling remain complex making superconductivity at ambient temperature elusive even to this day.

## II. PURPOSE

The Cooper theory of superconductivity by complex phonon and exciton mechanisms somehow allows electron pairs to attract in contradiction to the expected repulsion that are not self-evident in the search for zero electrical resistance at ambient temperature. Instead of superconductivity, the purpose here is to present the alternative of simple QED for a zero-resistance nanowire which is, indeed self-evident. The nanowire is illustrated in Fig. 1.

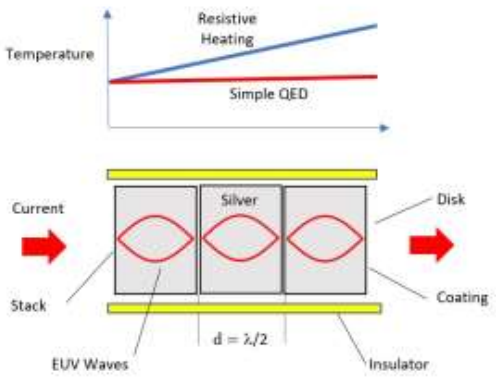


Figure 1. Zero-resistance Nanowire

## III. THEORY

Simple QED is a nanoscale heat transfer process based on the Planck law [3] of quantum mechanics (QM) differing significantly from classical physics by the kT heat capacity of the atom illustrated in Fig. 2.

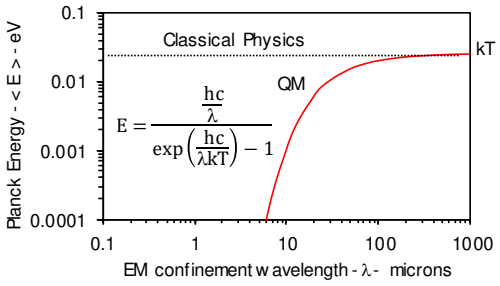


Figure 2. Planck law at 300 °K
In the inset, E is Planck energy, h Planck's constant, c light speed, k Boltzmann's constant, T absolute temperature, and λ the EM wavelength.

The Planck law at 300 K shows classical physics allows the atom constant kT heat capacity over all EM confinement wavelengths λ. QM differs as the heat capacity of the atom decreases for λ < 200 microns, and may be said to vanish < 0.1 microns. Implicitly, all nanotechnology comprising submicron nanostructures is subject to the same Planck constraint.

A decade ago, simple QED nanoscale heat transfer [4,5] was proposed based on the argument that the Planck law requires heat Q be conserved by creating non-thermal EM radiation. QED stands for quantum electrodynamics, a complex theory based on *virtual* photons advanced by Feynman [6] and others. In contrast, simple QED has nothing to do with Feynman's QED and only requires the heat capacity of the atoms in nanostructures to vanish allowing conservation to proceed by the creation of *real* photons forming EM waves [7] that stand across dimensions of the nanostructure. Hence, the Planck energy E of the simple QED state is,

$$E = \frac{hc}{2nd} \qquad (1)$$

where, n is the refractive index of the material over the dimension d of which the EM radiation stands

The heat Q flow across the dimension d depends on the time Δt for the EM wave to travel across and back thickness is, Δt = 2nd/c. Hence,

$$Q = N\frac{E}{\Delta t} = N\frac{h}{4}\left(\frac{c}{nd}\right)^2 \qquad (2)$$

where, N is the number of EUV waves. Importantly, simple QED based on EM waves requires the Joule heat $Q_J \geq Q$, otherwise Q = 0 as a EUV wave cannot form. This is an essential condition for the nanowire design presented in this paper.

## IV. APPLICATION

Simple QED is based on the conversion of Joule heat $Q_J$ to EM radiation in the nanowire. In Fig. 1, the wire comprises a stack of D = 200 nm diameter silver disks along the wire length housed in a loose-fitting evacuated insulator tube. Classically, current I through the stack encounters resistance R and produces Joule heat $Q_J = I^2R$ that increases the temperature along the wire length.

Simple QED differs by accepting the wire resistance R that exists for silver at ambient temperature. Unlike Cooper pairs, simple QED does not require the wire temperature to approach absolute zero. Instead, the Planck law precludes any temperature increase by Joule heat by spontaneously converting the Joule heat $Q_J$ into EUV radiation having a half-wavelength λ/2 standing across the thickness d of the disks. For silver with ionization potential E = 7.57 eV, λ =164 nm and d = λ/2 = 82 nm. EUV wavelengths ionize the silver disks by the photoelectric effect providing additional free electrons to enhance current flow. Simple QED makes Joule heat $Q_J$ an advantage and not the detriment of achieving the zero resistance of superconductivity.

The Planck law is valid across the D = 200 nm disk diameter and d = 82 nm thickness, but not along the nanowire length which may be several microns. The disks are separated by an evacuated gap g to allow metal to metal contact. To maintain the Planck law over wire length, separate circuits of Ionization and Control are provided as illustrated in Fig. 3.

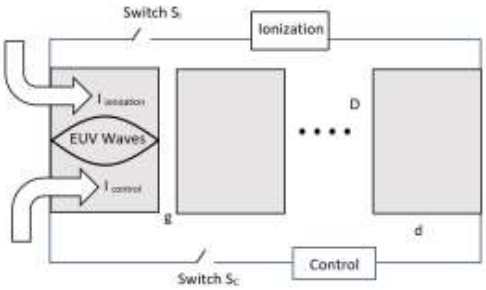


Figure 3. Nanowire Circuits at Zero-resistance

In operation, Ionization precedes Control by closing switch $S_I$ and opening $S_C$. Separate circuits are necessary as ionization requires much higher current than the Control circuit. Increasing the Ionization voltage should initiate an abrupt collapse of current $I_{ionization}$ as the silver in each disk ionizes. At this time, the switch $S_I$ is opened and $S_C$ closed. Any additional Joule heat $Q_J$ produced in the Control circuit is again converted to EUV radiation.

Simple QED converts Joule heat $Q_J$ in both circuits at any point along the wire to EUV radiation instead of temperature to achieve zero resistance. In contrast, zero resistance in superconductivity by Cooper pairs require temperatures along the wire to approach absolute zero.

The simple QED condition of Joule heat $Q_J > Q$ requires clarification. For silver in the EUV, the refractive index n ~ 1 and since only (N =1) is applicable to the nanowire, Eqn. 2 gives,

$$Q = \frac{h}{4}\left(\frac{c}{d}\right)^2 \qquad (3)$$

For disk thickness d = 82 nm, Q = 2.2 mW. The resistivity ρ of silver [8] is $1.62 \times 10^{-8}$ Ω·m. The resistance R = ρd/A: the disk diameter D = 200 nm area A = $3.14 \times 10^{-14}$ $m^2$ giving R = 0.0423 Ω. Since Joule heat $Q_J = I^2R$, the ionization current is 228 mA which is far larger than the 1-10 mA expected in Control circuits showing separate circuits are required as otherwise circuit elements are damaged.

Once the stack of nanowire disks is ionized, the wire resistance is expected to vanish allowing Control to operate at low currents with zero resistance.

## V. CONCLUSIONS

Superconductivity based on Cooper pairs that form from the attraction between free electrons in an electrical conductor by the interaction with phonons is questionable as phonons only exist at finite temperatures - not anywhere near absolute zero.

Electron attraction by exciton (electron-hole pairs) allowing the possibility of superconductivity at ambient temperature. However, producing the excitons using thin films is difficult, unless the photoelectric effect can be somehow implemented in superconductivity.

In this regard, superconductivity by simple QED differs from Cooper pairs produced by phonons or excitons as the focus shifts from achieving zero resistance at absolute zero to accepting the resistance at ambient temperature while converting the respective Joule heat to EUV radiation that ionizes the silver disks to increase the current flow offsetting resistance losses.

Simple QED is a nanoscale heat transfer process based on the Planck law that denies atoms in nanostructures the heat capacity to conserve heat by an increase in temperature. Instead, conservation proceeds by converting heat to EM radiation.

To illustrate superconductivity by simple QED, a nanowire is presented comprising a stack of 200 nm diameter - 82 nm thick silver disks in an evacuated insulative tube. The disk thickness is selected to be the half-wavelength of the first silver ionization potential, the Joule heat produced in the disk converted to EUV radiation that carries the current through the nanowire as an EM wave, the analysis of which is self-evident.

An alternative to stacking disks is stacking spherical NPs as shown in Fig. 4.

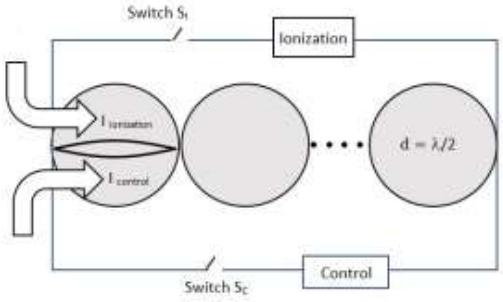


Figure 4. Spherical NP Design

The advantage of spherical NPs over cylindrical disks is the area of contact is well defined and fabrication is simplified, but the EM frequency across the wire diameter and along length are the same. Selecting UV at 254 nm as a compromise EM radiation, the spherical NP diameter d ~ 100 nm is suggested. Experiments are required to select the optimum nanowire design.

Similar to Joule heat $Q_J$ producing EUV radiation across the disk and spherical NPs, simple QED was proposed [9] as an alternative to chemiosmosis which is based on complex chemical reactions in converting adenosine diphosphate (ADP) to adenosine triphosphate (ATP). Mitochondria using body heat Q naturally produces UV in the 50-100 nm spaces between cristae as illustrated in Fig. 5

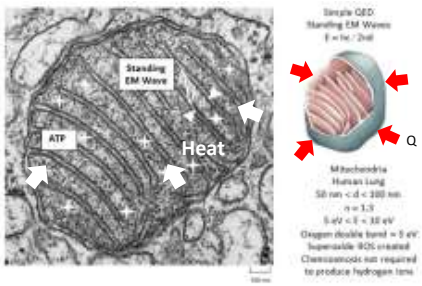


Figure 5. UV synthesis of ATP

In this way, ATP is directly synthesized from ADP by UV in the presence of phosphor in the mitochondria avoiding the complex sequential chemical reactions of chemiosmosis.

The work in this paper is still preliminary. Modifications of the nanowire design are reported when made.

**REFERENCES**

[1] Cooper L. N. [1956] Bound Electron Pairs in a Degenerate Fermi Gas. Phys. Rev. 156:1189-90.
[2] Bardeen J., et al. [1973] Model for an Exciton Mechanism of Superconductivity. Phys. Rev. B, 7:1020-1029.
[3] Planck M. [1900] On the Theory of the Energy Distribution Law of the Normal Spectrum, Verhandl. Dtsch. Phys. Ges., 2:2-37.
[4] Prevenslik T. 2013. Quantum Mechanics and Spin-valves. Proceedings of IEEE International Conference on Nanotechnology (IEEE-NANO 2013) Beijing, China.
[5] Prevenslik T., "Heat Transfer in Nanoelectronics by Quantum Mechanics," IEEE 12th Inter. Conf. Nanoelectronics, Birmingham UK, 20–23 August 2012
[6] Feynman R., QED: The Strange Theory of Light and Matter, Princeton University Press, 1976.
[7] Prevenslik T., [ 2015-2021] Simple QED Applications. https://www.nanoqed.org
[8] Silver Resistivity Resistivity (ρ) & Conductivity (σ) of Metals, Alloys, Rocks, and Soils - RF Cafe
[9] Prevenslik T. [2019] ATP by Endogenous UV Radiation. 10th Congress Targeting Mitochondria, Oct. 28-29, 2019 - Berlin, Germany.

*Proceedings of the World Congress on Recent Advances in Nanotechnology (RAN'16)*
*Prague, Czech Republic – April 1 – 2, 2016*
*Paper No. ICNMS 105*

# QED Heat Transfer

***Abstract -*** Classical heat transfer at the macroscale proceeds by three modes: conduction, radiation, and convection. However, at the nanoscale, heat transfer is not governed by classical physics, but rather by QM and a simplified form of QED. QM stands for quantum mechanics and QED for quantum electrodynamics. QED heat transfer is based on QM by the Planck law that requires the heat capacity of the atom to vanish under high EM confinement caused by the high surface-to-volume ratios of nanostructures thereby precluding the conservation of heat by the usual increase in temperature. EM stands for electromagnetic. Treating the nanostructure as a QM box with absorbed heat under high EM confinement, conservation proceeds by QED creating standing EM radiation that charges the nanostructure or is emitted to the surroundings. Diverse applications of QED heat transfer are described.

***Keywords*:** heat transfer, classical physics, quantum mechanics, QED

## 1. Introduction

In classical physics, heat transfer does not depend on the size of the structure allowing conservation of EM energy to always proceed by temperature changes. QM by the Planck law [1] differs by requiring the heat capacity of the atom under EM confinement at the nanoscale to vanish, and therefore the EM energy absorbed in nanostructures cannot be conserved by the usual change in temperature. Since EM energy is absorbed almost totally in nanostructure surfaces because of their high surface-to-volume ratios, surface atoms are naturally placed under high EM confinement that by the Planck law at nanoscale wavelengths precludes the atom from having the heat capacity to change in temperature with conservation proceeding by QED inducing EM radiation that charges the nanostructure or is lost to the surroundings.

## 2. Theory

### 2.1 QM Restrictions

Classically, atoms always have heat capacity to increase in temperature upon the absorption of heat irrespective of EM confinement, but QM does not. A comparison of the thermal $kT$ energy (or the heat capacity) of the atom by classical physics and QM by the Planck law is shown in Fig. 1.

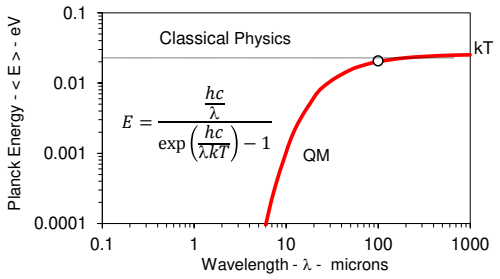


Fig. 1: Planck law of the Atom at 300 K
$E$ is Planck energy, $h$ Planck's constant, $c$ speed of light,
$k$ Boltzmann's constant, $T$ temperature, $\lambda$ wavelength

Fig. 1 shows QM allows the atom in macrostructures to have $kT$ energy and increase in temperature for $\lambda > 100$ microns. However, $kT$ decreases for structures having $\lambda < 100$ microns, while for nanostructures with $\lambda < 100$ nm, the atoms have virtually no heat capacity to conserve heat by an increase in temperature.

### 2.2 EM Confinement

QED heat transfer depends on the high surface-to-volume ratios of nanostructures. A closely related mechanism is TIR standing for total internal reflection. In 1870, Tyndall showed light is trapped by TIR in the surface of a body if its RI is greater than that of the surroundings. RI stands for refractive index. However, TIR usually occurs in the surface of macroscopic bodies having low surface-to-volume ratios where heat is absorbed throughout the volume of the body.

EM confinement of nanostructures differs from TIR because their high surface-to-volume ratios requires almost all of the absorbed heat to be spontaneously deposited in their surfaces, e.g., for a nanostructure of dimension $d$ between surfaces, atoms are placed under EM confinement solely by the high concentration of surface heat, i.e., there is no physical constraint of the atoms that produces the EM confinement. Hence, EM confinement is not permanent, sustaining itself only momentarily during absorption of heat, absent absorption of heat there is no EM confinement and QED induced EM radiation is not produced.

Since QM precludes the conservation of EM energy deposited in a surface by an increase in temperature, conservation proceeds by QED inducing the creation of standing EM radiation having half-wavelength $\lambda/2 = d$, where $d$ is the dimension between opposing nanostructure surfaces. Hence, the QED induced standing wave behaves as if it were external EM radiation momentarily absorbed and frequency up or down-converted to the EM resonance of the nanostructure. Because of the nanoscale thickness $d$, the short wavelengths $\lambda$ of QED induced EM radiation are in the UV and beyond having sufficient Planck energy to ionize and charge the nanostructure, and if not, the QED radiation is emitted to the surroundings.

QED is related to complex mathematics of light –matter interaction as described [2] by Feynman, but differs here in a far simpler form, i.e., supplying heat to a QM box with sides separated by distance $d$, QED creates standing EM radiation of half-wavelength $\lambda/2 = d$. Hence, QED conserves absorbed heat under the EM confinement of the QM box by frequency up or down -– conversion to the dimensions $d$ of the nanostructure, e.g., if the heat source is absorbed EM radiation, QED may blue or redshift the EM radiation. In simplified QED, the Planck energy $E$ of the EM radiation created is,

$$E = h\upsilon, \quad \upsilon = (c/n)/\lambda, \quad \lambda = 2d \tag{1}$$

where, the speed $c$ of light in vacuum is reduced by $n$, the RI of the nanostructure.

### 2.2 QED Emission

The wavelength of EM radiation induced by QED depends on the geometry and RI of the nanostructure. Typically, ZnO is used for electronics and YSZ for turbine blades. YSZ is yttrium-stabilized zirconia. QED induced EM radiation is shown in Fig. 2.

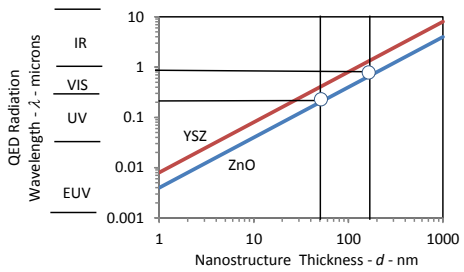


Fig. 2: QED Radiation Wavelength v. Nanostructure Thickness

## 3. Discussion

### 3.1. Thin Films

Cooling by QED radiation in nanoscale coatings is not new - first studied [3] by Kelemen. Since then, thin film data has been interpreted as reduced thermal conductivity because measured heat flow is lower than predicted by the Fourier equation. Because of this, the BTE was used [4] by Liu et al. to explain the reduced conductivity in thin films by the scattering of phonons. BTE stands for Boltzmann transport equation.

However, the BTE including the Fourier solutions are questionable [5] because heat balances did not include QED radiation beyond the UV lost to the surroundings, and therefore the thermal conductivity is concluded reduced from bulk. Alternatively, if the QED radiation loss is included in the balance, the conductivity remains at bulk, i.e., the heat to the film is almost totally converted to UV radiation. The exclusion of QED radiation from the heat balance is understandable [6] as frequencies beyond the UV would normally not be expected in thin film experiments.

### 3.2. Turbine Blades

Gas turbine blades are coated with TBC to insulate the blade from hot combustor gases. TBC stands for thermal boundary coating as described [7] by Lee. TBC stands for thermal boundary coating. In contrast, QED coatings [8] do not insulate the blade from high temperature, but rather cool the blade by converting combustor heat to non-thermal EM radiation that is dissipated in the surroundings. Under EM confinement in nanoscale TBCs, the heat capacity of the atom vanishes, and therefore the TBC cannot conserve heat from the combustor gases by the usual increase in temperature. Instead, conservation proceeds by the QED induced frequency up-conversion of combustor heat to non-thermal EM radiation at the EM confinement frequency of the TBC. QED cooling is passive avoiding the complexity of active fin and internal cooling by transferring the combustor heat away from the blades.

Turbine blade QED coatings differ from those in nanoelectronics because it is difficult, if not impossible to keep the coatings clean from fouling by combustor gas residues. Moreover, the application of nanoscale QED coatings of YSZ on nickel superalloys by APS and ALD is not yet demonstrated. APS stands for atmospheric plasma spray and ALD for atomic layer deposition. Conventional APS processes based on 10–100 microns particles are unlikely to produce submicron TBCs. ALD of nanoscale YSZ coatings on $Si_3N_4$ are encouraging, but research to determine whether ALD is capable of producing submicron TBCs on nickel based superalloy turbine blades remains to be proven.

### 3.3. EUV Lithography

Difficulties in extending Moore's law to 13.5 nm may be traced to LPP lithography. LPP stands for laser produced plasma. Based on classical physics, EUV light requires LPP to ionize [9] atoms at high temperature. EUV stands for extreme ultraviolet. LPP uses high power $CO_2$ lasers to heat solid and gas targets that produce EUV light by atomic emission. LPP systems are not only complex, but very expensive.

QED induced EUV lithography [10] based on QM offers a far simpler and inexpensive alternative in extending Moore's law, e.g., the EUV source comprises an ordinary spherical glass lens provided on the front surface with a nanoscale zinc oxide coating. A heater on the back surface supplies heat to the coating, but QM precludes any increase in coating temperature. Instead, QED converts the heat into the coating to a steady EUV light source. Lasers are not required.

The EUV wavelength is $\lambda = 2\ nd$, where n and d are the refractive index and thickness of the coating. For zinc oxide having $n \approx 2.5$, the QED radiation induced for coating thicknesses $d < 5$ nm is in the EUV having wavelengths < 20 nm, the degree of coherency depending on control of thickness variations. Extensions are made to mobile hand-held EUV sources for irradiating biological specimens.

### 3.4. Shock Waves

In shock waves, the work of gas compression is confined [11] almost totally in the surfaces of the nanoscale shock thickness because of its high surface-to-volume ratio. For shock thickness d, atoms between the surfaces are placed under temporary EM confinement by the high surface energy. Since the temperature cannot increase by QM, QED conserves the surface energy by creating standing EM radiation having wavelength $\lambda = 2\ nd$ within the shock thickness, where $n \approx 1$ for compressed gases. Because of the nanoscale shock thickness $d$, the QED radiation ionizes atoms and molecules in the shock thickness.

By QED, the shock wave thickness d may be estimated by experimentally measuring the wavelength $\lambda$ of EM radiation coming off the shock wave, i.e., $d \approx \lambda/2$ , e.g., QED radiation in the UV at $\lambda = 200$ nm suggests a shock wave thickness $d =$ 100 nm. But QED radiation in the EUV, say at $\lambda = 50$ nm corresponding to $d = 25$ nm may be difficult as EUV is immediately absorbed in air at the shock thickness surface and cannot be measured at any distance removed from the shock wave.

### 3.5. High Pressure Chemistry

Phenomena that occur at very high pressures - thousands or tens of thousands of atmospheres - are often observed at atmospheric pressure as quantified by optical spectra. Most notable is the nitric oxide dimer reaction $2\ NO_2 \rightarrow (NO)_2$ having a yield of less than 1 % dimer at atmospheric pressure, but in carbon nanotubes with ends open to atmospheric surroundings the yield is almost 100%. Assuming the dimers form under pressure, simple thermodynamic calculation shows that yields near 100 % would only be reached at pressures of 14,000 atmospheres. MC simulations allowing the consideration of other mechanisms confirm the observed high pressure enhanced dimer yields. MC stands for Monte-Carlo molecular dynamics.

However, MC simulations based on statistical mechanics assume [12] atoms in the confined phase have classical $kT$ thermal heat capacity. Indeed, the confined phase pressure $P$ is:

$$P = kT\left[\rho - \frac{1}{V}\ln\langle\exp\left(-\frac{\Delta U}{kT}\right)\rangle\right] \tag{2}$$

where, $\rho$ = density, $V$ = volume, and $\Delta U$ = energy. In contrast, QM by the Planck law restricts the atom heat capacity depending on the EM confinement. QM stands for quantum mechanics and EM for electromagnetic. Since the $kT$ heat capacity of the atom vanishes in the confined phase, the pressure P also vanishes. Hence, there are no high pressures and the dimer yield in the condensed phase is enhanced by another mechanism.

In this regard, atoms under EM confinement lacking heat capacity [13] cannot conserve the energy ΔU by the usual increase in temperature. Instead, conservation proceeds by the creation of standing QED induced non-thermal EM radiation inside the nanotube at frequencies in the EUV that by photolysis explain the enhanced dimer yield.

### 3.6. Near Field Enhancement

Recently, MIT mathematicians claimed [14] that if bodies are separated by small gaps, the blackbody-limit no longer applies. Moreover, if the gaps are nanoscale, say < 100 nm, the amount of heat transmitted between the bodies is claimed to exceed the blackbody limit by 100 to 1000 times. Since heat having wavelengths in the IR of a few microns cannot propagate across nanoscale gaps, the MIT claim is based on the assumption QM tunnels radiation across the gap from evanescent waves moving perpendicular to gap surfaces.

In near-field heat transfer, the theory [15] of evanescent waves assumes the long wavelength form of the Planck law to depend only on the temperature of the atom, i.e., for $\lambda$ > 100 microns in Fig. 1. However, for nanoscale gaps $g$ < 100 nm, atoms in the gap surfaces are under EM confinement corresponding to a standing half-wave, i.e., $\lambda/2 = g$, or $\lambda$ < 200 nm where the heat capacity of the atom vanishes. Hence, the fluctuating temperatures necessary to produce the charges and currents consistent with the FDT for radiative heat transfer do not exist. Indeed, evanescent waves in near-field heat transfer do not exist in nanoscale gaps. What this means is the claim that evanescent waves enhance near-field heat transfer beyond the blackbody limit is questionable.

In the alternative, QED radiation allows heat transfer across nanoscale gaps by creating standing EM radiation that tunnels [16] heat across the nanoscale gap at the wavelength of the EM confinement is $\lambda = 2\ g$. However, QED predicts no enhancement of heat beyond the blackbody limit in nanoscale gaps between bodies.

### 3.7. Superlens

In conventional optics, image quality depends on the diffraction limit. Recently, transformative optics using a superlens is proposed [17] to restore image quality below the diffraction limit. Indeed, superlens experiments [18] using a 35 nm silver film in contact with a 40 nm PMMA spacer under UV illumination at λ = 365 nm showed sub–diffraction-limited imaging of etched chromium objects down to 90 nm. PMMA stands for polymethyl methacrylate. When the superlens is removed, the diffraction-limited wavelength $\lambda^* = \lambda/n$ is controlled by the RI of PMMA, i.e., for $n$ = 1.5, $\lambda^*$ = 243 nm. With the silver film, the superlens was found to resolve the average cross section of the etched chromium objects to a line width of 89 nm.

Transformative optics depends on the evanescent enhancement across the thickness of the superlens and the condition the permittivity of the silver film and that of the adjacent PMMA are equal and of opposite sign. By QM, however, the silver film is under EM confinement across the thickness $d$ at wavelength $\lambda = 2\ nd$ that precludes

temperature fluctuations necessary for creating evanescent waves. Similar to near-field enhancement above, evanescent waves cannot be created across the thickness of the silver film. What this means is the observed enhancement of image quality has nothing to do with evanescent waves.

Instead, sub-diffraction-limited imaging in the super lens is proposed [19] to be a natural consequence of QED induced EM radiation in the silver film. In the QED interpretation, evanescent waves are not invoked. The QED process begins with the PMMA illuminated with UV at 365 nm giving diffraction limited EM radiation at $\lambda^* = 243$ nm. But the diffraction-limited EM radiation is absorbed in the silver film. Since the silver film cannot change in temperature because of QM, conservation proceeds by QED inducing the creation of EM radiation at wavelength $\lambda = 2\ nd$, where n is the RI of silver at wavelength $\lambda^*$ and $d$ is the silver film thickness. For $d = 35$ nm and silver at $\lambda^* = 243$ nm having $n = 1.28$, QED allows sub-diffraction-limited line-width of 89 nm consistent with experimental [18] observation.

### 3.8. Water Disinfection

UVC light as a disinfectant penetrates the cell wall of an organism to scramble the genes thereby precluding reproduction. Research has shown that the optimum UV wavelength range to destroy bacteria is between 250 and 270 nm.

QED induced UV radiation using hand-held nano-coated bowls is proposed [20] to allow West Africans to disinfect water at the point of use using body heat alone – no electrical power. QED disinfection is a consequence of QM that forbids the atoms under EM confinement inherent in the nano-coating to have the heat capacity to increase in temperature. By selecting a coating thickness, say 50 nm of ZnO having $n \approx 2.5$, the heat from the hand is conserved by QED inducing conversion to UVC radiation at $\lambda \approx 254$ nm. EPA guidelines for disinfection require a UVC dose of 38 mJ / cm$^2$. With body heat of about 6 mW / cm$^2$, the hand-held drinking bowl disinfects drinking water in about 7 seconds.

Currently, LED's in the UVC are limited [21] to EQE of a few percent and not expected to impact the disinfection market until 2017/2018. LED stands for light emitting diodes and EQE for external quantum efficiency. In contrast, the QED drinking bowl has 100% efficiency, but is limited by low body heat.

### 3.9. Cosmology by Cosmic Dust

In 1929, Edwin Hubble formulated the law that the velocity of a receding galaxy is proportional to its distance to the Earth. Hubble based his law on Doppler's Effect whereby the wavelength of light from the galaxy is redshift if the galaxy is moving away from us. Thus, by measuring the redshift of known spectral lines, Hubble claimed to know the recession velocity of the galaxy relative to the Earth.

However, cosmic dust comprising NPs of silicates permeate the vast reaches of the ISM. NP stands for nanoparticle and ISM for interstellar medium. If galaxy light is redshift upon absorption in dust which is also proportional to the distance to the Earth, velocity measurements of galaxies are no longer valid as the absorption of galaxy photons in NPs produces the redshift Z,

$$Z = (\lambda_o - \lambda)/\lambda \tag{3}$$

where, $\lambda$ is the wavelength of the galaxy photon which is redshift in the NP to wavelength to $\lambda_o = 2\ nd$.

Cosmological consequences are enormous as astronomers [22] based on the redshift of SN light have taken Hubble's law as proof the Universe is not only expanding, but the expansion is accelerating. SN stands for Supernovae. Redshift in dust means Universe expansion need not be occurring, let alone accelerating, thereby allowing the outstanding problems in cosmology to be simply resolved by Newtonian mechanics.

Regardless, the Hubble measurements of redshift may need correction for cosmic dust. In this regard, the Hubble redshift $Z_{Hubble}$ by the Doppler Effect gives the same Z for ALL galaxy photon wavelengths while QED induced redshift in dust depends on wavelength. A reasonable dust correction to Hubble's law depends on the difference between the shortest and longest wavelength galaxy photons, e.g., Ly$\alpha$ and H$\alpha$. Therefore, valid Hubble redshift from measured $Z_{Meas}$ is proposed [23] corrected using measured Z for individual Ly$\alpha$ and H$\alpha$ lines,

$$Z_{Hubble} = Z_{Meas} - (Z_{Ly\alpha} - Z_{H\alpha}) \tag{4}$$

where Ly$\alpha$ and H$\alpha$ stand for the $\alpha$ lines of Lyman and hydrogen.

### 3.10. Exoplanets

Discovery of exoplanets in far reaches of galactic space is a difficult task because of inherently faint images. Similar to the problems of black hole mass and galaxy rotation, proof of discovery is based on high-precision spectroscopy [24] to measure variations in light intensity as the planet spins. When observing a spinning exoplanet, half of the planet rotates away from Earth, while the other half rotates toward Earth. The spectrum of the side spinning away from us will show redshift, whereas the side spinning toward us will show a spectral blueshift.

The discovery by Oppenheimer et al. [25] of 4 planets orbiting the distant star HR8799 supported the theory that exoplanets surround other stars in the Universe is consistent with the planets that orbit our Sun. IR spectroscopic measurements of the suspected planets identified ammonia from 1450 to 1550 nm, acetylene from 1500 to 1550 nm, methane above 1650 nm, and possibly carbon dioxide from 1560 to 1630 nm, all of which are commonly observed in the atmospheres of planets in our solar system. However, molecular lines of carbon dioxide and methane should have been found in all 4 planets, but were only observed for 2 planets. In one planet, a weak carbon dioxide line initially not present appeared 4 months later. What this means is the spectra of HR8799 system are not likely produced by molecules.

QED redshift suggests the molecules thought measured by IR spectroscopy are in fact redshifted Lyα photons having a wavelength $\lambda_o$ depending on the NP properties. Indeed, NPs may produce near IR spectra similar to that of common molecules at high redshifts Z of Lyα photons. From Equation 3, the QED redshift wavelength $\lambda_o = (Z+1)\ \lambda$. A silicate NP having diameter $d \approx 500$ nm and $n \approx 1.5$ redshifts galaxy photons to a wavelength $\lambda_o = 2\ nd \approx 1500$ nm. For Lyα photons having $\lambda = 121.7$ nm, the redshift Z = 11.3. Hence, the NP redshift to 1500 nm could be mistaken as the ammonia line at 1450 - 1550 nm. Consistent with observation, the IR spectra has nothing to do with any molecular species, but most likely depends on cosmic dust NPs. Hence, redshifted Lyα radiation in dust to the near IR could be interpreted as proof of exoplanet discovery - when in fact the exoplanet may not even exist.

### 3.11. ISM Infrared Spectra

Dust NPs are thought to emit EM radiation by thermal emission at near to far IR wavelengths from non-equilibrium heating by single galaxy photons. In 1976, Purcell [26] showed single-photon heating produces a temperature spike of 40 K in very small NPs ($d$ < 0.005 microns) so that much of the absorbed energy will be radiated in the far IR near 60 microns. Today, Li and Draine [27] also propose NPs heated by single galaxy photons are the source of IR spectra.

However, the notion that NPs heat-up upon absorption of single galaxy photons is based on classical physics that allows the atom to have heat capacity. Contrarily, QM denies NP atoms under EM confinement the heat capacity to conserve the absorbed galaxy photon by a spike in temperature. Instead, QED produces IR in the ISM by redshift of Lyα photons as described above for exoplanets without increasing the NP temperature.

.

## 4. Conclusions

QED heat transfer finding basis in QM is proposed at the nanoscale as the mode of heat transfer alongside the classical modes of conduction, radiation, and convection at the macroscale.

At the macroscale, conduction is thought to be the most efficient mode of heat transfer. But at the nanoscale, the lack of heat capacity of the atom by QM precludes the temperature `changes necessary for thermal conduction, radiation, and convection. Unlike the macroscale, the Fourier heat equation is no longer applicable at the nanoscale.

Heat transfer at the macroscale conserves heat by changes in temperature, but at the nanoscale heat is conserved by creating charge or is lost to the surroundings.

Diverse applications of QED heat transfer presented based on QM suggest that classical physics at the nanoscale should henceforth be discontinued.

## References

[1] M. Planck, “On the Theory of the Energy Distribution Law of the Normal Spectrum,“ *Verhandl. Dtsch. Phys. Ges*., vol. 2, pp. 237, 1900.

[2] R. Feynman, *QED: The Strange Theory of Light and Matter*, Princeton University Press, 1985.

[3] F. Kelemen, "Pulse Method for the Measurement of the Thermal Conductivity of Thin Films," *Thin Solid Films*, vol. 36, pp. 199-203, 1976.
[4] W. Liu, Y. Yang, and M. Asheghi, "Thermal and Electrical Characterization and Modelling of Thin Copper Layers," Intersociety Conference on Thermal and Thermomechanical Phenomena in Electronic Systems, ITHERM,2005.
[5] T. Prevenslik, "Heat Transfer in Thin Films," Third Inter. Conf. on Quantum, Nano and Micro Technologies, ICQNM, Cancun, February 1-7, 2009.
[6] T. Prevenslik. (2010-2016). QED Theory and Applications [Online]. Available: http://www.nanoqed.org
[7] K. N. Lee, "Protective Coatings for Gas Turbines" In 'The Gas Turbine Handbook' (R. A. Dennis, Ed.) Section 4.4.2, NETL, 2006.
[8] T. Prevenslik, "QED Cooling of Gas Turbine Blades," Proc. ASME Turbo Expo 2014: Turbine Technical Conference and Exposition, June 16 – 20, 2014, Düsseldorf, Germany.
[9] B. A.M. Hansson, et al., "LPP EUV Source Development for HVM," in Emerging Lithographic Technologies X, Proc. of SPIE, vol. 6151, 2006.
[10] T. Prevenslik. (2014). Lithography [Online]. Available: http://www.prlog.org/12317992-lithography-by-qed-induced-euv-light-sources.html
[11] T. Prevenslik. (2015). Shock waves [Online]. Available: http://www.prlog.org/12474176-shock-waves-produce-qed-radiation-not-high-temperatures.html
[12] Y. Long, et al., "On the molecular origin of high-pressure effects in nanoconfinement: The role of surface chemistry and roughness," *J. Chem. Phys.*, vol. 139, 144701, 2013.
[13] T. Prevenslik. (2015). Confined Phases [Online]. Available: http://www.prlog.org/12501177-chemistry-in-confined-phases-by-quantum-mechanics.html
[14] O. D. Miller, S. G, Johnson, and A. W. Rodriguez, "Shape-Independent Limits to Near-Field Radiative Heat Transfer,"
*PRL*, vil. 115, 204302, 2015.
[15] K. Joulain, et al., "Surface electromagnetic waves thermally excited: Radiative heat transfer, coherence properties and Casimir forces revisited in the near field," *Surf. Sci. Rep.*, vol. 57, pp. 59, 2005.
[16] T. Prevenslik. (2015). Evanescent Waves [Online]. Available: http://www.prlog.org/12517435-evanescent-waves-do-not-exist-in-near-field-heat-transfer.html and "Near Field Radiation by Quantum Mechanics," Proc. ASME 2013 4th Micro/Nanoscale Heat & Mass Transfer Inter. Conf. MNHMT2013-22026, December 11-14, 2013, Hong Kong
[17] J. B. Pendry, "Controlling Light on the Nanoscale," *Progress in Electromagnetics Research*, vol. 147, 117, 2015.
[18] D. O. S. Melville and R. J. Blaikie, "Super-resolution imaging through a planar silver layer, *Optics Express*, vol. 13, 6, 2127, 2002.
[19] T. Prevenslik. (2015). Imaging [Online]. Available: http://www.prlog.org/12512936-super-image-quality-by-transformative-optics-or-qed.html
[20] T. Prevenslik, "QED Disinfection of Drinking Water in China," 2015 Inter. Conf. on Water Resource and Environment (WRE2015) July 25-28, Beijing, China.
[21] P. Mukish, 2015, UV LED - Technology, Manufacturing and Application Trends in disinfection, Yole Development.
[22] A. G. Riess, et al., "Type Ia Supernova Discoveries at Z >1 from the Hubble Space Telescope Evidence for Past Deceleration and constraints on Dark Energy Evolution," *ApJ*, vol. 607, 665, 2005.
[23] T. V. Prevenslik. (2015). Cosmic Dust and Cosmology [Online]. Available: Proc. of APRIM 2014: Galaxies, AGN and Cosmology – Daejon, Korea, http://aprim2014.org/08.php
[24] I. A. G. Snellen, et al. "Fast Spin of the Young Extrasolar Planet Beta Pictoris b," *Nature*, April 30, 2014.
[25] B. R. Oppenheimer, et al., "Reconnaissance of the HR 8799 exosolar system I: Near IR spectroscopy," arXiv:1303.2627v1 [astro-ph.EP]
[26] E. M. Purcell, "Temperature fluctuations in very small interstellar grains," *Astrophys. J.* , vol. 206, pp. 685, 1976.
[27] A. Li, and B. T. Draine, "Infrared Emission from Interstellar Dust. III. The Small Magellanic Cloud," *AsJ*, vol. 576, pp. 762–772, 2002.

# Sonoluminescence at Ambient Temperature?

**Abstract** Sonoluminescence (SL) is the light produced from the collapse of bubbles in water under ultrasound. Generally, SL is thought caused by the high temperatures that accompany the compression heating of air in bubble collapse. But the bubbles are filled with water vapor – not air, the water vapor during collapse condensing to liquid without any increase in temperature, and therefore the SL light is produced at ambient temperature. This is a significant finding in that some yet unknown mechanism exists by which SL light is produced at ambient temperature, thereby offering the economic potential of artificial lighting powered by a limitless source of clean renewable energy from the ambient thermal environment. SL at ambient temperature is proposed explained by a mechanism that treats the bubble as a quantum electrodynamics (QED) cavity having an electromagnetic (EM) resonant frequency that continually increases during collapse. This means EM radiation that resided in the QED cavity from the prior instant is continuously suppressed. But suppressed EM radiation in a QED cavity is energy loss that may only be conserved by an equivalent gain at its current resonant frequency, and therefore bubble collapse continually produces higher frequency EM radiation - the process called cavity QED induced EM radiation. Initially, the far infrared (IR) radiation from the ambient thermal kT energy of the water molecules in the bubble wall is suppressed to produce, say near IR radiation when the QED cavity collapses to near IR resonance. As the QED cavity resonance reaches visible frequencies, the near IR radiation is suppressed to produce visible radiation, and so forth. At ultraviolet (UV) resonance the visible radiation is suppressed to produce UV radiation while vacuum UV (VUV) radiation is produced from suppressed UV radiation at VUV resonances. Leakage of EM radiation from the bubble wall surface through the surrounding water appears as SL light having a broad featureless background spectrum from the near IR to the VUV. The VUV radiation produces OH* radicals that upon dissociation produce OH* emissions that superpose on the broad SL background spectrum. The generality of cavity QED induced EM radiation is shown applicable to SL from metal salt solutions, organics, and cryogenic liquids – including diverse applications in the solid state. Finally, a solid state device that produces light at ambient temperature is shown to satisfy limitations imposed by the 2nd law of thermodynamics.

**Keywords**: cavity QED, sonoluminescence.

## 1. Introduction

SL is the phenomenon of light emission [1] from a cavitation bubble generated within liquids irradiated with ultrasound, the light extended over a wide spectrum [2] from the near IR to the far VUV while having an extremely short duration [3] from 60 to 250 ps. SL is generally thought caused by high temperatures by the compression heating [4] of air during an adiabatic bubble collapse. Currently, the SL light is explained [5, 6] by the conversion of the air bubble into an Ar bubble as $N_2$ and $O_2$ are removed by chemical reaction at the high temperatures caused by adiabatic heating. But how air or Ar, and not water vapor fill a bubble nucleated in water under ultrasound has never been fully explained. Nevertheless, a consensus has emerged [7] that SL involves extraordinary temperatures in the bubble.

But there is a fundamental problem [8, 9] with high SL temperatures in bubbles nucleating and collapsing in water under ultrasound. Contrarily, the bubbles are not filled with air or Ar, but rather condensable water vapor as there is insufficient time at ultrasonic frequencies for air or Ar dissolved in the water to diffuse into the bubble. Vapor bubbles are required by Le Chatelier's principle[1] to maintain 2-phase equilibrium with the liquid bubble walls, and therefore the vapor tends to remain at ambient temperature and pressure as the

[1] Le Chatelier's principle states: "A system in equilibrium subjected to an external stress responds to reduce the effect of the stress." (1888). In a liquid-vapor system, an increase in pressure caused by a decrease in volume will cause the system to retreat from the increased pressure by the conversion of some vapor into liquid.

volume vanishes during bubble collapse – in sharp contrast to non-condensable gases like air or Ar where the gas temperature and pressure do indeed significantly increase as the volume vanishes [4].

Le Chatelier's principle is a statement of equilibrium between the water vapor and the liquid bubble wall. But the volume decrease in bubble collapse momentarily creates a non-equilibrium state of increased vapor temperature and pressure, and therefore some vapor condenses to liquid to lower the vapor temperature and pressure and restore thermal equilibrium with ambient conditions along a path governed by the Hertz-Knudsen [10] relation. Since the liquid bubble wall is a massive ambient temperature sink to the small quantity of vapor, the vapor remains at ambient temperature. Indeed, the Hertz-Knudsen relation was included [8,9] in computer solutions of bubble dynamics by the Rayleigh – Plesset (RP) equation [11] to show the temperature increase in a typical SL bubble is sufficiently small that the bubbles may be considered to collapse almost isothermally.

Yet, most of the early SL computer simulations [12] excluded water vapor in bubble collapse by making the assumption the bubbles are filled with air, and by treating the collapse as adiabatic instead of isothermal, air temperatures from 2000 to 10 million degrees were computed. More recently, RP simulations [13] including vapor condensation have been performed, but notably differ from [8,9] with regard to the condensation coefficient $\alpha_c$, and limits on the validity of the RP equation.

> The condensation coefficient $\alpha_c$ in the Hertz-Knudsen relation is defined as the probability of a vapor molecule sticking to the liquid water wall. If $\alpha_c = 0$, there is no sticking and the water vapor behaves as a non-condensable gas, such as air, giving bubble temperatures from 2000 to 10 million degrees. For $\alpha_c > 0$, the bubble temperature is reduced. But this is an academic exercise because the probability $\alpha_c$ the vapor molecule sticks to the wall can only be unity, i.e., even if sticking does not occur on the first collision, the molecule eventually sticks on subsequent collisions, as it cannot escape the bubble. Recent simulations [13] use $\alpha_c = 0.4$, and therefore predict far higher temperatures than actually [8, 9] occur.
>
> The RP equation is only valid if the bubble remains spherical during collapse, i.e., the water vapor pressure in the bubble is required to be greater than the pressure in the liquid wall. If not, the bubble wall fragments injecting microscopic liquid particles into the bubble cavity, and therefore the RP equation requires modification. One such modification [8, 9] replaces the RP equation with 1-D flow simulating the injection of particles into the bubble. Bubble wall break-up precludes spherical focussing of fluid flow to sonic velocities while limiting the bubble collapse velocity to 150 –200 $ms^{-1}$. Thus, the vapor molecules at ambient temperature having a RMS velocity of about 500 $ms^{-1}$ are always colliding to stick on the slower moving bubble wall as if the bubble wall is stationary.

It is therefore concluded based on Le Chatelier's principle and supported by computer simulations [8, 9] that the SL bubbles collapse almost isothermally at ambient temperature rather than by an adiabatic collapse at temperatures from 2000 to 10 million degrees.

## 2. Purpose

The SL light is most likely produced at ambient temperature – not at high temperature. The purpose of this paper is to present one such explanation of how SL light might be produced at ambient temperature – cavity QED induced EM radiation.

## 3. Objectives

Since SL is likely produced in an isothermal bubble collapse, a review of SL objectives is proper at this time to establish whether it is more promising to direct future SL research toward high or ambient temperature. The objective of SL at high bubble temperatures was to produce electricity by nuclear fusion in a bubble, the process called bubble fusion was first disclosed [14] in 1976. Recently, bubble fusion was even claimed [15] to be the discovery of the century in offering a source of limitless energy.

But the irony of science is that sometimes the converse of a premise proves more significant than the premise itself. Stated another way, SL at ambient temperature might instead truly embody the discovery of the century by providing a limitless source of artificial lighting from ambient temperature.

Because of Le Chatelier's principle, if the comparison of SL objectives were made over a decade ago, SL at ambient temperature might have been the more attractive choice. Indeed, the objective of SL at ambient temperature producing artificial light may be of far greater economic potential than by the electricity produced in miniature fusion reactors with inherent safety and radioactivity issues. Although not a direct producer of electricity, SL at ambient temperature may significantly reduce the burden of conventional power plants that otherwise supply the electricity for artificial lighting.

SL from liquids is not conducive to artificial lighting. In single bubble SL (SBSL), a single bubble is positioned at the center of a spherical pressure field by an arrangement of ultrasonic transducers. Since the intensity of light from a single SBSL bubble is faint even in a darkened room, the very large number of SBSL systems required to produce artificial light of commercial intensity renders SBSL impractical. In contrast, multi-bubble SL (MBSL) produces a swarm of SL bubbles from ultrasonic transducers spread over a wide region of liquid. But the spacing between the bubbles is still relatively large, and therefore a compact arrangement of MBSL bubbles is not possible. Both SBSL and MBSL require electrical energy to power the ultrasonic transducers, and therefore artificial light sources in liquids are not attractive economically.

Absent ultrasound, stationary nanoscale bubbles observed on solid surfaces under water that stabilize by nucleating on solid nanometer particles cannot be a source of commercial light because the particles quench the QED induced VUV radiation. Since the bubbles do not collapse, even if Ar.OH* excimers do form under VUV radiation there is no mechanism by which the Ar.OH* excimers may decompose to produce the SL light.

However, passive solid state materials fabricated into hollow nano shells might convert the steady heat flow from the ambient into VUV radiation that by photoluminescence is transformed into a commercial source of artificial light. See Appendix A.

## 4. Theoretical Background

Generally, the laws of thermodynamics preclude the spontaneous transformation of thermal kT energy from IR to VUV levels. But this is not true for IR radiation from the surface of a VUV resonant QED cavity. Indeed, the frequency up-conversion associated with transforming IR to VUV is the consequence of conserving EM energy in a QED cavity.

Cavity QED induced EM radiation follows from the most basic laws of physics – that low frequency EM radiation is suppressed in a high frequency QED cavity - the generality of the law applicable to QED cavities in both the solid and liquid state. Typically, IR radiation from QED cavity surfaces at ambient temperature is suppressed from atoms within the penetration depth of the resonant VUV radiation standing across the QED cavities. But in a QED cavity the EM energy loss from the suppression of IR radiation can only be conserved

by an equivalent gain at its resonant frequency, and therefore the atoms in the QED cavity surface are spontaneously excited by VUV radiation, the significance of which is that VUV radiation is produced at ambient temperature.

Generally, consider a spherical void of radius R in a solid or liquid as a QED cavity having an EM resonance emitting a VUV photon hυ shown in Fig. 1.

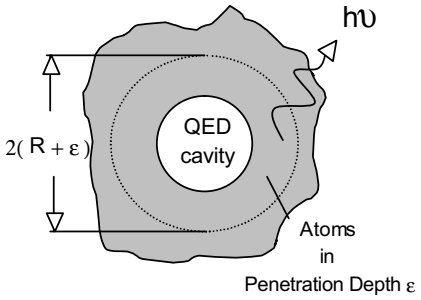


**Fig. 1** – Spherical Void in the Solid or Liquid State

The QED cavity extends beyond the surface of the void to include the penetration depth ε of the resonant standing EM wave. Initially for ε = 0, there are no atoms in the penetration depth of the standing EM wave for the respective IR radiation to be suppressed, and therefore the standing EM wave having an EM resonant wavelength λ = 4R is absent EM energy. But for ε > 0, the EM wave gains energy by conserving the loss from the IR radiation suppressed from the atoms. The EM wave has resonant wavelength λ and includes the depth ε necessary to assure absorptive (or reflective) boundary condition:

$$\lambda = 4(R + \varepsilon) \tag{1}$$

The Beer-Lambert law gives the depth ε by the absorption coefficient α of the cavity wall at the EM resonant wavelength λ = 4R of the QED cavity. The EM radiation intensity I at depth ε is related to the intensity $I_o$ at the QED cavity surface by,

$$I / I_o = \exp(-\alpha\varepsilon) \tag{2}$$

For αε = 5.15, over 99 % of the surface intensity is absorbed.

At ambient temperature, the thermal kT energy of atoms in depth ε is emitted as EM radiation at IR frequencies given [16] by the harmonic oscillator in Fig. 2.

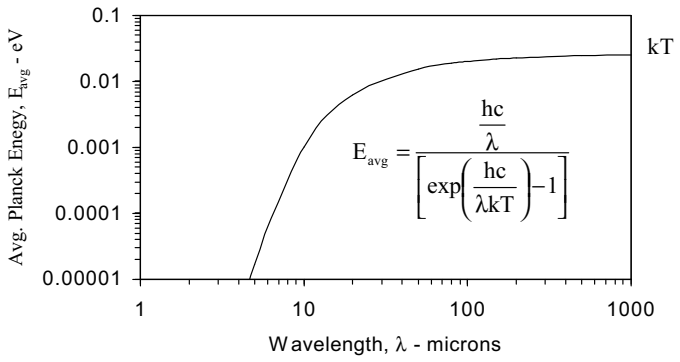


**Fig. 2** – Harmonic Oscillator at 300 K. In the inset, k is Boltzmann's constant, T is absolute temperature, h is Planck's constant, and c is the speed of light.

The suppression of IR radiation by cavity QED depends on the dimension [17] of the voids in the liquid and solid state. For IR radiation having wavelength $\lambda_{IR}$, the IR radiation is suppressed during bubble collapse at the instant $\lambda_{IR} > \lambda = 4(R + \varepsilon)$.

Rather than conserving the suppressed IR radiation by emitting a VUV photon, the temperature of the atoms in the penetration depth might approach absolute zero, but this takes time. Eventually, the loss of thermal kT energy does indeed lower the atom temperatures to absolute zero. However, the preferred path for prompt EM energy conservation is by the spontaneous frequency up-conversion of the suppressed IR radiation to the VUV resonant frequency of the QED cavity. Indeed, frequency up-conversion is the consequence of promptly conserving EM energy in a QED cavity.

Since the EM resonance of the QED cavity here is considered from the near IR to the VUV, the low frequency IR radiation of the atoms in the depth ε is suppressed. The total IR energy $U_{IR}$ suppressed,

$$U_{IR} = \frac{4\pi}{3}\Psi\left[(R+\varepsilon)^3 - R^3\right] \tag{3}$$

where, Ψ is the EM energy density, $\Psi \sim N_{dof}$ x ½ kT / $\Delta^3$, and Δ is the cubical spacing between atoms at solid or liquid density. $N_{dof}$ is the number of degrees of freedom of the atoms and molecules. Typically, for solids and liquids, $N_{dof}$ = 3 and 6, respectively.

Suppressed IR is a loss of EM energy that in a QED cavity may only be conserved by an equivalent gain in Planck energy at its resonant frequency. For QED cavities having EM resonance from the near IR to VUV, the conservation of EM energy may be expressed by,

$$NE = U_{IR} \tag{4}$$

where, N is the number of photons having average Planck energy E over the depth ε,

$$E = \frac{hc}{4(R+0.5\varepsilon)} \tag{5}$$

and if the leakage through the bubble walls during bubble collapse is neglected, then NE = $N_{near\ IR}\,E_{near\ IR}$ = $N_{visible}\,E_{visible}$ = $N_{VUV}E_{VUV}$. But the leakage of QED induced EM radiation is the well-known featureless SL background continuum, the simulation of which is presented later in this paper. Combining, the number N of photons having Planck energy E produced in the penetration depth ε,

$$N = \frac{8}{3}\pi\frac{kT}{hc}N_{dof}(R+0.5\varepsilon)\left[\frac{(R+\varepsilon)^3 - R^3}{\Delta^3}\right] \tag{6}$$

Generally, cavity QED induced EM radiation is produced at VUV frequencies *anytime* voids at the nanoscale are formed in solids and liquids thereby explaining why electrons by the photoelectric effect and photons by photoluminescence are observed at ambient temperature.

Although the IR radiation from the atoms in the penetration depth is incoherent, the VUV radiation becomes coherent [18] by the selective feedback of the QED cavity as an optical resonator. After emission of the VUV photon, the recovery of ambient temperature for the subsequent VUV emission depends on the liquid or solid state.

In the liquid state, the voids are nanobubbles. Under ultrasound, the thermal kT energy of the molecules in the penetration depth is recovered every cycle by the flow of liquid at ambient temperature. Work is required to flow the liquid, and therefore the 2nd law of thermodynamics is not violated. Although the number of SL photons produced by cavity QED induced EM radiation is discrete every cycle, the SL at ultrasonic frequencies appears as steady light.

The voids are nanogaps in the solid state. Solids absent fluid flow recover thermal kT energy in the penetration depth by conductive heat flow at ambient temperature across the boundary of the penetration depth. In the steady state, the suppression of IR radiation eventually causes the temperature of the atoms in the penetration depth to approach absolute zero. This enables heat to flow into the penetration depth from the ambient while cavity QED precludes any increase in temperature of the atoms in the penetration depth. Thus, EM energy is conserved by the spontaneous conversion of heat into VUV radiation.

In both liquid and solid states, the source of cavity QED induced EM radiation is *always* the thermal kT energy of the atoms at ambient temperature.

## 5. Applications

Cavity QED induced EM radiation is applied to SL at ambient temperature from liquid water, organics, metal-salt solutions in water and primary alcohols, and cryogens.

### 5.1 SL in Water

Historically, SL in water was first observed after saturation with Ar or air. But SL in water is also observed after saturation by other gases including $N_2$, $O_2$, He, Ne, and Xe. Similarity to Ar suggests the formation of OH* radicals by cavity QED induced EM radiation is common to all gases, the specifics depending on chemistry.

#### 5.1.1 Ar and Air Saturated Gases

Discoveries in the evolution of cavity QED induced EM radiation as a source of SL in water saturated with Ar or air are too numerous to cite, the more important beginning in 1939 with the finding [19] that SL in water was chemiluminescence. In 1983, radicals were identified [20, 21] in the ultrasonic irradiation of water and alkanes thereby supporting the notion that SL is caused by chemical reactions. In 1991, theoretical support [22] for SL by chemical reaction by radicals was established. The OH* emission in the dissociation of the OH* radical was first described [23] in 1996. In 1997, Ar gas doping was found [24] to be crucial to SL in water, the source of Ar in typical SL experiments being the ~ 1 % Ar in the atmospheric air naturally dissolved in water. In 2001, SL spectral lines were confirmed [25] to be the emission from dissociation of the OH* radical.

But how the OH* radical is produced at ambient temperature consistent with Le Chatelier's principle remains to be discovered. In this paper, the OH* radicals are proposed formed in the bubble wall by cavity QED induced EM radiation.

*Water Absorption, Planck Energy, and Number of VUV Photons and OH* Radicals*

The QED cavity walls are required to have absorptive (or reflective) boundary conditions to support momentary VUV standing waves. The absorption coefficient $\alpha$ of water [26] at ambient temperature is shown in Fig. 3.

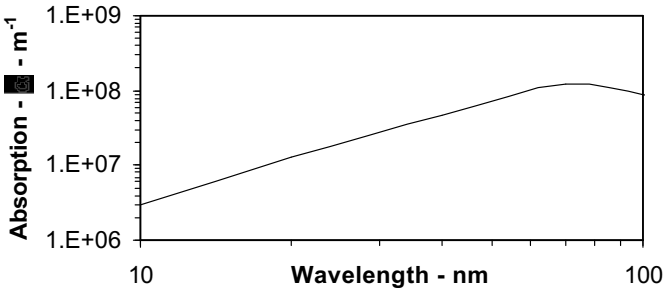


**Fig. 3** – Absorption coefficient α of Water

For αε = 5.15, the mean Planck energy E and number N of photons at fractions n of the penetration depth ε from the QED cavity surface are shown in Figs. 4 and 5. The maximum Planck energy E at n = 0.35, 0.1, and 0.05 is about 10, 16, and 20 eV, respectively. The corresponding number N of VUV photons are ~ $1x10^5$, $9x10^3$, and $3x10^3$. The VUV photons from 10 to 20 eV are consistent with the SL spectra [27] showing the spectral lines of the Ar atom and the $O_2^+$ ion are excited in sulfuric acid.

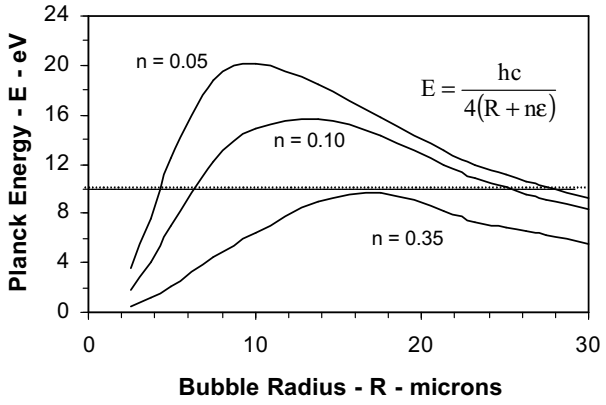


**Fig. 4** – Planck energy and Bubble Radius R

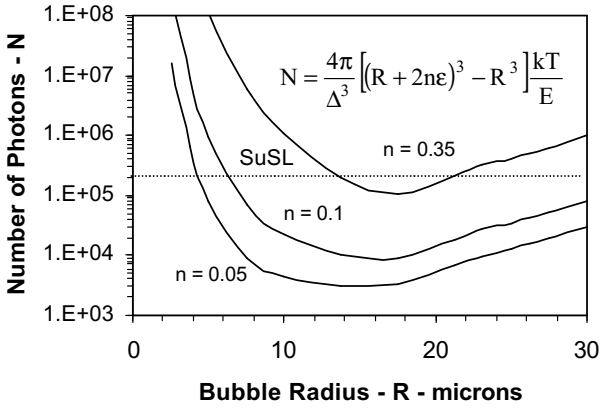


**Fig. 5** – Number of VUV photons and Bubble Radius

In water, the penetration depth ε as a function of bubble radius is depicted in Fig. 6. The minimum ε is about 30 nm and occurs at about R ~ 18 nm.

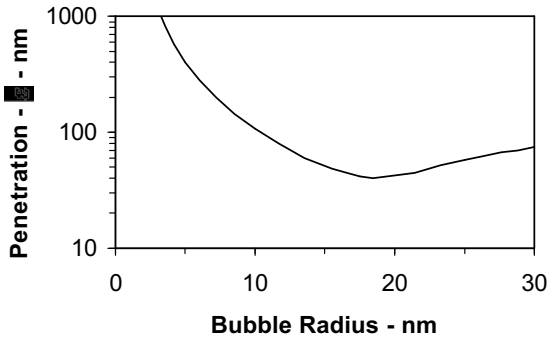


**Fig. 6** – Penetration Depth ε and Bubble Radius R

*Link between Ar Atoms and OH* Emissions*

In both SBSL and MBSL, water absent Ar [24] does not produce SL. Given the OH* emissions can only be caused by OH* radicals, it follows [28,29] the Ar atoms somehow initiate the formation of Ar.OH* excimers. Thus, cavity QED induced EM radiation forms Ar.OH* excimers either from excited (1) Ar* atoms, or (2) $H_2O$* molecules.

(1) *Argon Excited Excimers.* The VUV photons from cavity QED induced EM radiation at 9.85 eV at 126 nm [30] excite the Ar atom to produce the excited state Ar*. The excited Ar* atom efficiently combines with a pair of water neighbors by a three body reaction to form the Ar.OH* excimer,

$$\mathrm{Ar} + h\upsilon(126\ \mathrm{nm}) \rightarrow \mathrm{Ar}^* \tag{7}$$

$$\mathrm{Ar}^* + 2\mathrm{H_2O} \rightarrow \mathrm{Ar.OH}^* + \mathrm{H} + \mathrm{H_2O} \rightarrow 2\mathrm{H_2O} + \mathrm{Ar} + h\upsilon(310, 316, 318\ \mathrm{nm})$$

The excited Ar* can combine with a pair of Ar atoms in a three body reaction to form the excimer (Ar.Ar)*. However, the concentration of Ar in water is dilute, and therefore the three-body reaction is highly unlikely.

(2) *Water Excited Excimers.* Cavity QED induced EM radiation produces VUV photons that monotonically increase in Planck energy as the bubble collapses. The first singlet state $\mathrm{H_2O}^*(\tilde{\mathrm{A}})$ of the water molecule [29] is excited at ~ 7.5 eV and dissociates into H atoms and OH* radicals without producing SL light. Next, the $\mathrm{H_2O}^*(\tilde{\mathrm{B}})$ state at ~ 8.3 eV is reached but the yield is < 10% although excited radicals $\mathrm{OH}^*(^2\Sigma^+)$ are produced that emit SL light upon dissociation to H atoms OH radicals. The only significant SL light production of OH* radicals occurs upon the formation of the stable second singlet $\mathrm{H_2O}^*(\tilde{\mathrm{C}})$ state of water at 9.9 eV. Without Ar* or Ar.OH*, SL light from both $\mathrm{H_2O}^*(\tilde{\mathrm{C}})$ and $\mathrm{H_2O}^*(\tilde{\mathrm{B}})$ is possible.

$$\mathrm{H_2O}(\tilde{\mathrm{C}}) \rightarrow \mathrm{H_2O}(\tilde{\mathrm{A}}) \rightarrow \mathrm{OH}^*(^2\Sigma^+) \rightarrow \mathrm{OH}(^2\Pi) + h\upsilon(280, 310, 340\ \mathrm{nm}) \tag{8}$$

However, the $OH^*(^2\Sigma^+)$ radical [29] is quenched q by the water molecules.

$$OH^*\left(^2\Sigma^+\right) + H_2O \rightarrow OH\left(^2\Pi\right) + H_2O + q \tag{9}$$

Although the $OH^*(^2\Sigma^+)$ radical is formed by the VUV radiation, SL is not produced because the $OH^*(^2\Sigma^+)$ radical is quenched.

*Decomposition of Ar.OH* Excimers and Dissociation of OH* Radicals*

The Ar.OH* excimers decompose in the high pressures of bubble collapse. This is a likely event in that the energy of forming the Ar.OH* excimer is not high given the Ar.OH* dissociation [29] energy is ~ 0.02 eV. Indeed, the decomposition of the Ar.OH* excimer is the path for SL light production.

For SBSL, the 3-D stagnation pressure $P_S$ as the bubble walls collide, $P_S \sim 3 \times \frac{1}{2} \rho V_C^2$. From [8, 9], the bubble collapse velocity $V_C \sim 150$ - 200 $ms^{-1}$ and $P_S \sim 340$ to 600 atm. Since the dissociation pressure [29] of Ar hydrates is about 105 atmospheres, the Ar.OH* decomposition is likely. Lower collapse pressures are expected in MBSL.

*The Standard Unit of SL*

The standard unit of SL (SuSL) is the experimental [24] number of SL photons emitted from a SBSL bubble in air saturated water, i.e., SuSL ~ $2x10^5$. Figs. 4 and 5 show the excited Ar* state comprises N ~ $1x10^5$ photons at E ~ 10 eV, and therefore cavity QED induced EM radiation is consistent with the SuSL, i.e., N ~ SuSL is reasonable.

*RP Response at the Nanoscale*

RP simulations of bubble collapse give wall velocities $V_C$ and vapor pressure ratios $P_{vap} / P_{vapo}$ that depend on the minimum radius $R_{min}$. Early RP simulations [8, 9] at the microscale for $R_{min} \sim 0.5$ μm gave $V_C \sim 150 - 200$ $ms^{-1}$ and $P_{vap} / P_{vapo} \sim 5 - 10$. But cavity QED induced EM radiation having Planck energy E > 5 eV is produced at bubble radii R < 50 nm, and therefore requires the RP response at the nanoscale.

However, the microscale RP response [8, 9] is valid at the nanoscale if the mean free path MFP of the water vapor molecule is greater than the bubble diameter 2R, i.e., MFP > $2R_{min}$. If so, the vapor has condensed on the bubble wall. The condensation criterion,

$$2R_{min} < MFP = \frac{kT}{\sqrt{2}\pi P_{vapo} d^2} \tag{10}$$

where, d is the diameter of the water molecule, d ~ 0.2 nm. For $P_{vapo} \sim 2340$ Pa and T ~ 300 K, MFP ~ 10 μm and $R_{min} \sim 5$ μm. Following [8,9] under the constraints of the Hertz-Knudsen relation and unity condensation coefficient, the microscale RP response for a typical bubble dissolving under atmospheric pressure to radius $R_{min}$ is shown in Fig. 7.

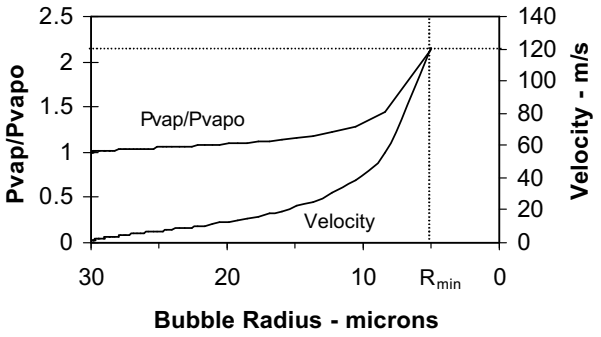


**Fig. 7** – Bubble Dissolving under Atmospheric Pressure - Microscale RP Response

The microscale RP response at radius $R_{min} \sim 5$ μm gives $V_C \sim 120$ ms$^{-1}$ and $P_{vap} / P_{vapo} \sim 2.2$. Thus, $P_{vap} \sim 5150$ Pa giving an equilibrium temperature T ~ 33 C for the water vapor that does not increase further as the bubble collapses to the nanoscale, i.e., the bubble collapses almost isothermally. Moreover, the velocity $V_C$ does not change significantly over the time it takes for the bubble walls to collide, and therefore the microscale RP response [8,9] for the velocity $V_C \sim 150 - 200$ ms$^{-1}$ is a reasonable estimate of $V_C$ at the nanoscale.

*Featureless SL Spectra*

In bubble collapse, SL light is continually produced in the bubble wall by cavity QED induced EM radiation. SL begins in the far IR, although recorded SL spectra begin in the near IR. Regardless, the EM radiation continues through the VIS and VUV until the bubble walls collide. Thus, the spectrum of SL light appears to have a continuous and featureless background consistent with [2] observation. If the EM radiation coincides with atomic lines or molecular bands of a species dissolved in the liquid or the liquid itself, the SL spectrum shows peaks above the background, e.g., the SL light from the decomposition of Ar.OH* excimers superposed on the featureless SL spectra from cavity QED induced EM radiation.

The featureless SL spectra may be understood by considering a spherical bubble of radius R described above dissolving under atmospheric pressure. Photons stand across the diameter in the penetration depth e at the EM resonance of the bubble. From Eqns. 5-6, the EM energy at any instant in the bubble collapse may be written,

$$U = \frac{1}{2} NE \tag{11}$$

where, N is the number of water molecules in the penetration depth e, ½ N is the number of QED photon pairs standing across the bubble, and E is the average Planck energy in the depth ε. Combining,

$$U = \frac{1}{6}\pi\left[\frac{(R+\varepsilon)^3 - R^3}{\Delta^3}\right]\left(\frac{hc}{R+0.5\varepsilon}\right)$$

For e << R,

$$U \cong \frac{\pi}{2\Delta^3} hc\varepsilon R \tag{12}$$

During bubble collapse, the SL power P emitted is the rate of change of the Planck energy in the penetration depth e and depends on the absorption coefficient α. Fig. 6 shows ε for water is lower bound at ~ 30 nm, and therefore is taken to lower bound the power P.

$$P = \frac{dU}{dt} = \left(\frac{\partial U}{\partial R}\right)\frac{dR}{dt} \cong \frac{\pi}{2\Delta^3} hc\varepsilon V_C \tag{13}$$

where, $dR/dt = V_C$ is the velocity of the bubble collapse. The absorption of the QED induced EM radiation between the bubble and the photomultiplier is assumed negligible, at least until VUV radiation is produced just before the bubble walls collide.

IR radiation is suppressed as the bubble collapses to radius $R_o \sim 25$ microns. Why this is so may be understood from Fig. 2. The kT energy at ambient temperature is observed to saturate at 0.0258 eV for $\lambda > 100$ microns. Since $\lambda = 4R$, the minimum R necessary to reach the full kT energy is 25 microns. During collapse, the suppressed IR is conserved by successively higher frequency photons by the increasing EM resonance of the bubble. The EM radiation that leaks out of the penetration depth produces the featureless broadband SL spectrum. If the EM radiation coincides with a quantum state of a chemical species in the bubble wall the emission appears as a spike on the broadband background.

Clearly, the IR radiation suppressed at the beginning of collapse leaks out apidly, thereby depleting the available kT energy to produce higher energy VIS and VUV photons. But the thermal kT energy of water molecules in the penetration depth ε is constantly being replaced by water molecules from the underlying bulk. The total amount of thermal kT energy $U_o$ available to supply the SL power P is that necessary to fill the bubble of radius $R_o$ at the beginning of collapse,

$$U_o = \frac{1}{2} N_o N_{dof} \frac{kT}{2} = \frac{2\pi}{3}\left(\frac{R_o}{\Delta}\right)^3 3kT = 2\pi kT\left(\frac{R_o}{\Delta}\right)^3 \tag{14}$$

where, $N_o$ is the number of water molecules in sphere of radius $R_o$. The thermal energy $U_o$ as the source of broadband EM emission is assumed far greater than that necessary to produce the broadband SL power spectrum. The RP equation is solved numerically by assuming the water molecules in the penetration depth are always maintained at ambient temperature T as the bubble collapses. The thermal kT energy U accumulates every time step,

$$U = U_{old} + Pdt \tag{15}$$

where, $U_{old} = 0$ at $t = 0$, and dt is the time step in the RP solution..

The SL power P emitted from the bubble and the fraction $U/U_o$ as a function of time t are shown in Fig.8. The maximum power P is found to be about 34 mW. This agrees with the SL power [47] of 30 mW measured in 1992. The fraction $U/U_o \sim 4x10^{-4}$ shows the available thermal kT energy in filling the bubble is hardly diminished by that necessary to produce the broadband EM radiation, and therefore the assumption that the penetration depth e is generally populated by water molecules at ambient temperature is justified.

The broadband SL spectrum produced as the bubble dissolves under atmospheric pressure is shown in Fig. 9. The SL spectrum does not begin in the near IR, but rather in the far IR at about 100 microns. In effect, cavity QED induced EM radiation is a continuous variable frequency excitation source that produces the spectral lines and broadband featureless of the liquid and impurities observed in SL spectra. The continuous nature of cavity QED induced EM radiation is important as otherwise the precise lines of Ar at 9.85 eV, bond breakage of $O_2$ and $O_2^+$ at 5.1 and 6.5 eV, and ionization of $O_2$ at 12.1 eV cannot be excited. Indeed, absent cavity QED induced EM radiation, the Ar.OH* excimers do not form and OH* spectral lines are not observed.

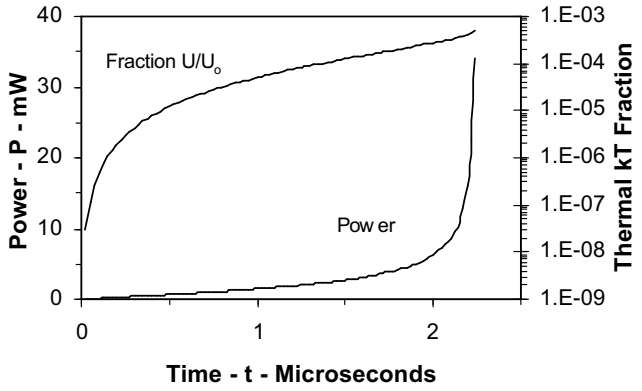


**Fig. 8** Bubble dissolving under Atmospheric Pressure – Power and Fraction of Available kT Energy Depleted during Bubble Collapse

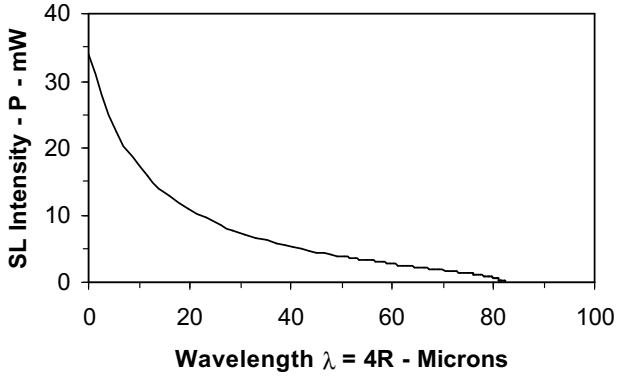


**Fig. 9** Bubble dissolving under Atmospheric Pressure - Broadband SL Emission Spectrum

The SL spectrum [27] for sulfuric acid and water is nearly flat over the range of wavelengths from 800 to 200 nm because of the uniform SL excitation produced in cavity QED induced EM radiation. The ~ $2x10^5$ VUV photons at ~ 20 eV having wavelength ~ 62 nm have always been present in SL but not previously observed because of the cut-off of water at about 200 nm. But ~20 eV photons are observed in SL from sulfuric acid because sulfuric acid is transparent down to and below 200 nm.

*SL Broadband Spectrum and Bremsstrahlung*

The broadband SL spectrum is the response of the liquid surrounding the bubble to cavity QED induced radiation from the near IR to the VUV as depicted above in Fig 10. Similar to sulfuric acid, the SL spectrum from water is a complex relation of transmission coefficients with wavelength. The correctness of cavity QED induced EM radiation may be assessed by comparing SL emission [31] to bremsstrahlung radiation from plasma at 100,000 K in water or from plasma at 200,000 K in sulfuric acid. This is not to say plasma exists in bubble interior in water or sulfuric acid during collapse, as the bubble remains at ambient temperature. But if the Planck energy E given by cavity QED induced EM radiation, say in water is equivalent to bremsstrahlung temperatures of 100,000 K, it is also consistent with the measured SL spectrum.

Taking the wavelength λ of the Planck energy E produced in the QED cavity as the minimum cutoff wavelength $\lambda_{min}$ associated with the bremsstrahlung radiation,

$$E = \frac{hc}{\lambda_{min}} = \frac{hc}{4(R + 0.5\varepsilon)} = kT_B \tag{16}$$

where, $T_B$ is the plasma temperature, or $T_B \sim 11{,}600$ K/ eV. Fig. 11 shows Planck energy E from cavity QED induced EM radiation is inversely proportional to $\lambda_{min}$ consistent with bremsstrahlung radiation. For E ~ 8.3 eV, $T_B \sim 100{,}000$ K, and therefore cavity QED induced EM radiation also closely follows the measured SL spectrum.

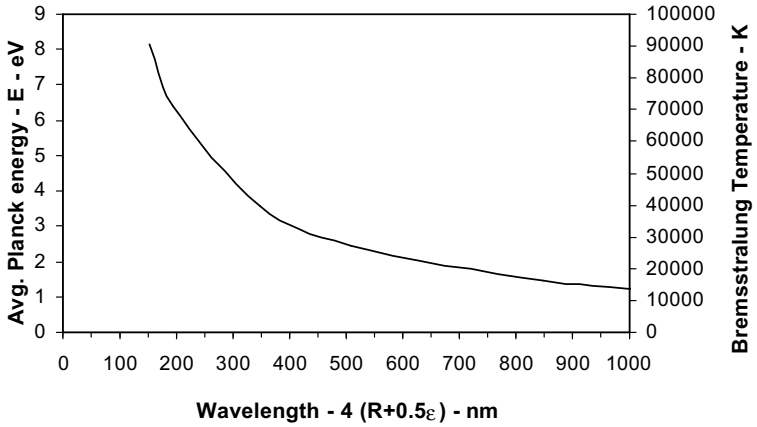


**Fig. 11** – Cavity QED induced EM radiation and equivalent bremsstrahlung temperatures

### 5.1.2 Saturated Gases other than Ar and Air

Although SL is commonly observed in water saturated with air containing Ar at atmospheric concentration, SL in water is also observed after saturation by other gases including $N_2$, $O_2$, He, Ne, and Xe that otherwise are absent Ar or air. In cavity QED induced EM radiation, SL in water saturated with *any* gas X follows that described above for Ar.

*Source of SL and the IR to VUV Continuum*

The source of SL for any gas X including Ar and air is cavity QED induced EM radiation from the IR to the VUV that in a photochemical process has the Planck energy at ambient temperature to produce the second singlet $H_2O^*(\tilde{C})$ state of water. Stated another way, the excited states of water are produced from the broadband excitation by cavity QED induced EM radiation in the manner of a variable frequency IR to VUV laser.

In contrast, the source of the IR to VUV continuum is thought [28] to be the OH* emissions caused by high temperatures (~ 15000-30000 K) in adiabatic bubble collapse. That high temperature alone is insufficient to explain SL follows from the fact that drastically different SL spectra are found for additives, i.e., small amounts of *n*-butanol suppress SL while carbon disulfide in small quantities does not change SL. Both $CS_2$ and *n*-butanol are dissociated at high temperatures, and therefore both additives would have similar – not drastically different effects on SL. On this basis, it was concluded [28] that the additives chemically react with the H atoms and OH radicals to yield the observed SL effects.

But the statement alone that chemical reactions explain the SL spectra of additives dissociated at high bubble temperatures is insufficient. Chemical reactions require highly specific time and temperature ranges both of which for diverse additives such as *n*-butanol and $CS_2$ are difficult to independently control in a typical adiabatic SL bubble collapse.

*MBSL*

In MBSL, chemiluminescence in water saturated by gas X comprising He, Ar, Kr, and Xe including $N_2$ and $O_2$ reacting with OH* radicals was formulated [29] over a decade ago because only OH* emission from X.OH* excimers provided a reasonable explanation for the observed SL spectra.

Recent MBSL spectra (Fig. 2 of [28]) for saturated Ar, Kr, and Xe in water show there is virtually no difference in the broadband IR to VUV continuum while the OH* emission at 310 nm decreases from Ar to Xe which for Xe becomes indistinguishable from the broadband continuum. The peak in the OH* emission at 310 nm is found to decrease in the order Ar > Kr > Xe as 4.2:3.2:2.2 as illustrated in Fig. 12.

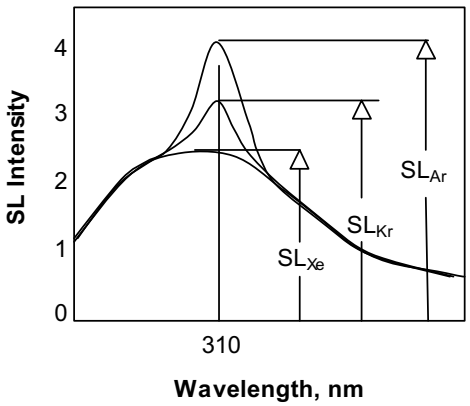


**Fig. 12** – SL Spectra of Water Saturated With Ar, Kr, and Xe

The SL intensity ratio $SL_X/SL_{Xe}$ of gas X to Xe may be approximated by assuming the number N ~ $1x10^5$ VUV photons of cavity QED photons at ~ 10 eV only excite the same number of X or Xe gas atoms, even though the number of X and Xe atoms in solution given by their solubility $\Phi$ in water may differ from each other, i.e., the ratio $SL_X/SL_{Xe}$ is independent of solubility. But the SL is quenched [29] by collisions of the excited X* or Xe* atoms with water molecules. Here the $SL_X/SL_{Xe}$ ratio is taken to be inversely proportional to the collision cross-sections $\sigma_X$ and $\sigma_{Xe}$ of X and Xe atoms,

$$\frac{SL_X}{SL_{Xe}} = \frac{\sigma_{Xe}}{\sigma_X} = \left(\frac{R_{Xe}}{R_X}\right)^2 \tag{17}$$

where, $\sigma_X \sim \pi R_X^2$ and $\sigma_{Xe} \sim \pi R_{Xe}^2$, and $R_X$ and $R_{Xe}$ are the radii of X and Xe atoms. The atomic radius $R_X$ of Ar < Kr < Xe increase in the order 0.88:1.03:1.24 angstroms. For $SL_{Xe}$ ~ 2.2, $SL_{Ar}$ and $SL_{Kr}$ ~ 4.37 and 3.18 reasonably approximate SL in Ar and Kr at 4.2 and 3.2.

*SBSL and MBSL*

SBSL is usually characterized by a featureless IR to VUV broadband spectrum absent the OH* emission bands that only appear in MBSL. However, the OH* emission at 310 nm was recently observed (Fig. 1 of [32]) in SBSL at low acoustic drive pressures.

In cavity QED induced EM radiation, SBSL is absent OH* emission bands because the high acoustic drive pressure compacts the excited X*states by water neighbors in the final collapse configuration and tends to quench the formation of the excited X.OH* excimers. In contrast, MBSL having lower acoustic drive pressures displays OH* emissions because fewer water neighbors are available to quench X.OH* formation. Indeed, the compact SBSL configuration likely consists of a single nanovoid; whereas, multiple nanovoids characterize MBSL. The compactness in the final SBSL and MBSL collapse configurations is illustrated in Figs. 13(a) and (b).

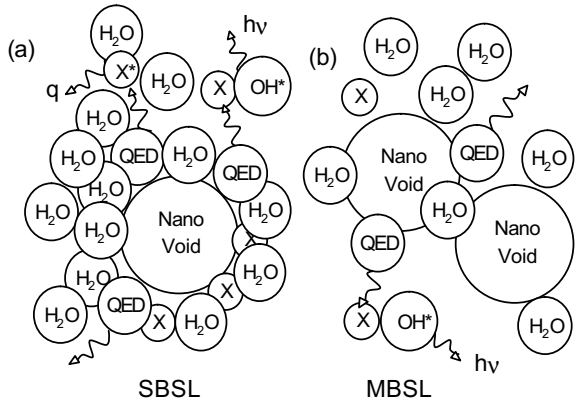


**Fig. 13** –SBSL and MBSL – Molecular Emission and Quench

In SBSL, the cavity QED photons travel through the water by the 3 paths depicted in Fig. 13(a). Most QED photons do not encounter an X atom and pass through the water to the spectrophotometer to be detected as the featureless IR to VUV broadband spectrum. Other QED photons form the X* state and by three body reaction with pairs of water neighbors form the X.OH* excimer that upon dissociation produces OH* emissions [29] detected by the spectrophotometer,

$$X^* + 2H_2O \rightarrow X.OH^* + H + H_2O \rightarrow 2H_2O + X + h\upsilon(310\ \text{nm}) \tag{18}$$

Still other X* states are quenched [29] by water molecules, and therefore fewer Ar.OH* excimers form. The quench q of the excited X* state may be described by,

$$X^* + H_2O \rightarrow X + H_2O + q \tag{19}$$

MBSL having a low acoustic pressure produces a less compact configuration of X atoms and water molecules than SBSL as illustrated in Fig. 13(b). Similar to SBSL, some QED photons do not encounter the X atoms and are detected by the spectrophotometer as the featureless IR to VUV broadband spectrum. The remaining QED photons excite the X atoms produce the X.OH* excimer. By Eqn. 18, the decomposition of the X.OH* excimer produces hυ photons that are detected by the spectrophotometer as OH* emission.

Thus, MBSL spectra or SBSL spectra at low acoustic pressures show OH* emission bands superposed on the broad IR to VUV background that are not observed in SBSL at high acoustic pressures.

## 5.2 SL in Organics

Cavity QED induced EM radiation is not only applicable to SL from water, but also to SL from organic liquids absent OH* radicals. It is emphasized that the QED induced broadband IR to VUV radiation is applicable to *any* liquid and is a *real* source of EM radiation from the atoms in the penetration depth of the bubble surface. Molecular emissions in the broadband IR to VUV background depend on the chemistry of the organic radicals R* and represent the optical response of the chemical species to the EM radiation induced by cavity QED.

In cavity QED induced EM radiation, the SL intensity from the organic liquid is proportional to the number of atoms in the penetration depth of the bubble surface at VUV frequencies, and therefore a comparison to that of another liquid may be made based on penetration depths. In this regard, water having the greatest penetration depth at VUV frequencies is the optimum SL liquid. Even so, small amounts of additives can reduce the penetration depth in water and significantly reduce the amount of IR suppressed in the surface, and therefore the depth estimate must include concentrations of additives intensity of SL. But absorption coefficients of water with additives are not readily known.

*SL from Non-Aqueous Solutions*

SL from non-aqueous solutions as a chemiluminescence process is summarized in [33]. Over a wide range of organic liquids comprising hydrocarbons under Ar, and systems containing nitrogen, oxygen, and chlorine, the SL spectra show the molecular emission of the chemical species superposed on the IR to VUV background.

For hydrocarbon dodecane under Ar, the SL spectrum shows the Swan transition bands of $C_2$ and CH superposed on a broadband continuum from 340 – 700 nm. Similar to OH* emission in water, the IR to VUV background is thought to caused by $C_2$* and CH* radicals. In SL from dodecane under15%$N_2$/85%Ar the $C_2$ and CN peaks are observed and attributed to $C_2$* and CN* radicals. SL from dodecane under 10%$O_2$/90%Ar show the $CO_2$, OH, CH, and $C_2$ peaks from the $C_2$* and $CO_2$* radicals. SL from tetrachloroethylene under Ar show the $C_2$ and $Cl_2$ emissions attributed to $C_2$* and $Cl_2$* radicals.

All of the SL chemistry from this diverse range of organic liquids was attributed [33] to chemiluminescence from radicals R* formed by high temperatures, but can be produced at ambient temperature by photochemical processes from cavity QED induced EM radiation.

*SL Quencher Experiments*

For some time, SL research has been guided by the emission of light taking place in the gaseous cavities - not in the bubble walls. In 1939, volatile organic compounds were found [19] to quench SL, and interpreted in [14] to mean that the emission of SL light takes place in the gas cavities. More recent experiments show:

(1) The most efficient quenchers of excited OH* states in a liquid – nonvolatile KI and α-naphthol – do not affect the total SL flux [34], and

(2) Benzene and aliphatic alcohols that quench OH* radicals in liquids lower the level of total SL flux more when the molecular weight and boiling point are higher [35].

On this basis, the conclusion was reached in [14,34] that absent the effect of SL quenching by non-volatile KI and α-naphthol in the liquid state while SL was quenched when alcohols were added indicate the SL light emission occur in the gaseous – not the liquid state. However, cavity QED induced EM radiation suggests the SL light emission occurs in the liquid state. Specifically,

> (1) Since the excited OH* states only produce feeble lines in the SL continuum, the total SL flux [34] is essentially the same as the SL continuum. By cavity QED induced EM radiation, the SL continuum does not depend on excited OH* states, and therefore the lack of reduction in total SL intensity observed is expected. Similar to a laser, cavity QED induced EM radiation can produce OH* radicals, but its intensity is unaffected by the presence of excited OH* state quenchers, and
>
> (2) Benzene and aliphatic alcohols are known [35] to be effective OH* scavengers in aqueous solution. In the gaseous state, similar scavenging is expected at high temperature, but bubble temperatures are near isothermal during collapse, and therefore it is unlikely the reduction in the SL continuum was caused by OH* quenching in the gaseous or liquid states. Given the OH* flux is a small fraction of the SL continuum, it is more likely the organic compounds act as impurities on the bubble surface that increase the absorption coefficient α of water, thereby decreasing the penetration depth. Since the suppressed IR radiation is reduced because of the reduced penetration depth, the SL continuum is reduced. But absorption coefficients α for water with organic impurities are not available to support this conclusion.

The SL quencher experiments not only affirm cavity QED induced EM radiation, but also give SL a luminescent nature [14, 34] occurring in cold cavitation bubble - not at high bubble temperatures as predicted by the hot spot [4] theory. Indeed, SL in a cold cavitation bubble is consistent with SL at ambient temperature by cavity QED induced EM radiation.

### 5.3 SL from Metal Salt Solutions in Water and Primary Alcohols

The application of cavity QED induced EM radiation to SL from metal salt solutions in water and alcohols like SL from other liquids is only qualitatively assessed. Beyond the large volume of literature, a quantitative evaluation similar to that described above for SL in water is not possible for lack of data, in particular the absorption coefficient α for the diverse liquids. The seminal paper [22] on SL from alkali-metal salt solutions in water and primary alcohols guides the following discussion.

*Mechanism of Chemical Excitation*

SL in water under Ar is described by the chemistry of OH* radicals formed by cavity QED induced EM radiation. Similarly, carbon P* and oxygen Q* based radicals are formed in the ultrasonic irradiation of primary alcohols under Ar. The generality of cavity QED induced EM radiation as a source of photochemical excitation is applicable to SL from *any* liquid under Ar, although the SL spectra of the liquids is likely to require highly specific and complex chemical analysis.

In the hot spot theory, the chemical excitation process is assumed to form in the high temperatures [22] within the bubble interior, the radicals diffusing rapidly out into the bubble wall where the reaction with alkali-metal atoms takes place. But this is unlikely because OH* radicals in water or P* and Q* radicals in alcohols cannot diffuse in the bubble wall and react with Ar atoms faster than their lifetimes. However, cavity QED induced EM radiation travels through the bubble wall to be absorbed by Ar impurities, the transfer of which to water neighbors forms the OH* radicals, or to alcohol neighbors forms the P* and Q* radicals.

Thus, cavity QED induced EM radiation promptly forms radicals in the bubble wall that readily explains SL from non-volatiles present in the liquid and not in the bubble.

*Effect of Vapor Pressure*

The SL intensity of K in 1-alcohols decreases exponentially with increasing vapor pressure (Fig. 3 of [22]). For optimum cavity QED induced EM radiation, the suppressed IR radiation is conserved by the gain in VUV radiation in the wall of an otherwise evacuated QED cavity. If vapor is present in a SL bubble, the VUV radiation in the wall as the source of chemical excitation is reduced because of that absorbed by the vapor, and therefore the SL intensity is reduced as the vapor pressure increases.

*Spectral Line Width and Position*

In the hot spot theory, the SL intensity is reduced with increased vapor pressure. Since SL is thought caused by high temperatures in the bubble, the hot spot theory expects the spectral line width and position to also change as a function of the vapor pressure. But this is contrary to the data (Fig. 4 of [22]). In fact, the observed line width and peak position are independent of cavitation conditions. The conclusion, therefore, is that the excited state atoms are not in the hot spot of the cavitation event when the emission occurs.

In contrast, SL by cavity QED induced EM radiation occurs by chemical excitation in the bubble wall, and therefore is consistent with the data (Fig. 4 of [22]) that shows the spectral line width and position are only dependent on the liquid state and do not depend on the vapor pressure within the bubble. Indeed, the spectral lines are naturally broadened by the quenching of photon emission by the solute in the liquid state, as shown for K in (Fig. 2 of [22]) from a hollow cathode lamp in a vacuum compared to the SL spectra in liquid water and 1- octanol.

*Atomic and Ionic emission*

The chemical reactions [22] by which radicals P* reduce alkali-metal cations $M^+$ to atoms M and photons $h\upsilon$ are,

$$\begin{aligned} P^* + MOH &\rightarrow M^* + ROH \\ M^* &\rightarrow M + h\upsilon \end{aligned} \qquad (20)$$

Recently, SL from metal salt solutions [36] in Ar saturated ethylene glycol showed the D-line of atomic Na, although only the $Na^+$ ion is present in the liquid state absent ultrasonic radiation. However, the P* radical produced in ultrasonic irradiation reduces the $Na^+$ ion to the Na atom before emitting the $h\upsilon$ photon. By extending the study to $CaCl_2$, it was thought emission from $Ca^{++}$ or $Ca^+$ might occur, and if only Ca lines were found would show the emission occurred in the gas phase rather than the liquid state. Indeed, only the Ca line near 422 nm was found. But this does not mean the Ca emission occurred in the gas phase because in the liquid state the P* radical can not only reduce $Ca^{++}$ to $Ca^+$, but also reduce $Ca^+$ to the Ca atom before emitting the $h\upsilon$ photon.

Whether the Ca emission is occurring in the liquid state may be deduced by the broadening of the spectral lines, not by the position of peak lines itself. In the hot spot theory, the high pressures that accommodate the high bubble temperatures in non-condensable gases are required to explain the broadened spectral lines. But in cavity QED induced EM radiation, the bubble is filled only liquid vapor at ambient temperature, and therefore pressure

broadening is insignificant. Instead, the SL spectra in ethylene glycol are naturally broadened because the SL emission is quenched by the liquid state.

*Nature of the Continuum*

In the hot spot theory, the discrete atomic lines and molecular bands in the SL spectra are well understood, but the nature of the underlying continuum in both SBSL and MBSL remains a mystery. The SL continuum has been thought [37] caused by confined electrons, blackbody radiation, electrical discharge, and emission from small molecules formed during the cavitation event. Current thought excludes plasma emission while claiming the continuum is produced by molecular excitations.

But a molecular continuum finds difficulty in explaining the almost continuous SL spectra found in the liquids. The molecular bands in the liquid would have to be continuously distributed from the IR through the visible to the VUV – a non-physical constraint on any molecular liquid. In cavity QED induced EM radiation, the SL light is produced from the near IR to the far VUV without any need to invoke the molecular continuum.

## 5.4 SL in Cryogenic Liquids

*SL under Ultrasound*

SL in cryogens by bubble nucleation and collapse under ultrasonic irradiation was first studied [38] in liquid helium at 1.8 K. Although the upper limit to the size of the bubbles was about 30 μm, the SL light intensity was found to be less than $10^{-4}$ of that from a comparable size SBSL bubble in water at 300 K. Cavity QED induced EM radiation explains the lower SL response in liquid helium to be primarily due the fact that liquid helium at 1.8 K has only 1.8/300 ~ 0.006 of the thermal kT energy available for suppression.

*Laser SL*

In 1979, SL was initiated [39] in liquid nitrogen (LN) by lasers. The process called laser SL focuses a laser in a container of pressurized LN. Upon absorption by impurities, the laser pulse vaporizes the LN to produce a vapor bubble that expands against the surrounding LN. After the bubble expands to the maximum radius R, the vapor promptly condenses with SL observed in the bubble collapse. It was found the LN required pressurization of a few atmospheres for SL to be observed. Estimates of the temperature in the cavity by adiabatic compression of the vapor were less than 1000 K, and therefore the high bubble temperature by the hot spot theory [4] was considered an unlikely explanation of laser SL.

Later in 1998, laser SL observed [40] in LN was found characterized by pulse widths of order 100-1000 ns. This is significant, as the pulse width for SBSL bubbles in water is of order 300 ps. In 2001, laser SL experiments in LN confirmed [41] the long pulse widths. Surprisingly, the OH* molecular band at 310 nm was observed for bubbles having a radius greater than 1000 μm, most likely because of impurities. Moreover, the SL intensity in laser SL was characterized by an integrated SL intensity more than 3 orders of magnitude greater than the single source of SBSL in water suggesting multiple sources in the LN bubble region.

In cavity QED induced EM radiation, laser SL in [38-41] is explained by the compression of microscopic voids formed during the condensation of LN. Prior to collapse, the pressure in the bubble balances the LN pressure. The bubble vapor temperature although initially hot, promptly cools to LN temperature thereby lowering the bubble vapor pressure causing the bubble wall to collapse. Because of the heterogeneity in condensation, the

condensed LN may be characterized by a bubble region of spherical shape containing voids distinct from the surrounding bulk LN.

For the purposes here, the spherical LN bubble region is considered to have a condensation radius Rc that corresponds to the mass of LN vapor in the bubble at maximum radius R. But the inertia of the collapsing bubble wall compresses the bubble region of radius Rc and reduces the size of the microscopic voids. Once the void size reaches nanoscale dimensions, say less than 20 nm, SL light is emitted spontaneously as cavity QED induced EM radiation. Depending on the homogeneity of the LN in the condensation process, voids may exist anywhere in the bubble region, and therefore SL light may be emitted at multiple locations. Since the bubble region is mostly LN, the SL pulse width may be estimated by the time $\tau$ it takes for a sound wave in LN to travel at velocity Vs from the surface of the bubble region at radius Rc to the center, and then back to the surface,

$$\tau \sim \frac{2Rc}{Vs} \tag{21}$$

where,

$$Rc = R\left(\frac{PM}{\rho R_G T}\right)^{\frac{1}{3}}$$

where, Vs is the sound velocity in LN, R is the maximum bubble radius, P is pressure of the LN and bubble vapor, M is the molecular weight of nitrogen vapor, $\rho$ is the density of LN, $R_G$ is the gas constant, and T is the absolute temperature of the vapor.

Numerically, $\rho = 807$ kg/m$^3$ and Vs = 869 ms$^{-1}$ at T = 66 K. Fig. 14 shows the pulse width $\tau$ versus the bubble radius R for pressures P = 6 and 12 bar in relation to the best fit of the experimental (Fig. 7 of [41]) data. Thus, cavity QED induced EM radiation is consistent with the pulse width in LN that is linear with the maximum bubble radius R.

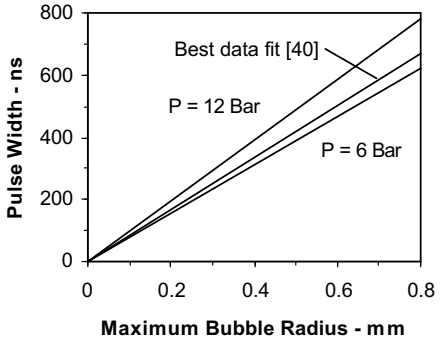


**Fig. 14.** Laser induced SL in LN – Pulse Width and Bubble Radius

In SBSL bubbles, only the water vapor at ambient temperature is present in the bubbles. At 20 C, the vapor pressure is about 2440 Pa in bubbles of radius about 30 μm having a condensation radius R ~ 0.78 μm. By cavity QED induced EM radiation, SBSL in water is produced with voids having radii < 20 nm, and therefore a single source of SL light is expected for SBSL. But the bubbles in LN by laser SL have a radius of about 1000 μm and a vapor pressure in excess of a few bars have respective condensation radii Rc ~ 200 to 300 μm, and as such are likely to have multiple sources. But the SL emission spot is likely to be concentrated over a smaller area. Indeed, observations in laser SL shows a near spherical emission spots of 70 μm, or radius of ~ 35 μm.

**6. SL Criterion**

In cavity QED induced EM radiation, the crucial SL parameter in *any* liquid is the minimum bubble radius $R_{min}$. For SL to be observed, $R < R_{min}$, where $R_{min} \sim 20$ nm. Indeed, $R_{min}$ is more than one order of magnitude smaller than the hard core radius $R_C \sim 0.8$ μm of non-condensable bubble gases usually assumed in SL. But the collapsed bubble need not have a radius $R > R_C$ because vapor bubbles only have traces of non-condensable gases. Although $R_{min}$ may be difficult to verify, it is unequivocal that all vapor bubbles collapse to the spacing $\Delta$ between molecules at liquid density. Since $R_{min} > \Delta$, the criterion that $R < R_{min}$ for SL to be observed is reasonable even though experimental proof of $R_{min}$ from 20 kHz to 1 MHz is lacking. Conversely if $R > R_{min}$, SL by cavity QED induced EM radiation is not observed.

**7. Summary and Discussion**

➢ The chemical excitation of atoms and molecules in the bubble walls at ambient temperature by cavity QED induced EM radiation explains both SBSL and MBSL as the consequence of the underlying cavity QED physics – suppressed IR radiation from atoms in the bubble surface is frequency up-converted to coherent VUV radiation, the VUV forming radicals that by chemical reaction with dissolved species produce the observed SL.

➢ In water, cavity QED induced EM radiation is a continuous IR to VUV excitation source that produces both the SL spectrum of a broadband continuum from the near IR to the VUV and superposed atomic lines and molecular bands of dissolved gases, or the liquid itself. The OH* spectral lines are produced by VUV excitation of Ar atoms that by three body reaction with water neighbors form Ar.OH* excimers. Indeed, OH* spectral lines are not produced absent Ar atoms.

➢ The broadband SL continuum is not produced by excited states of the atoms and molecules, but rather directly from cavity QED induced EM radiation. This is substantiated by the experimental fact that non-volatile SL quenchers only present in the liquid state do not affect the SL continuum. Additives that increase the absorption of water reduce the number of atoms in the penetration depth of the EM waves standing across the bubble, and therefore the SL continuum is reduced because the suppressed IR radiation is similarly reduced.

➢ The recent 'Nature' article [27] reported the finding of excited atomic argon and oxygen ion states in the SL spectra from argon saturated sulfuric acid. The finding is significant in that the excited states have not been previously observed. But the interpretation of this finding is that the SL light is caused by high temperature plasma from the compression heating of bubble vapor. Extensions to the 18 eV necessary to excite the oxygen ion suggests plasma temperatures of ~ 200,000 degrees. However, the high temperature plasma relied upon to explain the SL light is precluded by Le Chatelier's principle that requires the vapor to condense to liquid without an increase in temperature. Thus, the bubble collapses near ambient temperature – not at 200,000 degrees!!!

➢ Cavity QED induced EM radiation featuring variable frequency lasing produces high energy VUV photons to 20 eV and finds utility by producing photons, electrons, and ions at ambient temperature, the embodiments of which are protected by US patent pending.

➢ In the solid state, cavity QED induced EM radiation has explained static electricity [42], the Casimir effect [43], and thermophotovoltaics [44]. The QED cavities are not 3-D

spherical or near spherical bubbles as in liquids, but rather evacuated 1-D gaps between solid surfaces. But the QED physics remains the same – the EM energy loss from the suppression of IR radiation from atoms in the surfaces is conserved by the gain in VUV radiation at the resonant frequency of the gap - the VUV radiation producing: electrons by the photoelectric effect in static electricity, the electrostatic attractive force in the Casimir effect, and the electrical photocell current in the thermophotovoltaic effect.

➢ In SL from the liquid state, ultrasound is commonly used to repetitively nucleate and collapse bubbles. But what is called SL from liquids need not be initiated by ultrasound. SL light can be produced from any pressure fluctuation that induces hydrostatic tension in a liquid, even in a single nucleation and collapse event. Provided the bubbles collapse to, or nucleate from a radius $R < R_{min}$ the effects of acoustic energy and ultrasound frequency in SL bubbles are not of primary importance in producing the observed light.

➢ Unlike collapse, bubble nucleation requires hydrostatic tension to overcome surface tension. Typically, the smallest bubble that nucleates in water is about 3 microns in diameter, thereby precluding the formation of nanobubbles less than 100 nm. Recent observations [45] of nanobubbles in equilibrium on hydrophobic surfaces do not mean that nanobubbles are formed in the bulk because the bubbles may nucleate on solid nanoparticles. If so, the solid particle would quench the SL. Momentary nanobubbles absent nanoparticles that form in the non-equilibrium process of nucleating the 3 micron-sized bubbles are likely to produce VUV radiation that can electrify the liquid. In flow electrification, nanobubbles are proposed [46] as a likely source of VUV radiation, the VUV radiation producing electrons by the photoelectric effect or photons by photoluminescence.

➢ In thunderstorms, the electrification of the atmosphere is proposed to occur from the charge produced in the nucleation of nanobubbles in the volume expansion of supercooled particles in combination with the charge produced by collisions of upward moving supercooled particles and downward moving all-ice particles. Both sources of charge may be explained by the Planck energy formed by cavity QED induced EM radiation that dissociates water molecules into hydronium and hydroxyl ions that electrify the atmosphere.

➢ SL is produced from thermal kT energy extracted from the atoms in the penetration depth by the suppression of IR radiation. Effectively, the atom temperatures are lowered to absolute zero, and therefore the atoms are required to recover ambient temperature prior to the suppression of IR in the next cycle. To do this, water at ambient temperature is pumped to replace the water in the penetration depth. In effect, pump work raises the atom temperatures from absolute zero to ambient, and therefore the 2$^{nd}$ law of thermodynamics is not violated in SL by cavity QED induced EM radiation.

➢ Artificial light from solid state devices differs from SL under ultrasound in that the steady flow of heat replaces the cyclic flow of water. Since work is not provided, it might be thought the 2$^{nd}$ law of thermodynamics is violated. But this is not true. The time for the atoms in the penetration depth to recover ambient temperature is long in relation to the time for IR radiation to be suppressed, and therefore the atom temperatures tend to absolute zero. Heat from the ambient continues to flow into the penetration depth, but the temperature cannot increase because of cavity QED. Thus, EM energy can only be conserved by the spontaneous conversion of heat to VUV radiation that produces visible light by photoluminescence. Thus, the artificial light does not violate the 2$^{nd}$ law.

## References


[1] R. E. Verral and C. M. Segdal, "Sonoluminescence in *Ultrasound: Its Chemical, Physical and Biological Effects* (ed. K. S. Suslick), New York, 227, 1988.

[2] R. A. Hiller, S. J. Putterman, and K. R. Wenninger, "Time-resolved spectra of sonoluminescence," *Phys. Rev. Lett.*, 80, 1182, 1998.

[3] B. Gompf, R. Gunther, G. Nick, R. Pecha, and W. Eisenmenger, "Resolving sonoluminescence pulse widths with single photon counting," *Phys. Rev. Lett.*, 79,105, 1997.

[4] B. E. Noltingk and E. A. Neppiras, "Cavitation produced by ultrasonics," *Proc. Phys. Soc. B,* 63*,* 674-685, 1950.

[5] S. Hilgenfeldt, S. Grossman, and D. Lohse, "A simple explanation of light emission in a sonoluminescencing bubble," *Nature*, 398, 402, 1999.

[6] D. Lohse and S. Hilgenfeldt, "Inert gas accumulation in sonoluminescing bubbles," *J. Chem. Phys.*,107, 6986, 1997.

[7] Y. T. Didenko, W.R. McNamara III, and K.S. Suslick, "Molecular emission from single-bubble sonoluminescence," *Nature*, 407, 877, 19 October 2000.

[8] T. V. Prevenslik, "The paradigm of high temperatures in a collapsing bubble and sonoluminescence, sonochemistry, and D-D fusion," presented at Fifth biennial SSE European meeting, University of Amsterdam, October 2000. Unpublished.

[9] T. V. Prevenslik, "The cavitation induced Becquerel effect and the hot spot theory of sonoluminescence," *Ultrasonics*, 41, 312, 2003.

[10] P. Gajewski, A. Kulicki, A. Wisnewski, and A. Zgorzelski, "Kinetic theory approach to the vapor-phase phenomena in a nonequilibrim condensation process," *Phys. Fluids* 17, 321-27, 1974.

[11] C. E. Brennen, *Cavitation and Bubble Dynamics*, Oxford University Press, 1995.

[12] L. A. Crum, "Bubbles hotter than the sun," *New Scientist*, 36-40, 1995.

[13] M. P. Brenner, S. Hilgenfeldt, and D.Lohse, "Single-bubble sonoluminescence," *Reviews of Modern Physics*, 74, 425-452, 2002.

[14] M. A. Margulis, *Sonochemistry and Cavitation*, Gordon & Breach, 1995.

[15] L. A. Crum, "Sonoluminescence and Acoustic Inertial Confinement Fusion," Fifth International Symposium on Cavitation, Osaka, Japan, 1-4 November 2003.

[16] R. W. Christy and A. Pytte, *The Structure of Matter*: *Introduction to Modern Physics*, Benjamin, New York, 1965.

[17] S. Harouche and J-M Raimond, "Cavity Quantum Electrodynamics," *Scientific American*, 54, April 1993.

[18] R. van Zee, *Cavity-Enhanced Spectroscopies – Spontaneous Emission in a Microsphere: Cavity QED*, Vol. 40 in *Experimental Methods in the Physical Sciences* – Edited by: R. Celotta and T. Lucatorto, Academic Press, 2002.

[19] E. N. Harvey, "Sonoluminescence and Sonic Chemiluminescence," *J. Am. Chem. Soc.*, 61, 2392, 1939.

[20] M. Makino, M. M. Mossoba, and P. Riesz, "Formation of .OH and .H in aqueous solutions by ultrasound using clinical equipment," *J. Phys. Chem.*, 91, 3654, 1983.

[21] K. S. Suslick, J. J. Gawienowski, P. F. Schubert, and H. H. Wang, "Alkane Sonochemistry," *J. Phys. Chem.*, 87, 2299, 1983.

[22] E. B. Flint and K.S. Suslick, "Sonoluminescence from Alkali-Metal Salt Solutions," *J. Phys. Chem.*, 95, 1484-88, 1991.

[23] Y. T. Didenko, S. P. Pugach, and T. V. Gordychuk, "Sonoluminescence Spectra of Water: Effect of Ultrasonic Irradiation Power," *Optics and Spectroscopy*, 80, 821-826, 1996.

[24] R. T. Hiller, K. Wenninger, S. J. Putterman, and B.P. Barber, "Effect of noble gas doping on single bubble sonoluminescence," *Science*, 266, 248-250, 1997.

[25] T. Le Pointe, et al., "Observation of 'Ar-HO' van der Waals molecules in multibubble sonoluminescence," Ultrasonics International 2001, T. U. of Delft, 2-5 July 2001.

[26] D. J. Segelstein, "The complex refractive index of water," MS Thesis, University of Missouri, Kansas City, 1981.
[27] D. J. Flannigan and K. S. Suslick, "Plasma formation and temperature measurement during single-bubble cavitation," *Nature*, Vol. 434, 52-55, 2005.
[28] Y. T. Didenko and T. V. Gordychuk, "Multibubble Sonoluminescence Spectra of Water which Resemble Single-Bubble Sonoluminescence," *Phys. Rev. Lett.*, 84, 5640, 2000.
[29] Y. T. Didenko and S. P. Pugach, "Spectra of Sonoluminescence," *J. Phys. Chem.*, 98, 9742-49, 1994.
[30] M. Link, R. Mehnert, and L. Prager, "Design and Performance Characteristics of Windowless Argon Source," 5th Inter. Symposium on Ionizing Radiation and Polymers, 21- 26, September, 2002.
[31] Putterman, "Sonoluminescence: Sound into light," *Scientific American*, Feb.1995.
[32] J. B. Young, J. A. Nelson, and W. Kang, "Line Emission in Single-Bubble Sonoluminescence," *Phys. Rev. Lett.*, 86, 2673-2676, 2001.
[33] E. B. Flint and K. S. Suslick, "Sonoluminescence from Nonaqueous Liquids: Emission from Small Molecules," *J. Am. Chem. Soc.*, 111, 6987-92, 1989.
[34] M. A. Margulis and A. F. Dmitrieva, "Processes of sonoluminescence quenching by various additives," *Russ. J. Phys. Chem.*, 66, 751, 1992.
[35] C. Sehgal, R. P. Steer, R. G. Sutherland, and R. E. Verrall, "Sonoluminescence of Aqueous Solutions," *J. Phys. Chem.*, 81, 2618, 1977.
[36] V. H. Arakeri, "Sonoluminescence from Metal Salt Solutions," Fifth International Symposium on Cavitation, Osaka, Japan, 1-4 November 2003.
[37] W. B. McNamara III, Y. T. Didenko, and K. S. Suslick, "The Nature of the Continuum in Multibubble Sonoluminescence," *J. Am. Chem. Soc.*, 122, 8563, 2000.
[38] P. Jarman and K. Taylor, "The sonically induced cavitation of liquid helium,", *J. Low Temp. Phys.* 2, 389, 1970.
[39] P. I. Golubnichi, P. I. Dyadyushkin, G. S. Kaluzhnyi, and S. D. Korchikov, "Laser sonoluminescence in liquid nitrogen", *Sov. Tech. Tech. Phys.*, 24 (8) August 1979.
[40] O. Baghdassarian, B. Tabbert, and G. A. Williams, "Luminescence from laser-created bubble in cryogenic liquids," *Physica B*, 284-288, 392-394, 2000.
[41] O. Baghdassarian, H. C. Chu, B. Tabbert,and G. A. Williams, "Spectrum of Luminescence from Laser-Induced Bubbles in Water, and Cryogenic Liquids," CAV2001: Fourth International Symposium on Cavitation, California Institute of Technology, 20-31 June 2001.
[42] T. V. Prevenslik, "Cavity QED Induced Photoelectric Effect," *Proceedings ESA-IEJ Meeting*, Northwestern University, 230-40, 25-28 June 2002.
[43] T. V. Prevenslik, "The Casimir force – neutral or electrostatic?", 4th French Electrostatics Society Congress, Poitiers, 2-3 September 2004.
[44] T. V. Prevenslik, "The cavity QED induced thermophotovoltaic effect", 14th Inter. Photovoltaic Sci. & Eng. Conf., PVSEC-14, Bangkok, 27 Jan.-1 Feb.,2004.
[45] J. W. G. Tyrrell and P. Attard, "Images of Nanobubbles on Hydrophobic Surfaces and their Interaction," *Phys. Rev. Lett.*, 87, 176104, 2001.
[46] T. V. Prevenslik, "Flow electrification in micro porous filters," 5th International EHD Workshop, Poitiers, 30-31 August 2004.
[47] R. Hiller, S. J. Putterman, and B. P. Barber, "Spectrum of Picosecond Sonoluminescence," *Phys. Rev. Lett.*, 69, 1182-84, 1992.

Appendix A
Ambient Temperature Energy Source

Beyond SL, passive solid state devices that simulate cavity QED induced EM radiation might find utility by providing artificial lighting powered by IR radiation at ambient temperature. Typically, processed silica structures[2] having a large number of irregular voids are proposed as sources of visible light that might prove competitive with lighting powered by conventional sources of electricity. A hollow spherical structure representing one of a plurality of irregular shaped voids in the structure is depicted in Fig. A-1.

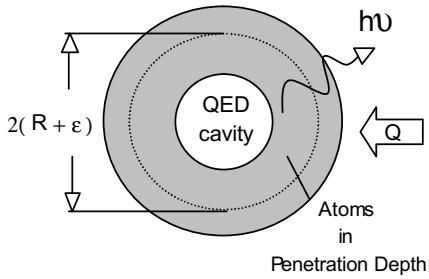


**Fig.** A-1
Artificial Light Source

Only IR radiation from thermal kT energy at ambient temperature is proposed to power the light source. For ( R + 0.5ε ) ~ 63.5 nm, the average wavelength λ ~ 4( R + 0.5ε ) ~ 254 nm. Thus, in the penetration depth ε, the average EM radiation is in the VUV. The VUV radiation then excites the silica[3] to produce red light. Processed structures having QED cavities with a random distribution of wavelengths λ < 254 nm produces white light. By extracting heat Q continuously from the environment, the ambient light source claims to produce a never ending supply of light !!

**What about the 2nd law of thermodynamics?**

*SL in water under ultrasound*

SL is produced from the VUV radiation induced by cavity QED by the suppression of IR radiation at ambient temperature from atoms in the penetration depth of the VUV radiation standing across the QED cavity every ultrasonic cycle. The thermodynamic diagram is illustrated in Fig. A-2(a). VUV radiation is produced by the suppression of IR radiation from the thermal kT energy of the atoms in the penetration depth. But suppression of IR radiation tends to reduce the atom temperatures to absolute zero, and therefore the atoms must be returned to ambient temperature prior to production of VUV radiation in the next ultrasonic cycle. In SL, the water in the penetration depth is recycled by the flow of water at ambient temperature. Since work W is expended to pump the water, SL by cavity QED induced EM radiation does not violate the 2nd law.

$$VUV = kT - W$$

[2] A. Colder, et al., "Strong visible photoluminescence from hollow silica nanoparticles," *Nanotechnology* 15, L1-L4, 2004.
[3] *Ibid.*

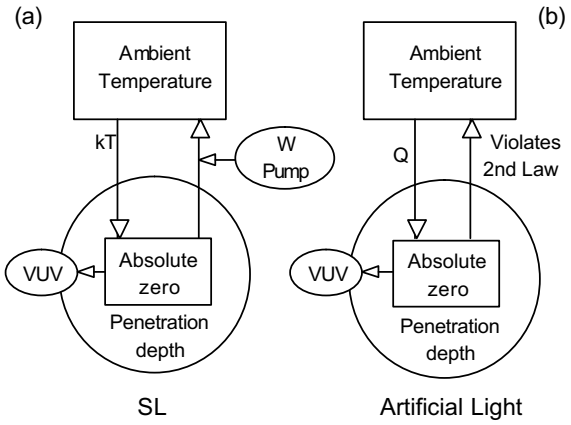


**Fig.** A-2
Cavity QED induced EM radiation
Thermodynamic Diagrams – (a) SL and (b) Artificial Light Source

*Artificial light source*

The thermodynamic diagram of the artificial light source is shown in Fig. A-2(b). In the solid state, the temperature of the atoms in the penetration depth is recovered by conductive heat Q through the thin walled hollow structure because of the temperature difference between the outer and inner surfaces at ambient $T_{amb}$ and near absolute $T_o$ temperatures,

$$Q = \frac{KA}{t^*}\left(T_{amb} - T_o\right)$$

where, K is thermal conductivity, A is area, and t* is a fraction of the wall thickness. But the thermal response of the atoms in the penetration depth takes time; whereas, the IR radiation is instantaneously suppressed by cavity QED. Thus, the heat Q is removed as soon as it flows into the penetration depth, and therefore the atom temperatures tend to absolute zero. Without expending work W to raise the temperature of the atoms to ambient, it might be thought the ambient light source violates the 2nd law.

But this is not true. Heat Q continues to flow into the penetration depth, but cavity QED precludes any increase in temperature. Moreover, the heat Q cannot escape from the penetration depth to the ambient because this would violate the 2nd law by a flow of heat from cold to hot temperatures. Thus, the only path available to conserve the 1st law is for the heat Q to undergo spontaneous conversion to VUV radiation,

$$VUV = Q$$

By making the wall thickness t of the hollow structures small, the heat flow Q converted to VUV radiation can be significant compared to SL which is limited to the thermal kT energy available to the atoms in the penetration depth.

# Chapter 6

# Astronomy

Controversial new studies suggest that the universe is not expanding and that dark matter does not exist. The simple QED theory of nanoscale heat transfer provides the basis for redshift in cosmic dust and refutes the theory that the universe is expanding, to the contrary it confirms that there is a static and infinite universe as once proposed by Einstein.


6.1 Redshift in Cosmic Dust precludes Universe Expansion and Dark Matter . . . . . 146

6.2 Dark Matter only Exists because of Cosmic Dust . . . . . 149

6.3 Cosmic Dust in an Expanding Universe? . . . . . 155

6.4 CMBR as Solar illumination of the Oort Cloud modified by Cosmic Dust . . . . 160

# Redshift in Cosmic Dust precludes Universe Expansion and Dark Matter

**Abstract:** Over the past century, Hubble's redshift of light from galaxies has intrigued scientists to ponder the current expansion rate of the Universe. Recently, a young schoolgirl published an article on the expansion of the Universe that illustrates how the misinterpretation of redshift of galaxies has falsely led astronomers over a century are being passed on to future generations. Indeed, the redshift of galaxies thought to support Hubbell's expansion of the Universe is nothing more than the redshift of a spectral line emitted from a galaxy upon interacting with nanoscopic cosmic dust. What this suggests is the Universe is not and never was expanding, nor does dark matter exist. Analysis is presented for the redshift of Balmer-lines over a range of silicate dust nanoparticle (NP) diameters. The interaction of the spectral line (SL) photon with the NP is by the simple QED method of nanoscale heat transfer that based on the Planck law denies the atoms in the NP the heat capacity to conserve the absorbed SL photon by an increase in temperature. In this regard, the NP diameter is required to be smaller than the SL photon wavelength which spontaneously immerses the NP in SL radiation. But the SL radiation cannot penetrate the NP surface as NP temperatures do not exist for Fourier conduction. Conservation may only proceed by creating temperature independent EM waves, the Planck constant divided by the time for the EM wave to travel across and back the NP diameter defining the Planck energy of the simple QED photon standing across the NP diameter. EM confinement of SL photon energy within the NP is provided by the inwardly disposed momentum of the SL radiation itself. Redshift in cosmic dust occurs when the wavelength of the simple QED photon is greater than that of the incident SL photon, and may accumulate in many successive NP interactions before reaching the observer on Earth.

***Keywords:*** Expanding Universe, cosmic dust, redshift, Hubbell, Planck law, nanoparticles, simple QED

## I. INTRODUCTION

Hubble's discovery [1] of an expanding Universe inferred from redshift measurements of spectral line emissions from distant galaxies has misdirected astronomy for the past century. Many scientists have devoted their lifetime work to the folly of an expanding Universe based on redshift measurements, a folly that is being passed on to future scientists.

Guided by her superiors, a young high school girl recently published [2] an article on calculating the expansion rate of the Universe. The work is representative of that published by senior scientists in astronomy. Nevertheless, the falsity of redshift as a basis for Universe expansion which is and has been a problem for astronomy remains. The velocity of Universe expansion in terms of redshift z is illustrated in Fig. 1.

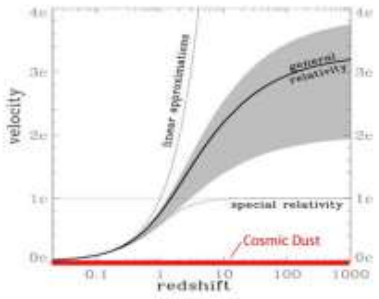


Figure 1. Universe expansion velocity and redshift

## II. PURPOSE

The purpose of this paper is to propose the redshift measured by Hubble and others over the past century is caused by cosmic dust having nothing to do with Universe expansion including dark matter. Indeed, cosmic dust precludes Universe expansion suggesting a static and infinite Universe once proposed by Einstein noted by the red line coincident with zero velocity in Fig. 1.

## III. THEORY

The simple QED theory of nanoscale heat transfer provides [3] the basis for redshift in cosmic dust. Based on the Planck law, heat from SL photons absorbed by cosmic dust NPs is not conserved by an increase in temperature, but rather by creating redshifted EM radiation in the NP.

### A. Planck law

The Planck law [4] of quantum mechanics (QM) denies atoms in NPs the heat capacity to increase in temperature upon absorbing heat. The average Planck energy E of the atom is,

$$E = \frac{\frac{hc}{\lambda}}{\left[\exp\left(\frac{hc}{\lambda kT}\right) - 1\right]} \quad (1)$$

and at 300 K is plotted in relation to classical physics in Fig. 2.

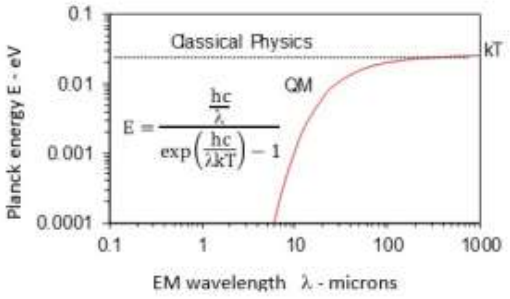


Figure. 2: Planck law of QM at 300 K
In the inset, E is Planck energy, h Planck's constant, c light speed, k Boltzmann's constant, T temperature, and λ the EM wavelength.

The Planck law at 300 K shows classical physics allows the atom to have constant thermal kT heat capacity over all EM wavelengths λ. QM differs as the kT heat capacity decreases for λ < 200 μm, and vanishes at the nanoscale for λ < 200 nm.

**B. Simple QED**

Simple QED is the consequence of the Planck law denying atoms in NPs the heat capacity to increase in temperature upon the absorption of heat. QED stands for quantum electrodynamics, a complex theory based on *virtual* photons advanced by Feynman [5] and others. Simple QED is far simpler only requiring the heat capacity of the atoms in NPs to vanish allowing conservation to proceed by the creation of *real* photons comprising EM waves that stand across the NP as shown in Fig. 3.

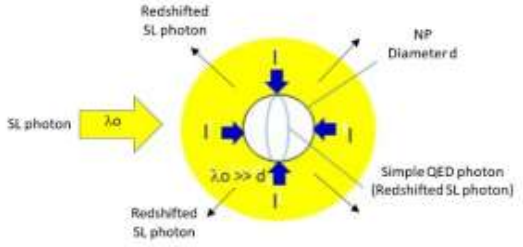


Figure 3. Simple QED redshifted SL photon

Fig. 3 depicts a SL photon having wavelength λo interacting with a NP of diameter d. For NPs having d < λo, the NP is instantly immersed in SL radiation. Inward disposed Poynting vector S ~ W/m$^2$ (yellow) carry SL momentum I (blue arrows) applying pressure to the NP surface to confine the EM energy of the absorbed SL photon to the shape of the redshifted simple QED photon.

Similar to atomic quantum states described by electrons in discrete orbitals, simple QED states are dependent on the diameter of the NP over which the EM waves stand. However, the simple QED photons can only be created by QM as classical physics requires very high temperatures to create photons.

By QM, the Planck law denies NPs the temperatures required for Fourier heat conduction and the heat flux Q cannot penetrate the NP surface. Conservation of Q may only proceed by non-thermal EM waves carrying the heat Q across and back the NP diameter d in time τ = 2d/(c/n), where n is the index of refraction of the NP. At this instant, the simple QED photon is created having Planck energy E = h/τ and wavelength λ = 2nd,

$$E = \frac{hc}{2nd} \qquad (2)$$

Importantly, the simple QED photon must be placed under brief EM confinement to produce the standing wave that fits the NP diameter. The EM confinement is not produced by some structuring of the NP surface, but rather by the momentum I of the heat Q flux itself. In effect, the momentum I briefly holds the absorbed SL photon energy until it forms a standing EM wave that fits the NP diameter d which defines the wavelength of the redshifted SL photon.

But the standing EM wave is stationary and cannot carry the redshifted SL photon into the surroundings. Energy Wave Theory (EWT) is invoked that requires [6] transverse EM waves accompany standing waves at the instant of formation thereby allowing transverse waves of redshifted SL photons to freely propagate into the surroundings.

Energy E is conserved between standing and transverse photon states, i.e., E = mc$^2$ and hc/2nd, respectively. Here, m is the standing photon mass. But photon momentum I = mV = h/2nd. Hence, V = c, i.e., the redshifted SL photon moves into the ISM at the speed of light.

## IV. ANALYSIS and DISCUSSION

Since the 1970's, dark matter was thought [7] to exist because the rotational velocities found in Andromeda M31 and other low-redshift galaxies (z < 0.001) were higher than expected by Newtonian mechanics which suggested the galaxies could not be held together as they appear. Following Hubble, the M31 rotation velocities were inferred from the redshift of the 658.3 nm nitrogen NII line, the consequence of which was flat rotation curves became the signature of dark matter holding galaxies together. The NII line is almost coincident with Hα.

However, high-redshift (0.6 < z < 2.6) galaxies in the distant Universe were recently [8] found to have falling rotation curves suggesting the absence of dark matter, at least at the galaxy periphery. Similarly, the recently discovered transparent Ghost galaxy was found [9] to have a falling rotation curve suggesting dark matter is not present absent cosmic dust.

Historically, galaxy redshift in cosmic dust went unnoticed for almost a century because the light-matter interaction of galaxy light including NII was assumed to follow classical physics allowing the heat capacity of the nanoscopic dust particle to conserve the galaxy

photon by an increase in temperature. But the heat capacity of the atom given by the Planck law of QM is not scale invariant being finite at the macroscale while vanishing at the nanoscale. Conservation of the galaxy photon is therefore only possible by a non-thermal mechanism proposed here to be simple QED and has been proposed [10] as alternative to Hubble redshift on numerous occasions.

Other alternatives to Hubble redshift have been proposed, one of which [11] is based on recently discovered large quantities of $H_2$ gas which is transparent and also may explain the missing mass in dark matter. Since light-molecule interactions are inelastic, the light is redshifted as very small amounts of energy are loss with each collision. But light from a galaxy would need to make many $H_2$ collisions to accumulate to high Hubble redshift levels.

In contrast, simple QED induced redshift in cosmic dust requires galaxies create SL photons of ionized H atoms by high temperatures or UV radiation, although SL of any element like NII used in M31 may be used. Unlike $H_2$, the interaction of SL of H interaction with a NP of cosmic dust may produce a high redshift in a single collision.

The Balmer series of H is important in astronomy as most of the Universe consists of the element hydrogen. Hydrogen is present almost everywhere and SLs of H are visible in most galaxy spectra. The cosmic dust redshift z for the Balmer series in relation to the dust diameter d is given in Fig. 4.

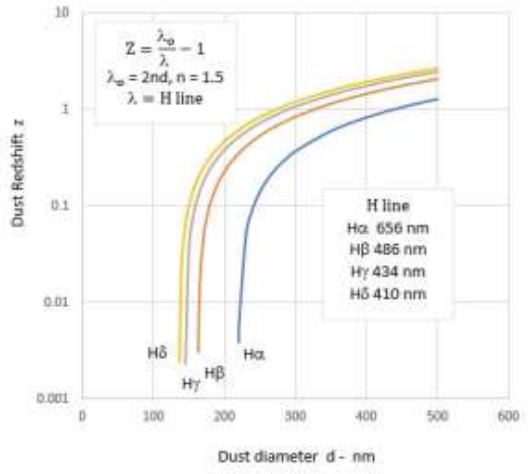


Figure 4. Balmer series - Cosmic redshift v. dust diameter

Fig. 4 shows high Hubble redshift (z~1) galaxies [12] are produced in 300-400 nm cosmic dust particles by a single interaction of a Hα line photon compared to a very large number $H_2$ collisions.

Of importance, cosmic dust redshift overstates velocities giving the impression dark matter is present to hold the galaxy together, i.e., cosmic dust is in effect creating dark matter which in reality does not exist.

Similarly, the overstated Hubble redshift of M31 by cosmic dust suggesting dark matter was present to keep the galaxy from flying apart, the higher rotational velocities at the periphery became known as the signature of dark matter having flat rotation curves rather than the falling curves of Newtonian mechanics.

Recently, the transparent Ghost galaxy having high redshift ($0.6 < z < 2.6$) and a falling rotation curve simply suggests cosmic dust is concentrated at the galaxy center and not at the periphery.

## V. CONCLUSIONS

For a century, Astronomy has been misdirected by cosmic dust to false notions of an expanding Universe and dark matter neither of which exist and can never be verified experimentally. Sadly, young scientists are nevertheless being guided to continue these false notions of Astronomy into the next century.

## REFERENCES

[1] Hubble E. [1929] A Relation between Distance and Radial Velocity among Extra-Galactic Nebulae. PNAS.
[2] Chen H. [2020] Calculating the expansion rate of the universe. Young Scientists Journal.
[3] Prevenslik T. Simple QED theory and applications. https://www.nanoqed.org, 2020 - 2021.
[4] Planck M. [1900] On the Theory of the Energy Distribution Law of the Normal Spectrum. Verhandl. Dtsch. Phys. Ges., 2:2-37.
[5] Feynman R., QED: The Strange Theory of Light and Matter. Princeton University Press, 1976.
[6] Photon Creation and Absorption – EWT (energywavetheory.com)
[7] Rubin, V. and Ford, W. [1970] Rotation of the Andromeda Nebula from a Spectroscopic Survey of Emission Regions. Astrophys. J., 159:379.
[8] Genzel, R., et al. Strongly Baryon-Dominated Disk Galaxies at the Peak of Galaxy Formation Ten Billion Years Ago. Nature., 543 (2017), 397–401.
[9] van Dokkum, P., et al.: A galaxy lacking dark matter. Nature., 555 (2018), 629.
[10] Prevenslik T. Cosmology and Redshift in Cosmic Dust to The Proceedings of The Conference "Cosmology on Small Scales" [2020] Conference Cosmology on Small Scales 2020. Michal Krizek and Yurii Dumin (Eds.) Institute of Mathematics CAS, Prague.
[11] Marmet P. [2000] Discovery of $H_2$, in Space Explains Dark Matter and Redshift. 21st CENTURY Science & Technology, Pages 5 - 7.
[12] Calzetti D. [1999] Properties of High Redshift Galaxies. https://arxiv.org/abs/astro-ph/9907025

*Buchalter 2017 Cosmology Submission*

# Dark Matter only Exists because of Cosmic Dust

Based on the Planck law of quantum mechanics, cosmic dust including neutral hydrogen atoms cannot conserve galaxy light by temperature fluctuations because their size requires heat capacities to vanish. With cosmic dust, conservation therefore proceeds by the re-emission of galaxy light redshifted beyond the Hubble redshift thereby overstating velocities to the extent that to hold galaxy clusters together dark matter is thought to exist. But if measured redshift is corrected for cosmic dust, dark matter need not exist as the galaxy clusters are held together by Newtonian mechanics. Because of the ubiquity of cosmic dust, all astronomical velocity measurements based on Hubble redshift are most likely overstated, e.g., the long-standing galaxy rotation problem may be resolved without the need for dark matter if the redshift measurements giving the higher than expected galaxy velocities are corrected for the redshift in cosmic dust. Moreover, an accelerating Universe expansion need not exist if the redshift showing supernovae brighter than expected is corrected for the redshift in the intervening cosmic dust. With regard to neutral hydrogen atoms, conservation of galaxy light thought to proceed by the thermal emission of the 21 cm hydrogen line is problematic as temperature fluctuations in hydrogen atoms are forbidden by quantum mechanics. Extensions of cosmic dust redshift corrections to historical astronomical observations are briefly discussed.

## 1. INTRODUCTION

Dark matter has a long history. In 1927, the Dutch astronomer Oort [1] applied Newton's laws to the motion of galaxies and showed the Milky Way rotated faster than expected suggesting dark matter was present to explain the flat rotation curves observed. In 1933, Zwicky found [2] the velocity dispersion of the Coma cluster of galaxies to be such that to keep the system together, the average mass density in the Coma system would have to be much higher than that deduced from observed visible matter. Similar to Hubble, early velocity measurements of galaxies were based on redshift [3] of optical emission wavelengths that continue to this day.

Since 1950, the computation of rotation curves became vogue after the radio astronomy discovery [4] of the 21 cm line of neutral hydrogen atoms. Unlike optical redshifts based on emission wavelengths, radio redshifts are determined from the frequencies of thermal emission.

In the 1970's, rotation curves based on both optical and radio redshifts were resolved [5] for the M31 spiral galaxy by assuming the presence of invisible mass thereby marking the beginning of the modern search for dark matter. Since then, a specific feature of these curves emerged: galaxy rotation curves tended to be flat instead of decreasing with radius consistent with Newtonian mechanics thereby suggesting a large amount of invisible dark matter pervaded the Universe.

Today, scientists generally agree that dark matter is invisible having about 5-times the mass of ordinary matter, but what it is and how it was formed has remained a mystery. Many dark matter dark matter theories are proposed. Until recently, dark-matter theory [6] rested on WIMPs thought created in the Big Bang. WIMP stands for Weakly Interacting Massive Particle. In LUX, the search for the WIMP was conducted in a large vessel containing liquid xenon. LUX stands for Large Underground Xenon collaboration. But LUX researchers recently reported [7] no evidence of WIMPS suggesting dark matter may not exist. The search for dark matter continues.

## 2. PROPOSAL

Cosmic dust generally comprises NPs of silicates having diameters < 500 nm that permeate the ISM. NPs stand for nanoparticles and ISM for interstellar medium. But the ISM is also filled with neutral hydrogen atoms. Both dust NPs and neutral hydrogen atoms affect optical and radio redshift measurements from which galaxy velocities are determined. In this paper, the light-matter interactions in deriving the optical and radio redshifts follow the Planck law of QM and not classical physics. QM stands for quantum mechanics.

QM affects the interpretation of optical and radio redshifts differently from that of classical physics. Upon the absorption of a galaxy photon, QM forbids temperatures fluctuations in both dust NPs and neutral hydrogen because their quantum size requires the heat capacities of constituent atoms to vanish.

What this means is both dust NPs and neutral hydrogen are required by QM to conserve galaxy photons by non-thermal mechanisms: (1) dust NPs by the optical re-emission of redshifted galaxy photons at a wavelength corresponding to the dimensions of the NP, and (2) the hydrogen atom by optical emission of the 21 cm hydrogen line. Both (1) and (2) processes require measurement by optical telescopes. In this regard, thermal radiation measured by radio telescopes is problematic as temperature fluctuations in dust NPs and hydrogen atoms are forbidden by QM.

In retrospect, classical physics that allows the atoms in quantum sized dust NPs and neutral hydrogen to have the heat capacity to fluctuate in temperature has led astronomy to a notion of redshift supportive of an expanding Universe. Another cosmology might have evolved for redshift based on QM.

The proposal here is dark matter is not a physical property of the Universe that can be discovered by experiment and only exists because optical redshifts are not corrected for cosmic dust. Radio redshifts of the 21 cm hydrogen line are simply problematic .

## 3. THEORY AND ANALYSIS

### 3.1. Optical Redshift

#### 3.1.1. Background

Light from a galaxy at wavelength λ may be optically redshift by the increment $\Delta\lambda_V$ by the recession velocity V of the galaxy. However, a further wavelength increment $\Delta\lambda_D$ occurs [8] as the galaxy light is absorbed in the cosmic dust D surrounding the galaxy. Hence, the redshift $Z_{meas}$ of the galaxy emission at wavelength λ measured on Earth is,

$$Z_{meas} = \frac{\Delta\lambda}{\lambda} = \frac{(\Delta\lambda_V + \Delta\lambda_D)}{\lambda} \quad (1)$$

In terms of the Hubble or recession redshift $Z_V = \Delta\lambda_V/\lambda$ and cosmic dust $Z_D = \Delta\lambda_D/\lambda$,

$$Z_{meas} = Z_V + Z_D \quad (2)$$

Unlike reddening where shorter wavelengths are not increased by scattering, cosmic dust redshift $Z_D$ corresponds to a physical increase $\Delta\lambda_D$ in the wavelength of galaxy light. Therefore, the galaxy velocity V is computed by correcting for the redshift $Z_D$ of cosmic dust,

$$\frac{V}{c} = \frac{[(Z_V + 1)^2 - 1]}{[(Z_V + 1)^2 + 1]} \quad (3)$$

where, $Z_V = Z_{meas} - Z_D$ and c is the velocity of light.

Today, the absorption of galaxy light by cosmic dust NPs is thought [9] to increase the dust temperature. Moreover, subsequent thermal emission from cosmic dust is thought [10] to create the observed IR spectra.

The conversion of galaxy light to a temperature increase in dust NPs assumes heat transfer is governed by classical physics where the constituent dust atoms have heat capacity. To date, the assumption of classical physics for dust NPs has not only misdirected IR spectra, but also cosmology by supporting an expanding Universe which by QM is problematic because of cosmic dust..

#### 3.1.2. Heat Capacity

By the QM Planck law, the NP heat capacity [11] of constituent atoms at temperatures of 300 and 2.7 K depends on the EM confinement wavelength λ as illustrated in Figure 1.

Classical physics (noted by dotted lines) allows NP atoms irrespective of EM confinement to always have kT heat capacity. QM differs by only allowing kT heat capacity at 300 and 2.7 K for λ > 100 and 3000 microns, while otherwise requiring kT heat capacity to decrease and vanish at λ < 1 micron.

In the ISM, NPs in the size range < 0.5 microns [12] therefore have vanishing heat capacity thereby precluding conservation of galaxy light by fluctuations in temperature.

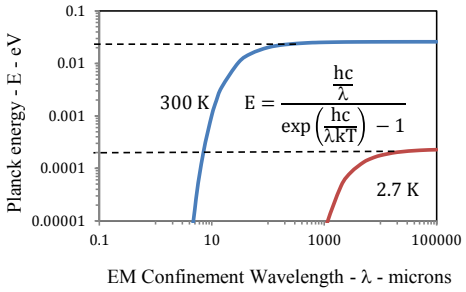


Figure 1: QM Planck law – Thermal Energy of the Atom
In the inset, E is Planck energy, h Planck's constant, k Boltzmann's constant, λ EM confinement wavelength, and T absolute temperature

However, the NPs require EM confinement at submicron wavelengths to achieve vanishing QM heat capacity. But cosmic dust is not observed to have any surface structure that might be construed as EM confinement suggesting the absorption of galaxy light in submicron dust NPs is itself the source of momentary EM confinement

#### 3.1.3. EM Confinement

Indeed, EM confinement of atoms in cosmic dust does not require any surface treatment, but is a natural consequence of the high S/V ratio of NPs. S/V stands for surface-to-volume. Upon absorption of galaxy light, almost all of the photon energy is therefore spontaneously deposited in the NP surface. What this means is the NP atoms are momentarily placed under EM confinement. Since the NPs are submicron, the EM confinement is also submicron and the heat capacity of the NP vanishes.

But the NPs in the ISM need not be submicron as the heat capacity of the atom at 2.7 K decreases about 3 orders of magnitude at λ < 1 microns, and therefore cosmic dust NPs > 1 micron also have reasonably high S/V ratios making EM confinement still valid. Regardless, size and not temperature is important as NPs > 1 micron also provide the sufficient EM confinement of constituent atoms necessary to conserve surface heat for creating non-thermal EM radiation.

#### 3.1.4. Simple QED

The QED of light-matter interaction in NPs is usually thought to proceed by the complex relativistic theory [13] advanced by Feynman and others. However, the simple QED proposed [14] to conserve the heat from absorbed galaxy light under EM confinement is far simpler and can be readily understood. Briefly stated:

Under the QM restriction that the heat capacity of the atom under high EM confinement vanishes, simple QED conserves the heat of galaxy light absorbed in a NP surface by spontaneously creating standing EM radiation inside the NP having half wavelength λ/2 = d, where d is the NP diameter.

The Planck energy E of the standing EM radiation is,

$$E = \frac{h\left(\frac{c}{n}\right)}{\lambda} = \frac{hc}{2nd} \quad (4)$$

where, the velocity of light c is corrected for the slower speed in the solid state by the refractive index n of the NP.

Once the EM confinement formed [14] as the galaxy light deposited in the NP surface is depleted in creating the standing EM radiation, the EM confinement vanishes allowing the standing EM radiation to escape the NP and travel to Earth as cosmic dust $Z_D$ redshifted galaxy light.

#### 3.1.5. Cosmic Dust Redshift

Upon absorption, the EM energy of the galaxy photon is redshift by simple QED depending [14] on the properties of the NP. Redshift only occurs as the NP absorbs a single galaxy photon because the probability of successive absorptions of galaxy photons by the same NP is extremely unlikely. In single photon absorption, only redshift occurs as blueshift with EM energy exceeding that of the galaxy photon is forbidden by the conservation of energy. The cosmic dust redshift $Z_D$ of the galaxy photon having wavelength $\lambda$ is,

$$Z_D = \frac{(2nd - \lambda)}{\lambda} \quad (5)$$

The redshift $Z_D$ for Lyman alpha (Lyα) and hydrogen alpha (Hα) photons is depicted in Figure 2.

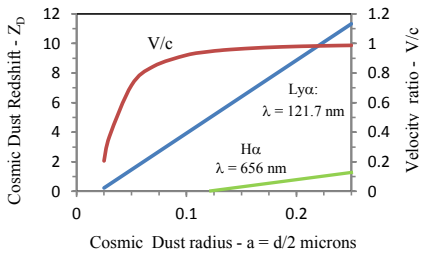


Figure 2: Cosmic Dust Redshift of Lyα and Hα lines for Amorphous Silicate n = 1.5

Of importance, the Lyα and Hα redshifts in (5) depend on the NP radius a = d/2 and refractive index n even if the emissions are from the same galaxy. Hence, the cosmic dust redshift does not follow the basic premise of Hubble redshift that the Doppler Effect is the same for both Lyα and Hα emissions from the same galaxy.

Because of this, cosmic dust was proposed [8] as the basis for correcting measured redshift $Z_{meas}$ for cosmic dust $Z_D$ to determine valid Hubble recession redshift $Z_V$.

#### 3.1.6. Corrected Redshift

Hubble redshift by the Doppler Effect gives the same Z for ALL emission wavelengths from the galaxy. Indeed, historical data [15] supports the Hubble redshift at low $Z < 0.05$, but excludes the Lyα and Hα lines that give the largest difference in redshift from cosmic dust. Therefore, to assess the validity of Hubble redshift, $Z_{meas}$ may be corrected with the difference in redshifts Z of individual Lyα and Hα lines.

$$Z = Z_{meas} - (Z_{Ly\alpha} - Z_{H\alpha}) \quad (6)$$

If $Z_{Ly\alpha} = Z_{H\alpha}$, $Z = Z_{meas}$ and the galaxy velocities given by the Doppler Effect are valid. Otherwise, cosmic dust invalidates the galaxy velocities.

### 3.2. Radio Redshift

#### 3.2.1. Background

The W-F effect [16] couples the spin temperature of neutral hydrogen to the Lyα excitation of the 21 cm line of hydrogen at 1420 MHz. W-F stands for Wouthuysen-Field. Most hydrogen in the Universe is in the ground state where the electron spins are parallel with higher energy than antiparallel spins, the relative occupation of the spin levels given by the spin temperature $T_s$.

The W-H effect assumes neutral hydrogen by absorbing and re-emitting Lyα photons may enter either of the two spin states. Since the spin state energy difference is very small, the hydrogen can wait on average a few million years before undergoing the 21 cm emission. Even so, the large amount of hydrogen gas in the Universe suggests hydrogen atoms are always emitting 21 cm radiation to allow detection with radio telescopes.

#### 3.2.2. Spin and Kinetic Temperatures

Radio telescopes measure the 21 cm recession velocity of hydrogen based on the thermal power P received per unit bandwidth by, $P = k T_k$, where $T_k$ is the kinetic temperature. But the spin temperature $T_s$ is only a descriptor of the electronic spin state. Only the kinetic temperature $T_k$ is a true thermodynamic temperature. The W-F effect is thought to provide the link between the spin temperature $T_s$ produced under Lyα absorption with the kinetic temperature $T_k$ of the hydrogen atom. But like cosmic dust NPs, the Planck law of QM precludes thermal fluctuations of kinetic temperature $T_k$ because the heat capacity of hydrogen atoms vanishes.

What this means is the W-F effect that couples the kinetic temperature $T_k$ to the spin temperature $T_s$ is forbidden by QM. The 21 cm hydrogen line emission is therefore optical and related to the spin temperature $T_s$ but has nothing to do with the kinetic temperature $T_k$ and thermal power P radiated from the neutral hydrogen atom.

.

#### 3.2.3. Thermal Noise

Galaxy velocities inferred from the thermal power P measured by the radio telescope that depend on the kinetic temperature $T_k$ of the hydrogen are questionable because of thermal noise. Signal to noise ratios of radio telescope power P may be < 1 suggesting noise is being interpreted as 21 cm radiation. What this means is radio measurements of 21 cm radiation may have nothing to do with galaxy velocities, or the existence of dark matter inferred [4, 5] from the flat rotation curves of the M31 galaxy. Non-thermal 21 cm emission is suggested, but optical measurements are difficult and radio telescopes only measure the power P of thermal radiation.

#### 3.2.4. Conclusions

QM by the Planck law questions the W-F effect in describing the excitation of the spin temperature $T_s$ of the hydrogen atom by the kinetic temperature $T_k$. In fact, the 21 cm hydrogen lines can only have a non-thermal origin and cannot be measured by radio telescopes. Indeed, radio redshift measurements based on thermal power P emitted by neutral hydrogen have no physical meaning as the atom is forbidden by QM to conserve the Lyα photon by temperature because of its vanishing heat capacity.

Radio telescopes measuring the thermal power P thought emitted by the 21 cm hydrogen line are most likely measuring thermal noise. Only galaxy redshifts measured by optical telescopes and corrected for cosmic dust provide credible galaxy velocities.

## 4. DISCUSSION

Today, cosmology is of great interest with regard to dark matter and Universe expansion, both relying on galaxy velocities computed by the Doppler Effect. The following discussions are made based on assessments of optical redshifts. Radio redshifts are excluded.

### 4.1. Dark Matter

The spiral galaxy M31 is thought [5] to have a flat velocity profile from the bulge to the edge while Newtonian mechanics suggests decreasing velocity with radius. But cosmic dust redshift $Z_D$ resolves the dilemma. The M31 spectra of galaxy light in an edge-on view gives a nearly constant redshift $Z_D$ along the galaxy radius because the galaxy illuminates about the same amount of cosmic dust NPs along the line-of-sight between the galaxy and the Earth based observer.

If the amount of cosmic dust in front of the galaxy is negligible, the velocity profile would appear Newtonian and not flat. But this is not expected as the Doppler velocities inferred from optical redshift $Z_D$ are expected to dwarf recession $Z_V$ redshifts, $Z_D >> Z_D$ giving the flat velocity profile. Regardless, Newton's equations are valid if corrections in (6) are made for cosmic dust.

Prior to the WIMP search, the MOND theory [17] based on spatially dependent gravitation force – laws was considered the leading explanation of dark matter. MOND stands for Modified Newtonian Dynamics. For spiral galaxies, MOND does reproduce the galaxy rotation curves. But for elliptical galaxies, galaxy groups, galaxy clusters, and larger-scale structures, MOND does not fit observations.

Interestingly, the presence of dark matter has been inferred [18] by kinematic measurements of redshifted galaxy positions. However, if the kinematics is based on actual galaxy positions excluding redshift, dark matter is shown [19] insignificant consistent with the corrections in (6) for redshift by cosmic dust.

More exotically, there is no compelling evidence [20] that PBHs produce dark matter. PBH stands for primordial black holes. To determine the mass of a PBH, the velocity of orbiting stars again rely on redshift measurements. However, the star velocities may be only a few hundred km/s that by the Doppler Effect correspond to $Z < 0.005$. Therefore, high precision spectroscopy [21] is required to resolve the redshift wavelength $\Delta\lambda$ which may only be a fraction of a nanometer. Therefore, PBHs need critical review for cosmic dust redshift.

### 4.2. Accelerated Universe Expansion

Since Hubble's discovery of galaxy redshift, an expanding Universe has dominated astronomy. However, by correcting for the redshift in cosmic dust, Hubble might have allowed astronomy to proceed on the basis of Newtonian mechanics instead of Einstein's general relativity. Nevertheless, astronomy still follows Hubble's redshift in explaining how the Universe is currently undergoing an accelerated expansion.

In 2001, the most distant Type Ia SN was found [22] brighter than expected for a distance corresponding to its redshift $Z = 1.7$. SN stands for Supernovae. Later 10 more distant SN were all found brighter than expected and interpreted as being closer to us than indicated by the redshift/distance relationship. Since dust can only make SN dimmer, but never brighter, the brighter SNs were explained [23] by accelerated Universe expansion.

It is correct that cosmic dust can never make the SN brighter, but incorrect to conclude dust does not redshift SN light. From (2), the redshift/distance relationship usually assumes $Z_{meas} = Z_V$ and not $Z_{meas} = Z_V + Z_D$. If redshift $Z_{meas}$ is not corrected for dust $Z_D$, the brightness B ($Z_V$) is greater than at B ($Z_V + Z_D$) consistent with [22] that the SN appears closer to us than expected from the distance based on the relationship with redshift.

However, if the redshift $Z_{meas}$ is corrected for cosmic dust redshift $Z_D$, the brightness B ($Z_V + Z_D$) is the same as expected B ($Z_V$) from the redshift/distance relationship. What this means is the accelerating Universe is not physical, but rather an anomaly of redshift in cosmic dust.

## 5. EXTENSIONS

### 5.1. Sunyaev-Zel'dovitch Effect

The SZE is thought to blueshift CMB radiation upon interacting with collapsing galaxy clusters. SZE stands for Sunyaev-Zel'dovich Effect. Both measured redshift $Z_{meas}$ and the SZE are usually thought proportional to the galaxy cluster mass M, so the SZE should be proportional to $Z_{meas}$. Contrarily, the SZE is found [23] to be independent of $Z_{meas}$. But $Z_{meas} = Z_V + Z_D$ includes cosmic dust redshift $Z_D$. Since $Z_D >> Z_V$, and since $Z_D$ does not originate within the collapsing galaxy clusters, but rather in the in the line-of-sight of the galaxy cluster to the Earth, it is likely $Z_{meas}$ does not depend on the SZE consistent with observations.

### 5.2. Supernovae Light Curve Decay

Studies of time dilation in SN light curves [24] showed that at low Z it takes 20 days to decay while at Z = 1 it takes 40 days. Cosmic dust redshift, $Z_D$ is proportional to the number of dust NPs surrounding the SN that in turn is proportional to the mass M of the SN. Hence, $Z_{meas}$ should be proportional to M, i.e., the SN at Z = 1 having larger M taking a longer time to decay than for smaller M at low Z.

But this has nothing to do with time dilation, rather the fact the NPs causing the redshift are simply cooling at a rate proportional the mass of the SN. What this means is time dilation based on redshift observed in SN light curves requires review for cosmic dust to avoid interpreting thermal cooling of SN as Universe expansion.

### 5.3. Tolman Test

In 1930, Tolman proposed correlating the brightness B of galaxies with redshift $Z_V$ as a test to determine whether the Universe is expanding. But Tolman did not consider the redshift $Z_D$ of the intervening cosmic dust. In fact, Tolman is only valid if $Z_D = 0$, i.e., $Z_{meas} = Z_V$. Since cosmic dust redshift $Z_D$ exist even if the galaxy is not receding $Z_V = 0$, Tolman fails as there is no Universe expansion. Nevertheless, the Tolman test was interpreted [25] as the reality of Universe expansion.

Recently, the brightness B of aging SN spectra was shown [26] to drop inversely with (1 + Z). Assuming only redshift $Z_D$ by dust alone, the brightness Bo at the observer is, Bo = hc / 2nd while at the galaxy B = hc / λ. Hence, the wavelength λ of galaxy light redshift by cosmic dust is $2nd = (1 + Z_D)\ \lambda \rightarrow Bo = hc / (1 + Z_D)\ \lambda = B / (1 + Z_D)$ and cosmic dust redshift $Z_D$ is consistent with the drop in brightness B of the SN spectra by $(1 + Z_D)$ even though the galaxy is not receding.

### 5.4. Exoplanets

Planets orbiting the distant star HR8799 are thought [27] to support the theory that exoplanets surround other stars in the Universe consistent with the planets that orbit our Sun. IR spectroscopic measurements of the suspected planets in the wavelength range from 995-1769 nm showed the presence of ammonia 1450-1550 nm, acetylene 1500-1550 nm, methane greater than 1650 nm, and carbon dioxide 1560-1630 nm, all observed in the atmospheres of the planets in our solar system. Unlike the distinct IR spectra observed on Earth, however, the exoplanet spectra are broadband with superposed small features identifying the IR lines of molecular gases.

Stars like HR8799 emit high intensity UV radiation that can be absorbed in the dust of surrounding debris haloes, but there is no mechanism known to convert UV radiation, say Lyα, to near IR radiation upon absorption in the dust of debris haloes. However, UV can be redshift by cosmic dust to the near IR. From (5), methane having cosmic dust redshift $Z_D$ wavelength 2nd > 1650 nm could be mistaken for Lyα radiation at Z > 12.6 and d > 550 nm. Broadband near IR spectra around suspected lines of exoplanet gases may be explained by variations in the diameters d of NPs in the cosmic dust debris.

### 5.5. Olbers Paradox

In 1823, Olbers made the paradoxical observation that the night sky is dark, but in a static infinite Universe the night sky should be bright. Indeed, Olbers paradox is often argued in supporting the Big Bang theory in an expanding finite Universe. Olbers argued in an infinite Universe the observer would see a nearby galaxy in one region of the sky and other more distant galaxies. Although the nearby galaxy would appear brighter, there would be more distant galaxies in the sky. Therefore, both the light from the nearby region and the total light from the distant region would be the same. Hence, the night sky should be bright if the Universe is infinite, but since the night sky is dark, Olbers concluded the Universe is finite.

But in a finite Universe, darkness requires absorption of starlight that by classical physics increases temperatures resulting in a bright night sky which is not observed. Hence, Olbers paradox requires the Big Bang to expand the finite Universe, the increased volume compensating for starlight heating to maintain the CMB at 2.7 K.

For cosmic dust, QM differs. In a static and infinite Universe, a bright night sky from starlight heated cosmic dust may be dismissed [14] because QM denies dust atoms the heat capacity to increase in temperature. Instead, visible galaxy starlight upon absorption in cosmic dust may only be cosmic dust redshift $Z_D$ to the IR, the IR visually appearing to the observer on Earth as a dark night sky and not bright. Unlike cosmic dust, starlight heats macroscopic matter, but the infinite mass in the static and infinite Universe precludes any measurable temperature increase, a fact supported by the thermal stability of the CMB.

Olbers paradox is resolved. Either static and infinite or finite and expanding Universes are possible, but the Universe is more likely static and infinite because the finite and expanding Universe requires the speculative Big Bang to maintain the CMB temperature at precisely 2.7 K.

## 6. CONCLUSIONS

The Buchalter Cosmology Prize was conceived on the premise that there are still fundamental gaps in our understanding of cosmology and that currently-accepted paradigms such as dark matter and Universe expansion are incomplete and perhaps even incorrect descriptions of our Universe.

The instant paper is presented in the manner of the Buchalter Prize not because it is ground breaking theoretical, observational, or experimental work in cosmology, but rather based on deductions from the well-known, but the long-forgotten Planck law of QM formulated over a century ago. Nevertheless, my paper challenges current cosmology on dark matter and Universe expansion from first principles hopefully spurring the formulation of a simpler cosmology that explains current observations while advancing our understanding of QM and classical physics. By credibly refuting current cosmological theories for dark matter and Universe expansion, perhaps cosmology will return to Einstein's once upon a time static and dynamic Universe.

## References


[1] J.H. Oort, "Observational evidence confirming Lindblad's hypothesis of a rotation of the galactic system," Bull. Astron. Inst. the Netherlands 3, 275–282, 1927.

[2] F. Zwicky, "Die Rotverschiebung von extragalaktischen Nebeln," Helv. Phys. Acta, 6, 110–127, 1933.

[3] E. Hubble, "Extragalactic Nebulae," Astrophys. J. 64, 321, 1926.

[4] J. L. Pawsey, "The interstellar hydrogen line at 1,420 Mc./sec., and an estimate of galactic rotation," Nature 168, 358 (1951).

[5] V. C. Rubin, W.K. Ford, "Radial Velocities and Line Strengths of Emissions Lines Across the Nuclear Disk of M31," Astrophys. J., vol. 170, pp 25, 1971.

[6] D. S. Akerib, et al., "The LUX Collaboration," Astropart. Phys. 45, 34, arXiv: 1210.4569 [astro-ph.IM] 2013.

[7] D. S. Akerib, et al., "Results from a search for dark matter in LUX with 332 live days of exposure," arXiv: 1608.07648v1 [astro-ph.CO] 27 Aug 2016.

[8] T. V. Prevenslik, "Cosmic Dust and Cosmology," Publications of the Korean Astronomical Society, vol. 30, pp. 327-330, September, 2015.

[9] E. M. Purcell, "Temperature fluctuations in very small interstellar grains, " Astrophys. J., vol. 206, pp. 685, 1976

[10] B. T. Draine, A. Li, "Infrared emission from interstellar dust. I. Stochastic heating of small grains," Astrophys. J., 551, 807, 2001.J. C.

[11] M. Planck, "On the Theory of the Energy Distribution Law of the Normal Spectrum," Verhandl. Dtsch. Phys. Ges., 2, 237, 1900.

[12] Weingartner, B. T., Draine, "Dust Grain Size Distributions and Extinction in the Milky Way, Large Magellanic Cloud, and Small Magellanic Cloud," Astrophys. J., vol. 548, pp. 296, 2002.

[13] R. Feynman, QED: The Strange Theory of Light and Matter. Princeton University Press, 1976.

[14] T. V. Prevenslik, See Simple QED Applications at http://www.nanoqed.org , 2010-2017.

[15] R. Minkowski, O. S. Wilson, "Proportionality of Nebular Red Shifts to Wave length," Astrophys. J., vol. 123, pp. 373, 1956

[16] S. A. Wouthuysen, "On the excitation mechanism of the 21-cm interstellar hydrogen emission line," Astrophys. J., vol. 57, pp. 31-32; April, 1952.

[17] M. Milgrom., "The MOND Paradigm," arXiv: 0801.3133v2 [astro-ph] 2008.

[18] D. Harvey, et al., "Dark Matter Astrometry: Accuracy of sub-halo positions for the measurement of self-interaction cross sections," arXiv:1305.2117v1 [astro-ph.CO] 2013.

[19] C. Moni Biden, et al., "On the local dark matter density," arXiv:1411.2625v1 [astro-ph.GA] 10 Nov 2014.

[20] B. Carr, F, Kuhnel, M. Sandstad, "Primordial Black Holes as Dark Matter," arXi: 1607.06077v3 [astro-ph.CO] 2016.

[21] E. A. Corbett, et al., "Emission line widths and QSO black hole mass estimates from the 2dF QSO Redshift Survey," arXiv: astro-ph/0304541v1, 2003.

[22] A. G. Riess et al., "The Farthest Known Supernova: Support for an Accelerating Universe and a Glimpse of the Epoch of Deceleration," Astrophys. J., vol. 560, pp.49-71, 2001.

[23] A. G. Riess, et al., "Type Ia Supernova Discoveries at Z > 1 from the Hubble Space Telescope Evidence for Past Deceleration and constraints on Dark Energy Evolution, Astrophys. J., vol. 607, pp. 665, 2004.

[24] J. E. Carlstrom, C. P. Holder, E. D. Reese, "Cosmology with the Sunyaev-Zel'dovich Effect," Ann. Rev. Astron. Astrophys., vol. 40, pp. 643, 2002.

[25] S. Blondin, et al., "Time Dilation in Type Ia Supernova Spectra at High Redshift," Astron. J, vol. 682, pp. 724, 2008.

[26] L. M. Lubin, A. Sandage, "The Tolman Surface Brightness Test for the Reality of the Expansion. IV. A Measurement of the Tolman Signal and the Luminosity Evolution of Early-Type Galaxies," Astron. J, vol. 122, pp. 1084, 2001.

[27] B. R. Oppenheimer, et al., "Reconnaissance of the HR 8799 exosolar system I: Near IR spectroscopy," Astron. J., 8 March, 2013.

# Cosmic Dust in an Expanding Universe?

**Abstract** Dust alters our observations of what we observe on Earth, but also our understanding of the Universe. Cosmic dust that permeates inter stellar space is not considered in Hubble's law that states the velocity of a receding galaxy is proportional to its distance to the Earth. Hubble's law is based on Doppler's Effect whereby the wavelength of light from the galaxy is redshift if the galaxy is moving away from us. Recently, redshift measurements of Supernovae explosions have been taken as proof the Universe is not only expanding, but the expansion is accelerating. Redshift measurements suggest high galaxy velocities that cannot be explained by Newton's law of motion unless the existence of invisible mass or dark matter is assumed. Yet, the amount of dust between us and the galaxy is also proportional to the distance from Earth, and if cosmic dust can be shown to redshift galaxy light, the implications of Hubble's law are significant. The Universe need not be expanding, let alone accelerating, dark matter would not exist with all other the outstanding problems in cosmology resolved by Newtonian mechanics

**Keywords** Expanding Universe, Hubble redshift of galaxy light altered by cosmic dust, quantum mechanics

## 1. Introduction

DUST 2016, the International Conference on Atmospheric Dust [1] is directed to the world of the atmospheric particles. Beyond our atmosphere, cosmic dust in the ISM comprising nanoparticles of primarily silicates permeate the vast reaches of the Universe. ISM stands for interstellar medim. Like atmospheric dust obscurring observations of what we perceive on Earth, our observations of the Universe are affected by cosmic dust.

In 1929, Edwin Hubble [2] formulated the law that the velocity of a receding galaxy is proportional to its distance to the Earth. Hubble based his law on Doppler's Effect whereby the wavelength of light from the galaxy is redshift if the galaxy is moving away from us. Thus, by measuring the redshift of known spectral lines, Hubble claimed to know the recession velocity of the galaxy relative to the Earth.

Based on the redshift of SN light, astronomers [3] now take Hubble's law as proof the Universe is not only expanding, but accelerating. SN stands for supernovae. If, however, the redshift has a non-Doppler origin, the Universe need not be expanding. Redshift without an expanding Universe is of utmost importance because many of the outstanding problems in cosmology would be simply resolved by Newtonian mechanics.

## 2. Theory

QED is proposed as the mechanism by which the EM energy of a galaxy photon is redshift upon absorption under EM confinement in cosmic dust NPs. QED stands for quantum electrodynamics, EM for electromagnetic, and NP for nanoparticle. QED induced redshift is a consequence of QM that forbids the atoms in NPs under EM confinement to have the heat capacity to increase in temperature upon absorbing the galaxy photon. QM stands for quantum mechanics. The EM confinement of NP atoms is a consequence of the high surface-to-volume ratio of NPs that requires the galaxy photon energy to deposit in the NP surface. Upon absorption, the EM energy of the galaxy photon is redshift depending on the size of the NP. Redshift only occurs as the NP absorbs a single galaxy photon, i.e., blueshift having energy greater than the galaxy photon violates the conservation of energy and does not occur.

The QM restriction on heat capacity may be understood by the Planck law [4] that requires atoms under EM confinement at short wavelengths λ to have vanishing thermal kT energy. The Planck law at ambient temperture of 300 K and the ISM at 2.7 K are shown in Figure 1.

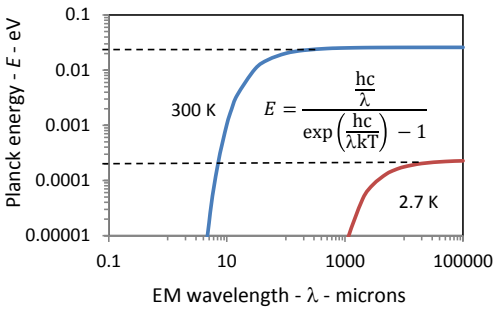


**Figure 1.** Planck law at 2.7 and 300 K
In the inset, E = Planck energy, h = Planck's constant, k = Boltzmann's constant, c = velocity of light, T = temperature, and λ = wavelength

Unlike classical physics allowing the atom to always have heat capacity, QM restricts the heat capacity of the atom to the macroscale. Classical physics at ambient and ISM temperatures noted by dotted lines at 300 and 2.7 K shows the macroscale corresponds to $\lambda > 30$ and 3000 microns, respectively. The QM heat capacity of NPs vanishes at $\lambda < 0.1$ microns at ambient temperature, although is significantly reduced for $\lambda < 6$ microns. In the ISM, the QM heat capacity of the atom vanishes even for much larger > 1 mm size particles.

### 2.1. Conservation of Energy

In classical physics, heat transfer in NPs does not depend on their size allowing conservation of EM energy to always proceed by temperature changes. QM differs by requiring the heat capacity of NP atoms under EM confinement at ISM temperatures to vanish, and therefore the EM energy of the galaxy photon cannot be conserved by the usual change in temperature. Instead, conservation proceeds by the creation of EM radiation inside the NP by QED.

QED as a mode of heat transfer depends on the high surface-to-volume ratios of nanostructures. A closely related mechanism is TIR standing for total internal reflection. In 1870, Tyndall showed light is trapped by TIR in the surface of a body if its RI is greater than that of the surroundings. RI stands for refractive index. However, TIR usually occurs in the surface of macroscopic bodies having low surface-to-volume ratios allowing absorbed EM energy to be absorbed throughout the volume of the body. QED differs from TIR in that EM confinement in NPs depends on the high surface-to-volume ratio which means almost all of the EM energy of the galaxy photon absorbed by the NP to be spontaneously deposited in its surface.

### 2.2. EM confinement

The EM confinement wavelength $\lambda$ of the NP depends solely on the deposition of the galaxy photon in the NP surface as there is no physical confinement. Regardless of NP shape, EM energy of any form is almost totally confined to surfaces because of the high surface-to-volume ratios inherent in NPs. Atoms interior to opposing NP surfaces are therefore spontaneously placed under EM confinement as illustrated in Figure 2.

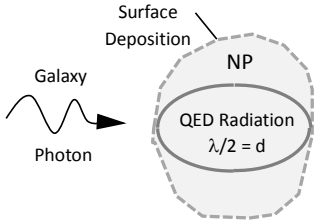


**Figure 2.** Momentary EM Confinement of absorbed galaxy photon in a NP

### 2.3. QED Radiation

QED relies on complex mathematics as described by Feynman [5] although the underlying physics is simple to understand, i.e., EM radiation [6] of wavelength $\lambda$ is created by supplying EM energy to a QM box with sides separated by $\lambda/2$. QED therefore induces the absorbed surface energy to be conserved by EM radiation standing within the EM confinement of the NP.

The NP as a QM box absorbs the EM energy of the galaxy photon in the minimum possible time, and therefore the characteristic dimension d is the minimum distance opposing NP surfaces. QED therefore induces the creation of standing EM waves having half-wavelengths $\lambda/2 = d$. Since the source of the standing QED wave is the EM energy of the absorbed galaxy photon in the confining NP surfaces, the EM confinement vanishes allowing the QED radiation to be emitted to surroundings at a wavelength depending on the characteristic dimension d of the NP. Since blue shift violates conservation of energy, the NP only redshifts the galaxy photon. All this occurs without a change in temperature. EM confinement is not permanent, sustaining itself only during absorption of the galaxy photon, i.e., absent absorption there is no EM confinement and the galaxy photon is not redshifted.

The Planck energy E of the galaxy photon having wavelength $\lambda$ is,

$$E = hc/\lambda \tag{1}$$

After absorption in the NP, the redshift wavelength $\lambda_o$ is,

$$\lambda_o = 2nd \tag{2}$$

where, n and d are the RI and characteristic dimension of the NP.

## 3. Application

The QED redshift galaxy photon [7] induced in dust NPs is observed on Earth at wavelength $\lambda$ giving the redshift Z,

$$Z = (\lambda_o - \lambda)/\lambda \tag{3}$$

is caused solely by the absorption of the galaxy photon in cosmic dust. Relative to the velocity of light c, the Doppler velocity V of galaxies with redshift Z is,

$$V/c = [(Z+1)^2 - 1]/[(Z+1)^2 + 1] \tag{4}$$

QED redshift depends on the wavelength of the galaxy photon and the size of the NPs. In this paper, only Ly$\alpha$ and H$\alpha$ galaxy photons are considered because of their abundance while representing the respective shortest and longest wavelengths in the ISM. The NPs are assumed to be amorphous silica having n = 1.5 with a range [8] of NP radii a where $0.0005 < a < 0.25$ microns, and $a = d/2$.

The QED redshift Z of Lyα and Hα lines in dust and the galaxy velocity ratio V/c based on the Lyα line is shown in Figure. 3.

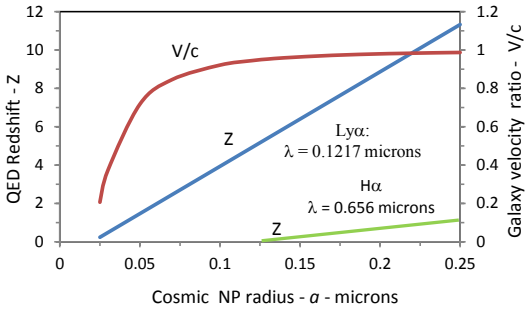


**Figure 3.** QED Induced Redshift of Lyα and Hα lines
Amorphous Silicate: n = 1.5

Unlike Hubble redshift where both Lyα and Hα photons always have the same Z, QED redshift of Lyα photons is far greater than that of Hα for the same NP radius, i.e., the Hubble redshift by the Doppler Effect gives the same Z for ALL wavelengths, but QED redshift in dust depends on wavelength. What this means is QED redshift allows an assessment of the validity [7] of the Hubble redshift if the Z's are not the same. Moreover, the galaxy velocity ratio V/c inferred by the Doppler redshift by dust may be a significant fraction of the velocity of light c making any astronomical measurement questionable as the galaxy need not be receding at all. Hence, cosmic dust most likely affects the accuracy of ALL astronomical ISM velocities inferred from Hubble redshift.

Historical [9] data by Minkowski & Wilson supports the Hubble redshift at low Z < 0.05, but excludes the Lyα line that gives the largest QED redshift in cosmic dust. Therefore, to assess Hubble redshift validity, measured Z is corrected [7] with the difference in redshifts of Lyα and Hα lines,

$$Z_{Hubble} = Z_{Meas} - (Z_{Ly\alpha} - Z_{H\alpha}) \qquad (5)$$

If redshift measurements of QED redshift of Lyα and Hα lines show,

$$Z_{Ly\alpha} = Z_{H\alpha}$$

Then

$$Z_{Hubble} = Z_{Meas}$$

and the effect of cosmic dust on Hubble redshift by the Doppler Effect may be neglected. If not, the validity of the Hubble redshift is questionable. At the upper bound NP radius of 0.25 microns, the Lyα and Hα lines have Z = 11 and 1.2, respectively. Hence, the cosmic dust correction to Hubble redshift for the Lyα line is far greater than Hα.

# 4. Discussion

### 4.1. Expanding Universe

QED induced redshift is caused solely by the absorption of the galaxy photon in cosmic dust having nothing to do with an expanding Universe. Given that galaxy light is unequivocally absorbed by cosmic dust on its way to the Earth, the high galaxy velocities V inferred from the Doppler interpretation of Hubble redshift Z may be meaningless as the galaxy need not be receding at all.

Relative to the velocity of light c, the Doppler velocity V of galaxies with redshift Z is shown in Figure 3. The galaxy velocity V inferred by the Doppler redshift of the Lyα photon is a significant fraction of c even at low Z, e.g., for a = 0.025 microns, Z = 0.23 and V = 0.2 c. Therefore, any implied relation of dark matter [3] from SN light to an expanding Universe is highly questionable. What this means is the Universe may still be expanding and dark matter and energy may still exist, but Universe expansion cannot be proven from redshift measurements of SN light. Moreover Hubble redshift is questionable proof the Universe began in the Big Bang suggesting the notion once proposed by Einstein of a static Universe in dynamic equilibrium is a more credible cosmology

### 4.2. Corrections of Hubble Redshift

The Hubble redshift $Z_{Hubble}$ by the Doppler Effect gives the same Z for ALL wavelengths while QED induced redshift depends on wavelengths. Historic data [9] supports the Hubble redshift at low Z < 0.05, but excludes the Lyα lines that give the largest QED induced redshifts. Today, support for the Doppler Effect at high Z is rarely reported. Therefore, to obtain valid Hubble redshift, measured Z is proposed corrected using measured Z for Lyα and Hα lines,

$$Z_{Hubble} = Z_{Meas} - (Z_{Ly\alpha} - Z_{H\alpha})$$

### 4.3. Sunyaev-Zel'dovich Effect

The CMB radiation upon interacting with collapsing galaxy clusters is thought to blue-shift by the SZE. CMB stands for Cosmic Microwave Background and SZE for Sunyaev-Zel'dovich Effect. Since redshift Z is thought proportional to galaxy mass M while SZE is proportional to M, the SZE is thought proportional to Z. Contrarily the SZE is found [10] to be independent of redshift Z. By QED redshift in cosmic dust, the Z does not originate inside the collapsing galaxy clusters, but rather from NPs in the line of sight of the galaxy cluster to the observer. The SZE is therefore independent of Z consistent with observations.

### 4.4. Black-Hole Mass

Astronomers based on the Doppler redshift measurements of stars orbiting black-holes infer 50 billion solar masses are required to allow the stars moving near the speed of light to stay in orbit. However, QED induced redshift Z in cosmic dust highly exaggerates the actual rotational speed of the stars. NPs of cosmic dust in the trailing debris of stars moving away from the observer suggest speeds approaching the velocity of light. Hence, the rotational speed of the star in orbit inferred from the $Z_{Meas}$ is highly exaggerated, thereby placing in question the presence of large solar masses in black-holes necessary to maintain the star in orbit. $Z_{Meas}$ of black hole masses needs to reviewed for a cosmic dust origin.

### 4.5. Supernovae Light Curves

Time dilation of SN light curves [3] at low Z that take 20 days to decay will take 40 days to decay at Z = 1. SN stands for Supernovae. By QED redshift, Z is proportional to number of NPs that in turn is proportional to the mass M of the SN, i.e., Z is proportional to M. At Z = 1 the SN having larger dust mass M takes a longer time to cool than at low Z. What this means is time dilation observed in SN explosions inferred from $Z_{Meas}$ requires corrections for cosmic dust to avoid interpreting time dilation as Universe expansion instead the thermal cooling of the SN mass.

### 4.6. Tolman Test

In 1930, Tolman proposed a test to determine whether the universe is expanding by measuring the brightness B of galaxies and redshift Z, but Tolman did not consider the brightness reduced by cosmic dust. Nevertheless, the Tolman test was interpreted by Lubin and Sandage [11] as the reality of Universe expansion. Recently, the brightness B of the aging of SN spectra was shown by Blondin, et al. [12] to drop inversely with (1+Z). By QED redshift, the brightness Bo at the observer is. Bo = hc/λo, where λo given by Equation (3) is wavelength at the observer caused by cosmic dust. But λo = (1+Z) λ → Bo = hc/(1+Z) λ. At the SN, the brightness B = hc/λ. Hence, $B_o$ = B/ (1+Z) and therefore QED redshift ion dust is consistent with the reduction in the brightness B of the SN spectra by (1+Z).

### 4.7. Galaxy Rotation Problem

Similar to black-holes, the galaxy rotation problem discovered in the 1960's by Rubin and Ford [13] suggests dark mass exists at the center of the galaxies to hold them together under high rotational speeds inferred from $Z_{Meas}$ and interpreted by the Doppler Effect. However, measured redshifts need to be corrected for QED redshift in cosmic dust NPs depending on whether the galaxy is rotating away or toward the observer. Dust in galaxies moving away from us will show more redshift than that in the galaxy moving toward us, and therefore the rotational velocity based on Hubble redshift is far greater than it actually is. What this means is dark matter may not be necessary to hold the galaxies together. Indeed, Newtonian mechanics may resolve the galaxy rotation problem. Therefore, there would be no need to modify Newton's equations as in MOND to explain [14] how dark matter added to galaxies explains how they stay together at rotational speeds near the velocity of light. MOND stands for Modified Newtonian Dynamics.

### 4.8. Exoplanets

Discovery of exoplanets in far reaches of galactic space is a daunting task because of inherently faint images. Similar to the problems of black hole mass and galaxy rotation, proof of discovery is based on high-precision spectroscopy [15] to measure variations in light intensity as the planet spins. When observing a spinning exoplanet, half of the planet rotates away from Earth, while the other half rotates toward Earth. The spectrum of the side spinning away from us will show redshift, whereas the side spinning toward us will show a spectral blueshift.

The discovery by Oppenheimer et al. [16] of 4 planets orbiting the distant star HR8799 supporting the theory that exoplanets surround other stars in the Universe is consistent with the planets that orbit our Sun. IR spectroscopic measurements of the suspected planets identified ammonia from 1450 to 1550 nm, acetylene from 1500 to 1550 nm, methane above 1650 nm, and possibly carbon dioxide from 1560 to 1630 nm, all of which are commonly observed in the atmospheres of planets in our solar system. However, molecular lines of carbon dioxide and methane should have been found in all 4 planets, but were only observed for 2 planets. In one planet, a weak carbon dioxide line initially not present appeared 4 months later. What this means is the spectra of HR8799 system are not likely produced by molecules on the planets.

QED redshift suggests the molecules thought measured by IR spectroscopy are in fact redshifted Lyα photons having a wavelength depending on the size of the dust. Figure 3 shows NPs may produce near IR spectra similar to that of common molecules at high redshifts Z of Lyα photons, i.e., Z ≅ 11 at NP radius a = 0.25 microns. From Equation 3, the QED redshift wavelength λo = (Z+1)λ ≅ 1460 nm which is comparable to ammonia at 1450 nm. Similarly, methane having wavelengths > 1650 nm would be observed at Z ≅ 14 and NP radii a ≅ 0.275 microns which is a reasonable extension of known dust distributions in the ISM. Consistent with observation, the IR spectra has nothing to do with any molecular species, but highly likely depends on cosmic dust NPs. Hence, redshifted Lyα radiation in cosmic dust to the near IR could be interpreted as proof of exoplanet discovery - when in fact the exoplanet may not exist.

### 4.9. ISM Infrared Spectra

Dust NPs are thought to emit EM radiation by thermal emission at near to far IR wavelengths from non-equilibrium heating by single galaxy photons. In 1976, Purcell [17] showed single-photon heating produces a temperature spike of 40 K in very small NPs (a < 0.0025 microns) so that much of the absorbed energy will be radiated in the far IR near 60 microns. Today, Li and Draine [18] are similarly proposing NPs heated by single galaxy photons are the source of IR spectra in the ISM.

However, the notion that NPs heat-up upon absorption of a single galaxy photon is based on classical physics that allows the atom to have heat capacity. Contrarily, QM denies NP atoms under EM confinement the heat capacity to conserve the absorbed galaxy photon by a spike in temperature. Instead, QED produces IR in the ISM by redshift of Lyα photons as described above for exoplanets without increasing the NP temperature.

## 3. Conclusions

Humans know life has a beginning and an end, and it is only natural to think the Universe also has a beginning and end. Yet, for thousands of years, the Universe was considered static and infinite - without a beginning and end. However, Einstein in 1916 introduced his field equations that required the Universe to be finite and either contracting or expanding. Since a static Universe is foreign to human experience, Einstein provided a theoretical basis to suggest the Universe does indeed have a beginning and an end. But lacking experimental proof, Einstein's theory lay dormant until 1929 when Hubble dismissed a static Universe by showing the light from distant galaxies was redshift. Interpreted by the Doppler Effect, the Hubble redshift was taken as proof the Universe is finite and expanding consistent with human experience now supported by Einstein's field equations that continues to this day.

However, cosmic dust NPs that permeate the ISM upon absorbing a galaxy photon undergo QED redshift without the galaxy receding thereby not only over-predicting the velocities of galaxies, but suggesting the Universe is static and not expanding.

QED redshift in dust NPs is a consequence of QM that requires the heat capacity of the atom to vanish under the EM confinement produced upon the momentary absorption of the galaxy photon in the surface of the NP, the latter because of its high surface-to-volume ratio. Lacking heat capacity, conservation cannot proceed by an increase in temperature. Instead, QED induces the creation of standing wave photons in the NP having a wavelength that is redshifted relative to that of the galaxy photon.

In a Universe with cosmic dust, the accuracy of velocity measurements of galaxies inferred from the Hubble redshift by the Doppler Effect may be simply assessed by the difference between the redshift of Lyα and Hα lines.

## REFERENCES


[1] DUST 2016 - 2nd International Conference on Atmospheric Dust, Castellaneta Marina – Taranto, Italy, 12-17 June 2016.

[2] E. Hubble, "A Relation between Distance and Radial Velocity among Extra-Galactic Nebulae," Proc. of the Nat. Acad. of Scie. Of the United States of America, 15, 3, 168-173, 1929.

[3] A. G. Riess, et al., "Type Ia Supernova Discoveries at Z >1 from the Hubble Space Telescope Evidence for Past Deceleration and constraints on Dark Energy Evolution," ApJ, 607, 665, 2004.

[4] M. Planck, "On the Theory of the Energy Distribution Law of the Normal Spectrum," Verhandl. Dtsch. Phys. Ges., 2, 237, 1900.

[5] R. Feynman, QED: The Strange Theory of Light and Matter, Princeton University Press, 1985.

[6] T. V. Prevenslik, Various QED Applications, See http://www.nanoqed.org , 2010-2016.

[7] T. V. Prevenslik, "Cosmic Dust and Cosmology," Proc. of APRIM 2014: Galaxies, AGN and Cosmology – Daejon, Korea, September 2015, See http://aprim2014.org/08.php

[8] J. C/ Weingartner, B. J. Draine, "Dust Grain Size Distributions and Extinction in the Milky Way, large Magellanic Cloud, and Small Magellanic Cloud," AsJ, 548, 296. 2001.

[9] R. Minkowski, O. S. Wilson, "Proportionality of Nebular Red Shifts to Wavelength," AsJ, 123, 373, 1956.

[10] J. E. Carlstrom, C.P. Holder, E. D. Reese, "Cosmology with the Sunyaev-Zel'dovich Effect," ARA&A, 40, 643, 2002.

[11] L. M. Lubin, A. Sandage, "The Tolman Surface Brightness Test for the Reality of the Expansion. IV. A Measurement of the Tolman Signal and the Luminosity Evolution of Early-Type Galaxies," AsJ, 122, 1084, 2001.

[12] S. Blondin, et al., "Time Dilation in Type Ia Supernova Spectra at High Redshift," AsJ, 682, 724, 2008.

[13] V. C. Rubin, W. K. Ford, "Rotation of the Andromeda Nebula from a Spectroscopic Survey of Emission Regions," AsJ, 159, 379, 1970.

[14] M. Milgrom, "The MOND Paradigm," arXiv:0801.3133v2 [astro-ph]

[15] I. A. G. Snellen, et al. "Fast Spin of the Young Extrasolar Planet Beta Pictoris b," Nature, April 30, 2014

[16] B. R. Oppenheimer, et al., "Reconnaissance of the HR 8799 exosolar system I: Near IR spectroscopy," arXiv:1303.2627v1 [astro-ph.EP]

[17] E. M. Purcell, "Temperature fluctuations in very small interstellar grains," Astrophys. J. 206, 685, 1976.

[18] A. Li, B. T. Draine, "Infrared Emission from Interstellar Dust. III. The Small Magellanic Cloud," AsJ, 576, 762–772, 2002.

CMBR as Solar illumination of the Oort Cloud modified by Cosmic Dust

**INTRODUCTION**

Cosmic Background Radiation (CMBR) evolved from models [1] of the Big Bang by Gamow beginning in 1948. Only later in 1965 did Penzias and Wilson [2] discover the microwave radiation coming from space. Dicke and others came to the conclusion that the Big Bang left behind residual radiation which would still be present in the Universe as black body EM radiation with a temperature of about 10 K. However, Dicke [3] did not believe that the radiation came from a cold source, and instead cold temperatures were produced during the Big Bang in the expansion of the Universe.

However, Universe expansion is not required as cold temperatures are a natural consequence of our Solar System. Beyond the Planetary System, the Oort Cloud [4] at 10,000 AU is naturally cold. In 1950, the Oort Cloud was inferred by studying the orbits of different comets as comets were permanent members of the Solar System and not random bodies. Unlike the disk-like Planetary System in the ecliptic of the Sun, the Oort cloud is spherical. The Oort Cloud in relation to the Planetary System is shown in Figure 1.

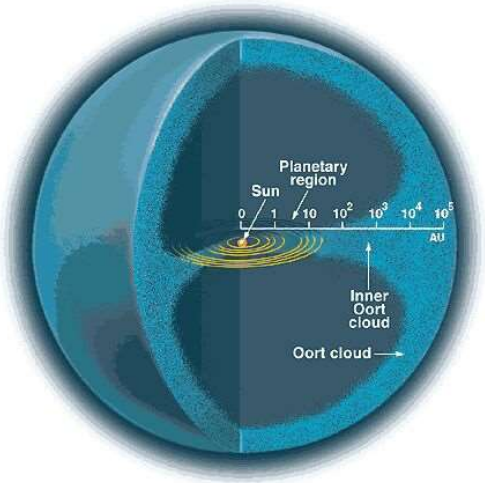


Figure 1. Sun and Planetary System in relation to the Oort Cloud

The equilibrium temperature T of the Oort Cloud may be estimated by assuming blackbody thermal radiation emitted by the Sun at temperature Ts is absorbed without refection by the Oort Cloud.

$$T = Ts\sqrt{\left(\frac{R_S}{2D}\right)}$$

where, Ts = 5800 K and Rs = 693 x $10^6$ m. From Figure 1, the distance D is arbitrarily taken as the inner radius of the Oort Cloud, D ~ 10,000 AU. For AU = 150 x $10^9$ m, T = 2.79 K. Similarly, the Earth at 1 AU from the Sun gives T = 279 K. The temperature of the CMBR at 2.725 K is close to the 2.79 K estimated from blackbody radiation at D = 10,000 AU as shown in Figure 2.

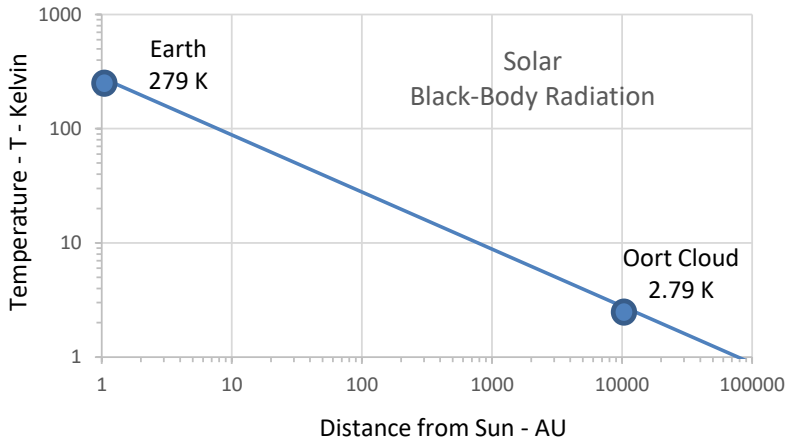


Figure 2. Blackbody approximation to CMBR Temperature

The notion the Solar System alone defines the CMBR radiation is supported by Planck's law,

$$\mathrm{Er} = \frac{h\upsilon^3}{c^2}\frac{1}{e^{\frac{h\upsilon}{kT}} - 1}$$

The peak of Spectral Radiance occurs at dEr/dυ = 0. Numerically, hυ/kT = 2.821. The CMBR at T =2.725 K corresponds to $\upsilon_{max} \sim 160$ GHz and $\lambda = 1.871$ mm as shown in Figure 3.

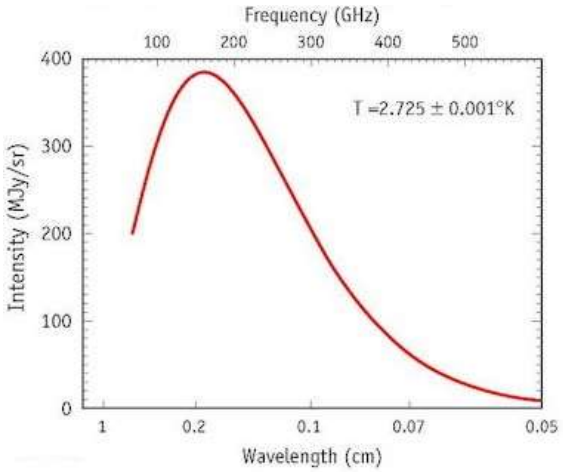


Figure 3. CMBR Spectrum

However, the CMBR is not uniform everywhere in the Universe. The anisotropy is evident as the resolution of the CMBR increases from COBE to WMAP to Planck shown in Figure 4.

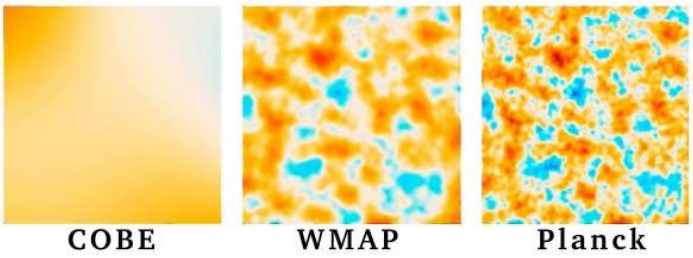


Figure 4. Anisotropy of the CMBR

In this paper, the CMBR anisotropy is given by the Anomalous Microwave Emission (AME) from cosmic dust in our Solar system. In order to do statistical tests on the true CMBR, the AME must be removed. But the effect of dust on EM radiation must be understood before CMBR is cleaned. Especially notable is the intense AME in the Galactic plane [5] shown in Figure 5. Dust rings [6] around Mercury, Venus and Earth also be cleaned as shown in Figure 6.

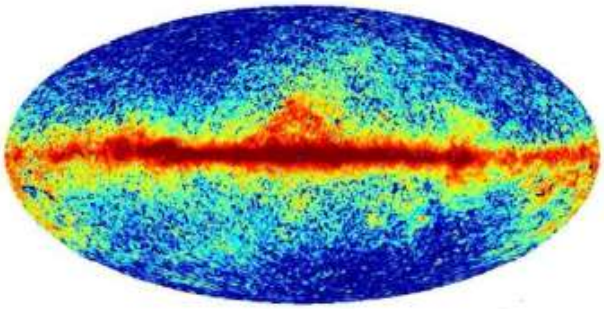

Figure 5. AME from dust in the Solar system

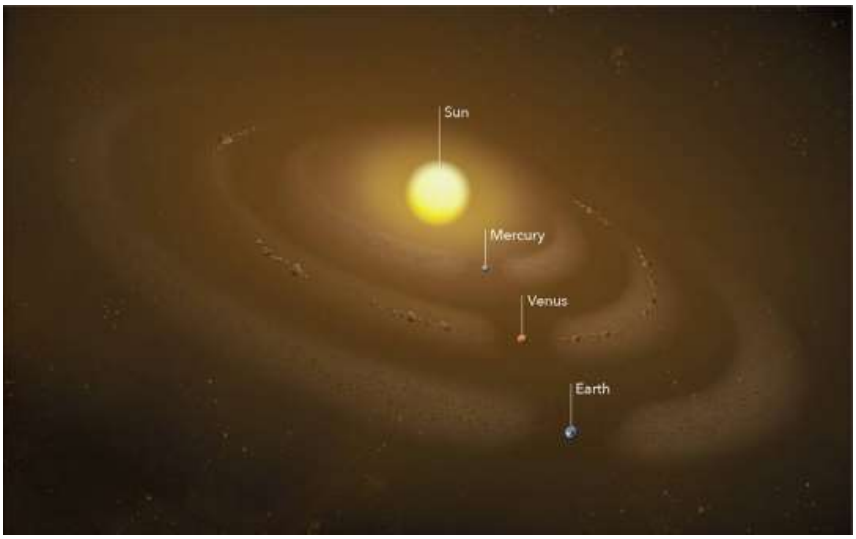


Figure 6. Dust rings around Mercury, Venus and Earth

In cosmology, the Copernican principle states the Earth is not a privileged location in the Universe, i.e., if the Universe appears isotropic in all directions from the Earth, then the Universe is isotropic everywhere. Locally, Figures 4 and 5 show the CMBR is anisotropic to about one part in a thousand, but on a large scale, the anisotropy is significant as shown in Figure 7. Indeed, the large scale anisotropy shows an 'Axis of Evil' suggesting the Copernican Principle is not satisfied, i.e., the quadrupole and octupole axes are almost coincident and aligned with the Galactic plane erroneously making the Earth the center of the Universe!!!

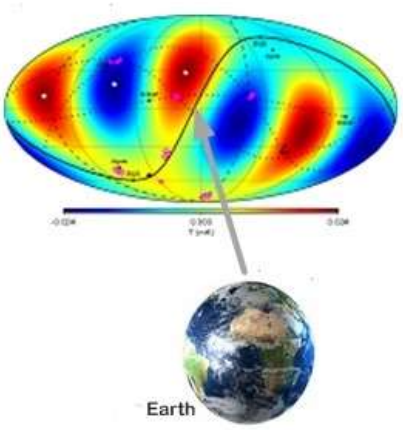


Figure 7. CMBR Quadrupole and Octupole Axes Aligned with Galactic plane

**DISCUSSION**

**Cosmic Dust and Redshift**

Light from galaxies beyond the Oort Cloud measured on Earth must pass through the Kuiper Belt and dust rings of the Planetary System. In this paper, the light absorbed in dust redshifts the galaxy light which if inferred by the Doppler effect highly overstates actual galaxy velocities. Indeed, visual observations of galaxy dynamics do not confirm the inferred Doppler velocities unless dark matter exists to slow the high velocities to Newtonian levels.

The difficulty with high galaxy velocities from overstated redshift is not new. Hubble found it difficult to believe the galaxy velocities were real and instead found it easier to suppose that the lines of the spectra are shifted to the red by some property of space acting on the light during its journey to the Earth. Following Hubble's reasoning, the galaxy velocities here are not real and cosmic dust that permeates the Solar System and Universe is the property of space that redshifts spectral lines. Later, Arp proposed the redshifts were intrinsic giving the false impression dark matter is present, when in fact it does not exist, perhaps explaining why the search for dark matter particles to date has not succeeded.

Based on classical physics, astronomers [7] claim the light from distant galaxies upon absorption in cosmic dust simply raises dust temperature and upon re-emission explains the IR spectra in the ISM. But the dust is nanoscopic governed by QM, the Planck law of which shows atoms in nanoparticles (NPs) of cosmic dust cannot conserve galaxy light by an increase in temperature [8] because their heat capacity vanishes. QM stands for quantum mechanics. The Planck law at 2.7 and 300 K is shown in Figure 8.

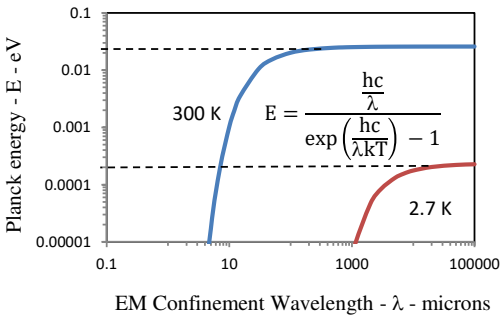


Figure 8: QM Planck law – Thermal Energy of the Atom
In the inset, E is Planck energy, h Planck's constant, k Boltzmann's constant,
λ EM confinement wavelength, and T absolute temperature

Classical physics (noted by dotted lines) allows NP atoms irrespective of EM confinement to always have kT heat capacity. QM differs by only allowing kT heat capacity at 300 and 2.7 K for $\lambda > 100$ and 3000 microns, while otherwise requiring kT heat capacity to decrease and vanish. In the ISM, NPs in the size range < 0.5 microns [8] therefore have vanishing heat capacity thereby precluding conservation of galaxy light by fluctuations in temperature.

However, vanishing QM heat capacity requires the NPs to have high EM confinement at submicron wavelengths. But cosmic dust is not observed to have any surface structure that might be construed as EM confinement suggesting the absorption of galaxy light in submicron dust NPs is itself the source of momentary EM confinement. Indeed, no special treatment of surfaces is required as EM confinement is a natural consequence of the high S/V ratio of NPs. S/V stands for surface-to-volume. Upon absorption of galaxy light, almost all of the photon energy is therefore spontaneously deposited in the NP surface. What this means is the NP atoms are momentarily placed under EM confinement. Since the NPs are submicron, the EM confinement is also submicron and the heat capacity of the NP vanishes.

But the NPs in the ISM need not be submicron as the heat capacity of the atom at 2.7 K decreases about 3 orders of magnitude at $\lambda < 1000$ microns, and therefore cosmic dust NPs > 1 micron also have reasonably high S/V ratios making EM confinement still valid, e.g., Lyman-alpha (Ly$\alpha$) and Hydrogen-alpha (H$\alpha$) photons are redshift to VIS and near IR levels in NPs $<$ 1 micron while far IR photons are produced from NPs $>$ 1 micron. Unlike classical physics thought to create IR spectra from NPs by increased temperature, QM produces VIS to far IR spectra by the nonthermal process [8] of simple QED as shown in Figure 9.

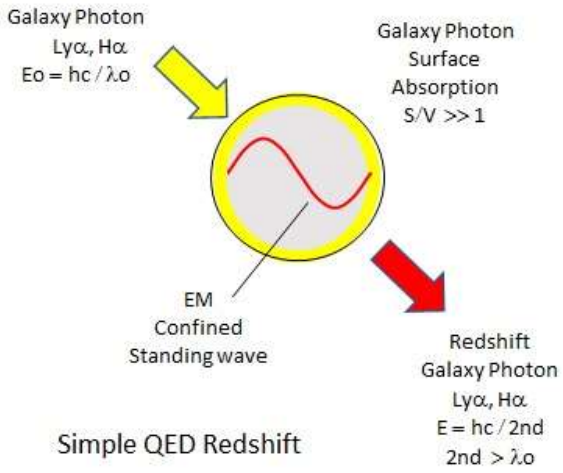


Figure 9. Simple QED induced Cosmic Dust Redshift

Simple QED produces EM radiation in NPs, but has nothing to do with the QED of light-matter interaction by Feynman and others. Simple QED [8] is far simpler and is readily understood.

Briefly stated:

Under the QM restriction that the heat capacity of the atom under high EM confinement vanishes, simple QED conserves the heat of galaxy light absorbed in a NP surface by spontaneously creating standing EM radiation inside the NP having half wavelength $\lambda/2 = d$, where d is the NP diameter. The Planck energy E of the standing EM radiation is,

$$E = \frac{h\left(\frac{c}{n}\right)}{\lambda} = \frac{hc}{2nd}$$

where, the velocity of light c is corrected for the slower speed in the solid state by the refractive index n of the NP. The standing wave is created under the EM confinement formed from the galaxy light deposited in the NP surface, but once depleted the EM confinement vanishes allowing the standing EM radiation to escape the NP and be observed on Earth as redshifted galaxy light. The cosmic dust redshift $Z_D$ of the galaxy photon having energy Eo and wavelength $\lambda o$ is,

$$Z_D = \frac{2nd - \lambda o}{\lambda o} > 0$$

Unlike reddening where shorter wavelengths are not increased by scattering, cosmic dust redshift $Z_D$ corresponds to a physical increase ($2nd-\lambda o$) in the wavelength of galaxy light. Therefore, the true galaxy velocity V is computed by correcting the measured redshift $Z_{meas}$ for the redshift $Z_D$ of cosmic dust,

$$\frac{V}{c} = \frac{[(Z_V + 1)^2 - 1]}{[(Z_V + 1)^2 + 1]}$$

where, $Z_V = Z_{meas} - Z_D$.

In Figure 10, the cosmic dust redshift $Z_D$ of Ly$\alpha$ and H$\alpha$ light is shown for amorphous silicate n = 1.5. The range of NP sizes [9] for radii r = d/2 from 0.025 to 0.25 microns shows simple QED produces cosmic dust redshifts of Ly$\alpha$ and H$\alpha$ photons at 0.25 microns of 11 and 1.5, respectively. If not corrected for cosmic dust redshift, dust redshift velocities approach the speed of light at d = 2r ~ 0.2 microns.

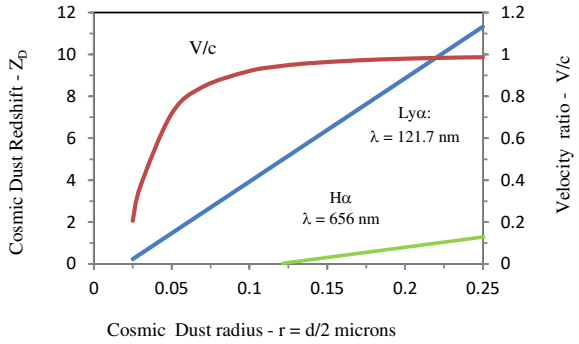


Figure 10. Cosmic Dust Redshift of Ly$\alpha$ and H$\alpha$ Light

**Cosmic Dust and CMB Anisotropy**

The Planck satellite surveyed the whole sky polarization [10] over a range of frequencies spanning the radio (30 GHz) to the submillimetre (857 GHz) for CMB anisotropies. Although the AME in BICEP2 measurements at 150 GHz supported the presence of gravitational waves formed in the rapid expansion following the Big Bang, the AME may be more simply produced by cosmic dust in the Solar System. Subsequent extrapolation of 353 GHz Planck satellite data to 160 GHz showed the AME was caused by dust [11] and not remnants of gravitational waves. Only dust is considered in this paper.

Currently, the AME mechanisms [12 ] by which dust radiates at microwave frequencies are:

1. Vibrational electric dipole emission due to thermal fluctuations in the charge distribution in the grain,
2. Magnetic dipole emission due to thermal fluctuations in the magnetization of grain material, and
3. Rotational electric dipole emission due to the rotating electric dipole moment of a spinning grain.

In the ISM, the power radiated by dust is due to vibrational electric dipole emission, peaking in the far-infrared at 100 microns ~ 300 GHz, the low-frequency tail of which can be extrapolated to microwave frequencies, but falls far below the observed 10-60 GHz AME. However, if grains contain magnetic materials, e. g., magnetite or iron the thermal fluctuations in the magnetization will result in strong magnetic dipole emission.

Classically, the absorbed Ly$\alpha$ photon is dissipated by an increase in temperature, but is forbidden by QM. Hence, the above dust mechanisms depending on thermal fluctuations must be rejected by QM. In large NPs, absorbed Ly$\alpha$ photons may only be conserved by redshift; whereas, small NPs conserve Ly$\alpha$ photon energy by spinning. In this regard, the Ly$\alpha$ photon having Planck energy Eo and wavelength $\lambda$o is the common galaxy light that is redshifted to VIS and IR levels. Typically, redshift occurs in a NP having simple QED inducedPlanck energy E $<$ Eo. After NP emission of a redshifted galaxy photon, the excess energy (Eo –E) is conserved by removing electrons to create positive charges q+ within the dust because E $>$ ionization potentials as illustrated in Figure 11.

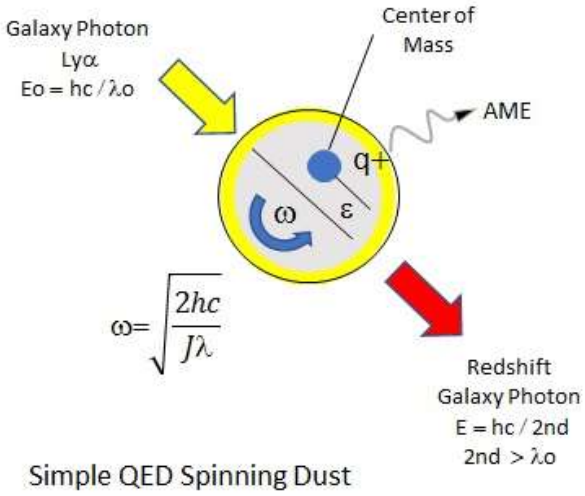


Figure 11. Simple QED Anomolous Microwave Emission

~~Since th~~e collision of the galaxy photon is likely to be offset ε from the center of mass of the dust, the Lyα momentum p = h/ λo produces a torque p·ε that spins the dust at rate ω, the consequence of which is the simple QED induced charge q+ produces microwave AME. Simple QED induced AME conserves the Lyα energy hc /λo with rotational energy ½ J $\omega^2$ of the NP giving the spin rate ω = √ (2 h c / J λo ), where, J the NP rotational moment of inertia, J = 2 m $a^2$ / 5 and m the NP mass. For amorphous silica having density 2650 kg / $m^3$, the spin rate ω over NP radii 0.001 < a < 0.04 microns corresponds to AME from 0.1 to 860 GHz as shown in Figure 12.

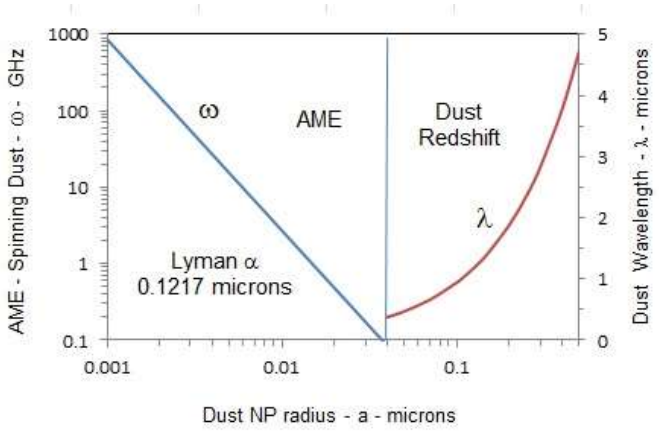


Figure 12. Cosmic Dust and Redshift

For large NPs having a > 0.04 microns, the Lyα photon produces redshift the emission wavelength λ from the VIS to the near IR. Smaller NPs having a < 0.04 microns produce AME. In Figure 12, the AME is based on E = 0 → (Eo – E) = Eo giving the upper bound AME rate.

**CONCLUSIONS**

The Big Bang and subsequent expansion of the Universe used to explain the 2.725 K black-body temperature of the CMBR never occurred. Instead, the 2.725 K is the consequence of the Sun as a black body heating our Solar System at distance comparable to the inner Oort Cloud boundary. The equilibrium 2.725 K temperature of the Oort boundary depends only on the size and temperature of the Sun and the distance from the Sun to the dust particles forming the Oort Cloud boundary dust particles, provided the particles are macroscopic and not nanoscopic.

Redshift of galaxies beyond the Oort Cloud are highly overstated on Earth by the dust in our Solar System. Although simple QED suggests dust absorption significantly redshifts emission lines from distant galaxies, any precise correction of galaxy velocities is difficult. Regardless, it can unequivocally be stated an expanding Universe based on redshift does not exist with Galaxy dynamics given by Newtonian mechanics.

Simple QED applied to the absorption of Lyα photons in dust NPs < 1 micron provides the basis for assessing CMBR anisotropy. Cosmic dust having radii $<$ 0.04 microns produce the AME while redshift occurs for NPs > 0.04 microns.

Current AME mechanisms that excite NP rotation by IR emission from thermal fluctuations cannot be valid by QM. Similarly, the UIR bands thought formed by increased temperatures of PAH molecules are also not valid.

Simple QED induced AME based on charge created upon absorption of Lyα photons exceeds the ionization potentials of most materials. Cosmic dust need not be magnetic to produce AME.

The AME is caused by dust – not as a relic of gravitational waves in an expanding Universe following the Big Bang. The CMB spectrum is produced by thermal blackbody radiation from the Solar System reaching an equilibrium temperature of 2.725 K at a distance comparable to the inner Oort Cloud boundary.

**References**

[1] Gamow G. (1948) The Origin of Elements and Separation of Galaxies, PRL, 74, 505-506.
[2] Penzias, A. A. and Wilson, R. W. (1965) A measurement of Excess Temperature at 4080 Mc/s, ASJ 142, 419-21.
[3] Dicke, R. H., et al (1965) Cosmic Black-Body Radiation, ASJ 142, 414-19
[4] Oort, J. (1950). The structure of the cloud of comets surrounding the Solar System and a hypothesis concerning its origin. Bulletin Astronomical Institutes Netherlands, 11, 91–110.
[5] Frejsel, A. M. (2015) Large Scale Anomalies of the Microwave Background with Planck, Niels Bohr Institute and Discovery Center, University of Copenhagen.
[6] Tran, L. (2019) https://solarsystem.nasa.gov/news/874/what-scientists-found-after-sifting-through-dust-in-the-solar-system/ NASA Goddard.
[7] Li, A. and Draine, B. T. (2001) Infrared Emission From Interstellar Dust. II. The Diffuse Interstellar Medium, AJ, 554, 778-802.
[8] Prevenslik, T. Simple QED by Quantum Mechanics. http://www.nanoqed.org, 2016-2019.
[9] Weingartner, J. C. and Draine, B. T. (2001) Dust Grain–Size Distributions and Extinction in the Milky Way, Large Magellanic Cloud, and Small Magellanic Cloud. The Astrophysical Journal, 548:296-309.
[10] Livio, M. and Kamionkowski, M. (2014) Bicep2's B Modes: Big Bank or dust? Physics Today, 8-10.
[11] Flauger, R., et al. (2019) Toward an Understanding of Foreground Emission in the Bicep2 Region. arxiv.org/pdf/1405.7351
[12] Draine, B. T. and Lazarian, A. (2001) Microwave Emission from Galactic Dust Grains

# Chapter 7

# Nanoparticle Physics and Molecular Dynamics

The high thermal conductivity of graphene and carbon nanotubes has received much attention in the heat dissipation of microelectronic devices. At the nanoscale, theories and methods based on classical physics like Molecular Dynamics and Finite Element Models analysis are no longer valid. Thermal conductivity and mechanical material properties can be modelled accurately on the nanoscale level.


7.1 Graphene: High Thermal Conductivity at the Nanoscale? . . . . . 172
7.2 Nanocomposites by Quantum Mechanics . . . . . 176
7.3 Molecular Dynamics by Quantum Mechanics . . . . . 181
7.4 Molecular Dynamics of Silver Nanowires Stiffened by QM . . . . . 187
7.5 Quantum Mechanics: Validity of Classical Molecular Dynamics . . . . . 192

# Graphene: High Thermal Conductivity at the Nanoscale?

**Abstract:** Over the last decade, the high thermal conductivity of graphene flakes and carbon nanotube (CNTs) at the nanoscale has received much attention in the heat dissipation of microelectronic devices. But Molecular Dynamics (MD) and Finite Element Models (FEM) analysis in support of high thermal conductivity based on classical physics are no longer valid at the nanoscale because the atoms in nanostructures are assumed to have temperature, when in fact the Planck law denies atoms at the nanoscale the heat capacity to conserve heat by an increase in temperature. Indeed, phonons dependent on temperature implicit in MD and FEM do not even exist at the nanoscale. In this regard, the simple QED method of nanoscale heat transfer based on the Planck law conserves heat by the emission of EM radiation instead of increases in temperature. Under steady laser heating at the center of a graphene flake, the in-plane thermal conductivity assumed proportional to the laser heat is highly overstated as soft X-ray emission normal to flake is not included as a significant heat loss. Similarly, most heat in CNTs is dissipated across the diameter making thermal conductivity based on heat transfer along the length also highly overstated. In contrast, the thermal conductivity of silicon nanowires (NWs) is not measured by assuming heat only flows along the NW length, but rather simply measures the temperature difference across the wire length, the consequence of which is the thermal conductivity of silicon at the nanoscale is not higher than bulk, but rather at least 100X lower than bulk consistent with simple QED.

***Keywords:*** Graphene flakes, carbon nanotubes, nanowires, thermal conductivity, Planck law, simple QED

## I. INTRODUCTION

Over the past decade, the discovery of graphene comprising a 2D layer of single atoms arranged in a honeycomb lattice has received considerable attention [1] as a promising material for future electronic circuits. Shortly thereafter, the promise of graphene attracted research [2] on the related thermal conductivity of 1D carbon nanotubes (CNTs) as interconnects in integrated circuits, both finding commonality in the nanoscale.

Later, the thermal conductivity of single atom 2D layers of graphene flakes [3] gained much interest as a non-contact method used was based on confocal micro-Raman spectroscopy as illustrated in Fig. 1.

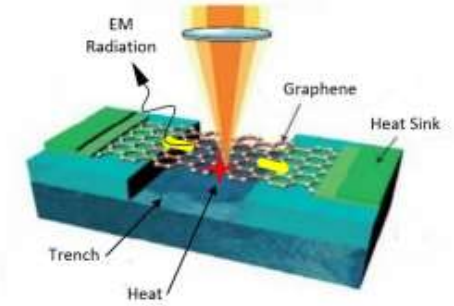


Figure 1. Thermal Conductivity Test

The Raman G peak temperature was used to monitor the temperature change produced by the variation of the laser excitation power focused on a graphene layer in Fig. 1. The graphene is suspended over a trench. Heat (red star) in the middle flows outward in-plane (yellow arrows) to heat sinks. The heat Q transferred to the heat sinks excludes the heat loss by EM emission (black arrows) from the graphene to the surroundings.

Since heat loss to contact with the trench edges is negligible, the graphene in-plane thermal conductivity K assumes all laser heat Q is transferred to the heat sinks giving,

$$K = (L/2S)\cdot(\Delta Q/\Delta T)$$

where L and S are the length and area of the suspended graphene, and $\Delta Q/\Delta T$ is the change in Q for a change in temperature. Here, S = wd with w and d the layer width and thickness. At room temperature, the single layer graphene was found to have K = 4800 to 5800 W/mK. Compared to bulk carbon having 2000 W/mK the nanoscale showed a significant increase.

The literature at that time generally showed carbon at the nanoscale had higher thermal conductivity than bulk carbon. Indeed, bulk crystalline diamond [4] gives K ~ 1000–2200 W/mK, multiwall CNTs [5] give 3000 W/mK, and K ~ 3500 W/mK for single-wall CNTs [2].

Theoretical estimates of CNT thermal conductivity mostly support [3] the experimental results, although some discrepancy exists. Molecular dynamics (MD) simulations [6] of diamond CNT give very high K ~ 6,600 W/mK by assuming the Tersoff potential for temperature dependence for a crystal at 300 K. The MD assumed cells across the diameter, but periodic boundary conditions along the length consistent with classical physics allow finite heat

capacity which is justified as the length L > a few microns, but is invalid through the thickness. Regardless, the MD results are consistent with reports that at 104 K, the thermal conductivity of diamond 410 W/cm K, or 41,000 W/mK which is the highest measured thermal conductivity [7] for a solid above liquid nitrogen temperature.

Experimental and theoretical estimates of thermal conductivity of graphene and carbon at the nanoscale were generally considered controlled by phonons. Today, the state of graphene [8] as of 2019 suggests the high thermal conductivity of graphene first reported [2,3] is still based on phonons guiding heat transfer at the nanoscale.

Indeed, the MD simulation and Abaqus finite element analysis [9] reported in [8] assume classical physics in the heat transfer of nano-thickness graphene flakes which also give far higher thermal conductivity than bulk consistent with work [2-7] a decade ago.

But there is a problem.

Well before the seminal findings [2,3] of high thermal conductivity of graphene and carbon at the nanoscale, silicon NWs were not found [10] to have enhanced thermal conductivity over bulk, but rather 100X less than bulk. Even today, the thermal conductivity of silicon NWs [11,12] is at least 2 orders of magnitude lower than bulk values. Theoretically, silicon should be no different than carbon materials at the nanoscale as both transfer heat by a ballistic process driven by infrequent phonon collisions compared to classical diffusive processes driven by frequent phonon collisions. Yet, nanoscale silicon is characterized by size dependence of the effective thermal conductivity (ETC) while carbon-based materials are not.

## II. PURPOSE

The purpose of this paper is to propose simple QED heat transfer [13] explains the stark differences between silicon and carbon-based materials at the nanoscale. Comparisons are made to experimental data and analytical predictions in the literature.

## II. THEORY

Simple QED is a nanoscale heat transfer process based on the Planck law [14] of quantum mechanics (QM) differing significantly from that of classical physics. Research in nanoscale heat transfer [15-17] has been reported. But despite advances, there are still challenges in understanding the mechanism of nanoscale thermal transport. Perhaps, researchers have not appreciated the significant difference between classical physics and the Planck law with regard to the heat capacity of the atom illustrated in Fig. 1.

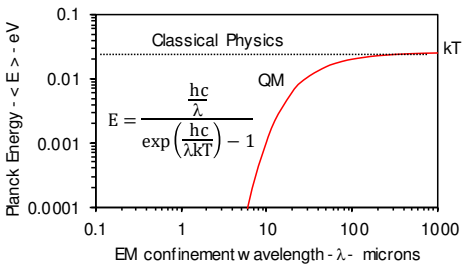


Figure. 1: Planck law of QM at 300 K
In the inset, E is Planck energy, h Planck's constant, c light speed, k Boltzmann's constant, T temperature, and λ the EM wavelength.

The Planck law at 300 K shows classical physics allows the atom to have constant kT heat capacity over all EM confinement wavelengths λ. QM differs as the heat capacity of the atom decreases for λ < 200 microns, and vanishes at the nanoscale for λ < 100 nm.

Indeed, simple QED by the Planck law denies atoms in nanostructures the heat capacity to increase in temperature upon the absorption of heat. QED stands for quantum electrodynamics, a complex theory based on *virtual* photons advanced by Feynman [18] and others. Simple QED is a far simpler theory that only requires the heat capacity of the atoms in nanostructures to vanish allowing conservation to proceed by the creation of *real* photons comprising EM waves that stand across the nanostructure.

Similar to atom quantum states of electrons in discrete orbitals, simple QED quantum states are dependent on the dimension of the nanostructure over which the EM waves stand. The Planck energy E of a photon standing across a distance d is given by the time τ for light to travel across and back, $\tau = 2d/(c/n)$, where n is the index of refraction of the nanostructure Hence, the Planck energy E of the simple QED photons is, $E \sim h/\tau$ and wavelength $\lambda = 2nd$,

$$E = \frac{hc}{2nd}$$

The laser heating Q of a nanoparticle (NP) of diameter d by a laser having wavelength $\lambda_o >> d$ immerses the NP in Q radiation to emit UV is illustrated in Fig. 2.

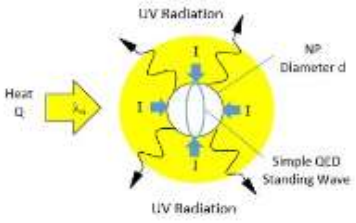


Figure 2. Laser Heating of a NP

The simple QED standing wave in the NP is shown under EM confinement by a Poynting vector of thermal momentum I (blue arrows) from the difference in temperature between the thermal surroundings at 300 K and the NP at 0 K. Absolute zero is justified as the Planck law denies the NP the heat capacity to change in temperature consistent with the constituent NP atoms absent thermal motion.

## IV. APPLICATION

The laser heated graphene flake [3] differs from the NP in that the heat Q focused at the center of the graphene layer flows in-plane and outward (red arrows) through the graphene to heat sinks as depicted in Fig. 3.

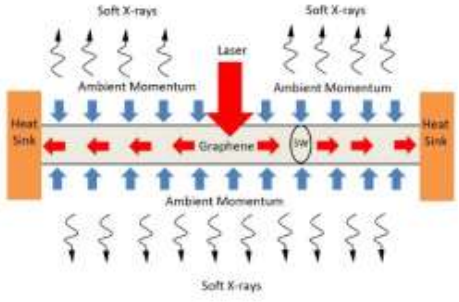


Figure 3. Laser heating of Graphene Flake

Along the graphene length, the heat flows by the Fourier law as EM confinement in the range of a few microns allows a classical treatment. However, the Planck law requires heat flow across the graphene thickness to be only EM radiation at soft X-ray levels. as illustrated shown in Fig. 3.

The EM standing waves (SW) noted across the graphene thickness are placed under EM confinement by the inward ambient thermal momentum (blue arrows) from the difference in temperature between the thermal surroundings at 300 K and the graphene which may be considered at 0 K.

The EM radiation at soft X-ray levels given by the Planck energy E of simple QED radiation, E = hc/2nd. Since the refractive index of graphite [19] from 50 - 1000 eV is n ~ 1, the single atom graphene thickness d = 0.337 nm gives wavelength 2nd = 0.674 nm and E = 1.8 keV which is near the short wavelength 3 keV limit of soft X-rays. The 1.8 keV fluoresces down to ~ 270 eV and excites the CK bands [20] of graphite as shown in Fig. 4.

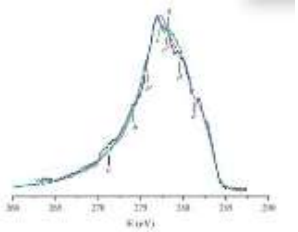

Figure 4. Soft X-ray emissions of carbons

Of importance is the significance of the soft X-ray emission in the enhancement of graphene thermal conductivity. Usually, simple QED only considers the minimum dimension of a nanostructure by Fermat's principle, the absorbed heat Q is dissipated in the least time which means in the direction of the shortest standing EM wave. By simple QED, the graphene flake has 3 quantum states characterized by EM waves standing across the thickness d, width w, and length L of the flake. The heat Q is dissipated by,

$$Q_d = hc/2nd$$
$$Q_w = hc/2nw$$
$$Q_L = hc/2nL$$

In the partitioning of heat Q in the flake, the ratio $Q_L/Q_d = d/L$ is of importance as the literature [2-7] assumes the heat loss $Q_d << Q_L$. In the experiment [3] shown in Fig. 1, the length L from the flake center to the trench edge is, L = 1.5 microns. For flake thicknesses d < 1 nm, d/L < 0.0005 which means little, if any, heat is conducted along the flake length. The heat Q is totally dissipated by soft X-ray emission.

Since flake lengths L of a few microns have finite heat capacity, the thermal conductivity along the length takes on bulk values K ~ 2000 W/mK. However, simple QED gives the ETC for the graphene flake, ETC = K(d/L) ~ 1 W/mK. Hence, reports [2-7] of nanoscale thermal conductivity from 4800 to 5800 W/mK are falsely overstated.

## V. CONCLUSIONS

The Planck law denies atoms in graphene layers the heat capacity to conserve heat across the thickness by an increase in temperature. Phonons depending on temperature do exist along the length of a few microns, but not through the < 1 nm graphene layer.

Simple QED based on the Planck law conserves heat Q across graphene layers by the emission of EM radiation at ~ 280 eV soft X-ray levels.

Assuming laser heat is conducted in-plane to the heat sinks is false as virtually all heat is loss by soft X-rays before ever reaching the sinks. MD and FEM programs ANSYS and ABAQUS based on classical physics are not valid at the nanoscale.

High thermal conductivity of graphene at the nanoscale does not exist as assuming all laser heat flows in-plane through the layer to heat sinks is invalid. In fact, the ETC of graphene layers vanishes in the same way as for silicon NWs.

The 100X lower thermal conductivity of silicon NWs at the nanoscale compared to bulk is determined experimentally by measuring the temperature difference across the wire length. Graphene experiments should do the same.

**REFERENCES**

[1] Novoselov K. C., et al. 2004. Electric Field Effect in Atomically Thin Carbon Films. Science 306:666-669.
[2] Pop E., et al. 2006. Thermal Conductance of an Individual Single-Wall Carbon Nanotube above Room Temperature. Nano Letters. 6:96-100.
[3] Balandin A. A., et al. 2008. Superior Thermal Conductivity of Single-Layer Graphene. Nano Letters. 8:902-907.
[4] Sukhadolou A. V., et al. 2005. Thermal conductivity of CVD diamond at elevated temperatures. Diamond Relat. Mater. 14:589:593.
[5] Kim. P., et al. 2001. Thermal transport measurements of individual multiwalled nanotubes. Phys. ReV. Lett. 87:215502.
[6] Berber S., et al. 2000. Unusually High Thermal Conductivity of Carbon Nanotubes. Phys. ReV. Lett., 84: 4613.
[7] Wei L., et al., 1993. Thermal Conductivity of Isotopically Modified Single Crystal Diamond. Phys. Rev. Lett., 70:3764-3767.
[8] Sang M., et al. 2019. Electronic and Thermal Properties of Graphene and Recent Advances in Graphene Based Electronics Applications. Nanomaterials. 9: 374-407.
[9] Bernal M. M., et al. 2018. Edge-Grafted Molecular Junctions between Graphene Nanoplatelets: Applied Chemistry to Enhance Heat Transfer in Nanomaterials. Adv. Funct. Mater. 28:1706954.
[10] Li D., et al., 2003. Thermal conductivity of individual silicon nanowires. App. Phys. Lett. 83: 2934- 2936.
[11] Calvo-Schwarzwälder M., et al. 2018. A slip-based model for the size-dependent effective thermal conductivity of nanowires. Intern. Commun. Heat and Mass Transfer. 91:57-63.
[12] Zhang Z., Chen J. 2018. Thermal conductivity of nanowires. Chin. Phys. B, 27: 035101.
[13] Prevenslik T. Simple QED Theory and Applications, nanoqed.org, 2015-2020.
[14] Planck M. [1900] On the Theory of the Energy Distribution Law of the Normal Spectrum, Verhandl. Dtsch. Phys. Ges., 2:2-37.
[15] Cahill D. G., et al. "Nanoscale thermal transport," Appl. Phys. vol. 93, pp. 93–818, 2003.
[16] Chen G., Nanoscale energy transport and conversion: parallel treatment of electrons, molecules, phonons, and photons, Oxford University Press, 2005.
[17] Cahill D. G, et al. "Nanoscale thermal transport. II. 2003–2012," Appl. Phys. Rev. vol. 1, pp. 011305, 2014.
[18] Feynman R., QED: The Strange Theory of Light and Matter, Princeton University Press, 1976.
[19] Jansing C., et al. 2018. Soft X-ray refractive index by reconciling total electron yield with specular reflection: experimental determination of the optical constants of graphite. J. Synchrotron Rad. 25, doi:10.1107/S1600577518010408
[20] Ilkiv B., et al. 2012. X-Ray Emission Spectra of Graphene Nanosheets. Journal of Nanoscience and Nanotechnology 12:8913-9.

# Nanocomposites by Quantum Mechanics

**Abstract** Nanocomposites with uniform dispersion of NPs offer significantly enhanced mechanical properties. NPs stand for nanoparticles. The composites comprise a large number of NPs in a mold of the desired final composite geometry. The NPs have a metal core encapsulated in a polymer shell. During thermal processing, the shells melt to form a composite that upon solidification form a nearly uniform NP spacing in a polymer matrix, the mechanical properties of which are enhanced as a consequence of QM. QM stands for quantum mechanics. In classical physics, the NP atoms have heat capacity allowing the atoms to increase in temperature during thermal processing. QM differs. By the Planck law, QM precludes the atoms in NPs from having the heat capacity to increase in temperature. Instead, conservation of heat during processing proceeds by QED inducing the NPs to create non-thermal EM radiation that charges the NPs by the photoelectric effect. QED stands for quantum electrodynamcis and EM for electromagnetic. The QED induced EM radiation wavelength is, $\lambda = 2\ nd$, where n and d are the refractive index and diameter of the NP. Coulomb repulsion between the charged NPs produces a triaxial stress state that increases the stiffness of the composite. MD simulations are presented to show that mechanical properties and specifically the Young's modulus of PP are significantly enhanced with a uniform dispersion of NPs. MD stands for molecular dynamics and PP for polypropylene. Absent uniform NP spacing, mechanical properties are not significantly enhanced.

**Introduction**

Avoiding agglomeration of NPs in a PP matrix is perhaps the central issue [1] in nanocomposites, yet even if avoided; it is unlikely the NP dispersion is uniform. The future of nanocomposites is therefore uncertain unless a process is developed that produces a matrix with a uniform NP dispersion.

In this regard, the process by which a matrix is fabricated with a uniform NP distribution is assumed to be eventually solved by material scientists. In this paper, a process is proposed that may appear difficult to implement, but necessary to proceed with MD simulations that show the Young's modulus of PP is significantly enhanced. The nanocomposite process envisions the production of a large number of preformed NPs placed in a mold of the desired composite geometry as illustrated in Figure 1.

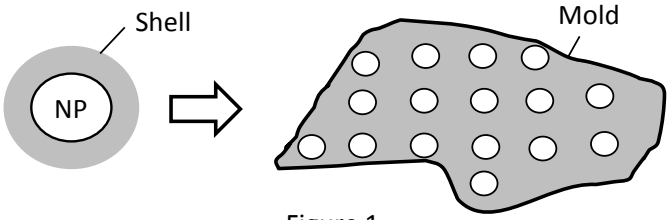


Figure 1
Nanocomposite Thermal Processing

The NPs are assumed to be Fe NPs in a PP shell. A very large quantity of NPs is required. The effort is akin to building a macroscopic object from the bottom–up assembly of atoms. For d = 80 nm Fe NPs in PP shell of thickness t = 210 nm, the NP spacing $\delta$ = d + 2t = 500 nm. The NPs are placed in a 3D mold of the desired final configuration as shown in Fig. 1. Thermal processing proceeds by slowly heating the mold to the PP melt temperature, but the mixture is not stirred. Hence, the PP shells melt to form a composite that after cooling forms a nearly uniform spacing of Fe NPs in a solid PP matrix. Experiments are required to determine how well the uniformity of NP spacing is preserved in thermal processing.

**Theory**

In a PP matrix of uniformly spaced Fe NPs, the mechanical properties are enhanced by the triaxial stress state induced by the Coulomb repulsion of charged NPs, the charging produced [2] as a consequence of QM. External charging is not required. In classical physics, the NP atoms have heat capacity allowing the atoms to increase in temperature during thermal processing. QM differs as shown in Figure 2.

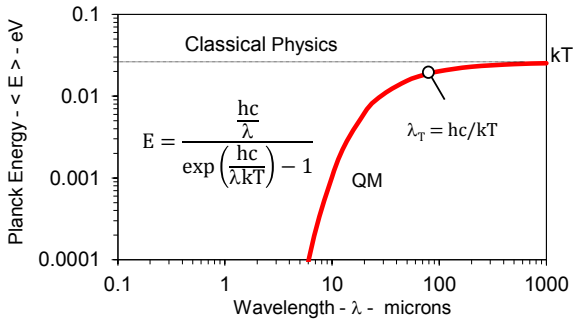


Figure 2. Planck law of the Atom at 300 K
E is Planck energy, h Planck's constant, c speed of light,
k Boltzmann's constant, T temperature, and $\lambda$ wavelength

By the Planck law at 300 K, QM precludes the atoms at EM confinement wavelengths $\lambda$ < 100 microns in NPs from having the heat capacity to increase in temperature. EM stands for electromagnetic. In NPs having EM confinement < 100 nm, the heat capacity vanishes, although is significantly reduced at $\lambda$ < 6 microns.

In thermal processing of NPs, conservation of heat during thermal processing proceeds by QED inducing [3] the NPs to create non-thermal EM radiation that charges the NPs by the photoelectric effect. Metal NPs including Fe are electron-rich and charge positive from ionizing QED radiation produced in the NPs. The QED induced EM radiation wavelength is, $\lambda$ = 2 nd, where n and d are the refractive index and diameter of the NP. Proper selection of NP properties assures NP ionization during thermal processing. QED induces ionizing EM radiation at 6.21 eV (200 nm) in Fe NPs having n = 1.5, giving the diameter d = 200 nm / 3 $\cong$ 70 nm.

Once the NPs are charged, the polymer should have a low dielectric constant $\kappa$ to maximize the Coulomb repulsion between other NPs in the matrix, e.g., PP and Teflon have $\kappa$ = 1.5 and 2, respectively. Moreover, after NP charging, the charge should not decay. In this regard, both PP and Teflon are electret fluoropolymers [4] are claimed to retain charges for a hundred years!

**MD Simulation**

The MD simulation of the tensile specimen having length L = 10,000 nm and cross-section width W = 2000 nm comprising 500 NPs is shown for a uniform spacing $\delta$ = 500 nm in Figure 3.

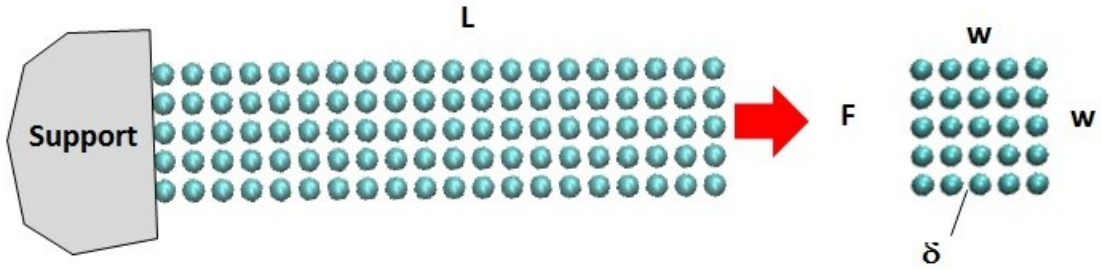


Figure 3
MD Model of only NPs in PP Composite Tensile Specimen

Of importance, the MD model only contains NPs. The PP atoms are not included. To maintain stability under the axial load F, the NPs were free to move in the UZ direction, but were constrained to zero UX and UY displacements in the plane of the cross-section. The UZ displacements at the support were specified to have zero displacement. The force F was imposed by specifying displacement $\Delta$ at the free end of the specimen, i.e., $F = (w^2E/L)\,\Delta$, where E is the Young's modulus of PP.

The Coulomb repulsive forces between all NPs alone induce the triaxial stress state that enhances mechanical properties. The Coulomb repulsion is long-range, and therefore all NPs are considered to interact with each other, i.e., no cut-off in force calculations is assumed. The Coulomb force $F_c$ is,

$$F_c = \frac{q^2}{4\pi\varepsilon_o\kappa\delta^2} \qquad (1)$$

where, q is the unit charge, $\varepsilon_o$ permittivity, and $\kappa$ the dielectric constant of PP.

The MD solutions were run at a time step of 5 fs. Convergence to Young's modulus E is rapid in 1000 iterations as shown for spacings 100, 120, 200, 300, and 500 nm in Figure 4. The inset shows simplified estimates the Young's modulus E is inversely proportional to the cube of the spacing between spacings of 100 and 120 nm. At 100 nm spacing, the PP modulus E = $27x10^6$ psi is found. Since the PP modulus = 20,000 psi, the enhancement is about 1000 times. Figure 5 shows at 500 and 1000 nm spacings are shown enhanced about 25 and 2 times, respectively.

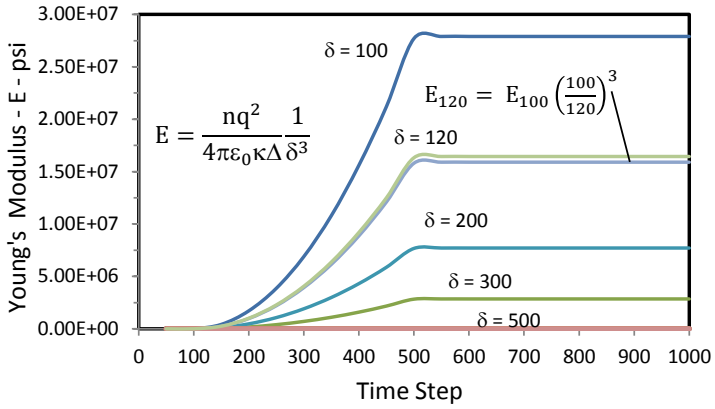


Figure 4
Enhanced Young's Modulus with NP Spacing < 500 nm

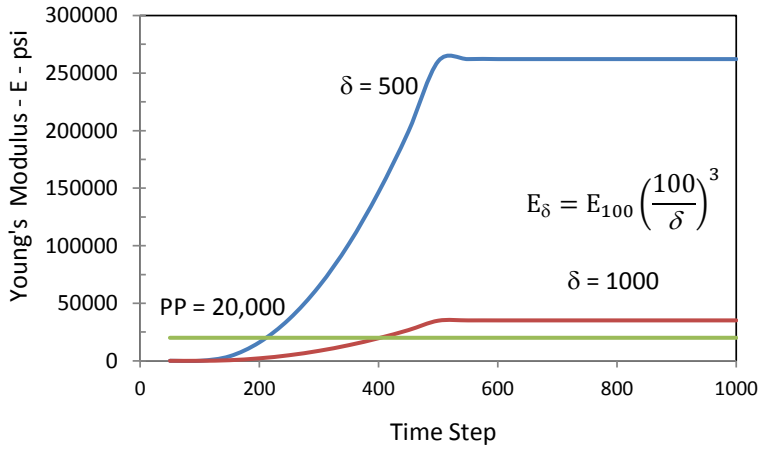


Figure 5
Enhanced PP modulus with NP Spacing < 1000 nm

**Discussion**

The significant stiffening of PP by uniform NP spacings from 100 to 1000 nm suggests the assumption of lateral constraint by specifying zero UX and UY displacement may be over restrictive. A way of assessing the constraint is to compare the magnitude of the Coulomb force $F_c$ to the lateral displacement $\Delta$ of the PP under the lateral F load as shown in Figure 6.

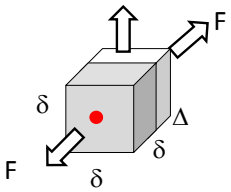


Figure 6

Lateral NP Displacement

The lateral force F is estimated by the Coulomb force Fc between a pair of NPs. For a spacing $\delta$ = 500 nm, Equation 1 gives Fc = 6.13x10 $^{-16}$ N. The lateral force F exerted on the NP depends on the elastic displacement $\Delta$ of the PP, i.e., F = $\delta E\Delta$. For $\delta$ = 500 nm and E = 130 MPa, F = 65$\Delta$. As an upper bound, taking F = Fc $\rightarrow$ $\Delta$ = 9 4x10$^{-18}$ m << $\delta$ = 500 nm. Hence, the PP restrains lateral motion of the NPs making the assumption of zero lateral NP displacements valid.

**Conclusions**

The MD simulations show triaxial stress state produced by QED induced Coulomb repulsion of charged FE NPs in a PP matrix is significant.

Other forms of charging the Fe NPs should be investigated. Indeed, the electret literature [4] suggests charging under electric fields may suffice. Regardless, the production of electret polymers with submicron uniform NP spacing may be difficult to achieve. Without uniform NP spacing, triaxial stress throughout the extent of the composite cannot be achieved making significant enhancement of mechanical properties unlikely.

**References**

[1] F. Mirjalili, L. Chuah, and E. Salahi, "Mechanical and Morphological Properties of Polypropylene/Nano $\alpha$-$Al_2O_3$ Composites," Scientific World Journal, Volume 2014, Article ID 718765.

[2] M. Planck, "On the Theory of the Energy Distribution Law of the Normal Spectrum," Verhandl. Dtsch. Phys. Ges., 2, 237, 1900.

[3] T. V. Prevenslik, Various QED Applications, See http://www.nanoqed.org , 2010-2016.

[4] B. Gross, *Charge storage in solid dielectrics; a bibliographical review on the electret and related effects*, New York, Elsevier Pub. Co., 1964.

# Molecular Dynamics by Quantum Mechanics

**Abstract**

Traditional MD simulations of chemical reactions with temperatures given by the equipartition theorem are problematic as atom temperatures are forbidden by the Planck law of quantum mechanics. MD proceeds without temperature with thermal effects simulated with the momentum of heat flow from IR lasers. MD simulations of RIXS experiments proceeds by specifying X-ray momentum.

## 1.0 Introduction

Traditionally, MD simulations of chemical reactions are thought [1] mediated through changes in the positions of the reactant atoms induced by temperature induced molecular vibrations based on the equipartition theorem. MD stands for molecular dynamics. MD assumes the temperature T of the atoms is given by the average kinetic energy <KE> of atoms in an ensemble by the equipartition theorem of statistical mechanics,

$$\mathrm{T} = 2 < \mathrm{KE} > /3\mathrm{N} \tag{1}$$

where, <KE> is the average kinetic energy of the atoms and N the number of atoms in the ensemble. MD simulates changes in atom positions in a continuum of chemical reactants by applying PBC to an ensemble of a small number of atoms in a computational box. PBC stands for periodic boundary conditions. Although the equipartition theorem and PBC are traditional in MD, there are questions as to the validity of the MD simulations.

One question is whether atoms in a continuum under PBC do indeed simulate the chemical reactions. The finite size of computation box [2] is likely to introduce interaction between molecules in the continuum of periodic images, especially if long range electrostatic forces are simulated. Moreover, the equipartition theorem is violated [3] in MD simulations with PBC if fluctuations are not allowed for the center of mass of the computation box. Regardless, chemical reactions occur locally between atoms of reactant molecules having nothing to do with the average temperature of atoms in the ensemble representative of the continuum. A more fundamental question is whether MD based PBC and the equipartition theorem can be extended to discrete molecules.

In applying MD to discrete molecules, PBCs are problematic. Indeed, the MD simulations of protein folding are commonly performed with PBC, even though folding is a discrete process unrelated to the continuum. Moreover, application of the equipartition theorem of classical physics to discrete molecules is precluded by the Planck law of QM that requires atoms have vanishing heat capacity, i.e., positional changes of atoms in discrete molecules therefore have nothing to do with temperature. QM stands for quantum mechanics. Figure 1 shows the Planck law at ambient 300 K temperature giving the heat capacity of the atom in terms of the wavelength $\lambda$ of EM confinement.

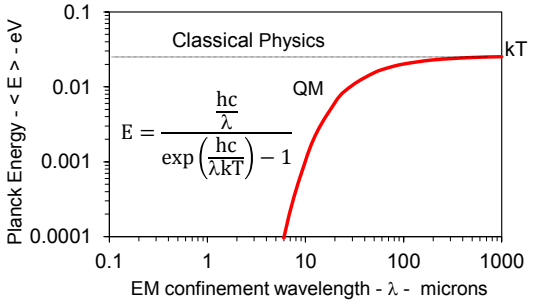


Figure 1. Planck law of QM at 300 K

Classical physics is depicted by a horizontal line allowing the atom to always have kT energy from the macroscale > 1000 microns to the nanoscale < 1 micron. QM differs by requiring the kT energy of the atom to decrease below 100 microns and vanish at the nanoscale < 1 micron. Hence, heat cannot be conserved in a molecule < 1 micron by an increase in temperature, thereby precluding the notion of relating the velocity of atoms in discrete molecules to their temperature. However, the equipartition theorem is valid in MD simulations of the continuum >100 microns under PBC as atoms have kT energy and do indeed change in temperature.

**2.0 Problem**

MD aside, the fact discrete molecules are precluded by QM from increasing in temperature while the equipartition theorem is not applicable to single molecules suggests molecules cannot vibrate, a false conclusion refuted by observation. Indeed, chemical reactions obviously do occur as atoms change position by molecular vibration. So the question is:

Why do molecules vibrate?

Indeed, the same question may be asked why MD finds basis in the equipartition theorem. There is no question temperature is somehow connected to molecular vibration, but a physical mechanism is required which cannot be the esoteric equipartition theorem.

**3.0 Background**

In RIXS, an external source of X-rays [4] positions the atoms in a molecule. But what about ordinary chemical reactions absent X-rays? Since QM precludes temperature changes, whether the heat Q from an ambient thermal bath can accumulate for electronic energy in core electrons to reach the K-edge level was considered [5] and found to take < 100 ps. But X-ray absorption in RIXS typically occurs in < 100 fs. Since a 1000 fold reduction in absorption times is unlikely, ordinary chemical reactions cannot be initiated by X-rays created from an ambient thermal bath,

What is the mechanism inducing the molecular vibrations
that positions atoms and yet be consistent with QM?

**4.0 Purpose**

The purpose of this paper is to present MD simulations of heat Q from IR lasers to show how traditional programs may be modified consistent with QM for discrete molecules without invoking the equipartition theorem. The nitrogen molecule in the stretch mode is used to show how directional heat flow Q from IR lasers can control ordinary chemical reactions

**5.0 Mechanism**

A molecular vibration is excited when the molecule absorbs a photon with a quantum n = 1 of energy E = hυ. When two quanta are absorbed the first overtone is excited, and so on to higher overtones. A transition from level n to level n+1 due to absorption of a photon, the frequency of the photon is equal to the classical vibration frequency. For the H·Cl molecule, the overtones may even lead to dissociation at $D_o$ as illustrated in Figure 2.

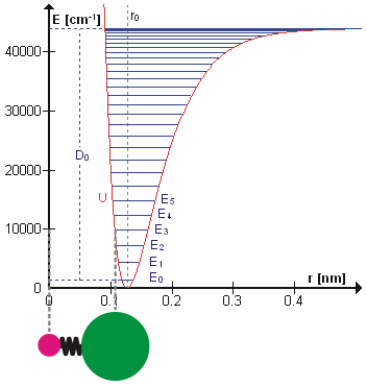


Figure 2. Vibration levels of the H·Cl molecule

However, excitation of molecule by photons differs with heat flow rate Q from a thermal bath. Photons must have precise frequencies to match the overtone levels, but atom temperatures from classical physics are continuous and not discrete. Because of the nanoscopic size of molecules, QM by the Planck law forbids the classical heat transfer as temperatures cannot change. Hence, the molecule directly converts heat flow Q into n quanta of E = hυ in the ground state,

$$Q\Delta t = n\, h\upsilon \tag{2}$$

where, Δt is the time of heat Q absorption, but must be sufficiently spontaneous. Following RIXS, say Δt < 100 fs.

Over time Δt, the heat flow Q under the EM confinement of the vibrational ground state hυ, that for nitrogen is in the IR. Overtones are not excited. Under the same EM confinement frequency υ of the vibrational ground state, the heat flow Q creates n identical IR photons, each having energy E = hυ exciting molecular vibration in the IR.

Similar QM arguments have been made [6] for the creation of UV, VIS, and IR photons from absorbed heat Q in nanostructures. Like vibration, the photons are created because QM forbids the conservation of heat Q by temperature. Instead, the high surface-to-volume ratio of nanostructures places interior atoms under high EM confinement as the heat Q is concentrated in their surfaces allowing photons to stand across the nanostructure. Once the photons are created, the EM confinement vanishes and the photons are absorbed by the material of the nanostructure or escape to the surroundings. The frequency $\upsilon$ of photons created is, $\upsilon = c/\lambda$, where $\lambda$ is the wavelength of the standing photon, $\lambda = 2\, n_r\, d$, and $n_r$ is the refractive index of the nanostructure.

**6.0 Analysis**

Similarly, MD by QM initiates chemical reactions by molecular vibration from the conversion of directional heat flow Q to the mode of the nitrogen molecule. The heat Q provided by a IR laser having frequency $\upsilon$ matched to the vibration frequency of the nitrogen molecule,

$$Q \sim n\left(\frac{hc}{\lambda}\right) / \left(\frac{\lambda}{c}\right) = \frac{Pc^2}{\lambda}\ J/s \tag{3}$$

where, P is the photon momentum, $P = n\, h/\lambda$, and n is the number of IR photons confined to the stretch quantum state. Heat flow Q directed along the bond direction of the nitrogen molecule to excite the stretch mode having frequency $\upsilon$ is shown in Figure 3.

Figure 3. Momentum of Heat Flow

However, the heat flow Q is restricted by the time $\tau$ to reach the quantum $E = h\upsilon$ by $\tau = n\, h\upsilon/Q$. Over time $\Delta t$, the momentum P is constant and force $F = P/\Delta t$. In the MD solution, the initial velocity V of the atom mass m is imposed in the first iteration, $V = F\Delta t/m = P/m$.

**7.0 Simulation**

Standard MD programs are modified for QM by updating the impulse force F at each iteration depending on the direction of momentum P, but temperature fluctuations are excluded consistent with QM. The implementation is simple as the directionality of momentum forces $\Delta F = P/\Delta t$ between a pair of atoms is already implicit in the L-J computation of forces, say in the leapfrog algorithm [1] prior to computing atom velocities. L-J stands for Lennard-Jones. Figure 4 depicts a 2D (x, y) model of a molecule driven by forces F from momentum P of an IR or X-ray source.

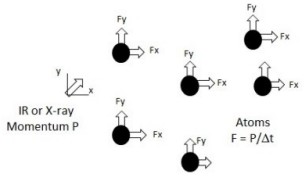


Figure 4 2D Model for Impulse Forces

The MD of the nitrogen molecule in the stretch mode is simulated with a half-model by fixing the central anti-node of the molecule shown in Figure 5.

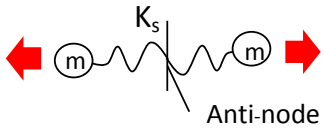


Figure 5 Model of Nitrogen Molecule

The nitrogen stretch mode is modelled by a bead-spring force $F = K_s(x - d/2)$, where d is the bond length. Spring stiffness $K_s$ is selected to simulate experimental nitrogen resonance in the IR at 2330 /cm ~ $7x10^{13}$ Hz.

The MD solutions for the nitrogen molecule in the stretch mode for the heat flux Q of 320 mW comprising $10^5$ IR photons having frequency $\upsilon = 7x10^{13}$ Hz matched to the stretch mode of the nitrogen molecule. The integration time step $\Delta t = 1 \times 10^{-17}$ s. The MD response for the amplitude X and velocity V of the nitrogen atom are shown in Figure 5.

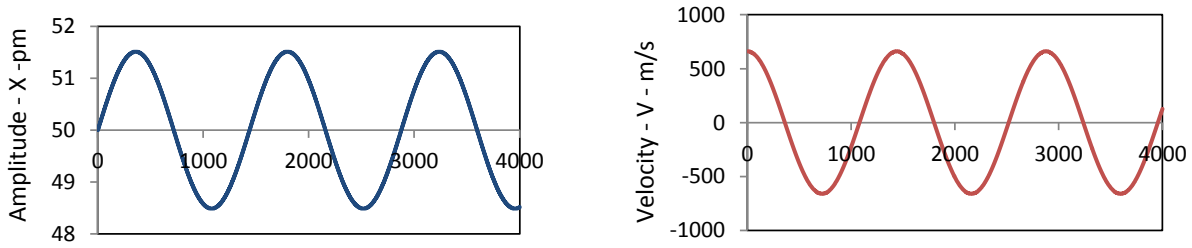


Figure 5 Amplitude and velocity of the Nitrogen atom
under 320 mW IR laser excitation at $7x10^{13}$ Hz

In the first iteration, the Q = 320 mW IR laser supplies the nitrogen atom with $n = 10^5$ IR photons in time $\tau = n h\upsilon/Q = 14.5$ fs. What this means is the nitrogen molecule stretch mode is filled with photons as Bosons in time $\tau < 100$ fs that is sufficiently spontaneous to justify the superposition of quantum states. Moreover, the momentum P provided by $10^5$ IR photons is actually 2 orders greater than that from a single 434 eV ray photon having wavelength $\lambda = 2.86$ nm. But unlike IR lasers, synchrotron X-ray radiation is not always available for the common chemical reaction.

Regardless, a continuously variable IR laser capable of being tuned to the frequency of stretch and bending vibration modes of typical molecules is required, but is not available. However, if developed may lead to IR control of chemical reactions. In this regard, study is now underway.

**8. Conclusions**

The path toward a theory for MD by QM holds the promise of improving the IR or X-ray control of chemical reactions. This paper has taken a step in that path by demonstrating agreement between atomistic MD simulations of the stretch mode of molecular nitrogen. A summary of the findings is as follows.

MD by QM supersedes traditional MD simulations of RIXS experiments under synchrotron radiation by avoiding the erroneous temperature changes in X-ray heating predicted by the equipartition theorem of classical physics.

Ordinary chemical reactions absent X-rays may be initiated by the QM induced conversion of directional heat flux Q from common strip heaters in thermal baths. But heat Q from continuously variable IR lasers is preferred as the IR frequency can be tuned to the specific stretch or bending modes of reactant molecules as in RIXS with X-rays. Indeed, the momentum $P = n\ h/\lambda$ from only $n \sim 10^3$ IR photons is comparable to a single X-ray photon having wavelength $\lambda = 3$ nm. Hence, IR lasers and not X-rays from synchrotrons are suggested for the practical control of chemical reactions.

In MD simulations of X-rays in controlled synchrotron experiments, implementation of QM by the Planck law is straightforward because the traditional leapfrog algorithm that updates the L-J forces every iteration depending on the directionality between a pair of atoms may readily include the impulse forces from IR or X-ray sources.

Heat flow Q from the momentum of IR or X-ray lasers for the nitrogen stretch mode is not significant to change bond lengths because of the high stiffness suggesting the bending modes having greater flexibility in combination with L-J forces actually mediate chemical reactions.

**References**

[1] Allen, M.P. and Tildesley, D. J., *Computer Simulation of Liquids*, Oxford University Press, 1987.

[2] Hou, C., Xu, J., Ge, W., Li, J. "Molecular dynamics simulation overcoming the finite size effects of thermal conductivity of bulk silicon and silicon nanowires," Modeling Simulation Mat. Scie. Eng., **24**, 2016.

[3] Siboni, N. H., Raabe, D., Varnik, F.," Maintaining the equipartition theorem in small heterogeneous molecular dynamics ensembles," Phys. Rev. E **87**, 030101(R), 2013.

[4] Couto, R. C. et al., "Selective gating to vibrational modes through resonant X-ray scattering," Nature Comm., **8**, 14165, 2017

[5] Prevenslik, T., "Molecular Dynamics by X-rays," 2nd Global Conference Applied Computing Science and Engineering (ACSE2), Canary Islands, 26-28 July, 2017

[6] Prevenslik, T. See diverse QM applications at http://www.nanoqed.org, 2010-2017

# Molecular Dynamics of Silver Nanowires Stiffened by Quantum Mechanics

***Abstract*—Over the past decade, the observation of significant stiffening of nanowires or NW's has been reported, although some findings suggest there is no stiffening. Because of this uncertainty, research on the mechanism for stiffening has been a subject of great interest. Numerous mechanisms have been proposed that depend on high surface-to-volume ratio of NW's including surface stress and strain – all of which rely on classical physics. However, classical physics in the interpretation of nanoscale behaviour typically leads to unphysical results that are avoided by quantum mechanics. In NW's, quantum mechanics precludes the atoms in NW's from having the heat capacity to conserve the absorption of thermal energy from macroscopic supports by an increase in temperature. Instead, absorbed energy is conserved by frequency up-conversion to the total internal reflection resonance of the NW by quantum electrodynamics, the consequence of which is the production of photons that create charge by the photoelectric effect. Molecular dynamics simulations show the stiffening of NW's is caused by the charge repulsion between atoms creating a state of hydrostatic tension that changes the usual uniaxial stress to a triaxial stress state that by the Poisson effect enhances the Young's modulus consistent with elasticity theory.**

## I. Introduction

OVER the past decade, the observation of significant stiffening of NW's has been reported, although some findings suggest there is no stiffening. Because of this uncertainty, research on the mechanism for stiffening has been a subject of great interest. Numerous mechanisms [1] have been proposed including: high surface-to-volume ratio, surface stresses, bulk nonlinear elasticity, surface stiffness, surface tension, surface reconstruction, surface strain and stress, and skin depth energy pinning.

Generally, the stiffening of NW's is not based on direct measurements of material properties, but rather inferred from indirect measurements of increased resistance to buckling, enhanced resonant frequencies, and the like. In contrast, the traditional uniaxial tensile test of a NW gives mechanical properties directly, but is difficult to perform because of the nanoscopic size of the tensile specimen. Nevertheless, Young's modulus and yield stress of fivefold twinned silver NW's was recently [2] measured in tensile tests and found to show stiffening consistent with indirect measurements, the stiffening mechanism thought to be the high surface-to-volume ratio in combination with the annihilation of dislocations at free surfaces and enhanced strain hardening from fivefold twinning. The stiffening mechanisms proposed to date find basis in classical physics [3] contrary to the fact stiffening is not observed at the macroscale, but rather a QM effect only observed in < 100 nm diameter NW's. QM stands for quantum mechanics. Unlike classical physics, only QM having a size effect may explain stiffening of NW's.

Manuscript received September 10, 2012.

In this paper, the QM requirement is invoked that the heat capacity of the atom vanishes at the nanoscale thereby precluding the conservation of thermal energy from macroscopic supports by an increase in temperature, say from the grips in uniaxial tensile tests of NW's. Instead, the absorbed thermal energy is conserved by the creation of photons *inside* the NW by frequency up-conversion to its TIR resonance. QED stands for quantum electrodynamics and TIR for total internal reflection.

## II. Theory

### A. QM Restrictions

Unlike classical physics, QM restricts the heat capacity of nanostructures through the thermal $kT$ energy of the atom thereby precluding conservation of any form of EM energy by an increase in temperature. EM stands for electromagnetic. A comparison of the $kT$ energy of the atom by classical physics and QM by the Einstein-Hopf relation [4] is shown in Fig. 1.

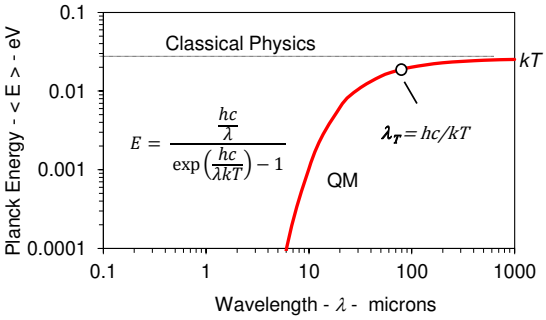


Fig. 1 Heat Capacity of the Atom at 300K
$E$ is Planck energy, $h$ Planck's constant, $c$ speed of light
$k$ Boltzmann's constant, $T$ absolute temperature, and $\lambda$ wavelength

Classical physics allows the atom to have the same $kT$ energy in submicron nanostructures as in macroscopic bodies. QM differs in that $kT$ energy is only available for $\lambda > \lambda_T$ and otherwise is < $kT$. At ambient temperature, $\lambda_T \sim 40$ microns. Fig. 1 shows the thermal energy or heat capacity of the atom is < $kT$ for $\lambda < 40$ microns. By QM, atoms under

EM confnement wavelengths $\lambda$ < 1 micron have virtually no heat capacity to conserve energy from any EM source by an increase in temperature.

### B. TIR Confinement

Lack of heat capacity by QM precludes heat absorbed from EM sources to be conserved in nanostructures by an increase in temperature. The EM energy is proposed conserved by the creation of non-thermal EM radiation by the QED induced frequency up-conversion to the TIR resonance of the nanostructure.

In 1870, Tyndall showed light is trapped by TIR in the surface of a body if the refractive index of the body is greater than that of the surroundings. TIR has an important significance in nanostructures and need not be limited to light absorption. Unlike macroscopic bodies, nanostructures have high surface to volume ratios, and therefore EM energy from any source (lasers, mechanical and Joule heat, electron beam irradiation) is absorbed almost entirely in their surface. Since the nanostructure surface coincides with the TIR wave function, QED induces the absorbed EM energy to undergo spontaneous conversion to surface QED photons However, TIR confinement sustains itself only during EM energy absorption, i.e., absent absorption of EM energy, there is no TIR confinement and QED radiation is not created.

QED relies on complex mathematics as described by Feynman [5] although the underlying physics is simple, i.e., photons of wavelength $\lambda$ are created by supplying EM energy to a submicron QM box with sides separated by $\lambda/2$. In this way, QED frequency up-converts absorbed EM energy to the TIR resonance described by the characteristic dimension $D_C$ of the nanostructure. The QED photon energy $E$ and frequency $\upsilon$ are:

$$E = h\upsilon, \quad \upsilon = \frac{c}{\lambda}, \quad \lambda = 2nD_c \tag{1}$$

where, $n$ is the refractive index of the nanostructure.

### C. QED Induced Hydrostatic Tension

In NW's, the prompt conversion of thermal heat from the supports to QED photons at the speed of light is far faster than the phonons at acoustic velocities can respond, thereby essentially negating thermal conduction by phonons. Under TIR confinement across the wire diameter, the QED photons *inside* the wire have Planck energies beyond the ultraviolet (UV). By the photoelectric effect, the QED photons promptly eject electrons to the surroundings leaving positive charge that by electrostatic repulsion produces a stress state of hydrostatic tension.

### D. Triaxial Stress State

Unlike the uniaxial stress state in macroscopic tensile specimens, NW's under tension are under a triaxial stress state. Taking the x-y directions in the plane of the wire cross-section and the z direction along its length, the hydrostatic pressure $P$ in terms of stresses $\sigma_x$, $\sigma_y$, and $\sigma_z$,

$$P = \frac{\sigma_x + \sigma_y + \sigma_z}{3} \tag{2}$$

In hydrostatic tension, $\sigma_x = \sigma_y = \sigma_z = P$.

### E. QED Induced Pressure

The QED induced pressure $P$ produced in the tensile specimen from thermal $kT$ energy acquired from the grips is obtained by computing the electrostatic repulsion from positive charges produced by the photoelectric effect. However, the pressure $P$ may be upper bound by assuming all the atoms in the NW acquire $kT$ energy at the support temperature $T$. Provided the QED photon energy $E$ > 5 eV, the QM pressure is,

$$P_{QM} = \frac{NkT}{V} = \frac{kT}{\Delta^3} \tag{3}$$

where, $N$ is the number of atoms in the volume $V$ of the NW, i.e., $V/N = \Delta^3$ and $\Delta$ is the atomic spacing. . For the silver with $\Delta = 0.409$ nm with grips at $T = 300$ K, $P_{QM} < 6.05 \times 10^7$ Pa ~ 8770 psi.

Other forms of absorbed EM energy also stiffen the NW, e.g., mechanical heat from hysteresis in loading and unloading the tensile specimen.

### F. Enhanced Young's Modulus and Yield Strength

In tensile tests of NW's, elasticity theory for the triaxial stress state gives the strain $e_z$ along the wire length,

$$e_z = \frac{1}{Y_o}\left[\sigma_z - \nu\left(\sigma_x + \sigma_y\right)\right] \tag{4}$$

where, $\nu$ is Poisson's ratio and $Y_O$ the bulk Young's modulus in the uniaxial stress state.

$$\begin{aligned} \sigma_x' &= \sigma_x + P \\ \sigma_y' &= \sigma_y + P \\ \sigma_z' &= \sigma_z + P \end{aligned} \tag{5}$$

where, σ' includes the pressure stress. Hence, the Young's modulus $Y$ in the triaxial stress state is,

$$Y = \frac{\sigma}{e_z} = \frac{Y_O}{1 - \nu\left(\sigma_x' + \sigma_y'\right)/\sigma_z'}$$

Or,

$$\frac{Y}{Y_O} = \frac{1}{1 - \nu\left(\sigma_x + \sigma_y + 2P\right)/(\sigma_z + P)} \tag{6}$$

For $\sigma_x + \sigma_y < 2P$ and $\sigma_z > P$, the QED enhancement $Y/Y_O$ ratio for Poisson's ratio of silver $\nu = 0.37$ and the incompressible limit is shown in Fig. 2.

Taking the yield of silver $\sigma_z = 6550$ psi and the QM pressure P= 8770 psi, $P / \sigma_z = 1.33$ and $Y/Y_O \sim 63$. But this is only a simplification to describe the basic physics of stiffening in NW's. By the Poisson effect, the $\sigma_x$ and $\sigma_y$ stresses reduce the $e_z$ strain from that of the uniaxial stress state, thereby increasing the Young's modulus. Detailed stresses are derived in the molecular dynamics (MD) simulations. Regardless, the enhancement of Young's modulus is significant. The silver yield strength is enhanced the same as that for Young's modulus.

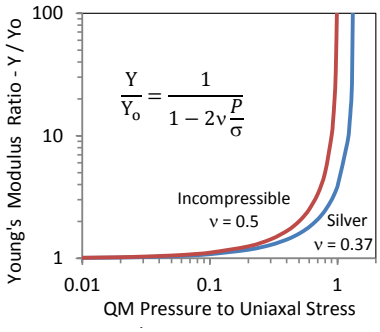


Fig. 2 QED Enhancement of Young's Modulus

## III. Simulation

Standard MD computer programs based on statistical mechanics that implicitly assume the atoms have heat capacity could not be used to derive the Young's modulus of silver NW's. Because of this, the Leapfrog algorithm [6] was modified to accommodate the QM restrictions that require the atom's heat capacity to vanish.

### A. NW Model

The NW model geometry selected was a square cross\-section having sides w and length L as illustrated in the VMD graphics in Fig. 3. The silver wire was modeled in the FCC configuration with an atomic spacing of 4.09 A comprising 550 atoms having sides w = 8.18 A and length L = 87.9 A.

Fig. 3 MD Model of NW under Longitudinal Loading

### B. Lennard-Jones Potential

The L-J potential [7] was used to simulate the atomic potential U of the silver NW.

$$U_{ij} = 4\varepsilon\left[\left(\frac{\sigma}{R_{ij}}\right)^{12} - \left(\frac{\sigma}{R_{ij}}\right)^{6}\right] \tag{7}$$

where, $R_{ij}$ the interatomic spacing and for silver σ = 2.644 A and ε = 0.345 eV.

### C. Electrostatic Repulsion

The QM pressure is caused by the electrostatic repulsion of atoms from charges created by the QED induced photoelectric effect. The electrostatic potential $U_{ES}$, for the atom as a sphere of radius $R_{atom}$ having electron charge e,

$$U_{ES} = \frac{3e^2}{20\pi\varepsilon_o R_{atom}} \tag{8}$$

where, $\varepsilon_o$ is the permittivity of the vacuum.

### D. Thermal kT Energy

In the NW, the thermal kT energy $U_{kT}$ of the atom depends on the temperature $T_{grip\ of}$ the grips,

$$U_{kT} = \frac{3}{2}kT_{grip} \tag{8}$$

### E. Stress Calculation

The MD response gives pressure within the specimen and not the stresses. In the controversy [8] as to whether the virial stress gives the Cauchy stress, the virial stress in terms of the dimensionality n of the constraints is::

$$\sigma_{ij}^{V} = \frac{1}{V}\sum_{\alpha}\left[\sum_{\beta=1}^{N}\left(R_i^{\alpha} - R_i^{\beta}\right)F_j^{\alpha\beta} - nkT\right] \tag{9}$$

where, β takes values 1 to N neighbors of atom α, $R_i^{\beta}$ is the position of atom β along direction i, $F_j^{\alpha\beta}$ is the force (along direction j) on atom α due to atom β, and *V* is the volume.

However, the controversy over virial and Cauchy stress may be irrelevant at the nanoscale as by QM the thermal kT energy of the atom vanishes. Hence, the virial stress $\sigma_{xx}$ is,

$$\sigma_x^{V} = \frac{1}{V}\sum_{\alpha}\sum_{\beta=1}^{N}\left(R_x^{\alpha} - R_x^{\beta}\right)F_x^{\alpha\beta} \tag{10}$$

with the $\sigma_y$ and $\sigma_z$ stress is similarly defined.

### F. MD Pressure

The MD pressure P within the NW model [6] during equilibration and loading is,

$$P = P_{QM} + \left(NkT + \frac{1}{3}\sum_{\alpha}\sum_{\alpha>\beta} r\frac{dU}{dr}\right)/V \tag{11}$$

### G. Equilibration and Loading

1. Equilibration During equilibration, the NW was fixed at the left end and free at the right end. At the fixed end, only the z-coordinates of the atoms on were fixed; the x and y atom positions were free to move. With the atoms in the plane of the left end corresponding to the origin of the xyz system, the free end is located at z = L

Consistent with the QM requirement that the atoms have vanishing heat capacity, the absolute temperature was held at < 0.1 K by the Nose-Hoover thermostat. During equilibration, the QM pressure $P_{QM}$ is not used.

2. Loading The NW was displacement loaded by a step change δ in the z-direction at z = L. The force $F = AY_O\,\delta / L$ where the axial stress σ = F/A and strain ε = δ / L.

The QM pressure $P_{QM}$ tending to separate the atoms is simulated by defining the fraction η of the electrostatic $U_{ES}$ energy corresponding to the thermal kT energy of the atom.

$$\eta = \frac{U_{kT}}{U_{ES}} = \frac{10\pi\varepsilon_o k R_{atom} T_{grip}}{e^2} \tag{12}$$

Taking $T_{grip}$ = 300 K for the silver atom having $R_{atom}$ = 1.45 A, e = $1.6\times10^{-19}$ C, the fraction η = 0.0065. During the MD solution, the Nose-Hoover thermostat maintained the temperature T < 0.01 K.

*H. Response*

The MD response was obtained for uniaxial and triaxial stress states at time steps from 1-5 fs.

1. Uniaxial In the uniaxial response, the QM pressure induced electrostatic repulsion was excluded. Equilibration for 5000 steps was followed by displacement loading to 10000 steps. For $\delta$ = 0.5 A, the displacement loading is shown in Fig. 4.

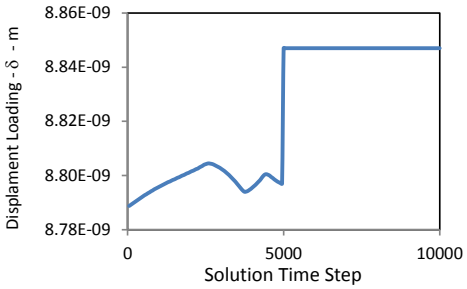


Fig. 4 Displacement Loading

Before the displacement load, the $\sigma_x$, $\sigma_y$, and $\sigma_z$ stresses < 100 psi. Upon displacement $\delta$ loading, the stresses increased and at convergence, the $\sigma_x$ and $\sigma_y$ stresses vanished leaving only the $\sigma_z$ stress. The $\sigma_x$ and $\sigma_y$ stresses were identical as shown for $\delta$ = 0.5 A in Fig. 5.

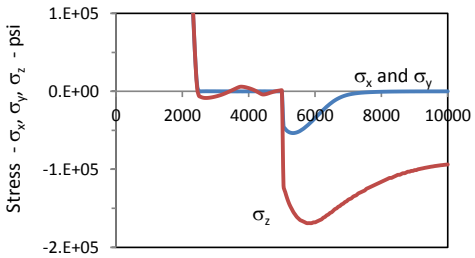


Fig. 5 Uniaxial Stress State

Upon convergence at 10000 steps, the displacement loading $\delta$ = 0.15, 0.25, and 0.5 A was found to be approximately linear giving Young's moduli $Y_o \sim 16x10^6$ psi as shown in Fig. 6.

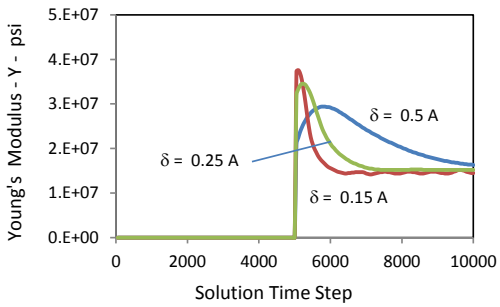


Fig. 6 Uniaxial Young's Modulus

2. Triaxial The triaxial response included the QM pressure through the electrostatic repulsion. For full kT energy corresponding to $\eta$ = 0.0065, the MD solution for displacement $\delta$ = 0.5 A consisted of equilibration for 5000 steps followed by loading for an additional 5000 steps as shown in Fig. 7. Unlike uniaxial stress, the $\sigma_x$ and $\sigma_y$ stresses did not vanish after equilibration and loading. It is of note, that attempts to use a constant QM pressure alone instead of electrostatic repulsion failed as the $\sigma_x$ and $\sigma_y$ stresses vanished as for the uniaxial stress state.

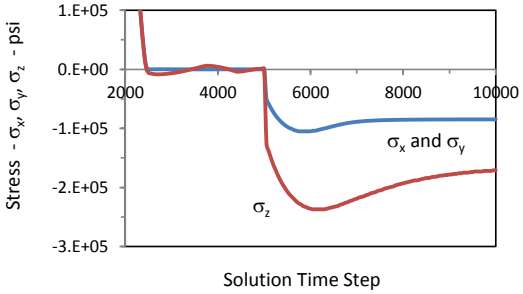


Fig. 7 Triaxial Stress State - Stresses

The Young's modulus Y and Poisson's ratio $\nu$ for displacement loading $\delta$ = 0.5 A at fractions $\eta$ = 0.0065, 0.003 and 0.001 are shown in Fig. 8 and 9.

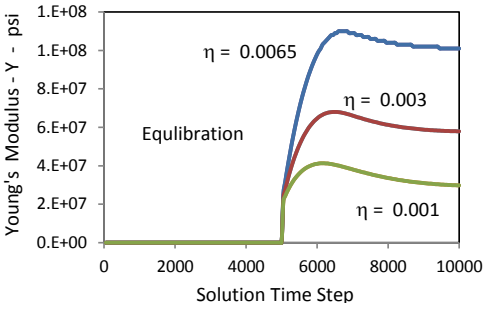


Fig. 8 Triaxial Stress State – Young's Modulus

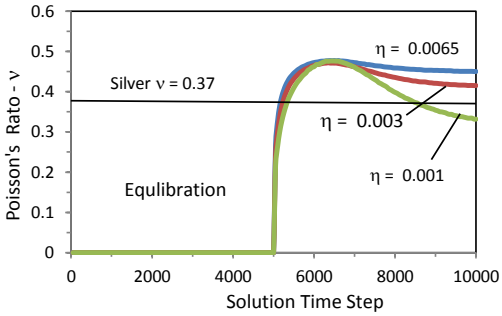


Fig. 9 Triaxial Stress State – Poisson's Ratio

## IV. DISCUSSION

### A. MD Solution and Comparison to Data

Simulating the QM pressure with the fraction η of the kT energy by electrostatic repulsion produces the solutions shown in Fig. 8. After convergence at 10000 steps, full kT energy corresponding to $\eta = 0.0065$ gives Young's modulus $Y = 100 \times 10^6$ psi; while $\eta = 0.003$ and 0.001 give $Y = 60$ and $30 \times 10^6$ psi, respectively. The correct Young's modulus is determined from the Poisson/s ratio of silver $\nu = 0.37$. Interpolation gives the $\eta = 0.002$ solution is close to that for silver as shown in Fig. 9. Hence, the Young's modulus of the NW is about $45 \times 10^6$ psi. With the uniaxial Young's modulus Yo ~ $16 \times 10^6$ psi, the stiffening enhancement is Y/Yo ~ 3. The MD solution for $\eta = 0.002$ of silver NW's means only 2/6.5 or about 30 % of the full kT energy stiffens the NW, the remaining kT energy lost to the surroundings as QED radiation.

Experimental data ( Table I of [2] ) on 34 nm diameter silver NW's show Young's moduli of $Y = 26 \times 10^6$ psi. In contrast, the MD solution for the smaller 8 A square silver NW gave $Y = 45 \times 10^6$ psi, although the MD solution appears reasonable at about 2x that for the 34 nm NW.

### B. EM Energy Sources and Stiffening

Only the kT energy of the grips was considered as the heat source, but any EM energy absorbed by the NW also produces the stiffening effect. In this regard, the strain hardening ( Fig. 2(a) of [2] ) under a sequence of loading and unloading to raise the ultimate tensile strength (UTS) to about 300,000 psi, or about 45x that of the yield of bulk silver at 6550 psi. The strain hardening is explained by dislocation-induced shear, but the dislocations produce mechanical heat that like the thermal kT energy of the grips cannot be conserved by an increase in temperature. Instead, it is more likely conservation of dislocation induced mechanical heating proceeds by QED induced triaxial stress states that enhance the UTS by strain hardening as depicted for the Young's modulus Y in Fig. 2.

Passing current through NM's is a source of Joule heat that again is induced by QED to enhance the Young's modulus. Indeed, electron beam irradiation is shown [9] to enhance the Young's modulus of tin oxide NW's by 40%.

### C. Shape of Fracture Surface

In the tensile tests of silver NW, the fracture surface is unusual. Unlike macroscopic tensile specimens, the NW specimen showed no diameter reduction or necking prior to failure as shown in Fig. 10.

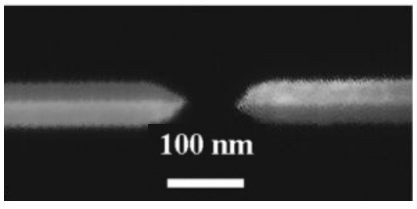


Fig. 10 Fracture Surface of Silver Nanowire

Dislocation-induced shear is thought [2] to explain the localized fracture surface. However, it is more likely the shape fracture surface is caused by the removal of silver atoms by Coulomb explosion from QED induced charge repulsion during strain hardening. Verification of Coulomb explosion of NW's by searching the SEM chamber for silver atoms or monitoring their emission during tensile testing is suggested. MD simulations of Coulomb explosions in NW's under tensile testing are planned.

## V, CONCLUSIONS

Classical physics assumes the atom always has heat capacity. QM differs by restricting the atom's heat capacity to vanishing small levels in nanostructures. Conserving absorbed EM energy by the QED induced creation of photons in the nanostructure surface avoids unphysical findings and heat transfer anomalies.

In tensile tests of silver NW's, the QED photons are created by EM energy from the temperature of the grips that hold the NW in combination with the heat associated with strain hardening. The QED photons charge the silver atoms by the photoelectric effect to induce electrostatic repulsion placing the NW under high hydrostatic tension. The Young's modulus of NW's is enhanced above bulk because the hydrostatic tension pressure reduces the longitudinal strain by the Poisson effect of classical elasticity.

MD solutions of 8 A square NW show the QED induced charge repulsion of silver atoms give Young's moduli of $45 \times 10^6$ psi comparable to data of for the 34 nm NW. MD solutions are computationally intensive and require computing power beyond the PC, especially for the larger 34 nm diameter NW's.

The QED induced stiffening of NW's in tensile tests occurs anytime EM energy is absorbed including thermal energy from grips, mechanical heat from repeated loading and unloading, and electron beam irradiation.

## REFERENCES

[1] X. J. Lu, J. W. Li, Z. F. Zhou, L. W. Yang, Z. S. Ma, G. F. Xie, Y. Pan, and C. Q. Sun, "Size-induced elastic stiffening of ZnO nanostructures: Skin-depth energy pinning," *App. Phys. Lett.*, vol. 94, 131902, 2009.

[2] Y. Zhu, Q. Qin, F. Xu, F. Fan, Y. Ding, T. Zhang, B. J. Wiley, and Z. L. Wang., "Size effects on elasticity, yielding, and fracture of silver nanowires: In situ experiments," *Phys. Rev. B*, 85, 045443, 2012.

[3] C. Kittel, *Introduction to Solid State Physics*, 7th ed. Wiley, New York. 1996.

[4] A. Einstein and L. Hopf, "Statistische Untersuchung der Bewegung eines Resonators in einem Strahlungsfeld," *Ann. Physik*, vol. 33, pp. 1105-1120, 1910.

[5] R. Feynman, *QED: The Strange Theory of Light and Matter*. Princeton University Press, 1985.

[6] M. P. Allen and D. J. Tildesley, *Computer Simulations of Liquids*, (Oxford: Clarendon Press: 1987).

[7] P. Guan, D. R. Mckenzie and B. A. Pailthorpe, "MD simulations of Ag film growth using the Lennard-Jones potential,", *J. Phys.: Condens. Matter 8,* pp. 8753–8762, 1996.

[8] A. K. Subramaniyan and C. T. Sun, "Continuum Interpretation of Virial Stress in Molecular Simulations," *Int. J. of Solids and Structures*, vol. 3, pp. 16, 2008.

[9] J. Zang, L. Bao, R. A. Webb, and X, Li, "Electron Beam Irradiation Stiffens Zinc Tin Oxide Nanowires," *Nano Lett.*, vol. 11, pp. 4885–4889, 2011.

## Quantum Mechanics: Validity of Classical Molecular Dynamics

Modern physics in the form of QM was born in the beginning of the twentieth century from the collapse of classical physics relating to light as EM waves described by Maxwell's equations, the consequence of which led to the ultraviolet catastrophe that required the atom to have infinite energy at high frequency or short wavelengths. QM stands for quantum mechanics. In 1900, Planck departed from the concept of light as a deterministic wave phenomenon described by Maxwell's equations to a statistical description of light as particles or quanta of energy called photons. Planck's derivation of blackbody radiation therefore returned light to Newton's corpuscular theory previously rejected by Maxwell's wave theory. Light by the Planck law was then consistent with the new particle statistics of thermodynamics developed by Boltzmann.

Today, the emphasis on nanotechnology has renewed the controversy between classical physics and QM thought resolved by Planck a century ago. Indeed, classical physics is still used in heat transfer analysis of nanostructures by assigning macroscopic heat capacity to the atoms. But by the Planck law, the heat capacity of the atom vanishes under EM confinement in nanostructures, a natural consequence of their high surface-to-volume ratio that concentrates almost all of the absorbed energy in the nanostructure surface, thereby placing interior atoms under high EM confinement. Since absorbed EM energy cannot be conserved by the usual increase in temperature, conservation proceeds by QED inducing the creation of photons in the manner of standing waves from atoms under EM confinement between nanostructure surfaces. The Planck energy of the QED standing wave photons is sufficient to ionize the atoms that charge the nanostructure as the distance between nanostructure surfaces is $< 100$ nm. But the creation of the QED induced standing wave photons depletes the surface energy forming the EM confinement, and if ionization does not occur, the standing wave QED photons are free to escape to the surroundings. QED induced EM radiation is a consequence only possible in QM as charge is not created in classical physics.

Applications include nanotechnology in general and discrete MD specifically. MD stands for molecular dynamics. For QM in the validity of MD by classical physics, see:

Prevenslik T., Quantum Mechanics: Validity of Classical Molecular Dynamics. In: Saleem Hashmi (editor-in-chief), Reference Module in Materials Science and Materials Engineering. Oxford: Elsevier; 2016. pp. 1-6. ISBN: 978-0-12-803581-8

# Chapter 8

# Geoengineering and Engineering

The Simple QED theory has a wide range of applications in engineering. Applications include injection of absorptive black carbon aerosols into the stratosphere as a means to reduce solar radiation at the Earth surface to compensate for increasing carbon dioxide levels, the conversion of Joule heat in circuit elements to non-thermal QED radiation and models for the memristor, Phase Change-Random Access Memory devices and $1/f$ noise in nanowires. The concluding patent presents QED devices that rely on the cavity QED induced vacuum ultraviolet light to produce photons in the visible spectrum, electrons and ions.


8.1 Global Cooling by Injecting Black Carbon into the Stratosphere? . . . . . 194
8.2 Heat Transfer in Nanoelectronics by Quantum Mechanics . . . . . 201
8.3 1/f Noise in Nanowires by Quantum Mechanics . . . . . 209
8.4 Cavity QED devices United States Patent . . . . . 214

# Global Cooling by Injecting Black Carbon into the Stratosphere?

**Abstract** Global cooling by injecting black carbon (BC) aerosols into the stratosphere is currently not considered a viable geoengineering solution to compensate for global warming. However, geoengineering analysis methods assume the BC particles upon under absorbing solar radiation follow classical physics and increase in temperature. But for sub-micron nanoparticles (NPs) the Planck law denies atoms in BC particles the heat capacity to increase in temperature in absorbing solar radiation, the consequence of which allows BC to be effective in compensating for global warming. In thus paper, classical physics is superseded by simple QED - a nanoscale heat transfer process based on the Planck law - is used to show the advantages of radiative forcing by BC absorption compared to reflective aerosols. The analysis uses the simple QED heat transfer process based on the Planck law that conserves heat by creating standing EM radiation inside the BC particle having wavelength $\lambda = 2nd$, where n and d are the refractive index and diameter of the spherical BC particle. For BC having n = 2.4, the desired $\lambda$ = 10-micron wavelength for emission through the 8-12 microns atmospheric window requires d ~ 2 microns. The BC particles injected at the top of the stratosphere having high absorb all incident UV-VIS-NIR solar radiation. For a 1% absorption of solar radiation in the stratosphere or negative radiative forcing of -1.6 W/m$^2$ at the Earth's surface, $3.4 \times 10^6$ tons of BC are required at a cost from $ 1-2 trillion. Alternative geoengineering using Earth based BC mirrors is discussed.

**Keywords:** Global cooling, Black carbon, geoengineering, Classical physics, Planck law,

## I. INTRODUCTION

Global warming over the past decades has primarily concentrated on scientific research directed to the control of greenhouse gases, and specifically limiting carbon dioxide in emissions from burning fossil fuels. Despite controls on carbon dioxide, global temperatures continued to increase suggesting research on other ways to limit the rise in global temperature. One promising area of research [1-3] was to inject aerosols of sulfates into the stratosphere that reflect solar radiation back into space and thereby cooling the Earth surface even though carbon emissions do not decrease.

Indeed, the dispersion of submicron nanoparticles (NPs) in the atmosphere was proposed [1] to scatter solar irradiation while being transparent IR radiation at 10 microns emitted by the Earth. In effect, the feasibility of controlling the global temperature without reducing the emission of greenhouse gases was studied. NPs of inexpensive alumina ($Al_2O_3$) that do not absorb solar irradiation. By Mie scattering theory, the NPs in the stratosphere scatter solar irradiation having wavelengths ranging from 0.2 to 4.0 micron. The NPs having an optimum size of 350-450 nm were assumed dispersed in the stratosphere at an altitude of 30 km. The total NP mass of $3 \times 10^7$ tons in the stratosphere was found to reduce 3% of the solar irradiation.

Because of high scattering efficiency, titania was proposed [2] as an alternate to alumina aerosols over 2020-2100 period. However, titania efficiently absorbs solar UV radiation producing a significant stratospheric warming > 20 C offering little benefit when compared to sulfate aerosols from the injection of sulfur dioxide. In this regard, black carbon (BC) having high absorption was shown to have a much lower injection rate than titania produced stratospheric temperature changes > 70 C. BC more commonly known as soot that like carbon dioxide is produced in the combustion of fuels. Because of atmospheric heating, BC aerosols were considered [2] excluded from geoengineering.

Similarly, earlier [3] studies of BC aerosols showed 1 Tg/year of BC injected into the lower stratosphere would cause little surface cooling for 0.3-micron NPs while 0.16-micron NPs produced large surface cooling, but stratospheric warming of over 60 C. Stratospheric warming caused global ozone loss by up to 50% for 0.16 micron NPs. Using diesel fuel to produce the aerosols is also prohibitively expensive. Compared to reflecting sulfate aerosols, absorbing BC aerosols carry too many problems to be a viable option for climate control.

However, there is a dark side to sulfate aerosols because they are not totally reflective, and in fact are absorptive [4] because the sulfate aerosols also contain BC. Contrarily, the sulfate aerosol particles actually heat the atmosphere.

## II. PROBLEM

Prior studies of aerosols containing alumina, titania, and BC NPs in the atmosphere based on Mie theory and classical physics are questionable because the Planck law denies NPs the heat capacity to conserve absorbed solar radiation by an increase in temperature. Instead, solar radiation is conserved by the NPs creating EM radiation that is emitted to the atmosphere. The Planck law depends on NP temperature and maximum size. NPs larger than the maximum are macroscopic particles that follow classical physics and increase in temperature upon absorption of solar radiation.

## III. PROPOSAL

To propose absorptive BC aerosols injected into the stratosphere provide geoengineering with a means to reduce solar radiation at the Earth surface to compensate for increasing carbon dioxide levels. Specifically, 2-micron spherical NPs of graphite comparable to BC injected at the top of the stratosphere. The solar radiation spectrum from UV to near IR is absorbed and converted to 10-micron radiation that escapes to space through the 8-10 micron atmospheric window. The graphite NPs produce 10-micron IR radiation without heating the atmosphere.

## IV. METHOD

The analysis method is based on simple QED which is a nanoscale heat transfer process (nothing to do with Feynman's QED). Unlike elastic Mie theory having the emission frequency to be the same as the excitation frequency, simple QED changes the frequency of absorbed light in size dependent EM quantum states of the nanostructure. Since NPs are small compared the wavelength of incident light, simple QED assumes light is absorbed over the NP surface consistent with the high surface surface-to-volume ratio of NPs. But the Planck law precludes conservation of absorbed light by a temperature increase, and therefore simple QED asserts standing EM radiation is created inside the NP, the absorbed surface heat itself providing the EM confinement to constrain standing EM radiation inside and across the NP diameter. In effect, simple QED conserves EM heat in nanoscale regions by creating EM radiation - not temperature.

Simple QED energy E is quantized by the dimension d of the nanostructure that defines the half-wavelength $\lambda/2$ of the nanostructure. Fig. 1 illustrates the standing EM radiation in a spherical NP has a single quantum state corresponding to NP diameter d, but NP atoms still follow their quantized electron energy levels.

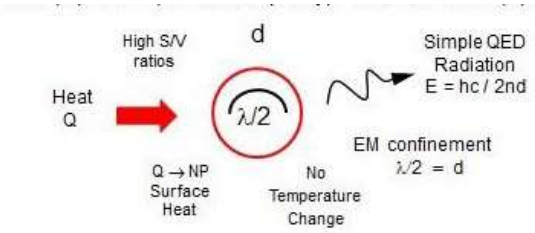


**Fig. 1: Planck Energy of EM Radiation**

In a rectangular NP with different dimensions of width, thickness, and length there are 3 simple QED quantum states corresponding to the different dimensions of the NP. Continuous variation in internal nanoscopic dimensions produces a broadband spectrum of simple QED quantum states. Fig. 1 shows simple QED absorbs heat Q in the NP surface because of the high EM confinement. Unable to conserve the surface heat by a change in temperature, conservation requires the creation of simple QED radiation. The Planck energy $E = h \cdot c/2nd$, where h is Planck's constant and c the velocity of light. The refractive index n of the NP corrects for the velocity c of light within the NP.

## V. ANALYSIS

Solar radiation at 1365 W/m$^2$ at the Earth's surface is reduced by a factor of 4 to 340 W/m$^2$ as only a quarter of the Earth is illuminated at any time. Of the 340 W/m$^2$, Figure 1 shows reflected radiation is 29% while radiation absorbed in the atmosphere is 23%. Radiation that is absorbed by the Earth surface is 48%.

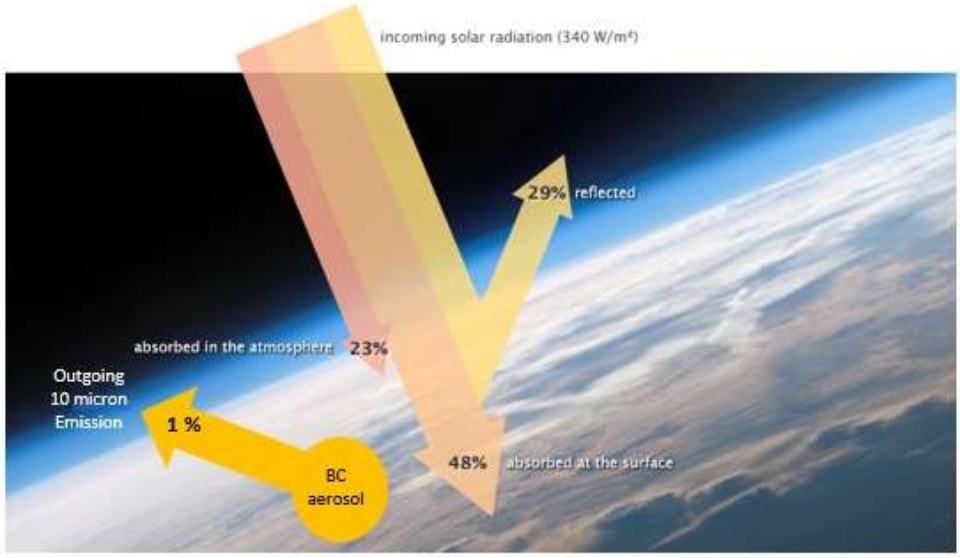


**Figure 1. Distribution of Solar Radiation on Earth**

In this analysis, the BC aerosol absorbs 1 % of the incoming solar radiation 340 W/m$^2$ or 3.4 W/m$^2$. Hence, 48 % of 3.4 W/m$^2$ or 1.6 W/m$^2$ that otherwise would have increased Earth temperature can correct for limited global warming.

Simple QED gives the emission wavelength $\lambda$ = 2nd. Since $\lambda$ = 10 microns, the particle diameter d = 5/n. From [5] the BC refractive index n at 10 microns is, n = 2.4. Hence, d ~ 2 microns. As discussed later, simple QED converts the heat from broadband UV-VIS-NIR solar radiation to 10-micron IR that is radiated back into space as 10-micron radiation through the 8-12 microns atmospheric window.

### 1. Number of BC Particles

For the Earth as a sphere of radius R and N spherical BC particles of diameter d, the ratio of solar radiation absorbed is,

$$\frac{NA_p}{A/4} = \frac{1.6}{340 * 0.48} = 0.01$$

where, $A = 4\pi R^2$ and $A_p = \pi d^2/4$.

Taking R = 6.37x10$^6$ m and d = 2 microns, A = 5.1x10$^{14}$ m$^2$ and $A_p$ = 3.1x10$^{-12}$ m$^2$ giving, N = 4.1x10$^{23}$. The BC particle weight w = $\pi\rho d^3/6$ and total BC mass W = w·N that for $\rho$ = 2000 kg/m3, w = 8.4x10$^{-15}$ kg and W = 3.4x10$^9$ kg or 3.4x10$^6$ tons for the BC aerosol absorbing 1 % of the solar radiation. In comparison, 3 % reflection of solar radiation [1] required 3x10$^7$ tons of alumina, about 10x more mass than the BC aerosol.

**2. Simple QED and the Planck law**

The 2-micron BC particle chosen for the aerosol was selected to have the 10-micron emission and allow the solar radiation from the UV to near IR to dissipated to space, but only if BC particle heat capacity vanishes. Otherwise, the particle temperature increases to heat the atmosphere. For the stratosphere having temperatures at top and bottom of the stratosphere of 220 and 270 K, the Planck law for atoms in the BC particle is shown in Fig. 2.

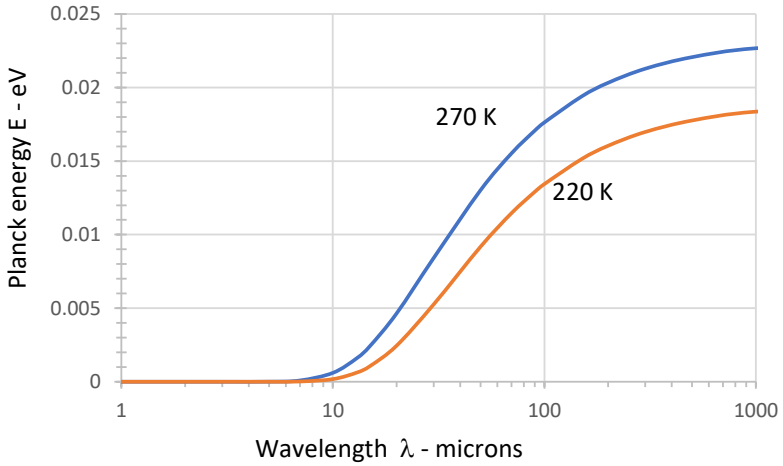


**Figure 2. Planck law at 220 and 270 K**

The Planck law shows the kT energy of the atoms in the BC particle at both 220 and 270 K vanishes to E < 400 μeV at wavelengths λ < 10 microns. What this means is all solar radiation from the UV to the near IR absorbed as heat by the 2-micron BC particle is emitted back into space at 10 microns.

## VI. DISCUSSION

**1. Classical Physics vs. Simple QED**

Classically, the 2-micron BC particle atoms have heat capacity by the Planck law. The increase in temperature ΔT upon absorption of 1.6 W/m$^2$ solar radiation is,

$$\Delta T = \frac{1.6A_p}{wC}$$

where, w and C are mass and specific heat of the BC particle. For BC specific heat C = 708 J/kg-°C, the temperature rate is, ΔT = 0.83 °C/s.

In contrast, simple QED creates photons isothermally. The number Np of 10-micron IR photons emitted to space is,

$$N_p = \frac{1.6A_p}{E}$$

where, E = hc/λ. For λ = 2nd = 10 microns, E = 1.98x10$^{-20}$ J, the rate of 10-micron photons emitted to space through the 8-12 microns atmospheric window is, $N_p$ = 253x10$^6$ /s.

**2. Health Concerns**

The BC aerosol proposal to block 1 % of solar radiation carries the danger of health concerns. Indeed, BC geoengineering is thought [3] not viable as a means of modifying the climate. The problem with BC is soot is considered a major factor in respiratory illness and has been labeled as carcinogenic. The World Health Organization has estimated that up to 500,000 globally each year may be associated air quality exceeding the PM2.5 soot standard.

However, the PM2.5 standard includes not only micron sized particles, but also NPs. PM stands for particulate matter. By simple QED, the NPs emit EM radiation in the UV that causes inflammation and DNA damage leading to health problems. Micron sized particles in the PM2.5 standard emit EM radiation in the Near and far IR which does not cause health problems. In vaccinations, adjuvants to stimulate activation of the immune system antigens, the adjuvants comprising $<$ 100 nm aluminum NPs. Upon vaccine injection, the adjuvant accumulates in the brain. Simple QED converts heat from the brain tissue [6] into UV radiation that activates the immune system, but also damages DNA leading to neuro-degenerative disease and autism. approved by the FDA about a century ago. Similarly, soot NPs cause health problems and micron sized particles are benign. Fig. 3 shows a typical PM2.5 soot particle extends over a few microns and meets the PM2.5 standard. However, the soot particle consists of numerous nanoscopic filaments noted in white circles. Simple QED induced EM radiation E is shown emitted from the filaments that cause health problems - not the micron agglomerate. Coating 2-micron solid spherical BC particles not only avoids health effects, but also ozone loss from chemical reactions between BC and ozone.

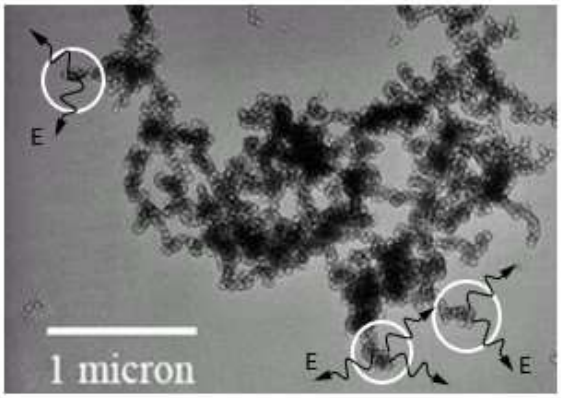


**Figure 3. PM2.5 Soot - Micron Particles and NPs**

**3. Thermal Ozone Damage**

Based on classical physics, injecting BC aerosols in the stratosphere [3,7] will cause stratospheric heating estimated above for 1.6 W/m2 as about 1°/s. Nuclear winter simulations [8] suggest catastrophic ozone losses would rapidly destabilize the stratosphere.

In contrast, the Planck law at stratosphere temperatures shows the atoms in 2-micron BC particles are denied the thermal kT heat capacity to increase in temperature as shown in Fig. 2. Contrary to classical physics, the BC particles do not increase in temperature at all, let alone cause stratospheric heating. At 1.6 W/m$^2$, there is no loss of ozone due to excessive stratosphere temperatures. However, the BC particles absorb UV radiation and preclude ozone formation, but comprising only 1 % of the Earth's surface area allow ozone formation without any significant difference.

**4. BC Cost**

Geoengineering with BC aerosols is usually based on NPs < 100 nm produced from soot in the burning of diesel fuel. Carbon black (CB) differs by being produced from combustion of heavy fuel oil in low oxygen. Both BC and CB therefore have similar density and refractive indices. However, a typical BC particle aerosol is approximately 0.1 micron while CB particles are larger of few mm. Hence, grinding mm size CB particles down to the 2-micron BC size is necessary. Either way, the annual cost of BC or CB aerosol is estimated [3] at about 2 trillion USD.

## VII. CONCLUSION

The injection of BC aerosols into the stratosphere to absorb solar radiation and provide obtain negative -1.6 W/m$^2$ radiative forcing avoids the problem that reflection of solar radiation also includes an absorptive fraction that increases stratosphere temperature. Regardless of whether absorptive or reflective forcing surpass each other, the problem is the practicality of injecting 3 million tons of BC or sulfur aerosols in the stratosphere. A more practical BC global cooling alternative is suggested.

## VIII. ALTERNATIVES

One alternative to injecting BC particles into the stratosphere is an Earth based extension of placing a number space mirrors in orbit [10,11] to reflect solar radiation back into space. The mirrors having an area of a square kilometer made of thin plastic reflective films to illuminate photovoltaic devices producing electricity.

Another alternative extends the injection of 2-micron BC particle aerosols into the stratosphere by providing a large number of flat 100 m square BC mirrors on the Earth surface. Although avoiding the difficulty of injecting BC particles into the stratosphere, geoengineering of many Earth based BC mirrors is still formidable. The BC mirrors are flat having a 2-micron BC layer on a silicon substrate, the BC layer facing the sun and the back-silicon surface facing the Earth surface as shown in Fig. 4.

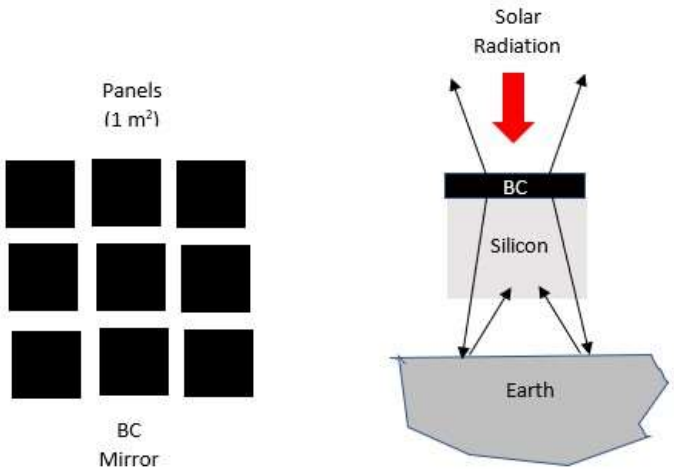


**Fig. 4 Earth based Global Cooling BC Mirrors**

Similar to BC particles, the BC mirrors have thickness of 2 microns, consistent with the same simple QED emission wavelength $\lambda$ = 2nd ~ 10 microns. Hence, simple QED converts the heat from the absorption of all UV-VIS-NIR solar radiation at the Earth's surface to 10-micron radiation that escapes the Earth through the 8-12 microns atmospheric window.

From the above 2-micron spherical BC particle design, the total BC mirror area $A_T = N \cdot A_p = 1.23 \times 10^{12}$ m$^2$ required is distributed with many BC mirrors spread over the Earth's surface. Each mirror area $A_m$ is 100 m on a side having $A_m = 1 \times 10^4$ m$^2$ comprised of 1 m$^2$ panels, each panel consisting of a 2-micron

BC front surface on a supporting substrate transparent to 10-micron radiation, e.g., silicon. What this means is a very large number 123 million BC mirrors are required, the economic feasibility of which is yet to be determined. Nevertheless, the Earth based BC mirrors offer advantages over injecting 2-micron spherical BC particles into the stratosphere as health effects and the cost of continual BC particle injection into the stratosphere are avoided. Moreover, Earth based BC mirrors are more feasible than reflective mirrors deployed in space. Indeed, earth-based BC mirrors are more feasible than injection of BC or any reflective aerosol into the stratosphere and would be even more attractive if IR photocells are developed to utilize the 10-micron emission from the silicon substrate.

Nevertheless, geoengineering with BC mirrors is still prohibitively expensive, but may be necessary for the survival of the human species. Since removing carbon dioxide from the atmosphere is a decades long solution, the recommendation here follows [4] in that the near-term BC emissions be immediately reduced while Earth-based BC mirror technology is developed.

**References**

[1] Maruyama S., et al. 2015: Possibility for controlling global warming by launching nanoparticles into the stratosphere. Journal *of Thermal Science and Technology* - 10, DOI: 10.1299/jtst.2015jtst0022.

[2] Jones A.C., et al. 2016: Climatic impacts of stratospheric geoengineering with sulfate, black carbon and titania injection. *Atmos. Chem. Phys.*, 16, 2843–2862.

[3] Kravitz B., et al., 2012: Sensitivity of stratospheric geoengineering with black carbon to aerosol size and altitude of injection. *J. Geophys. Res.*, 117, D09203, doi:10.1029/2011JD017341.

[4] Jacobson M.T. 2001: Strong radiative heating due to the mixing state of black carbon in atmospheric aerosols. *Nature*, 409, 795-797.[5] Donaldson K.., et al.: 2005. Combustion-derived nanoparticles: a review of their toxicology following inhalation exposure. *Part. Fibre Toxicol*., 2, 10.

[5] Jacobson, M.T. Fundamentals of Atmospheric Modeling. Second Edition, Cambridge University Press 2005.

[6] Prevenslik T. 2019. The Causal Link Between Vaccination Adjuvants and Autism. Inter. J. Research - Granthaalayah, 7, 288-295.

[7] Ferraro A. J., et al. 2011. Stratospheric heating by potential geoengineering aerosols, *Geophys. Res. Lett.*, 38, L24706, doi:10.1029/2011GL04976.

[8] Mills M. J., et al. 2008. Massive global ozone loss predicted following regional nuclear conflict, *Proc. Natl. Acad. Sci. U. S. A*., 105(14), 5307–5312, doi:10.1073/pnas.0710058105.

[9] Robock, A., L. Oman, and G. L. Stenchikov. 2008. Regional climate responses to geoengineering with tropical and Arctic SO2 injections, *J. Geophys. Res*., 113, D16101, doi:10.1029/2008JD010050.

[10] Angel, R. 2006. Feasibility of cooling the Earth with a cloud of small spacecraft near the inner Lagrange point (L1). *PNAS*, 103: 17184–17189.

[11] Lior N. 2013. 93, Mirrors in the sky: Status, sustainability, and some supporting materials experiments, *Renewable and Sustainable Energy Reviews*, 18, 401–415.

**ASME 2013 International Conference on Packaging and Integration of Electronic and Photonic Microsystems**
**InterPACK2013**
**July 16-18, 2013, Burlingame, California, USA**

**InterPACK2013-73173**

# HEAT TRANSFER IN NANOELECTRONICS BY QUANTUM MECHANICS

## ABSTRACT

Today, the transient Fourier heat conduction equation is not considered valid for the derivation of temperatures from the dissipation of Joule heat in nanoelectronics because the dimension of the circuit element is comparable to the mean free path of phonon energy carriers. Instead, the Boltzmann transport equation (BTE) for ballistic transport based on the scattering of phonons within the element is thought to govern heat transfer. However, phonons respond at acoustic frequencies in times on the order of 10 – 100 ps, and therefore the BTE would not have meaning if the Joule heat is conserved by a faster mechanism.

Unlike phonons with response times limited by acoustic frequencies, heat transfer in nanoelectronics based on QED induced heat transfer conserves Joule heat in times < 1 fs by the creation of EM radiation at optical frequencies. QED stands for quantum electrodynamics. In effect, QED heat transfer negates thermal conduction in nanoelectronics because Joule heat is conserved well before phonons respond.

QED induced heat transfer finds basis in Planck's QM given by the Einstein-Hopf relation in terms of temperature and EM confinement of the atom as a harmonic oscillator. QM stands for quantum mechanics and EM for electromagnetic. Like the Fourier equation, the BTE is based on classical physics allowing the atom in nanoelectronic circuit elements to have finite heat capacity, thereby conserving Joule heat by an increase in temperature. QM differs by requiring the heat capacity of the atom to vanish. Conservation of Joule heat therefore proceeds by QED inducing the creation of excitons (hole and electron pairs) *inside* the circuit element by the frequency up-conversion of Joule heat to the element's TIR confinement frequency. TIR stands for total internal reflection. Under the electric field across the element, the excitons separate to produce a positive space charge of holes that reduce the electrical resistance or upon recombination are lost by the emission of EM radiation to the surroundings.

TIR confinement of EM radiation is the natural consequence of the high surface to volume ratio of the nanoelectronic circuit elements that concentrates Joule heat almost entirely in their surface, the surfaces coinciding with the TIR mode shape of the QED radiation. TIR confinement is not permanent, present only during the absorption of Joule heat.

Charge creation aside, QM requires nanoelectronics circuit elements to remain at ambient temperature while dissipating Joule heat by QED radiation to the surroundings. Hot spots do not occur provided the RI of the circuit element is greater than the substrate or surroundings. RI stands for refractive index.

In this paper, QED radiation is illustrated with memristors, PC-RAM devices, and $1/f$ noise in nanowires, the latter of interest as the advantage of QM in avoiding hot spots in nanoelectronics may be offset by the noise from the holes created in the circuit elements by QED induced radiation.

## OVERVIEW

Heat transfer in nanoelectronics is governed by QM, the consequence of which is that the heat capacity of the circuit element vanishes. Joule heat is no longer conserved by an increase in temperature. Instead, conservation proceeds by the QED induced conversion of Joule heat to non-thermal EM radiation to create excitons that upon separation produce space charge of positive charge holes. Thermal management of nanoelectronics is proposed to proceed based on the time dependent Fourier equation using commercial 3D finite element FE programs such as ANSYS and COMSOL. Although FE programs based on classical physics are perfectly valid for circuit boards, cooling systems, and surroundings, QM requires the sub-micron circuit elements to be simulated in the FE model as point or line sources of QED radiation. Hot spots do not occur in nanoelectronics because the QED radiation emitted by the elements is absorbed over large areas of the system. Instead, management of electronic noise may very well control the design of future nanoelectronics.

## BACKGROUND

Nanoelectronics heat transfer is thought [1] unconventional because the transient Fourier heat conduction equation or continuum assumption fails as the characteristic dimension of the circuit element is comparable to the mean free path of phonon energy carriers. Instead, the BTE based on ballistic transfer is employed to derive conductive heat flow based on the scattering of phonons by the lattice. Because of this, the BTE and phonon variants thereof abound [2-4] the literature.

Today, the BTE is primarily directed to the steady state derivation of thickness dependent thermal conductivity of thin films, although the reduced conductivity of thin films has been known [5] for over 30 years. Over this time, the Fourier heat conduction equation has failed to explain thickness dependent thermal conductivity. In contrast, the BTE is claimed [1, 6] to explain reduced thin film conductivity.

However, the BTE [1, 6] and Fourier solutions are questionable because of the heat balances assumed for the films. The problem is thin films emit QED radiation beyond the UV to the surroundings [7] that is not included as a loss in the heat balance, and therefore the thermal conductivity is concluded to be reduced from bulk. Alternatively, if the QED radiation loss is included in the balance, the conductivity remains at bulk. The exclusion of QED radiation from the heat balance is understandable as frequencies beyond the UV would normally not be observed during thin film experiments.

Further, the BTE finds basis in classical physics, and therefore the thermal conductivity of the thin film or collectively the nanoelectronic circuit element is explained by phonons at steady state. However, phonons respond [8] at frequencies < 10 GHz in times > 100 ps, and therefore conduction of Joule heat at acoustic frequencies is just too slow to compete with QED radiation at optical frequencies beyond the UV. In nanoelectronics, QED induced heat transfer therefore conserves Joule heat in circuit elements well before phonons respond.

Moreover, the BTE is generally only applied to steady conductive heat flow. Thermal transients are usually not studied, especially in complex 3D nanoelectronic geometries. Typically, the BTE is limited [9] to steady 1D phonon simulations while transient response is limited to simple estimates [8] of temperatures based on classical physics, e.g., transient temperature changes $\Delta T$ for response times $\tau$, electrical power $P$, heat capacity $C$, and volume $V$, are: $\Delta T = P\tau/CV$, i.e., $\Delta T$ is bounded as heat capacity $C$ is assumed finite.

In contrast, QM requires the heat capacity $C$ in nanoelectronics circuit elements to vanish. By QM, divergent transient $\Delta T$ temperatures are avoided by the creation of QED radiation that charges the element or is emitted to the surroundings.

## THEORY

### QM Restrictions

Classical physics allows the atom to have thermal $kT$ energy or equivalently the heat capacity necessary to conserve absorbed Joule heat by an increase in temperature. A comparison of the thermal $kT$ energy of the atom by classical physics and QM by the Einstein-Hopf relation [10] is shown in Fig. 1.

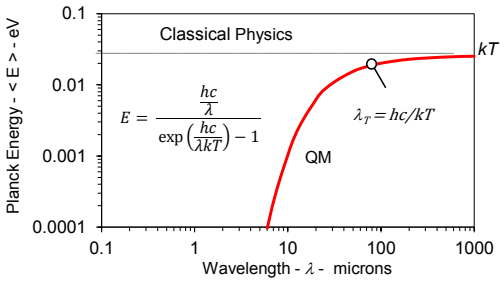


Fig. 1 Heat Capacity of the Atom at 300K
$E$ is Planck energy, $h$ Planck's constant, $c$ speed of light
$k$ Boltzmann's constant, $T$ temperature, and $\lambda$ wavelength

Both the Fourier equation and the BTE follow classical physics and allow the atom to have the same $kT$ energy in nanoelectronic circuit elements as in conventional electronics. QM differs in that $kT$ energy is only available for $\lambda > \lambda_T$ and otherwise is < $kT$. At ambient temperature, $\lambda_T \sim 40$ microns. By QM, atoms in nanoelectronics circuit elements under TIR confnement wavelengths $\lambda < 1$ micron therefore have virtually no heat capacity to conserve Joule heat by an increase in temperature.

### TIR Confinement

Absent heat capacity, QM precludes conservation of Joule heat in nanoelectronics by an increase in temperature. Instead, Joule heat is conserved by the creation of non-thermal EM radiation from the QED induced frequency up-conversion to the TIR resonance of the circuit element.

In 1870, Tyndall showed light is trapped by TIR in the surface of a body if the RI of the body is greater than that of the surroundings. However, TIR need not be limited to the confinement of light. Any form of EM energy may be confined by TIR, although in nanoelectronics the confined EM energy is Joule heat.

In nanoelectronics, circuit elements have high surface to volume ratios. Provided the element has a higher RI than the substrate, the Joule heat is almost entirely absorbed in its surface. But the surface fully participates with the shape of the

TIR wave function, and therefore QED induces the absorbed Joule heat to undergo spontaneous conversion to surface EM radiation. TIR confinement induces the creation of excitons from QED radiation without any external EM confinement. Indeed, TIR confinement is not permanent, sustaining itself only during the absorption of Joule heat, i.e., absent Joule heat, there is no TIR confinement and excitons from QED radiation are not produced.

QED relies on complex mathematics as described by Feynman [11] although the underlying physics is simple, i.e., photons of wavelength $\lambda$ are created by supplying EM energy to a QM box with sides separated by $\lambda/2$. In this way, QED frequency up-converts Joule heat to the TIR resonance described by the characteristic dimension $d$ of the circuit element. The Planck energy $E$ of the QED radiation,

$$E = h\upsilon, \;\; \upsilon = \frac{c}{\lambda}, \;\; \lambda = 2nd \tag{1}$$

where, $n$ is the RI of the circuit element. For film and spherical or cylindrical geometries, $d$ is the thickness or diameter.

## APPLICATIONS

Applications of QED induced heat transfer to nanoelectronics [12-15] find commonality in the conversion of Joule heat in circuit elements to non-thermal QED radiation. Subsequently, the QED radiation creates excitons or is emitted to the surroundings as EM radiation. Summaries for the memristor, PC-RAM devices, and 1/ $f$ noise in nanowires are as follows.

### Memristors

In 1971, Chua [16] hypothesized a passive two-terminal circuit element existed having a resistance that depended on the time–integral of the current. Based on symmetry arguments alone, the notion was held that electronic circuitry based on the three circuit elements - the resistor, capacitor, and inductor was incomplete. For completeness, a fourth element called a memristor was proposed. But lacking an actual prototype, the memristor lay dormant for almost 40 years.

Hewlett-Packard (HP) in 2008 announced [17] the development of a switching memristor circuit element comprising a thin film of titanium dioxide sandwiched between platinum electrodes. HP memristors claim positive charged holes from oxygen vacancies are the source of switching. But the HP theory is phenomenological lacking physical basis to allow extensions to memristors without vacancies.

Indeed, experiments over the past 50 years show memristor behavior without oxygen vacancies. Even electrodes are not necessary, as memristor behavior is observed in a single material, e.g., gold and silicon nanowires. Absent vacancies, memristor behavior in nanowires is explained by the presence of space charge, but the source has never been identified. In contrast, QED theory predicts space charge creation from excitons anytime Joule heat is dissipated in nanoelectronics.

*QED Radiation and Excitons* QM restrictions on heat capacity require the dissipative Joule power $P$ be conserved by creating number $N_P$ of QED photons in the memristor having Planck energy $E$. The QED radiation is created at the rate $dN_P/dt$,

$$\frac{dN_P}{dt} = \frac{P}{E} \tag{2}$$

where, $P$ is power, $P = IV = I^2R$, and $V$, $I$, and $R$ are the voltage, current, and resistance.

By the photoelectric effect, the rate $dN_{ex}/dt$ of excitons created depends on the yield $Y$ of excitons / QED photon,

$$\frac{dN_{ex}}{dt} = Y\frac{dN_P}{dt} \tag{3}$$

Only a fraction $\eta$ of excitons created change the memristor resistance, the remainder (1-$\eta$) upon recombination produce EM radiation that is lost to the surroundings.

*Source of Holes* The number of holes and electrons in the memristor is given by $Q_H$ and $Q_E$, respectively. The rate $dN_{ex}/dt$ of excitons created is balanced by the electron $Q_E$ and hole $Q_H$ charges moving toward voltage terminals by their respective $\mu_E$ and $\mu_H$ mobility in the electric field $F$. The charge balance is,

$$\frac{dQ_E}{dt} = \frac{\eta YP}{E} - Q_E\frac{\mu_E F}{d} \tag{4}$$

$$\frac{dQ_H}{dt} = \frac{\eta YP}{E} - Q_H\frac{\mu_H F}{d} \tag{5}$$

where, $d$ is the memristor thickness. Both exciton electron and hole equations are symmetric allowing the hole response to represent the electron for the same mobility. Taking $F = V/d$ and $V = Vo \sin \omega t$ gives the number $Q_H$ of hole charges,

$$\frac{dQ_H}{dt} = \frac{\eta YP}{E} - \frac{\mu_H V_o \sin \omega t}{d^2}Q_H \tag{6}$$

where, $\omega$ *is* circular frequency, $\omega = 2\pi f$, and $f$ is frequency. Conservation of the charge for the number $Q_E$ of electrons is in the excitons is similar.

The hole $Q_H$ solution by the integrating factor method,

$$Q_H \exp\left(-\frac{\mu_H V_o}{\omega d^2}\cos \omega t\right) = \frac{\eta YP}{E}\int \exp\left(-\frac{\mu_H V_o}{\omega d^2}\cos \omega t\right) dt \tag{7}$$

*Electrical Response* On average, the exciton holes and electrons are centered in the film $d$ and need to move $d/2$ to reach opposite polarity voltage terminals. The resistance $R$ is,

$$R = \rho\frac{d}{2A} = \frac{d}{2A}\frac{1}{\mathrm{e}(\mu_E Q_{EO} + \mu_H Q_{HO})/Ad} \approx \frac{d^2}{4\mathrm{e}\mu_H Q_H} \quad (8)$$

where, e is the unit electronic charge. For simplicity, the resistivity $\rho$ assumes $\mu_E = \mu_H$ with the same number $Q_E$ of electrons as $Q_H$ holes. Note the resistivity $\rho$ requires units of per unit volume, where volume is $Ad$ and $A$ is memristor area. The initial resistance $R_o$ gives the initial number $Q_{HO}$ of hole charges,

$$Q_{HO} = \frac{d^2}{4\mathrm{e}\mu_H R_O} \quad (9)$$

The current $I$ is,

$$I = \frac{V}{R} = \frac{V_O \sin \omega t}{R} \quad (10)$$

*Simulations* Memristor resistance $R$ depends on the instantaneous number of holes $Q_H$ during each cycle of applied harmonic voltage. The QED induced $I$-$V$ hysteresis loop of memristors characterized by the "bow-tie" shape reported by Chua [16] and HP [17] is shown in Fig. 2.

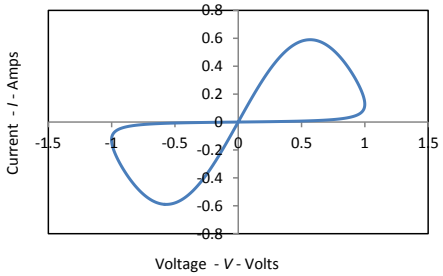


Fig. 2 Memristor $I$-$V$ Curve
$d$ = 50 nm, $\mu_H = 2\text{x}10^{-6}$ cm$^2$/V-s

## PC-RAM Devices

In the 1960's, Ovshinsky initiated scientific research in the field of amorphous and disordered GST materials of fundamental importance in the storage of data in PC-RAM devices that continues to this day. GST stands for GdSbTe chalcogenide type glasses and PC-RAM stands for phase-change - random access memory.

The Ovshinsky [18] effect is the significant reduction in resistance of submicron thick GST films under low voltages. In contrast, Chua's [16] memristor gives a continuous decrease and recovery of resistance over the same harmonic cycle, but is superseded by QED induced charge consistent with Ovshinsky's charge carriers [18].

However, PC-RAM theory is not without controversy. Ovshinsky [18] thought the resistance of GST films changed by the redistribution of charge carriers; whereas, others at that time including PC-RAM researchers today [19, 20] argue the resistance changes because the GST crystalline state is transformed to the amorphous state by melting, the Joule heat supplied by lasers and heaters. In this controversy, QM asserts the heat capacity of submicron GST films vanishes, and therefore melting cannot occur, as the Joule heat supplied is not conserved by an increase in temperature. By precluding melting, QM re-opens the controversy between the melting and charge carrier PC-RAM mechanisms.

Instead of increasing GST film temperature, conservation proceeds by the QED induced creation of excitons from EM radiation under TIR confinement. The TIR confinement of QED radiation is enhanced by the fact the Joule heat absorbed in the GST film is concentrated in the TIR mode because of its high surface to volume ratios. The QED radiation having Planck energy beyond the UV produces excitons by the photoelectric effect, the electrons and holes of which change the GST film resistance without melting. QM precludes temperature increases during switching provided submicron GST films are sandwiched in materials of a lower RI. However, thick supramicron GST films follow classical physics and do indeed melt upon heating. In this regard, Chua's [16] conjecture that memristors are the missing fourth element in electronic circuits is superseded by Ovshinsky's [18] charge carriers, the charge carriers being the consequence of QM.

*Mobility* In PC-RAM devices and memristors, mobility of hole charge carriers is of great importance in defining the current that transfers the charge from excitons to the voltage terminals, but data is limited. In this paper, current is proportional to both mobility and conductivity, Chen et al. [21] expressed mobility $\mu$ at ambient temperature by,

$$\mu = \mu_o \exp\left(\alpha F^{1/2}\right) \quad (11)$$

where, $\mu_o$ is the mobility at zero field. Organic light emitting tris-(8-hydroxyquinolate) aluminum (Alq3) film correlates by $\alpha = 9.22\text{x}10^{-3}$ (cm/V)$^{1/2}$. The typical GST mobility is independent of GST film thickness, i.e., $\mu = 2\text{x}10^{-5}$ cm$^2$/V-s.

*Source of Holes* Similar to memristors, excitons in GST films change resistance in proportion to the fraction $\eta P$ of QED radiation absorbed and the yield $Y$. The rate $dN_{ex}/dt$ of excitons created is balanced by the electron $Q_E$ and hole $Q_H$ charges lost by neutralization at opposite polarity terminals by their respective $\mu_E$ and $\mu_H$ mobility in the field $F$. For constant voltage $V = V_o$, the hole $Q_H$ balance is,

$$\frac{dQ_H}{dt} = \frac{\eta Y P}{E} - \frac{\mu_H V_o}{d^2} Q_H \quad (12)$$

The hole $Q_H$ solution,

$$Q_H = \frac{d^2}{\mu_H V_o}\left\{\frac{\eta Y P}{E}\left[1 - \exp\left(-\frac{\mu_H V_o}{d^2}t\right)\right] + \frac{\mu_H V_o}{d^2}Q_{H0}\exp\left(-\frac{\mu_H V_o}{d^2}t\right)\right\} \quad (13)$$

*Simulations* The Alq3 mobility [21] was used in the simulations. The electric field $F$ assumed constant voltage $V_o$ = 1 V that for GST film thickness from 10 to 10000 nm, correspond to $F = Vo / d$ of $10^6$ to $10^3$ V/cm. Equation (11) gives Alq3 hole mobility from $3.04 \times 10^{-3}$ to $4.03 \times 10^{-7}$ cm$^2$/V-s. The resistance $R$ transients are shown in Fig. 3.

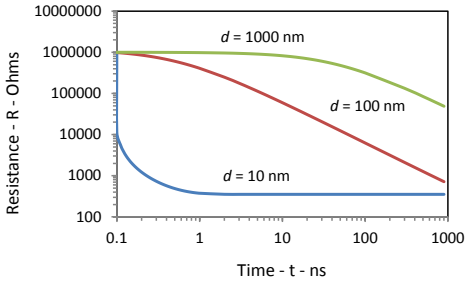


Fig. 3 Transient $R$ – Alq3 Mobility

All GST films were assumed to have an initial resistance $R_o = 1 \times 10^6$ ohms. The 10 nm film resistance $R$ is reduced to 350 ohms in less than 1 ns – a 99.965 % reduction approaching superconductivity. The 100 and 1000 nm films respond far slower. All GST films change resistance by QED induced space charge as Ovshinsky envisioned over 50 years ago.

**1/*f* Noise in Nanowires**

1/*f* noise is commonly observed in EM measurements of electronic circuits comprising capacitors, resistors, and inductors. Research in 1/*f* noise began in 1925 with Johnson [22] and Nyquist [23] who found vacuum tubes emitted white noise. White noise has a constant power spectrum generated by the thermal agitation of charges inside the resistor itself without any applied voltage. In contrast, 1/*f* noise sometimes called pink noise differs in that under applied voltage the frequency $f$ of the power spectrum is not constant, but rather increases as $f$ is lowered, i.e., having a slope of -1 on a log-log plot of noise vs. frequency.

Over the past 80 years, explanations of 1/*f* noise have proved elusive. Schottky [24] proposed a 1/ $f$ model of exponentially decaying current pulse $I$ caused by the release of electrons from the cathode of a vacuum tube, i.e., $I = Io \cdot e^{-bt}$, For a train of such pulses at an average rate, the power spectrum is of the Lorentzian form which is constant near $f = 0$ and for large $f$ is proportional to $1/f^2$ with a narrow transition region where the power spectrum resembles that of 1/$f$ noise.

Today, 1/$f$ noise is generally explained by free electrons in the Hooge [25] relation,

$$\frac{S_R}{R^2} = \left(\frac{S_I}{I^2}\right)_V = \frac{\alpha}{fN} \quad (14)$$

where, $S_R$ and $S_I$ are the spectral power density of resistance $R$ and current $I$, and $f$ is the frequency at which the noise is measured, $N$ is the total number of free electrons, and α is an empirical dimensionless constant.

Hooge claimed the 1/$f$ noise is caused by lattice scattering of electrons. However, this is unlikely as phonon frequencies are far higher than LFN frequencies. LFN stands for low frequency noise. It is difficult to reconcile LFN with the residence time of the electron in the size of the sample. If 1/$f$ noise is a summation of Lorentzians having long characteristic times t >> 1 s, the electrons must stay in the sample much longer than a few seconds. But in a sample with a length of 1 cm, an electron only stays about 0.1 s as its diffusion coefficient $D$ is of order 0.001m$^2$/s. In nanoelectronics, the residence time of the electron in the circuit element is far smaller. The Hooge relation based on electrons therefore cannot be correct.

*Source of Holes* Unlike Hooge's relation for LFN based on electrons, QED radiation [15] created by conserving Joule heat produces charge by the photoelectric effect.

$$\frac{dN_P}{dt} = \frac{P}{E} \text{ and } \frac{dN_{ex}}{dt} = Y\frac{dN_P}{dt} \quad (15)$$

where, $dN_p/dt$ is the rate of QED radiation created. By the photoelectric effect, $dN_{ex}/dt$ is the rate of excitons produced and $Y$ is the exciton yield / QED photon. Like the memristor and PC-RAM devices, only a fraction $\eta$ of the excitons created produce 1/$f$ noise, the remaining (1-η) excitons upon recombination emit EM radiation to the surroundings. Unlike the probabilistic creation of excitons from an external source of EM radiation having $Y << 1$, QED radiation created *inside* the circuit element surface have $Y = 1$. For voltage $V_o$ across the nanowire, the field $F = V_o / L$,

$$\frac{dQ_H}{dt} = \frac{\eta P}{E} - \frac{\mu_H V_o}{L^2}Q_H \quad (16)$$

The hole $Q_H$ solution is,

$$Q_H = \frac{L^2}{\mu_H V_o}\left\{\frac{\eta P}{E}\left[1 - \exp\left(-\frac{\mu_H V_o}{L^2}t\right)\right] + \frac{\mu_H V_o}{L^2}Q_{H0}\exp\left(-\frac{\mu_H V_o}{L^2}t\right)\right\} \quad (17)$$

In contrast to LFN based on electrons given by the Hooge relation, QED induced excitons are produced by a step change in charged hole $Q_H$ carriers as current enters the NW. Since the step in charge $Q_H$ with time $t$ is a step in current $I = dQ_H/dt$ and since the voltage $V_o$ across the NW is constant, the LFN in NWs is caused by a step change in power $P = V_o I$.

*Fourier Transform of Step Change* In NWs, the LFN is given by the Fourier transform (FT) of a step change in power, the general form [26] of which is,

$$u(t)t^{\alpha} \leftrightarrow \text{Mag} = \Gamma(\alpha+1)\omega^{-(\alpha+1)}$$

$$\text{Phase} = -\pi(\alpha+1)/2 \qquad (18)$$

where, $\alpha$ is a constant. In the time domain, the unit step function u($t$) is defined as u($t$) = 0 for $t < 0$, and u($t$) = 1 for $t \geq 0$. For $\alpha = 0$, the Gamma function $\Gamma(\alpha+1) = 1$ and the FT($f$) for the step in power has the magnitude of $1/f$ in the frequency $f$ domain at phase angle $\theta = -\pi/2$, i.e.,

$$FT(f) = \int_{-\infty}^{\infty} 1e^{-j2\pi ft}\, dt = -\frac{j}{2\pi f} = \frac{1}{2\pi f}\text{at}\,\theta = -\frac{\pi}{2} \quad (19)$$

LFN therefore consists of a $1/f$ noise spectrum given by the FT($f$) of the step change in hole charges $Q_H$ created by QED as current enters the NW.

*Simulations* QED induced $1/f$ noise simulations of $SnO_2$ NWs were made for the current PSD at a drain bias $V_D = 0.1$ V and gate voltages $V_G = 2.5$ V over the frequency band from 1 to 1000 Hz. PSD stands for power spectral density. See (Fig. 3(a) of [27]). The NW diameter $d$ and length $L$ are 50 nm and 1.5 microns, respectively.

*Signaling Power* QED theory requires the Joule heat dissipated in the PSD of the NW at a given $V_G$. However, the PSD in [27] is expressed in signaling [28] terminology,

$$I^2(f, f_o) = \frac{KF \cdot I_D}{C_{cap}L^2} f_o \int_{f_o}^{f} \frac{df}{f} \quad \text{A}^2/\text{Hz} \qquad (20)$$

where, $I^2(f)$ is the current PSD in $A^2$/Hz. From [27], at $V_G = 2.5$ V and $f_o = 1$ Hz, the PSD = $1.4\text{x}10^{-17}$ $A^2$/Hz. The constant $KF = 8.14\text{x}10^{-32}$ was fit to the PSD using capacitance $C_{cap} = 1.593\text{x}10^{-16}$ F given in [27]. Integration to $f = 1000$ Hz,

$$I^2(1000,1) = 1.4\text{x}10^{-17}\ln\left(\frac{1000}{1}\right) = 9.66\text{x}10^{-17}\ \text{A}^2 \quad (21)$$

The NW physical current $I_{phys}$ is,

$$I_{phys} = \sqrt{I^2(1000,1)} = 9.83\text{x}10^{-9}\text{A} \qquad (22)$$

The Joule heat is the power $P = V_D I_D$, where $V_D$ and $I_D$ are drain voltage and current. From (Fig. 2(a) of [27]), the $I_D = 0.2\text{x}10^{-6}$ A at $V_D = 0.1$ V. Hence, the power $P = 2\text{x}10^{-8}$ W.

Only a fraction $\eta$ of the power $P$ produces the excitons in $1/f$ noise, i.e., $\eta P = I_{phys}V_D = 9.83\text{x}10^{-10}$ W $<< P = 2\text{x}10^{-8}$ W, where $\eta \sim 0.05$. The remaining $(1\text{-}\eta)$ excitons upon recombination emit EM radiation to the surroundings. The TIR confinement barrier of the $SnO_2$ NWs having $d = 50$ nm diameter and $n = 1.73$ from (1) has Planck energy $E = 7.1$ eV, the barrier confining (and exciting) all lower $SnO_2$ quantum states, e.g., the 2 eV VIS luminescence of $SnO_2$ [29] nano rods. Hence, the excitons $\eta P/E$ in (17) are created at $E \sim 2$ eV.

*Step Change in Hole Charges* The hole $SnO_2$ mobility $\mu_H$ = 172 and 40 $cm^2$/V-s were simulated. Assuming $Q_{H0} = 0$, the transient hole $Q_H$ charges from (17) simplified to:

$$Q_H = \frac{\eta PL^2}{\mu_H EV_o}\left[1 - \exp\left(-\frac{\mu_H V_o}{L^2}t\right)\right] \qquad (23)$$

where, $\eta P = I_{phys}V_D$ and $V_o = V_D$. Fig. 4 shows the $Q_H$ response for mobilities of 172 and 40 $cm^2$/V-s is constant in ~ 5 ns at 4 and 17 holes, respectively. Hence, the $1/f$ spectrum for LFN in the frequency domain is justified by the FT of the step in power of holes $Q_H$ in the time domain.

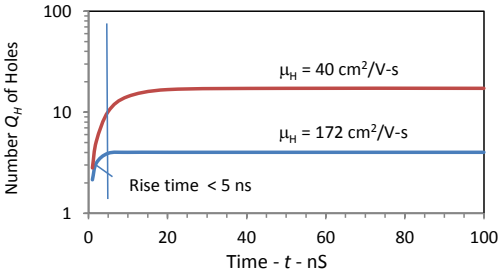


Fig. 4 QED Induced step change in Hole charges

In NWs, the number $N$ of holes is estimated [27] with the modified Hooge relation,

$$I^2(f) = \frac{\alpha_H I_D^2}{Nf} \qquad (24)$$

where, $\alpha_H = 0.045$. For $V_G = 2.5$ V, the PSD gives $I^2(f) = 1.4\text{x}10^{-17}$ $A^2$/Hz at $f = 1$ Hz. Hence, $N \sim 128$ holes which is greater than the QED induced holes. However, it is noted Hooge [25] based his experimental $1/f$ correlation on electrons – not holes.

.

*QED Spectral Density* QED induced PSD argues the step in charge $Q_H$ created as the current enters the NW under constant voltage $V_o$ produces a step change in power the FT of which establishes LFN has form of a $1/f$ spectrum, but the amplitude requires the physical current $I_{phys}$ to be estimated. From (16),

$$I_{phys} = \mathrm{e}\left(\frac{P}{E} - \frac{\mu_H V_o}{L^2} Q_H\right) \tag{25}$$

and

$$I^2(f, f_o) = \frac{I_{phys}^2}{ln\left(\frac{f}{f_o}\right)} \tag{26}$$

Unlike (23) with $\eta P$ ($\eta = 0.05$), the fraction ($\eta = 1$) is used in (25) because the physical current $I_{phys}$ to create all excitons depends on total power $P$, i.e., $\eta P$ produces $1/f$ noise while $(1\text{-}\eta)P$ is lost by VIS luminescence to the surroundings. Taking $Q_H = 4$ holes, $I_{phys} = 9.95\text{x}10^{-9}$ A. From (26), $I^2(f_o) = 1.43\text{x}^{-17}$ $A^2$/Hz. The experiment [27] is lower at $I^2(f_o) = 1.4\text{x}^{-17}$ $A^2$/Hz, but for clarity is depicted even lower in Fig. 5.

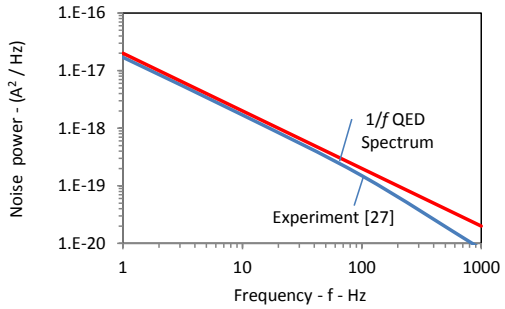


Fig. 5 $1/f$ QED Spectrum and Experimental [27] Data

The QED induced $1/f$ PSD is observed coincident with experiment for $f < 10$ Hz, but deviates for $f > 100$ Hz because the data does not follow $1/f$, but rather $1/f^{\beta}$, where $1 < \beta < 1.5$. Otherwise, the QED induced $1/f$ spectrum simulates experiment without any fitting parameters

**EXTENSIONS**

Nanowires provide nanoelectronics with interconnects between circuit elements. The abrupt decrease in resistance shown for QED induced photoelectric effect in GST films by Ovshinsky suggests superconductivity already exists or at least may be approached for nanowires at ambient temperature. Indeed, UV induced photo-conductivity [30] has already been observed for $GdBa_2Cu_3O_{6.5}$. Hence, the Ovshinsky Effect may supersede magnetic effects in spintronics, a review of which is planned in a subsequent paper.

**SUMMARY**

In nanoelectronics, the classical Fourier equation is not thought applicable to heat transfer for circuit elements because the characteristic dimension of the element is comparable to the mean free path of phonon energy carriers. Instead, the BTE is considered acceptable. However, QM suggests both Fourier equation and BTE derivations are invalid in nanoelectronics.

Over the past 30 years, thickness dependent thermal conductivity of thin films derived by both the Fourier equation and the BTE has been based on heat balances that exclude QED radiation losses to the surroundings. Because of this exclusion, the thermal conductivity of thin films is found reduced from bulk, but if included, QED induced radiation allows the thermal conductivity to remain at bulk for all thicknesses.

The BTE based on classical statistical mechanics currently used in heat transfer of nanoelectronics is a method of deriving the thermal conductivity of a circuit element under conditions of steady heat flow. The BTE is also claimed to derive transient thermal response, but like the Fourier equation the BTE assumes the atom has heat capacity at the nanoscale. BTE derivations of both steady and transient temperatures in nanoelectronics circuit elements are therefore invalid by QM.

QED induced heat transfer finding basis in QM differs from both the classical Fourier equation and BTE in that the heat capacity of the atom vanishes in nanoelectronics circuit elements. Joule heat is not conserved by an increase in temperature, but rather by the creation of non-thermal EM radiation that produces excitons to charge the element or upon recombination is emitted as VIS radiation to the surroundings.

By QED induced radiation, the circuit elements, e.g., memristors, PC-RAM devices, and nanowires do not increase in temperature under Joule heating. For QED to be valid, the RI of the element is required to be greater than the surroundings. If so, memristors need not rely on oxygen vacancies, GST films change resistance by charge and not by melting, and the $1/f$ noise based on large numbers of electrons in the long–standing Hooge relation based on electrons is superseded by a small number of QED induced charged holes. In nanoelectronics, QED radiation always creates excitons, the holes of which act as charge carriers as first envisioned in GST films by Ovshinsky.

The QED simulation of $1/f$ noise in $SnO_2$ NWs differs from memristors and PC-RAM devices in that the low power level of the PSD suggests the LFN is produced by only a few holes. Indeed, the experimental data was found simulated by < 20 carrier holes and for a mobility 172 $cm^2$/V-s only a few QED induced hole charges are required. In contrast, the modified Hooge relation predicts the creation of about 100 holes. More

study is required to confirm or refute whether a few hole charges do indeed produce 1/*f* noise in NWs.

NWs aside, the long-standing puzzle of generic 1/*f* noise may be explained by the FT of abrupt step changes in the time domain, e.g., the sound in striking a piano key and the electronic recording of changes in the stock market index.

The significant reduction in resistance of memristors and GST films as supported by QED induced radiation suggests nanowires as interconnects between circuit elements in nanoelectronics may indeed approach superconductivity at ambient temperature.

Applications of QED induced heat transfer in the thermal management of nanoelectronics are trivial compared to those required for the BTE. Given the BTE is invalid by QM, there is no need to perform tedious phonon scattering derivations of thermal conductivity in circuit elements. The magnitude and frequency of QED radiation may be simply estimated from Joule heat by hand calculations and input as point or line sources into standard FE computer programs such as ANSYS and COMSOL. Unlike conventional electronics, thermal management of hot spot temperatures is not expected to be a problem in nanoelectronics as the QED radiation emitted from a circuit element is absorbed over large areas of the surroundings. Instead, management of electronic noise may pose the greater challenge to nanoelectronics.

## REFERENCES


1. M. Aseghi and W. Liu, "Microscale heat transfer," Electronics Cooling, February, 2007.
2. G. Chen, "Ballistic-Diffusive Heat-Conduction Equations," PRL, vol. 86, pp. 2297-2300, 2001.
3. M. Xu and H. Hu, "A ballistic-diffusive heat conduction model extracted from Boltzmann transport equation," Proc. R. Soc., 26 January 2011.
4. A. J. Minnich, et al., "Quasiballistic heat transfer studied using the frequency-dependent Boltzmann transport equation," Phys. Rev. B, vol. 84, 235207, 2011.
5. P. G. Kelemen, "Pulse Method for the Measurement of the Thermal Conductivity of Thin Films," Thin Solid Films, vol. 36, 1976, pp. 199-203
6. W. .Liu, Y. Yang, and M. Asheghi, "Thermal and Electrical Characterization and Modeling of Thin Copper Layers," Intersociety Conference on Thermal and Thermomechanical Phenomena in Electronic Systems ITHERM, San Diego, 2006.
7. T. Prevenslik, "Heat Transfer in Thin Films," Third Inter. Conf. on Quantum, Nano and Micro Technologies, ICQNM, Cancun, February 1-7, 2009,
8. E. Pop, "Energy Dissipation and Transport in Nanoscale Devices," Nano Research, vol. 3, 147, 2010.
9. S.Sinha and K.E. Goodson, "Thermal conduction in sub-100nm transistors," Microelectronics Journal, 37, pp. 1148–1157, 2006.
10. A. Einstein and L. Hopf, "Statistische Untersuchung der Bewegung eines Resonators in einem Strahlungsfeld," Ann. Physik, vol. 33, pp. 1105-1120, 1910.
11. R. Feynman, QED: *The Strange Theory of Light and Matter*. Princeton University Press, 1985.
12. T. Prevenslik, "Memristors by Quantum Mechanics," Inter. Conf. on Intelligent Computing," ICIC 2011, Zhengzhou, August 11-14, 2011.
13. T. Prevenslik, "Quantum Mechanics and Nanoelectroncs," ICMON: International Conference on Microelectronics, Optoelectronics, and Nanoelectronics, Venice, November 28-30, 2011.
14. T. Prevenslik, "Heat Transfer in Nanoelectronics by Quantum Mechanics," IEEE NANO 2012, 12th Inter. Conf. on Nanotechnology, 20-23 Augusr 2012, Birmingham, UK.
15. T. Prevenslik, "1/*f* Nose by Quantum Mechanics," 2012 Inter. Conf. on Circuits, System, and Simulation (ICCSS 2012), Hong Kong, August 3-5, 2012.
16. L. O. Chua, "Memristor - the missing circuit element," IEEE Trans. Circuit Theory, vol. 18, pp. 507–519, 1971.
17. D. B. Strukov, et al., "The missing memristor found," Nature, vol. 453, pp. 7191, 2008.
18. S. R. Ovshinsky, "Reversible Electrical Switching Phenomena in Disordered Structures," PRL, vol. 21, pp. 1450-3, 1968.
19. S. Hudgens and B. Johnson, "Phase Change Chalcogenide Nonvolatile Memory Technology," MRS Bulletin, pp. 1-4, November 2004.
20. M. Wuttig and N. Yamada, "Phase-change materials for rewriteable data storage," Nature Materials, vol. 6, pp. 825-32, 2007.
21. B. Chen, et al., "Improved Time-of-Flight Technique for Measuring Carrier Mobility in Thin Films of Organic Electroluminescent Materials," Jpn. J. Appl. Phys., vol. 39, pp. 1190-1192, 2000.
22. J. B. Johnson, "The Schottky effect in low frequency circuits," Phys. Rev., vol. 26, pp. 71-85, 1925.
23. H. Nyquist, "Thermal agitation of electric charge in conductors," Phys. Rev., vol. 32, pp. 110-113, 1928.
24. W. Schottky, "Small-shot effect and flicker effect," Phys. Rev., vol. 28, pp. 74-103, 1926.
25. F. N. Hooge, "l/*f* noise is no surface effect," Phys. Lett., vol. 29 A, pp. 139, 1969.
26. S. Smith, "An Interesting Fourier Transform – 1/f Noise," http://www.dsprelated.com/showarticle/40.php
27. S. Ju, et al., "1/*f* noise of SnO2 nanowire transistors," Appl. Phys. Lett., vol. 92, pp. 243120, 2008.
28. P. E. Allen and D. R. Holberg, *CMOS Analog Circuit Design*, Oxford Unversty Press, 2002.
29. S. Brovelli, et al., "Ultraviolet free-exciton light emission in Er-passivated $SnO_2$ nanocrystals in silica," Appl. Phys. Lett., vol. 89, pp. 153126, 2006.
30. R. S. Decca, et al., "Photoinduced superconducting nanowires in GdBa2Cu3O6.5 films," Appl. Phys. Lett., vol. 73, pp. 120-122, 1998.

# 1/f Noise in Nanowires by Quantum Mechanics

**ABSTRACT**

The 1/f noise commonly observed in power measurements of circuit elements - capacitors, resistors, and inductors - is perhaps one of the oldest puzzles of contemporary physics. Simulations of 1/f noise made by a summation of Lorentzians for step changes of power in time, or by a Markov chain of such steps in a stochastic stationary process do indeed produce 1/f noise in the frequency domain, but lack a physical basis. The dramatic increase in 1/f noise in nanoelectronic circuit elements, and nanowires in particular suggest a physical basis may be found in the size effect of QM and even extended to submicron regions of ordinary circuit elements. QM stands for quantum mechanics. In nanowires, QM precludes atoms from the heat capacity necessary to conserve Joule heat by an increase in temperature. Instead, conservation proceeds by the creation of charge that produces a step change of power in time, the Fourier transform of which gives the 1/f noise spectrum in the frequency domain.

## 1. Introduction

The 1/f noise is commonly observed in power measurements of electronic circuits comprising capacitors, resistors, and inductors. Other processes in the natural world also display this behavior including stock prices and music suggest [1] a generic origin might exist, but no generally recognized physical explanation of 1/f noise has been proposed. Indeed, the ubiquity of 1/f noise is one of the oldest puzzles of contemporary physics.

Of interest is the origin of the 1/f noise in nanoelectronics, say in nanowires of tin oxide [2] having submicron diameters of 10-50 nm and lengths greater than about 10 microns. In 1925, Johnson and Nyquist discovered [3,4] electronic noise or white noise in vacuum tubes. White noise has a constant power spectrum generated by the thermal agitation of charges inside a resistor by itself without any applied voltage. In contrast, 1/f noise sometimes called pink noise differs in that under applied voltage the frequency f of the power spectrum is not constant, but rather increases as f is lowered, i.e., having a slope of -1 on a log-log plot.

Over the past 80 years, explanations of 1/f noise have proved [1] elusive. Schottky [5] proposed a mathematical model of exponentially decaying current pulse I caused by the release of electrons from the cathode of a vacuum tube, i.e., $I = Io \cdot e^{-bt}$, where Io is the initial step, b is the relaxation rate and t is time. For a train of such pulses at an average rate, the power spectrum is of the Lorentzian form which is constant near f = 0 and for large f is proportional to $1/f^2$ with a narrow transition region where the power spectrum resembles that of 1/f noise. Later, Bernamont [6] pointed out only a superposition of such processes with a variety of relaxation rates yield 1/f noise for a reasonable range of frequencies.

Given that 1/f noise as a stochastic stationary process has a mean and variance that do not change over time, Erland et al. [1] showed observations of such processes may be modeled as a Markov chain in which one observation depends stochastically only on the immediately previous one.

To date, mathematical models [1,3-6] are presented that simulate 1/f noise,

> But what is the physical basis that underlies the mathematical models of 1/f noise?

In this regard, Hooge [7,8] in an effort to systematically collect data on l/f noise from the literature proposed,

$$\frac{S_R}{R^2} = \left(\frac{S_I}{I^2}\right)_V = \frac{\alpha}{fN} \qquad (1)$$

where, $S_R$ and $S_I$ are the spectral power density of resistance R and current I, f is the frequency at which the noise is measured, N is the total number of free electrons, and α is an empirical dimensionless constant. Many years later, Vandamme and Hooge [9] concluded there is no theory behind (1). The relation normalizes [8] the relative noise to one electron. The only assumption is that whatever the electrons do, they do it independently.

Hooge [8] noted the difficulty of reconciling LFN with the residence time of the electron in the size of the sample. LFN stands for low frequency noise. If 1/f noise is a summation [1,5,6] of Lorentzians having long characteristic times t >> 1s, the electrons must stay in the sample much longer than a few seconds. However, in a sample with a length of 1 cm, an electron only stays about 0.1 s as its diffusion coefficient D is of order 0.001 $m^2/s$. For nanowires, the residence time of the electron is far shorter, yet LFN is still observed.

> How can electrons that stay in the nanowire for such short times produce LFN at frequencies below 1 Hz?

Hooge [8] argued that the 1/f noise is caused by lattice scattering of electrons, but this is unlikely because phonon frequencies are far higher than the low frequencies of 1/f noise. The number N of free electrons in (1) therefore has nothing to do with 1/f noise.

Nevertheless, 1/f noise theories based on electron scattering continued. Handel [10] proposed a quantum

1/f theory that claimed LFN is caused by low-frequency photons that are absorbed or emitted in each scattering event. However, the half-wavelength of LFN is far longer than the dimensions of the samples, and therefore QED at least, cannot be invoked as the mechanism by which the EM energy in scattering of electrons can produce 1/f noise. QED stands for quantum electrodynamics and EM for electromagnetic. The van Vliet [11] claim that the absence of an EM confinement mechanism to create the low frequency photons is not a serious problem must simply be rejected. It suffices to say the experimental results cited by Hooge [8] did not support the quantum 1/f theory.

**2. Scope**

In this paper, 1/f noise is hypothesized to be a consequence of the QM restriction that Joule heat cannot be conserved by an increase in temperature of the nanowires. Generally, the scope is nanoelectronics, although extensions may be made to submicron regions of ordinary electronic circuit elements. No attempt is made to provide a generic explanation of 1/f noise in areas such as stock prices and music [1] unless a connection can somehow be made to the dissipation of electrical current by Joule heat. .

**3. Purpose**

The purpose of this paper is to support the hypothesis that 1/f noise is a QM effect that occurs naturally upon passing current through a nanoelectronic circuit element, specifically a nanowire.

**4. Methodology**

QM in the 1/f noise of nanowires by the creationof charge finds similarity with nanoelectronics by Prevenslik [12] including memristors and the Ovshinsky Effect in PCRAM devices, the latter related to the creation of charge that locally reduces the resistance of the GST film to allow encoding of information based on difference in resistance. QM in combination with QED avoids the difficulties cited by Hooge [8] of producing LFN with long residence times in small samples, the methodology of which is described as follows.

1. QM precludes the atoms in nanostructures from having the heat capacity to conserve the Joule heat ($P = I^2R$) by an increase in temperature, and therefore QED is invoked to induce the conversion of Joule heat to photons within the nanowire.

2. The QED photons are created because of the EM confinement that is naturally provided by TIR under the high surface to volume ratio of the nanowire. TIR stands for total internal reflection. What this means is the Joule heat is almost totally absorbed in the surface of the nanowire that is the TIR mode of the QED photons, i.e., the QED photon provides its own EM confinement.

3. Charge is created in the nanowire by Einstein's photoelectric effect because the Planck energy of the QED photons created is beyond the ultraviolet. The charge in the form of excitons (holes and electrons) is created promptly as the current enters the nanowire.

4. The nanowire resistance drops abruptly that under a constant applied voltage causes the current to increase. The drop in resistance is caused by the increased conductance from the excitons in the nanowire. Power dissipated through the nanowire undergoes a steady step change. Repetitive Markov steps are not necessary.

5. The step change in power occurs abruptly because of the high mobility of the excitons and the short length of the nanowires. The shape of the steady power pulse may vary, but approximates the perfect step.

6. The Fourier transform (FT) of step change in power gives the 1/f slope in the frequency domain with variations thereof depending on the exact shape of the step. Hooge's [8] difficulty with long residence times in small samples is overcome because the FT naturally produces LFN from the step change in power.

**5. Theory**

5.1 QM Restrictions

The QM restrictions on the thermal energy of an atom in a nanowire depends on the EM confinement as given by the Einstein-Hopf [13] relation for the Planck energy E of the atom as a harmonic oscillator,

$$E = \frac{\frac{hc}{\lambda}}{\exp\left(\frac{hc}{\lambda kT}\right) - 1} \qquad (2)$$

where, h is Planck's constant, c the speed of light, k Boltzmann's constant and T absolute temperature. The Planck energy E with wavelength λ is shown in Fig. 1.

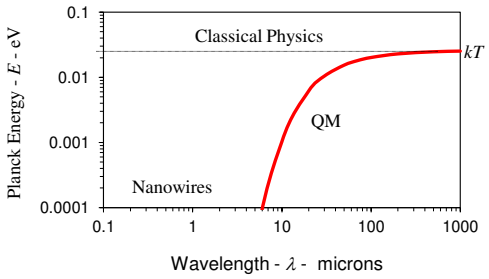


Fig. 1 Atom as a Harmonic Oscillator at 300 K

Classical physics allows the atom to have heat capacity at the nanoscale. QM differs by allowing the atom to only have heat capacity for λ > 50 microns. Unlike classical physics, QM precludes the atom from conserving absorbed EM energy at the nanoscale by an increase in temperature.

5.2 TIR Confinement

Nanowires lack of heat capacity by QM precludes conservation of Joule heat by an increase in temperature. However, the absorbed heat must still be conserved, and therefore conservation is proposed to proceed during TIR confinement by creating QED induced radiation *inside* the nanowire.

TIR has a long history beginning with Tyndall in 1870 who observed if the refractive index of a body is greater than that of the surroundings, absorbed light is trapped at its surface. However, TIR in nanostructures has an important significance and need not be limited to light absorption. Unlike the macro world, nanostructures have high surface to volume ratios, and therefore heat from any EM source (lasers, molecular collisions, Joule heat, etc.) is absorbed almost totally in the nanostructure surface. Since the nanostructure surface corresponds to the TIR wave function of the absorbed EM energy, QED induces the absorbed heat to undergo the spontaneous creation of photons *inside* the nanostructure. TIR confinement is not permanent, but rather sustains itself only during the absorption of EM energy, i.e., absent EM energy absorption, there is no TIR confinement and QED radiation is not created.

Similar to creating QED photons of wavelength $\lambda$ by supplying EM energy to a QM box with sides separated by $\lambda/2$, the absorbed EM energy is frequency up-converted to the characteristic dimension $D_C$ of the nanostructure. The QED photon energy E and frequency f are

$$E = hf,\ \ f = \frac{c}{\lambda},\ \ \lambda = 2nD_c \tag{3}$$

where, n the refractive index. For a nanowire, $D_C$ is the diameter d.

5.3 QED Photons and Rate

Classical heat transfer conserves absorbed heat by an increase in temperature, but is not applicable to nanowires because of QM restrictions on heat capacity. Instead, the power P of the Joule heat pulse is conserved by creating number $N_P$ of QED photons *inside* the nanowire. The rate of QED photon creation is,

$$\frac{dN_P}{dt} = \frac{\eta P}{E} = \frac{\eta I^2 R}{E} \tag{4}$$

where, t is time. Only a fraction $\eta$ of the power P creates excitons, the remainder (1-$\eta$) is lost to the surroundings. By the photoelectric effect, the rate $dN_{ex}/dt$ of excitons created, each comprising an electron and hole is,

$$\frac{dN_{ex}}{dt} = Y\frac{dN_P}{dt} = \frac{\eta YP}{E} \tag{5}$$

where, Y is the exciton yield. Unlike the probabilistic creation of excitons from an external source of radiation having Y<< 1, photons are created by the QED conservation of EM energy in the nanowire at Y = 1.

5.4 QED Photons, Excitons, and Charge

The creation of charge carriers in the nanowire requires QED photons having Planck energy greater than the energy Eg of the band gap, E > Eg. The excitons comprising electron-hole pairs form as the QED photons produce an electron charge $Q_E$ and positive charged hole $Q_H$ that separate under the field F.

The nanowire resistance R depends on the conductivity $\sigma$ and resistivity $\rho$ given by the number density of electrons $Q_E$ and holes $Q_H$,

$$\sigma = \frac{1}{\rho} = e\left(Q_E\mu_E + Q_H\mu_H\right) \tag{6}$$

where, $\mu_E$ and $\mu_H$ are the electron and hole mobility.

5.5 QM Charging

Excitons form in proportion to the fraction $\eta$P of QED photons absorbed and the yield Y. The $Q_H$ and $Q_E$ are the number of created positive charged holes and negative charged electrons. Under the high electric field F, the charge carriers separate to form independent charges that rapidly move to opposite polarity terminals.

The rate $\eta$YP/E of excitons created is balanced by the electron $Q_E$ and hole $Q_H$ charges lost in moving toward opposite polarity terminals by their respective $\mu_E$ and $\mu_H$ mobility in the electric field F.

$$\frac{dQ_E}{dt} = \frac{\eta YP}{E} - Q_E\frac{\mu_E F}{L} \tag{7}$$

$$\frac{dQ_H}{dt} = \frac{\eta YP}{E} - Q_H\frac{\mu_H F}{L} \tag{8}$$

Both exciton electron and hole equations are identical allowing the hole response to represent that of the electron for the same mobility. Taking F = Vo/d,

$$\frac{dQ_H}{dt} = \frac{\eta YP}{E} - \frac{\mu_H V_o}{L^2}Q_H \tag{9}$$

The hole $Q_H$ solution is given by,

$$Q_H = \frac{L^2}{\mu_H V_o} * \tag{10}$$

$$* \left\{\frac{\eta YP}{E}\left[1 - e\left(-\frac{\mu_H V_o}{L^2}t\right)\right] + \frac{\mu_H V_o}{L^2}Q_{H0}e\left(-\frac{\mu_H V_o}{L^2}t\right)\right\}$$

On average, the holes and electrons are centered in the nanowire and need to move L/2 to reach the voltage terminals, the resistance R is,

$$R = \rho\frac{L}{2A} = \frac{L}{2A}\frac{1}{e(\mu_E Q_{EO} + \mu_H Q_{HO})/AL} \approx \frac{L^2}{4e\mu_H Q_H} \tag{11}$$

The resistivity $\rho$ assumes $\mu_E = \mu_H$ with the same number $Q_E$ of electrons as the $Q_H$ holes. Note $\rho$ requires units of per unit volume, where volume is AL and A is the nanowire area. The initial resistance $R_o$ gives the initial number $Q_{HO}$ of holes,

$$Q_{HO} = \frac{L^2}{4e\mu_H R_O} \tag{12}$$

The current I is,

$$I = \frac{V_o}{R} \tag{13}$$

**6. Analysis**

Comparisons of QED theory with experimental data [2] for 1/f noise are made for $SnO_2$ nanowires. The assumed mobility $\mu_H$ = 0.0172 $m^2$/V-s, is higher than the typical range of 0.004 to 0.01 $m^2$/V-s. Wire diameters d ranged between 10-50 nm with a length L > 10 microns. The initial resistance Ro = $25x10^6$ ohm was taken from (Fig. 1(a) of [2]) for Vo = 2.5 volts at a current I = 0.1 μA. The power P ranged from 1 to 3 μW.

The Planck energy E and rate $dN_p/dt$ of QED photons created at power of 1 and 3μW shown in Fig. 2. The fraction η = 1 assumes there is no loss of QED radiation to the surroundings. The exciton velocity $\mu_H Vo/L$ and rise time of power pulse are shown in Fig. 3. The initial $QH_O$ and final QH number of holes in the nanowire is given in Fig.4.

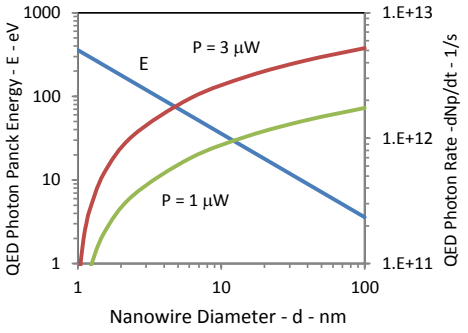


Fig. 2 QED Photon Energy and Rate

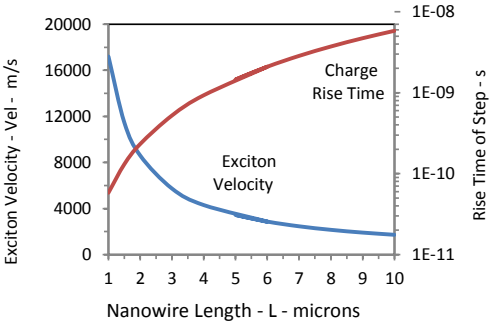


Fig. 3 Exciton Velocity and Rise time of Power Pulse

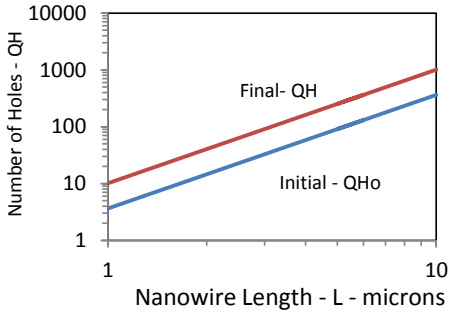


Fig. 4 Initial and Final Number of Holes

The charge creation as the current enters the nanowire is abrupt, i.e., the time constant from (10) is less than 6 ns at lengths L < 10 microns. Indeed, the time for the charge to traverse the full wire length is less than 10 ns for lengths L < 10 microns as shown in Fig. 3 What this means is the step in charge may be treated as a step function in power.

The FT of a unit step change of power in the time domain gives the 1/f spectrum in the frequency domain,

$$G(2\pi f) = \int_{-\tau/2}^{\tau/2} 1e^{-j\omega t}\, dt = \frac{\sin(\pi f \tau)}{\pi f} \qquad (14)$$

as illustrated to have the same -1 slope as 1/f and not $1/f^2$ in Fig. 5.

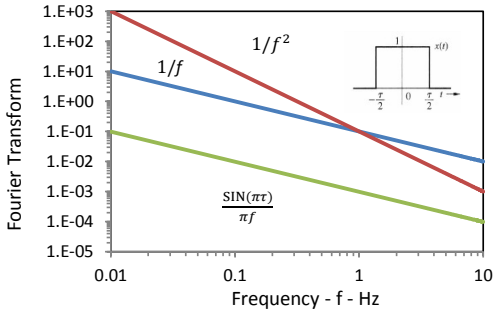


Fig. 5 FT - Step Change of Power in Frequency Domain

**7. Discussion**

7.1 Physical Markov Process

In nanowires, QED induces the Joule heat to produce a train of step changes in QED power each of which decay in the otherwise macroscopic circuit. In this way, a Markov process is formed with each step change in power effectively depending on the previous one.

However, stochastic Markov processes may not be necessary. Indeed, the 1/f spectrum may be considered deterministic and caused by the FT of a steady step change in power produced by simply passing current through the nanowire. .

7.2 Fourier Transforms

The FT of power [14] as an arbitrary step function $t^a$ in time gives $f^{-(a+1)}$ in the frequency domain, where a is a rational number not necessarily an integer. For a = 0, the FT of a step is 1/f and as depicted in relation to the reference 1/f. Clearly, the FTs of $t^a$ in [14] for a = +0.5 and -0.25 are not sufficient to bracket the 1/f noise. Numerical FTs of $t^a$ for a = -1.1 and – 0.9 are required.

7.3 Crystal Damage

Hooge [8] notes damaging the crystal by mechanical stress or by irradiation strongly increases the l/f noise. The electron concentration and the mobility hardly change; but the noise increases by orders of magnitude. The first explanation is that the defects act as

generation recombination centers that in some unexplained way generate l/f noise. If correct, 1/f noise in damage is a fluctuation in the number of free carriers or number noise. However, the defects may act as scattering centers and generate l/f noise according to fluctuations in mobility. Generally, damaged crystals are thought to be number rather than mobility noise.

Perhaps the difficulty in explaining the dramatic increase in 1/f noise upon crystal damage is that electrons and their mobility have nothing to do with 1/f noise. The literature does not suggest that excitons are created by mechanical stress or irradiation, yet low levels of QED induced charge may be induced from local heating of submicron regions. Heat is produced in damaging the crystal by any means, and therefore likely excitons formed from QED photons created in conserving local heating of submicron regions. Subsequently, the local resistance was lowered thereby increasing the 1/f noise upon passing current through the damaged crystal.

The problem is Hooge [8] and others never considered the possibility that charge was created in the damaged crystal. Electrons cannot explain 1/f noise.

7.4 Number of Carriers

QED theory asserts only a small number of holes need be created to explain 1/f noise in $SnO_2$ nanowires. For carbon nanotubes (CNTs) having length 600 nm, 1/f noise is caused [15] by about 40 holes in the ON state that decrease in the OFF state. Fig. 4 shows a comparable number of holes for the final and initial conditions of the 1-micron long $SnO_2$ nanowire.

7.5 External Step Change

The hypothesis that 1/f noise is caused by a step change in power induced by QED charge may be easily verified by applying an external step change in voltage to a nanowire. Perhaps this has already been done.

**8. Summary and Conclusions**

1. Charge continuously created in nanowires by QM is consistent with a Markov chain of step changes in power in the manner of a stochastic stationary process.

However, a Markov chain may not be necessary as a step change in power occurs naturally upon passing current through nanowires.

2. The physical process that underlies the 1/f spectrum in nanowires begins with the QED induced conservation of Joule heat by non-thermal EM radiation instead of by an increase in temperature.

The EM radiation having the Planck energy necessary to create excitons by the photoelectric effect momentarily lowers the nanowire resistance causing an increase in the current to produce a step change in QED power.

In the manner of producing LFN by imposing a step change of current or voltage in an ordinary circuit element, the 1/f noise is produced as the step in QED power is sustained by current through the nanowire.

3. Damaged crystal show increased 1/f noise because heat is locally produced that by QED theory creates charge in the form of excitons that lower the resistance of the crystal, thereby increasing the 1/f noise.

4. 1/f noise in SnO2 nanowires and CNTs depends on the creation of a small number of holes.

5. Imposing a step change of voltage or current in a nanowire is expected to increase the 1/f noise, thereby verifying the hypothesis of QED theory that charge is produced upon passing current through a nanowire.

**References**

[1] S. Erland, P. E. Greenwood, L. M. Ward, “1/f noise” is equivalent to an eigenstructure power relation,” EPL, 95 (2011) 60006.
[2] S. Ju, et al., ”1/f noise of SnO2 nanowire transistors,” Appl. Phys. Lett., Vol 92 (2008) 243120.
[3] J.B. Johnson, “The Schottky effect in low frequency circuits,” Physical Review 26 (1925), 71–85.
[4] H. Nyquist, “Thermal agitation of electric charge in conductors”, Phys. Rev., Vol. 32 (1928) 110-113.
[5] W. Schottky, “Small-shot effect and flicker effect,” Physical Review 28 (1926), 74–103.
[6] J. Bernamont, “Fluctuations de potential aux bornes d’un conducteur metallique de faible volume parcouru par un courant,” Ann. Physik (Leipzig) 7 (1937), 71.
[7] F. N. Hooge, “l/f noise is no surface effect,” Phys. Lett., 29 A (1969) 139.
[8] F. N. Hooge, “1/f Noise Sources,” IEEE Trans. Elec. Dev., 41 (1994) 1926.
[9] L. K. J. Vandamme, F. N. Hooge, “What Do We Certainly Know About 1/*f* Noise in MOSTs?” ,” IEEE Trans. Elec. Dev., 55 (2008) 3070.
[10] P. J. Handel, “1/ f noise-an infrared phenomenon,” Phys. Rev. Lett., 34 (1975) 1492.
[11] C. M. van Vliet, “Further comments on Handel’s theories of quantum l/f noise,” Physica, A150 (1988) 244.
[12] T. Prevenslik, “Quantum Mechanics and Nanoelectronics,” ICMON 2011 : International Conference on Microelectronics, Optoelectronics, and Nanoelectronics, Venice, November 28-30, 2011
[13] A. Einstein, L. Hopf, “Statistische Untersuchung der Bewegung eines Resonators in einem Strahlungsfeld,” Ann. Physik, 33 (1910) 1105.
[14] S. Smith, ”An Interesting Fourier Transform – 1/f Noise” http://www.dsprelated.com/showarticle/40.php
[15] Y. M. Lin, et al., “Low-Frequency Current Fluctuations in Individual Semiconducting Single-Wall Carbon Nanotubes,” Nano Letters, 6 (2006) 930.

US 20030178616A1

(19) **United States**

(12) **Patent Application Publication** (10) **Pub. No.: US 2003/0178616 A1**

**Prevenslik** (43) **Pub. Date: Sep. 25, 2003**

(54) **CAVITY QED DEVICES**

(76) Inventor: **Thomas V. Prevenslik**, Youngwood, PA (US)

Correspondence Address:
**Thomas V. Prevenslik**
**PO Box 515**
**Youngwood, PA 15697 (US)**

(21) Appl. No.: **10/179,641**

(22) Filed: **Jun. 25, 2002**

**Related U.S. Application Data**

(60) Provisional application No. 60/366,855, filed on Mar. 25, 2002.

**Publication Classification**

(51) **Int. Cl.**[7] ..... **H01L 29/06**; H01L 31/0328; H01L 31/0336; H01L 31/072; H01L 31/109

(52) **U.S. Cl.** ..... **257/14**

(57) **ABSTRACT**

QED devices emitting EM radiation are disclosed comprising structures in microscopic cavities. Steady EM radiation is produced from structures essentially permanently separated from the cavity walls, while transient EM radiation occurs by providing means to cause the temporary separation of the structures from the cavity walls. At ambient temperature, the EM radiation from atoms in structures not separated from the cavity walls is emitted at IR frequencies. However, the IR radiation is suppressed from atoms in structures separated from the cavity walls because the cavities have higher EM resonant frequencies. To conserve EM energy, the suppressed IR radiation from the structures is spontaneously emitted and combines at the QED cavity surfaces to collectively produce VUV light, the process called cavity QED induced VUV light. QED devices are disclosed utilizing cavity QED induced VUV light to excite the atoms and molecules on the cavity surfaces to produce VIS light, electrons, and ions.

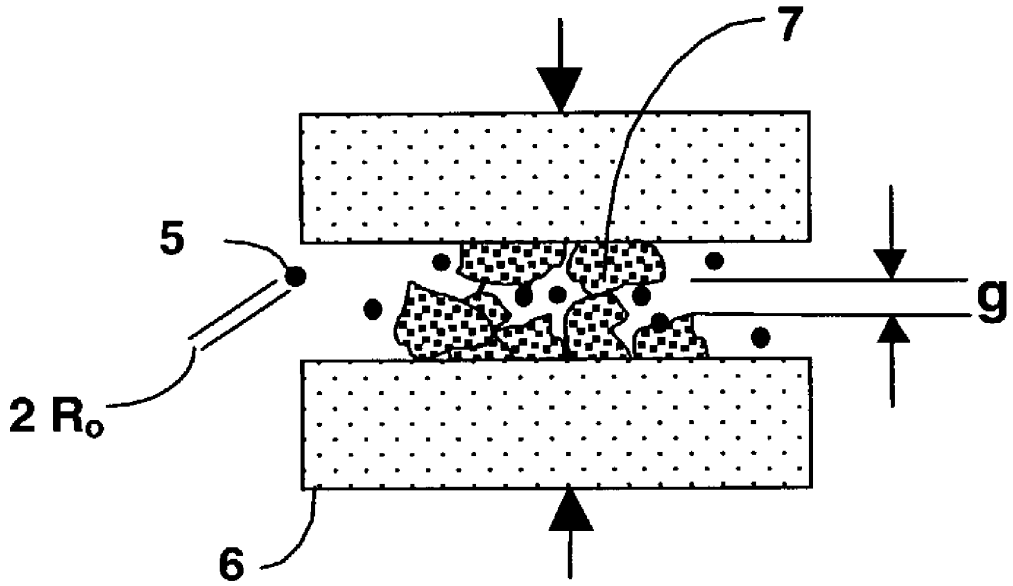

Patent Application Publication Sep. 25, 2003 Sheet 1 of 9 US 2003/0178616 A1

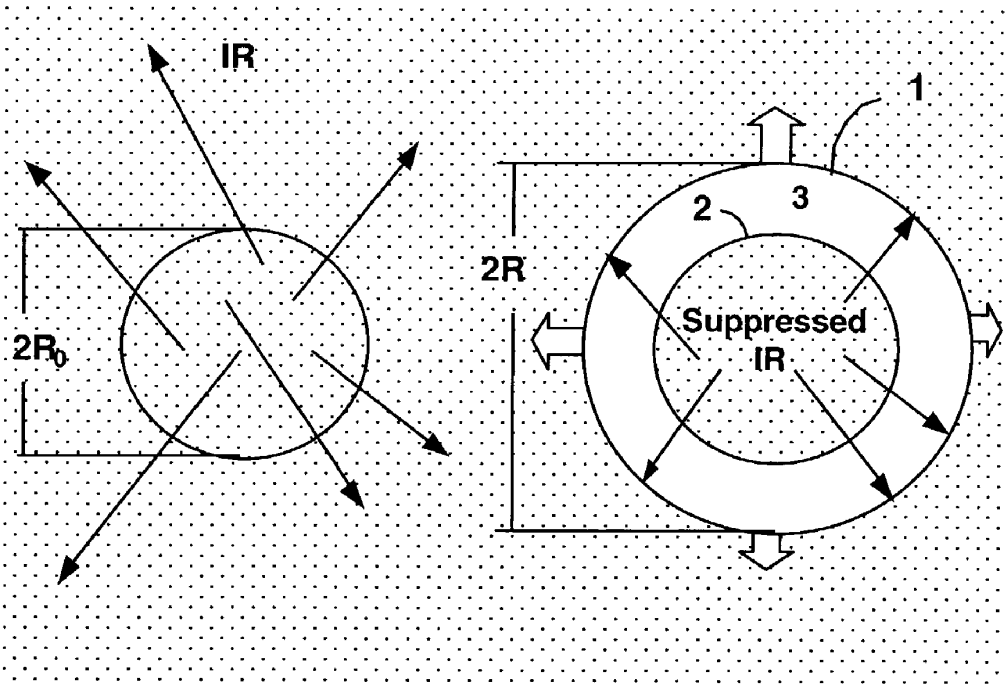


FIG. 1




FIG. 2

Patent Application Publication Sep. 25, 2003 Sheet 2 of 9 US 2003/0178616 A1

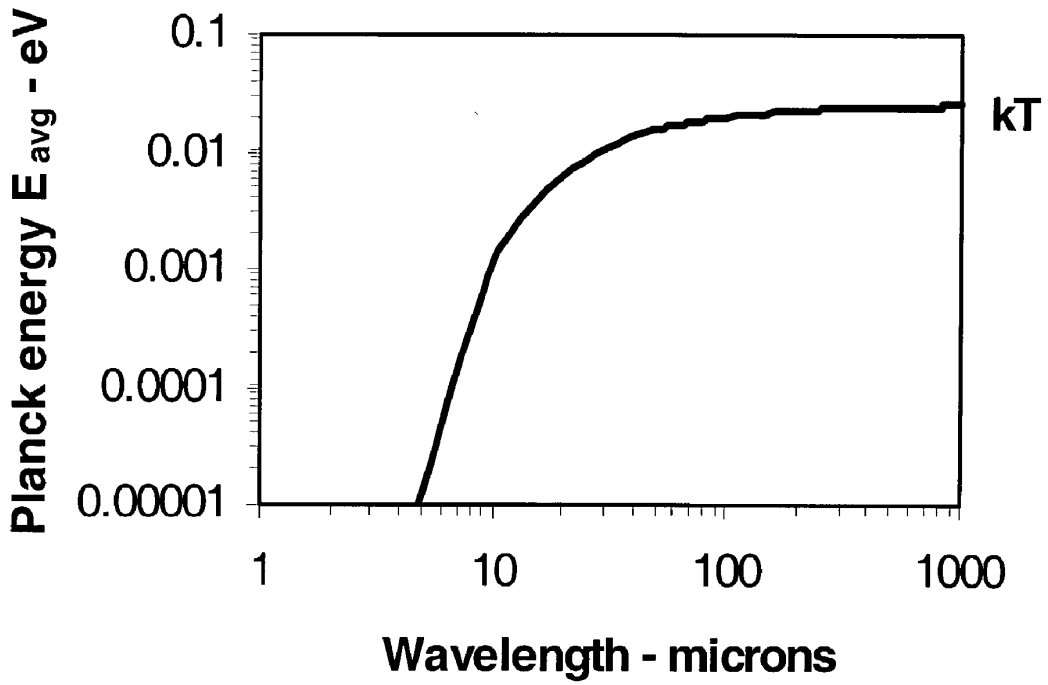


FIG. 3

Patent Application Publication Sep. 25, 2003 Sheet 3 of 9 US 2003/0178616 A1

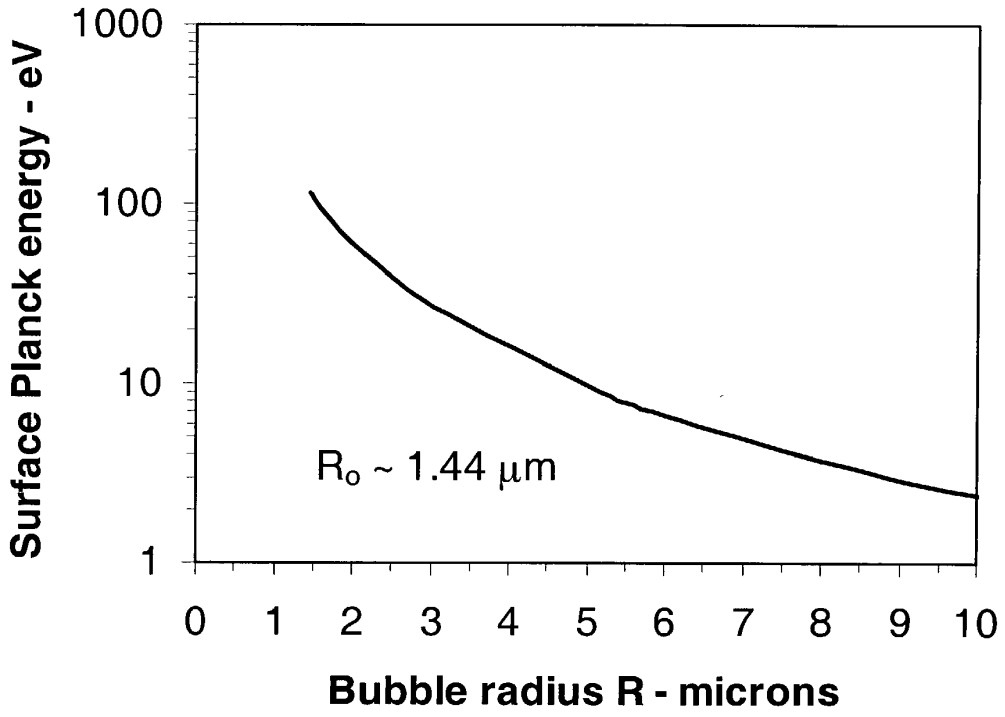


FIG. 4

Patent Application Publication Sep. 25, 2003 Sheet 4 of 9 US 2003/0178616 A1

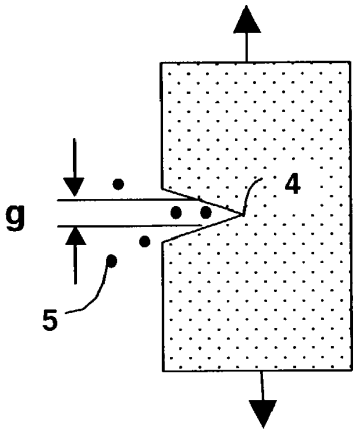


FIG. 5

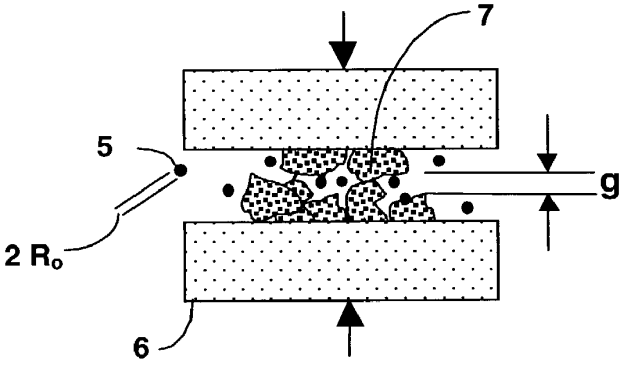


FIG. 6

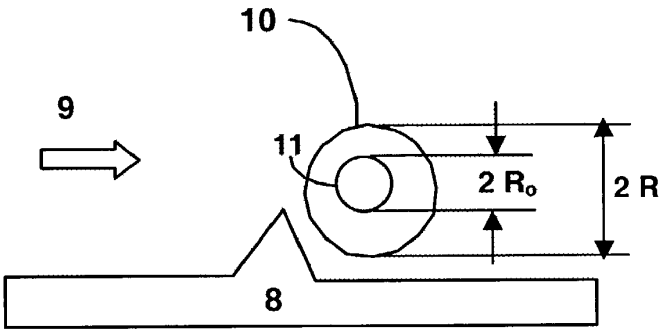


FIG. 7

Patent Application Publication Sep. 25, 2003 Sheet 5 of 9 US 2003/0178616 A1

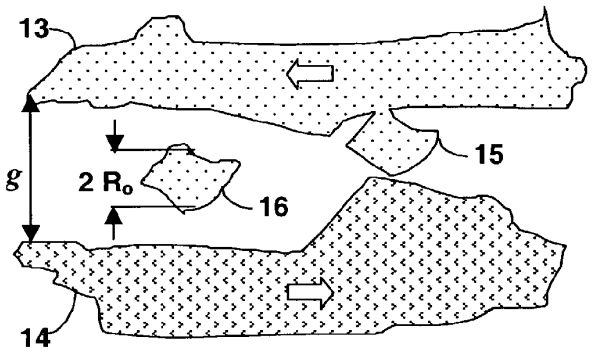


FIG. 8

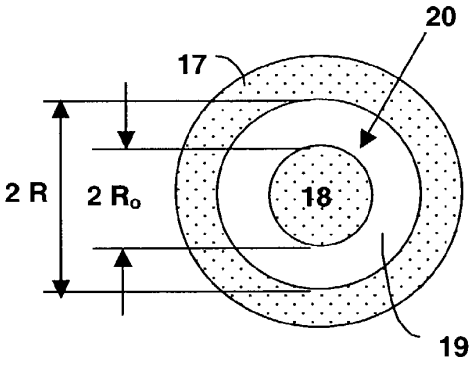


FIG. 9

FIG. 10

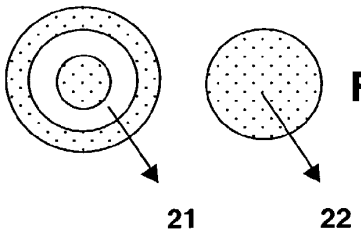


FIG. 11

Patent Application Publication Sep. 25, 2003 Sheet 6 of 9 US 2003/0178616 A1

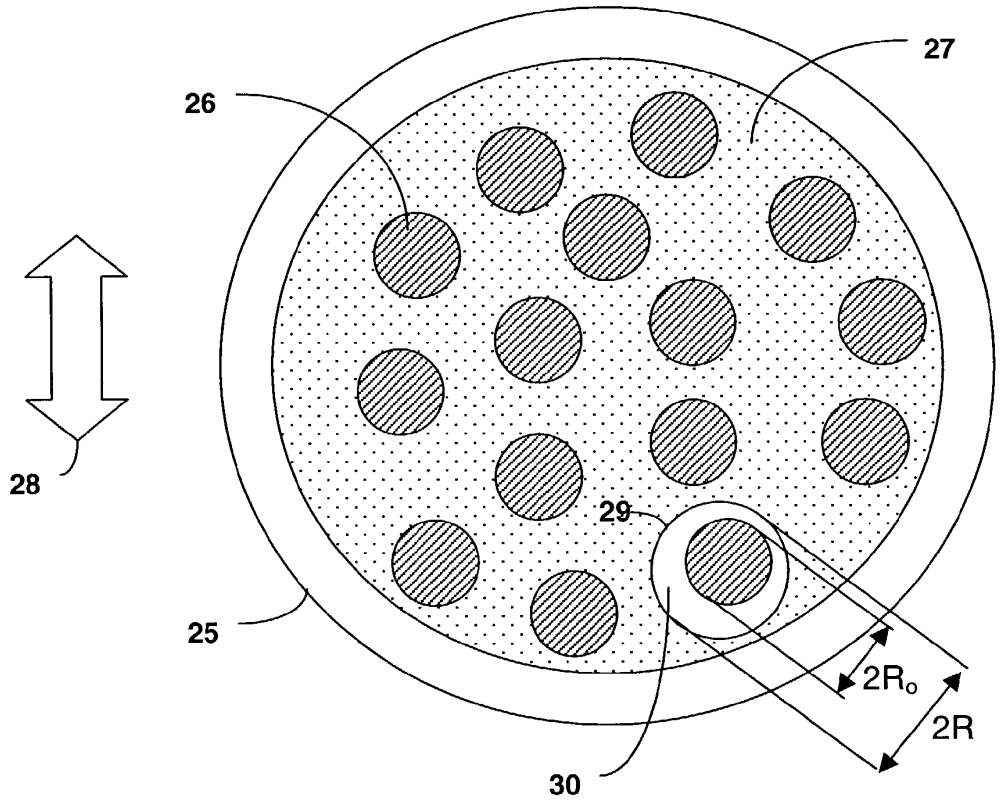


FIG. 12

Patent Application Publication Sep. 25, 2003 Sheet 7 of 9 US 2003/0178616 A1

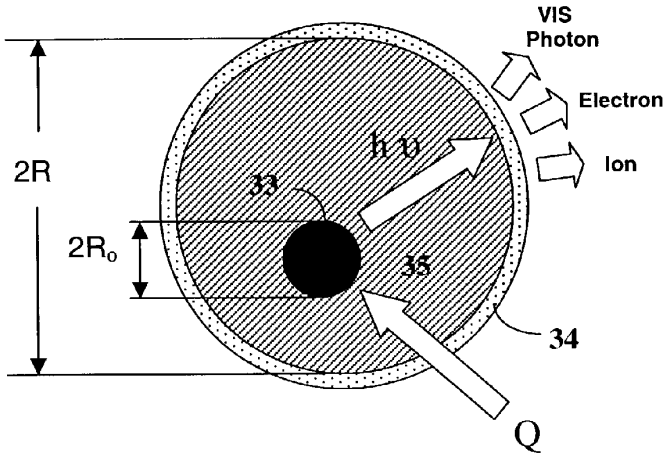


FIG. 13

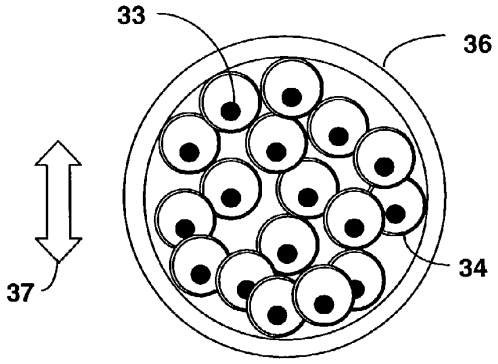


FIG. 14

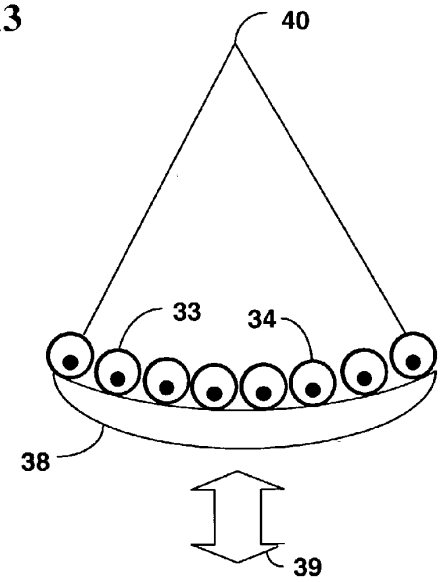


FIG. 15

Patent Application Publication Sep. 25, 2003 Sheet 8 of 9 US 2003/0178616 A1

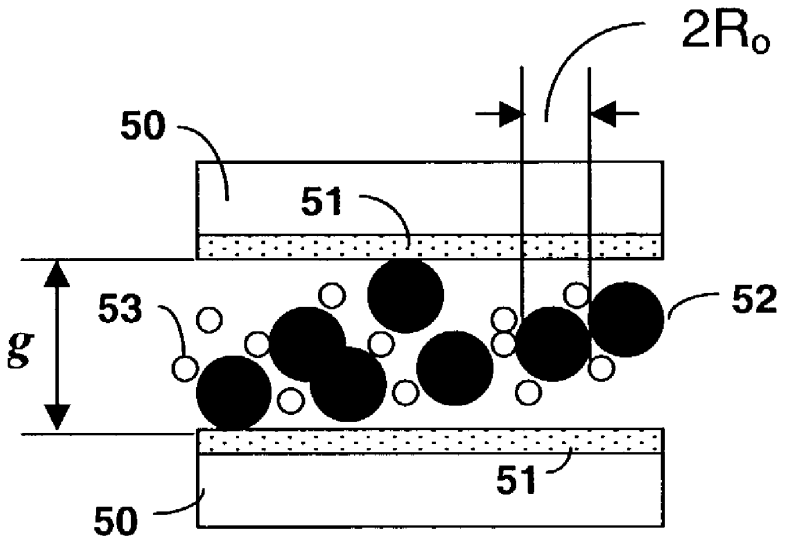


FIG. 16

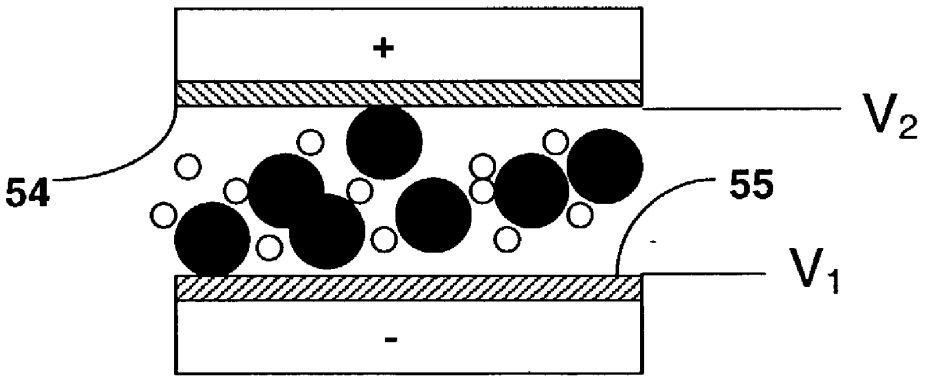


FIG. 17

Patent Application Publication Sep. 25, 2003 Sheet 9 of 9 US 2003/0178616 A1

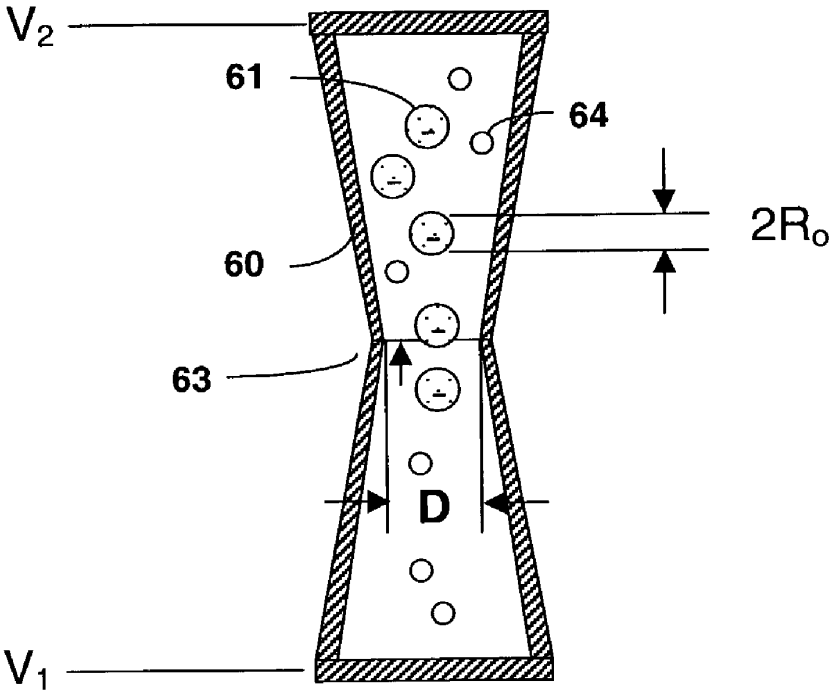


FIG. 18

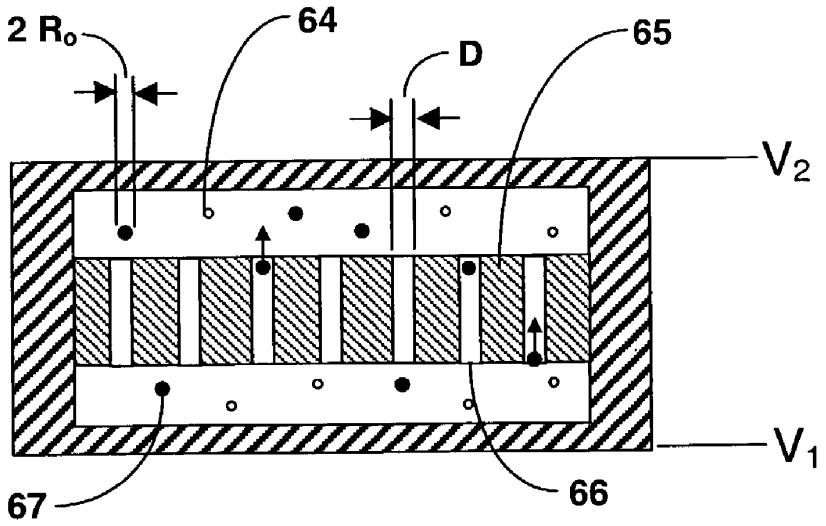


FIG. 19

US 2003/0178616 A1 Sep. 25, 2003



# CAVITY QED DEVICES

## CROSS-REFERENCE TO RELATED APPLICATIONS

[0001] Pursuant to 35 USC §119(e), the timely filing of this non-provisional patent application claims the benefit of provisional patent:

[0002] Application No. 60/366,855

[0003] Filing Date: Nov. 26, 2001

[0004] Applicant: Thomas V. Prevenslik

[0005] Title of Invention: Cavity QED induced photoelectric effect

## FEDERALLY SPONSORED RESEARCH OR DEVELOPMENT

[0006] Not Applicable.

## COMPACT DISK REFERENCES

[0007] Not Applicable.

## SUMMARY

[0008] Quantum electrodynamics (QED) devices are disclosed that spontaneously emit electromagnetic (EM) radiation, and specifically infrared (IR) radiation at ambient temperature from structures within microscopic cavities, the IR radiation combining to produce vacuum ultra violet (VUV) light at the cavity surfaces, the process called cavity QED induced VUV light. QED devices are disclosed that utilize the VUV light to excite cavity surfaces to produce electrons, ions, and visible (VIS) photons. The QED devices include:

[0009] (1) Ultrasonic VIS Lamp

[0010] (2) Microsphere Light Source

[0011] (3) Thermal Laser and Thermoelectric Battery

[0012] (4) Particle Filter

[0013] The preceding QED devices are illustrative examples, and do not in any way limit the generality of cavity QED induced VUV light. The disclosure will permit those skilled in the art to devise many other QED devices utilizing cavity QED induced VUV light.

## BACKGROUND OF THE INVENTION

[0014] 1. Field of the Invention

[0015] The present invention is related to the field of QED devices emitting EM radiation. Specifically, the invention relates to the field of QED devices that induce the spontaneous emission of IR radiation from atoms in structures within microscopic cavities, the IR radiation finding origin in the thermal kT energy of the atoms at ambient temperature.

[0016] 2. Related Art and Present Invention

[0017] Related art to the present invention may be summarized in terms of unexplained observations of VIS photons, electrons, and ions in diverse physical phenomena. These phenomena are commonly regarded as mysterious because they do not occur at high temperature or in the presence of external sources of EM energy where they are readily explained, but rather occur at ambient temperature absent external sources of EM energy. Heretofore, explanations have been proposed to explain these phenomena, but have never included cavity QED induced VUV light. Alternatively, the present invention is the first disclosure that cavity QED induced VUV light is the common source of EM energy in these diverse phenomena by which VIS photons, electrons, and ions are produced.

## DESCRIPTION OF RELATED ART

[0018] Diverse physical phenomena producing VIS photons, electrons, and ions at ambient temperature in related art include sonoluminescence, triboluminescence, flow electrification, static electricity, and atmospheric electricity.

[0019] In the drawings:

[0020] **FIGS. 1 and 2** are an illustration of the QED process of cavity QED induced VUV light operating in the nucleation of bubbles during the acoustic cavitation of liquid water, known in the prior art as sonoluminescence, heretofore an unexplained phenomenon;

[0021] **FIG. 3** is a graph showing the average Planck energy $E_{avg}$ of an atom represented by a harmonic oscillator as a function of the wavelength $\lambda$ of thermal kT energy at an ambient temperature of 300 K;

[0022] **FIG. 4** is a graph illustrating the Planck energy produced by cavity QED induced VUV light on the surface of the bubble wall of radius R from sonoluminescence in water;

[0023] FIGS. **5-11** illustrate how other physical phenomena in the related art may be explained by the cavity QED induced VUV light disclosed in the present invention. One such phenomenon is triboluminescence. **FIGS. 5 and 6** depict the emission of electrons and VIS light from the fracture and crushing of solids. **FIG. 7** depicts QED induced VUV light at play in flow electrification, known in prior art by the electrical charge buildup in jet fuel and automobile gasoline. **FIG. 8** shows the VUV light producing electrons in static electricity that has been unexplained since the early Greeks. FIGS. **9-11** illustrate stages in the QED induced VUV light process that produces the electrical charge in atmospheric electricity. It will become readily apparent to those versed in the art that the finding of QED induced VUV light is a discovery of fundamental importance in physics.

[0024] Sonoluminescence

[0025] Sonoluminescence is the production of coherent VIS light during the acoustic cavitation of water. Currently, sonoluminescence is thought produced by high temperatures caused by compression heating of bubble gases during collapse. However, except for traces of air and other non-condensable gases, the bubble gases are condensable water vapor. Water vapor in 2-phase equilibrium with the bubble walls maintains ambient temperature and vapor pressure as the bubble volume vanishes. Thus, high temperatures in bubble collapse do not occur and some mechanism other than high temperatures is necessary to explain sonoluminescence. The present invention produces sonoluminescence by cavity QED induced VUV light at ambient temperature. Sonoluminescence is prior art and not patentable, but QED

devices that rely on cavity QED induced VUV light to produce VIS light are novel and patentable.

[0026] **FIGS. 1 and 2** illustrate how cavity QED induced VUV light produces sonoluminescence. **FIG. 1** shows liquid water in a state of hydrostatic compression at ambient pressure P. A hypothetical spherical volume of radius Ro is depicted. At ambient temperature T, all water molecules in the continuum emit IR radiation having a long wavelength compared to the size of the hypothetical volume. If the liquid continuum is perturbed to produce a state of hydrostatic tension, a bubble nucleates as shown in **FIG. 2**. Because of surface tension S, the size of the bubble can not be less than a prescribed limit. Hence, the expanding liquid bubble wall **1** of radius R separates from a tightly bound spherical particle **2** of water molecules at liquid density, the particle depicted by the hypothetical radius $R_0=2S/P$. For water having a surface tension S of 0.072 N/m at atmospheric pressure, $R_0$~1.44 microns. The formation of the spherical particle is almost instantaneous and produces an annular gap **3** between the surfaces of the particle and bubble wall.

[0027] Prior to nucleation, the water molecules in the liquid continuum under hydrostatic compression emit $N_{dof}\times\frac{1}{2}$ kT of EM radiation, where k is Boltzman's constant, T is the absolute temperature, and $N_{dof}$ is the number of degrees of freedom. For water, $N_{dof}=6$. At ambient temperature, the EM radiation is emitted from the continuum at IR frequencies. But at the instant the particle separates from the bubble wall, the bubble is a 3-dimensional QED cavity having a high EM resonant frequency that suppresses the low frequency IR radiation from the water molecules in the particle.

[0028] Generally, suppressed radiation by cavity QED occurs as the frequency of the radiation emitted from the atoms within a cavity is lower than the EM resonant frequency of the cavity (for example, see Harouche and Raimond, "Cavity quantum electrodynamics", *Scientific American*, 1993, pp. 54-62). Simply stated, the only EM radiation that can stand in the bubble is required to have a half wavelength $\frac{1}{2}\lambda$ less than the bubble diameter 2R, where, R is the bubble radius. Thus, the resonant wavelength $\lambda_c$ is, $\lambda_c=4R$. Conversely, EM radiation is suppressed for $\lambda>\lambda_c$. However, the bubble surface is required to be highly reflective to achieve the optical quality for suppressing IR radiation by cavity QED. Water is opaque (and highly reflective) at IR wavelengths $\lambda>3$ microns. But this condition is nicely satisfied in sonoluminescence, as the bubble nucleates at a radius $R\sim R_0$ having a resonant IR wavelength $\lambda_0=4\ R_0\sim 6$ microns where water is highly reflective.

[0029] The amount of thermal kT energy suppressed at ambient temperature is given by the harmonic oscillator and depends on the wavelength $\lambda$ of the IR radiation. **FIG. 3** shows the average Planck energy $E_{avg}$ at ambient temperature to only be significant at IR wavelengths $\lambda>10$ microns, saturation occurring at kT~0.025 eV for $\lambda>100\ \mu$m. About 4% of the available thermal kT energy is contained at $\lambda<10$ microns, and therefore if the particle radius $R_0<\frac{1}{4}\lambda\sim 2.5$ microns at the instant of separation, the IR radiation suppressed is greater than 96% of the available thermal kT energy.

[0030] Provided the spherical particle of water molecules has a radius $R_0<2.5$ microns, the suppressed IR energy $U_{IR}$ is,

$$U_{IR} < \frac{4\pi}{3} R_0^3 \Psi \tag{1}$$

[0031] where, $\Psi$ is the EM energy density, $\Psi\sim N_{dof}\times\frac{1}{2}$ $kT/\Delta^3$ and $\Delta$ is the spacing between water molecules at liquid density, $\Delta$~3.1 angstroms.

[0032] Suppressed IR radiation is a loss of EM energy that is conserved by the spontaneous emission of IR radiation, the spontaneous emission absorbed by the bubble surface because of its high optical quality provided by the water molecule at IR frequencies. But the annular gap is resonant at VUV frequencies, and therefore the Planck energy in the gap increases with frequency from the IR to the VUV. The Planck energy in the gap is reduced because of the leakage of photons in the VIS, but does not detract from the production of VUV light. In this way, sonoluminescence produces VUV light in the annular gap from the cavity QED induced spontaneous emission of IR radiation at ambient temperature.

[0033] During spontaneous emission, the IR energy accumulates as multi-IR photon energy at the cavity radius R. If all the available EM energy $U_{IR}$ suppressed during nucleation is conserved with the Planck energy E of the surface molecules at bubble radius R,

$$E = \frac{N_{dof}}{6}\left(\frac{R_0}{R}\right)^2\left(\frac{R_0}{\Delta}\right)kT \tag{2}$$

[0034] At T~300 K and a particle radius $R_0$~1.44 microns, the Planck energy E accumulated by multi-IR photons at radius $R\sim R_)$ is about 120 eV and decreases with increasing radius as shown in **FIG. 4**.

[0035] In sonoluminescence, the coherent VIS light observed from bubbles in water is generally not thought produced by photoluminescence of the water by VUV radiation, but rather as Ar*OH excimers decompose in the high pressures developed in bubble collapse. In cavity QED induced sonoluminescence, the excited OH states necessary to form the Ar*OH excimers are produced following the dissociation of water molecules in the annular gap into hydronium $H_3O^+$ and hydroxyl $OH^-$ions by cavity QED induced VUV light.

[0036] The multi-IR photon energy at radius R may be quantified by the number $N_{VUV}$ of VUV photons having sufficient Planck energy $E_{VUV}$ to dissociate the water molecule and raise the hydroxyl ion to excited *OH states,

$$N_{VUV} = \frac{U_{IR}}{E_{VUV}} = \frac{2\pi}{3} N_{dof}\left(\frac{R_o}{\Delta}\right)^3\left(\frac{kT}{E_{VUV}}\right) \tag{3}$$

[0037] where, $E_{VUV}=N_{IR}$ kT and $N_{IR}$ is the number of multi-IR photons. The number $N_{OH}$ of OH ions formed from the cavity wall depends on the hydroxyl yield $\gamma_{OH}$ by,

$$N_{OH}=\gamma_{OH}N_{VUV} \tag{4}$$

[0038] At VUV frequencies, the yield $\gamma_p$ is unity. Taking the dissociation of water to occur at $E_{VUV}$~4.9 eV and a particle radius $R_0$~1.44 microns, the number of ions $N_{OH}$~$6.6\times10^9$.

[0039] Argon dissolved in the water combines with the excited hydroxyl states to form the Ar*OH excimers by the mole fraction solubility $\phi$~$2.75\times10^{-5}$. Hence, the number $N_{Ar^*OH}$ of Ar*OH excimers is, $N_{Ar^*OH}>\phi N_{OH}$~$1.8\times10^5$. In bubble collapse, high pressures develop in the collision of the bubble walls, the magnitude of pressure proportional to the size of the bubble prior to collapse, e.g., a bubble radius of about 35 microns develops a collapse pressure of about 200 bars. At this pressure, argon excimers decompose giving one VIS photon per excimer, or $1.8\times10^5$ VIS photons. This is consistent with the experimental standard unit of sonoluminescence, i.e., the $2\times10^5$ VIS photons found for the collapse of a typical bubble in air saturated water.

[0040] Cavity QED induced sonoluminescence is optimal for liquid water. Weak sonoluminescence is observed from liquid helium and nitrogen as low surface tension limits the size of the particle at nucleation that controls the number of atoms that spontaneously emit thermal kT energy, but also because of the low thermal kT energy at cryogenic temperatures. Water is the optimum liquid for the QED device because water has a high surface tension while still providing significant thermal kT energy even at ambient temperature.

[0041] Triboluminescence

[0042] Unlike sonoluminescence that occurs in the liquid state, electrons and VIS light in triboluminescence is emitted from materials as they fracture under tension or crush under compression. Triboluminescence is known from the prior art and is not patentable, but the QED process of cavity QED induced VUV light to produce triboluminescence is novel and patentable.

[0043] Triboluminescence by fracture under tension of a material by crack growth as the opening of gap g between fragments is depicted in **FIG. 5**. Cracks open during periods the crack tip is subjected to hydrostatic tension, the crack growth process providing a flow of microscopic particles **4** from the crack tip **5**, the particles **4** comprising atoms and molecules at solid density. **FIG. 6** depicts platens **6** crushing material **7**. Crushing acts to close cracks to microscopic dimensions, the crushing process reducing fragments to particle sizes comparable to the dimensions of the space between platens.

[0044] Fracture and crushing as QED processes treat the microscopic gaps between fragments as 1-dimensional QED cavities having a EM resonant wavelength $\lambda_c$~2 g, where g is the gap dimension in **FIGS. 5 and 6**. QED processes in triboluminescence produce EM energy from the spontaneous emission of IR radiation at the instant the particles separate from the fragments in fracture, or as the fragments close on the particles during crushing.

[0045] Prior to fracture or crushing, atoms and molecules in the solid state emit $N_{dof}\times$½ kT of EM radiation. For most solid state materials, $N_{dof}$~3. Similar to the liquid state, the EM radiation from the continuum in the solid state is emitted as IR radiation at ambient temperature as shown in **FIG. 3**.

[0046] Since the space in the gap g between crack and fragment faces has a high EM resonant frequency, the low frequency IR radiation from the atoms in the separated particle is momentarily suppressed. Suppressed IR radiation is a loss of EM energy that must be conserved, and therefore the EM energy is spontaneously emitted as multi-IR photons that accumulate to VUV levels in the atoms and molecules of fragment surfaces. For a particle of radius $R_0$, the Planck energy E at a distance X from the center of the particle,

$$E=\frac{1}{2}\left(\frac{R_0}{X}\right)^2\left(\frac{R_0}{\Delta}\right)kT \tag{5}$$

[0047] Taking $R_0$~1 micron and $\Delta$~3 angstroms, the Planck energy E at the particle surface is about 40 eV. The number $N_{VIS}$ of VIS photons produced depends on the photoluminescence yield $\gamma_{pl}$ and the number of $N_{VUV}$ of VUV photons,

$$N_{VIS}=\gamma_{pl}N_{VUV} \tag{6}$$

[0048] In triboluminescence, the VIS light observed from fracture of the solid state is the result of the cavity QED induced VUV light, the VIS light produced from the excitation of gases in the crack and by the photoluminescence of the solid state materials forming the crack surfaces.

[0049] Flow Electrification

[0050] In the flow of jet fuels and automobile gasoline, the fuel is electrified posing a danger caused by discharge of the charge buildup. Flow electrification is known from the prior art and is not patentable, but the QED process of cavity QED induced VUV light to produce flow electrification is novel and patentable.

[0051] **FIG. 7** illustrates the QED induced flow electrification. Protrusions **8** in the pipe wall perturb the flow **9** to cause low-pressure regions. In QED induced flow electrification, the QED cavities are microscopic bubbles **10** that nucleate in the low-pressure regions. Because of surface tension, the nucleation produces a spherical particle **11** of fuel molecules at liquid density. Fluids that electrify including aviation fuel and automobile gasoline are insulators having low electrical conductivity, thereby permitting the buildup of electrical charge. In contrast, water has an electrical conductivity about 7 orders of magnitude greater than fuels, i.e., charge buildup does not occur in water during acoustic cavitation. In the flow of insulator fuels, cavity QED induced VUV light charges the fluid positive by the liberation of electrons by the photoelectric effect.

[0052] Prior to nucleation, the fluid molecules in the liquid continuum under hydrostatic compression emit $N_{dof}\times$½ kT of EM radiation, which at ambient temperature is emitted from the continuum as IR radiation. For fuels, $N_{dof}$~6. But at the instant the particle separates from the bubble, the low frequency IR radiation from the fluid molecules in the particle is suppressed as the bubble has a high EM resonant frequency. Suppressed IR radiation is a loss of EM energy that is conserved by the spontaneous emission of IR radiation that accumulates to VUV levels on the bubble surface. For a particle of radius $R_0$, the Planck energy E on the bubble wall at a distance R from the center of the particle,

$$E = \left(\frac{R_0}{R}\right)^2 \left(\frac{R_0}{\Delta}\right) kT \quad (7)$$

[0053] where, the particle radius $R_0$~2S/P. For fuels, S~0.02 N/m. At atmospheric pressure, $R_0$~0.4 microns. For n-Heptane having a molecular weight of 100 and density 684 kg/m$^3$,Δ~6.2 angstroms, the Planck energy E at the particle surface is about 16 eV.

[0054] The number $N_e$ of electrons produced by a single bubble from the VUV irradiation of the bubble wall depends on the electron yield $\gamma_e$ by,

$$N_e = \gamma_e N_{VUV} \quad (8)$$

[0055] where, the number of VUV photons $N^{VUV}$~1.77×$10^7$ from Eqn. (3). For $\gamma_e$>0.0001, $N_e$>2000 with an equivalent number of charged molecular states in the fluid.

[0056] In flow electrification, the charged fluid and electrons are the result of the cavity QED induced photoelectric effect, the electrons produced by the VUV irradiation of the bubble wall at the instant of bubble nucleation.

[0057] Static Electricity

[0058] Since the time of the early Greeks, static electricity is a well-known phenomenon in the prior art and not patentable, but the QED process of cavity QED induced VUV light to produce static electricity is novel and patentable.

[0059] **FIG. 8** illustrates the cavity QED induced static electricity. Microscopic gaps g that open and close as materials **13** and **14** are made to contact each other are 1-dimensional QED cavities. Particles **15** that are part of material **13** rub off to produce free particle **16** in the gap, although the free particle **16** may be present in the surroundings as the QED cavity opens or closes. Otherwise, QED induced static electricity process and triboluminescence are similar.

[0060] Prior to confinement in the QED cavity, the atoms in the particles have $N_{dof}$×½ kT of EM energy, which at ambient temperature is emitted as IR radiation. But at the instant the 1-D cavities open or close to an EM resonant wavelength $\lambda_e$<10 microns, or gap g <5 microns, the low frequency IR radiation from the water molecules in the particle is suppressed. To conserve EM energy, the suppressed IR radiation is spontaneously emitted and accumulates to VUV levels on the adjacent material surfaces.

[0061] In cavity QED induced static electricity, the VUV radiation produces electrons from the contacting materials by the photoelectric effect. The number $N_e$ of electrons produced from the VUV irradiation of the particles depends on the electron yield $\gamma_e$ of the materials [see Eqn. (6)] and the number $N_{vuv}$ of VUV photons [see Eqn.(3)]. For dissimilar materials irradiated with VUV light, both materials lose electrons. But the material with the highest electron yield per VUV photon loses more electrons than it gains and charges positive, the one gaining a net number of electrons is charged negative.

[0062] Atmospheric Electricity

[0063] In atmospheric electricity, storms producing lightning and thunder are well-known from the prior art and not patentable, but the QED process of cavity QED induced VUV light to produce atmospheric electricity is novel and patentable.

[0064] FIGS. **9-11** illustrate cavity QED induced atmospheric electricity. **FIG. 9** shows a microscopic bubble **17** nucleates around a central particle **18** during the large volume expansion in graupel, the graupel a liquid-ice mixture that forms as moisture carried by updrafts of the storm supercools at high altitudes. Bubble nucleation produces VUV light by cavity QED induced spontaneous emission that dissociates the water molecules in the annular gap **19** between the particle and bubble surfaces into hydronium and hydroxyl ions. Unlike sonoluminescence where little air is drawn into the expanding bubble because of the short time available at acoustic frequencies, graupel expansion is prolonged allowing air **20** to be drawn into the bubbles.

[0065] Ionic charge separation occurs by the pH of the raindrops. Typically, rainwater has an acid pH, and therefore the bubble particle and walls carry a positive background charge. The cavity QED produced hydronium ions are repulsed to the bubble vapor while the companion hydroxyl ions are attracted to the surfaces of the particle and the bubble wall.

[0066] The hydronium and hydroxyl ions react with water and nitrogen molecules to form positive charge proton-hydrate (PH) and negative charge non-proton-hydrate (NPH) clusters.

[0067] The graupel volume contracts to collapse the bubbles as depicted in **FIG. 10**. But the water vapor is not compressed because it is a condensable vapor in 2-phase equilibrium with the liquid bubble walls. Only the air drawn into the graupel after nucleation is compressed to a high pressure. Hence, air with PH vapor **21** is forced out of the graupel, the vapor promptly forming positive charged micro-droplets; whereas, the NPH ions are attracted to the graupel.

[0068] **FIG. 11** shows the graupel later falling to the earth, the NPH ions subliming as a negative charged vapor. Charge separation that began at bubble nucleation is completed by the formation of light PH cluster clouds that remain buoyant in the stratosphere while the heavier NPH clouds fall to the earth.

[0069] In cavity QED induced atmospheric electricity, cloud-to-ground lightning is caused by the discharge of negative charge NPH clouds with the positive charge earth; whereas, cloud-to-cloud lightning is caused by discharge between the negative charged NPH clouds and positive charge PH clouds.

## DESCRIPTION OF THE INVENTION

[0070] The present invention is described by QED devices that rely on the cavity QED induced VUV light to produce VIS photons, electrons, and ions.

[0071] In the drawings:

[0072] **FIG. 12** is a cross-section elevation view of a preferred embodiment of the present invention for a QED device comprising an ultrasonic lamp producing VIS light.

[0073] **FIG. 13** is a cross-section elevation view depicting another preferred embodiment of the present invention for QED devices comprising a solid particle encapsulated in a microsphere to produce VIS photons, electrons, and ions. **FIG. 14** shows how the microsphere light sources may be arranged in a small container to produce VIS light by manual shaking. **FIG. 15** shows how the light sources may be placed on acoustically driven optical elements.

[0074] **FIG. 16** shows the present invention in a cross-section elevation view for still another preferred embodiment for a QED device to produce VIS photons and electrons comprising layered optical windows utilizing thermal energy from the surroundings to drive a QED thermal laser. A similar layered configuration for a QED device of a thermoelectric battery is shown in **FIG. 17**.

[0075] **FIG. 18** and **19** depict the present invention in a cross-section elevation view of a QED device as a particle filter. **FIG. 18** shows a microscopic cell producing VIS light. A particle filter producing comprising a plurality of microscopic cells is shown in **FIG. 19**.

[0076] The foregoing are given only as illustrative examples of the use of cavity QED induced VUV light in QED devices disclosed in the present invention, and do not in any way limit the generality of QED devices embodied in the present invention.

[0077] Ultrasonic Lamp and Battery

[0078] In one preferred embodiment, cavity QED induced VUV light is used in a QED device to produce VIS light in an ultrasonic lamp.

[0079] **FIG. 12** illustrates the cavity QED induced ultrasonic VIS lamp. A transparent container **25** houses a large number of microscopic solid particles **26** in liquid water **27**. The particles are essentially spherical and fabricated from a metal oxide, such as zinc oxide or the like having a high photoluminescence yield of VIS photons at VUV frequencies. Acoustic crystals **28** the container in orthogonal directions to immerse the particles **26** in a spherical acoustic field.

[0080] During periods of hydrostatic tension in the acoustic cycle, the bubbles **29** having a radius R nucleate in the liquid around the solid particles of radius $R_0$. In contrast, the particle in sonoluminescence is comprised solely of water molecules at liquid density formed by surface tension. Metal oxides are hydrophobic in water, and therefore the nucleation process in the ultrasonic lamp exposes a dry surface. An annular gap **30** promptly forms between the particle and bubble wall surfaces, providing the particle radius $R_0$ is slightly less than the surface tension radius for water, i.e., $R_0<2S/P\sim1.44$ microns. Hence, particles **26** are required to have a diameter radius $2R_0<2.88$ microns.

[0081] Prior to nucleation, the metal oxide molecules in the particle emit $N_{dof}x½$ kT of EM radiation. At ambient temperature, EM radiation is emitted from the particle as IR radiation. But at the instant the bubble wall separates from the particle, the bubble having a high EM resonant frequency suppresses the low frequency IR radiation from the metal oxide molecules in the particle. Suppressed IR radiation is a loss of EM energy that is conserved by the spontaneous emission of IR radiation. Hence, the IR photons are absorbed [see Eqn. 3] because of the high optical quality of the QED cavity provided by the absorption of the water molecule at IR frequencies. Subsequently, the VUV resonance of the annular gap [see Eqn. 6] excites the surface of the particles at VUV frequencies.

[0082] In the cavity QED acoustic lamp, VIS light is produced by photoluminescence of the metal oxide particles by the cavity QED induced VUV light from the spontaneous emission of IR radiation.

[0083] The QED acoustic lamp may be converted to a QED acoustic battery by replacing the water **27** with liquid n-Heptane having a low electrical conductivity, the electrons produced from the n-Heptane from the cavity QED induced VUV light by photoelectric effect.

[0084] Microsphere Light Source

[0085] In another preferred embodiment, cavity QED induced VUV light is used in a microsphere light source.

[0086] **FIG. 13** shows the solid particle **33** of radius $R_0$ encapsulated by an IR transparent solid **35** within a shell **34** having radius R. Both particle **33** and shell **34** are fabricated from zinc oxide having high photoluminescence yield. The particle **33** is encapsulated in silicon **35** that is transparent in the IR from about 1 to 20 microns.

[0087] In macroscopic cavities absent cavity QED effects, the particle **33** gains and loses heat Q the usual way by conduction with the shell **34** as shown in **FIG. 7**(*a*). However, cavity QED effects modify the heat transfer by including the rapid loss of thermal kT energy by spontaneous emission of EM radiation hυ compared to the slow heat Q loss by conduction. Heat Q gained by the particle by conduction is promptly lost by the spontaneous emission of EM radiation hυ. The QED device finds application as a steady QED laser or thermoelectric device driven by the temperature of the surroundings.

[0088] Microspheres fabricated with the particles **33** in a vacuum without a solid IR transparent material **35** are depicted to be vibrated in **FIG. 14** and **15**. A vacuum requires intermittent contact to transfer heat from the shell **34** to the particle **33**. **FIG. 14** shows microspheres in a transparent container **36** vibrated manually by hand **37** to produce VIS light. **FIG. 15** shows a concave optical lens **38** coated with a microsphere layer excited by an acoustic drive **39** to produce a beam of VIS light focussed at point **40**.

[0089] Provided the gap between the particle **33** and the shell **34** is IR transparent, the shells **34** are prescribed to have a radius R <2.5 microns, or a wavelength $\lambda<10$ microns consistent with the suppression of IR radiation at ambient temperature as shown in **FIG. 2**. Suppressed IR radiation is spontaneously emitted by cavity QED provided the particle is separate from the microsphere.

[0090] For a silicon **35** encapsulated particle **33**, the QED induced VUV light produces a number of VUV photons [see Eqn. 3] that are converted to VIS light [see Eqn. 6] by photoluminescence, e.g., for a microsphere of zinc oxide, a VIS green light is produced. In the alternative particle **33** encapsulated in an evacuated shell **34** provided with a filler gas, the VUV light excites the filler gas, which if nitrogen produces blue VIS light.

[0091] Thermal Laser and Thermoelectric Battery

[0092] In still another preferred embodiment, cavity QED induced VUV light is used to provide a steady QED thermal laser and thermoelectric battery.

[0093] The VIS laser shown in **FIG. 16** comprises optical quartz windows **50** about 1 cm in diameter separated to form a 1-dimensional QED cavity having a gap g of about 5 microns, thereby providing the suppression of IR radiation at wavelength $\lambda > 2$ g~10 microns. The interior window surfaces **51** are coated with metal oxide, such as zinc oxide or the like having a high photoluminescence yield of VIS photons at VUV frequencies. A zinc oxide powder **52** having a diameter $2R_0 < 3$ microns is provided in the gap. The QED cavity carries a filler gas **53**, such as nitrogen.

[0094] **FIG. 17** depicts the cavity QED thermoelectric battery that except for the window coating materials is otherwise identical to the QED thermal laser shown in **FIG. 8**(*a*). The QED thermoelectric battery requires one coating **54** to have a high photoelectric yield while the other **55** is reflective at VUV frequencies to optimize the potential difference and electron yield between the materials.

[0095] In both QED laser and thermoelectric battery, thermal energy from the surroundings is converted to a continuous steady low-level source of VIS light or electrons. Heat is transferred by convection from the windows **50** to the powder **52** by collisions of the filler gas molecules with to maintain the zinc oxide powder **52** at ambient temperature, the heat compensating for the loss of IR radiation by spontaneous emission induced by cavity QED.

[0096] In the QED thermal laser, the powder atoms spontaneously convert thermal kT energy to VUV light [see Eqn. 3]. The QED thermal laser produces VIS light from the metal oxide coated windows, e.g., zinc oxide produces a green light by photoluminescence [sse Eqn. 6]. In the alternative, the VUV light excites the filler gas, e.g., nitrogen produces blue VIS light.

[0097] The QED thermoelectric battery converts the thermal energy of the surroundings to a potential difference $V_2 - V_1$ and a source of electrons. The cavity QED induced VUV light produces electrons [see Eqn. 7] from both materials **54** and **55** depending on their photoelectric yields, the material with the higher yield losing more electrons and acquires a positive charge [see Eqn. 8]. Material **54** is depicted to acquire a positive charge owing to its higher electron yield, while the reflective material **55** gains electrons and charges negative.

[0098] Particle Filter

[0099] In a still another preferred embodiment, the QED device is used in a filter having microscopic pores resonant with the flow of solid spherical particles to provide a source of VIS photons and electrons.

[0100] **FIG. 18** illustrates a microscopic QED flow cell. Solid particles **61** of n-type semiconductor material having a diameter $2R_0 < 3$ microns move in tube 62 through a restriction **63** under the influence of an external electric field produced by voltages $V_1$ and $V_2$. The particles **61** carry a negative charge and the tube **62** is fabricated from an electrical insulator material. VUV light is produced as the particles move through the restriction **63** having a dimension D with an EM resonance that suppresses IR radiation. The channel is evacuated and filled to a low-density nitrogen gas **64**. At ambient temperature, IR radiation is suppressed at a wavelength $\lambda$ of about 10 microns, or a diameter D of 5 microns.

[0101] A resonant filter comprising a plurality of microscopic pathways is illustrated in **FIG. 19**. The filter body **65** is an electrical insulator provided with a plurality of microscopic pathways **66** having a nominal diameter D <10 microns. Solid particles **61** of n-type semiconductor material having a spherical diameter $2R_0 < 3$ microns move through the pathways **65** under the influence of an external electric field produced by voltages $V_1$ and $V_2$.

[0102] VIS photons are caused by the excitation of the nitrogen gas by cavity QED induced VUV light produced as the particles move through the restrictions in FIGS. **9**(*a*) and (*b*). The VUV light excitation produces a positive charged insulator material from the electron loss by the photoelectric effect, the electrons lost by the insulator carried away by the electric field to a collector of the battery.

What I claimed is:

**1**. A QED device producing cavity QED induced VUV light comprising: structures in a microscopic cavity, said structures of essentially temporary construction, said QED device utilizing the thermal kT energy of atoms in said structures as the source of EM energy, said cavity providing a QED confinement of IR radiation from said atoms defined by the harmonic oscillator at ambient temperature T. said QED device provided with means of separating said structures from the walls of said cavity, said atoms emitting IR radiation provided said structures are not separated from said cavity walls, said IR radiation from said atoms momentarily suppressed as said structures separate from said cavity walls, said QED confinement inducing spontaneous emission of said suppressed IR radiation from said atoms, said spontaneous IR emission combining at said cavity wall to produce said cavity QED induced VUV light.

**2**. A plurality of QED devices as recited in claim 1.

**3**. The QED device as recited in claim 1, wherein material of said cavity wall is selected to enhance VIS photon yield by photoluminescence from said cavity QED induced VUV light.

**4**. A plurality of QED devices as recited in claim 3.

**5**. The QED device as recited in claim 1, wherein material of said cavity wall is selected to enhance electron yield by the photoelectric effect from said cavity QED induced VUV light.

**6**. A plurality of QED devices as recited in claim 5.

**7**. The QED device as recited in claim 1, wherein material of said cavity wall is selected to enhance ionic yield from said cavity QED induced VUV light.

**8**. A plurality of QED devices as recited in claim 7.

**9**. A QED device producing cavity QED induced VUV light comprising: structures in a microscopic cavity, said structures of essentially permanent construction, said QED device utilizing the thermal kT energy of atoms in said structures as the source of EM energy, said cavity providing a QED confinement of IR radiation from said atoms defined by the harmonic oscillator at ambient temperature T, said QED confinement inducing spontaneous emission of IR radiation from said atoms in said structures, said spontaneous emission of IR radiation reducing said thermal kT energy of said atoms, said reduction in said thermal kT energy compensated by convection and conduction heat flow from the thermal surroundings through cavity walls to said atoms in said structures, said spontaneous IR emission combining at said cavity walls to produce said cavity QED induced VUV light.

**10**. A plurality of QED devices as recited in claim 9.

**11**. The QED device as recited in claim 9, wherein material of said cavity wall is selected to enhance VIS photon yield by photoluminescence from said cavity QED induced VUV light.

**12**. A plurality of QED devices as recited in claim 11.

**13**. The QED devices as recited in claim 9, wherein material of said cavity wall is selected to enhance electron yield by the photoelectric effect from said cavity QED induced VUV light.

**14**. A plurality of QED devices as recited in claim 13.

**15**. The QED devices as recited in claim 9, wherein material of said cavity wall is selected to enhance the ionic yield from said cavity QED induced VUV light.

**16**. A plurality of QED devices as recited in claim 15.

**17**. A QED device of an ultrasonic VIS lamp at ambient temperature comprising: a transparent container housing a large number of microscopic solid particles in liquid water, said particles essentially spherical and fabricated from zinc oxide having a nominal diameter of about 3 microns, said housing driven by acoustic crystals in orthogonal directions, said drives immersing the particles in a spherical acoustic field, said particles producing cavity QED induced VUV light at the water interface, said cavity QED induced VUV light producing VIS photons from said particles by photoluminescence.

**18**. A QED device of a microsphere producing VIS light at ambient temperature comprising:

a solid particle encapsulated in a thin shell by a layer of IR transparent silicon, said particle essentially spherical having a nominal diameter of about 3 microns, said layer of silicon having a nominal thickness of about 1 micron, said particle and said shell fabricated from zinc oxide, said shell forming a spherical QED cavity having a resonant wavelength of about 10 microns, said QED cavity inducing spontaneous emission of IR radiation from atoms in said particle at ambient temperature, loss of thermal kT energy by said atoms by said spontaneous emission of said IR radiation compensated by conduction heat gain from ambient surroundings, said spontaneous emission of IR radiation combining to produce cavity QED induced VUV light at said shell, said cavity QED induced VUV light producing VIS light from said shell by photoluminescence.

**19**. A plurality of QED devices as recited in claim 18.

**20**. The QED device as recited in claim 18, wherein said thin shell is a metal or semi-conductor material selected to enhance the electron yield under said cavity QED induced VUV light, said QED device finding application as a thermoelectric battery providing a source of electrons.

**21**. A plurality of QED devices as recited in claim 20.

**22**. A QED device for a thermal laser comprising: a pair of optical quartz windows coated with zinc oxide, coated window surfaces separated by a gap of about 5 microns, said gap providing a QED cavity having a resonant wavelength of about 10 microns, said QED cavity provided with zinc oxide powder having a nominal diameter of about 3 microns, said QED confinement inducing spontaneous emission of IR radiation from atoms in said powder at ambient temperature, loss of thermal kT energy by said spontaneous emission of IR radiation from said atoms in said powder compensated by convection heat gain from the thermal surroundings, said heat converted by said spontaneous emission of IR radiation from said particles to produce cavity QED induced VUV light at said coated window surfaces, said cavity QED induced VUV light producing VIS light from said coated window surfaces by photoluminescence.

**23**. The QED device in claim 22, wherein one of said window pair is coated with a metal having a high electron yield, the other of said windows coated with a VUV reflective material, said cavity QED induced VUV light producing electrons by the photoelectric effect, said QED device finding application as a thermoelectric battery.

**24**. A QED device for a flow filter producing electrons comprising: a plurality of microscopic pathways having an nominal diameter of about 10 microns, said pathways formed in an electrical insulator material, said QED device provided with solid particles fabricated from n-type semiconductor material having a spherical diameter of about 3 microns, said QED device provided with an electric field to move said particles within said pathways, atoms in said particles emitting IR radiation before entering said pathways, said IR radiation momentarily suppressed upon entering the pathways, said suppressed IR radiation spontaneously emitted from said particles to conserve EM energy, said spontaneous IR emission accumulating in the surfaces of said pathways to produce cavity QED induced VUV light, said cavity QED induced VUV light liberating electrons by the photoelectric effect.

* * * * *

# Acknowledgements

If it were not for the expertise of two dedicated, enthusiastic, conscientious persons studying and working at Technische Universität Berlin, Germany, this book would not have come to life!

The family of Thomas Prevenslik wishes to thank them for undertaking this challenging project of sorting and classifying over 300 research articles written from 2004 to 2021 by the late Thomas Prevenslik and posted chronologically on his website nanoqed.org.

All the articles in this book are the original publications in their original format as selected from the nanoqed website. The innovative theories and ideas presented are those developed by Thomas V. Prevenslik.

## About the Author

Thomas Prevenslik [1937-2021] grew up near Pittsburgh Pennsylvania. He was a serious student with a particular interest in science, wanting to know how things work and why; questioning the status quo.

"You don't know the future!"

He attended Carnegie Mellon and the University of Pittsburgh where he obtained his Bachelor and Master Degrees in Mechanical Engineering respectively. He designed non-vibrating structures to support the telescopes and cameras aboard the Apollo 11. In 1970, he worked for major companies in the area of nuclear reactors as a source of energy.

In 1994, Tom began a new career in Physics and entered a doctorate program at the University of Hong Kong. He developed the simple QED theory based on quantum mechanics and founded his own company: QED Radiations. He presented his research at numerous conferences throughout Europe, Asia and the USA.

## Topics

- Covid-19 Treatment by Nanoparticles
- Health Risks of Nanoparticles and Genetically Modified Food
- Cellular Biology
- UV Disinfection by Heat
- Simple QED
- Astronomy
- Nanoparticle Physics and Molecular Dynamics
- Geoengineering and Engineering